Advancing Chain Elongation Technology for Medium Chain Carboxylic Acids Production from Waste Streams

by

Shilva Shrestha

A dissertation submitted in partial fulfillment
of the requirements for the degree of
Doctor of Philosophy
(Environmental Engineering)
in The University of Michigan
2021

Doctoral Committee:

Professor Lutgarde Raskin, Chair
Assistant Professor Matthew T. Agler, Friedrich Schiller University Jena
Professor Glen Daigger
Associate Professor Xiaoxia Lin
Professor Steve Skerlos

Shilva Shrestha

shilva@umich.edu

ORCID iD: 0000-0001-5062-3634

DEDICATION

To Baba and Mama for their innumerable sacrifices and unparalleled love that paved the way to where I am today, and to my late grandmother, Pushpa Shrestha for seeding confidence and self-belief in a little girl.

ACKNOWLEDGEMENTS

This dissertation research was financially supported by the National Science Foundation Sustainability Research Networks (grant no 1444745) and the Department of Energy Small Business Innovation Research grant. I was fortunate to receive several fellowships during my graduate studies that gave me the flexibility to pursue my research without any financial constraints. I would like to acknowledge the Water Environment Federation Canham Graduate Scholarship, the Burroughs Wellcome Fund Integrated Training in Microbial Systems (ITiMS) Fellowship, and the University of Michigan Rackham Predoctoral Fellowship.

I would like to express my sincere thanks to my PhD advisor, Lutgarde Raskin, for her mentorship and wisdom, for helping me grow as an independent researcher, for believing in me and giving me the freedom to shape my dissertation research according to my interest, and for her endless support as my career goals evolved. I would like to express my gratitude to my committee members Steven Skerlos, Glen Daigger, Nina Lin, and Matthew Agler for lending me their expertise and providing constructive feedback throughout my PhD. I am thankful to Steve for his insightful suggestions and guidance with the life cycle assessment work.

Several PhD, Master's, and undergraduate students were instrumental in making this research possible. I would like to sincerely thank Dianna Kitt, Hang (Alex) Song, Caro Tryuers, Siqi Xue, Maxim Muermans, Brittany Colcord, Lucy Aley, and Liem Ellen Setiawan for their hard work and significant contributions at various stages of this research. Working with such a dedicated team of individuals and learning from each of them was one of the most gratifying experiences of my graduate life at the University of Michigan.

Samir Khanal, my master's thesis advisor, has supported me from the day I arrived from Nepal until today. I got the opportunity to interact and collaborate with wonderful researchers like Xavier Fonoll, Ilse Smets, Matt Scarborough, Josh Neufeld, Ryan Ziels, and Pranav Sampara and would

like to thank them for all the discussions and helpful input on my research. The bioreactor work was made possible through the technical assistance of CEE Technical Staff, especially Steve Donajkowski, Ethan Kennedy, and Jan Pantolin. I would like to extend my thanks to Thomas Yavaraski for helping me troubleshoot the analytical methods. Thank you to the CEE administrative team for their help with purchases and reimbursements.

A heartfelt thanks to my Environmental Biotechnology family, particularly all the current and former members of the Raskin Research Group for their friendship, doses of encouragement and fun over coffee and happy hours, and invaluable feedback on research and conference presentations. I have thoroughly enjoyed being a part of such a collaborative and stimulating research environment and have learned a tremendous amount from this exceptionally talented group of researchers. Many thanks to my friends Molly, Binita, Ramila, Indu, Shikha, Prashamsha, Abhishek, and Swechchha for having my back and lifting my spirits during some of the challenging times of my PhD.

Finally, my deepest love and appreciation to my family for their unconditional love and encouragement. I am indebted to my mom, dad, and brother, my biggest supporters through every step of this journey, for providing me with resources, often beyond their capacity, that made it possible for me to come this far. My sincere gratitude also goes to my grandparents for their love and my in-laws for their unfailing support. Last but not the least, I am grateful to my husband, Bibhushan, who has been by my side throughout, for his unwavering love, companionship, and relentless support. His perseverance, optimism, and encouragement have helped me keep life challenges in perspective.

TABLE OF CONTENTS

DEDICATION ii
ACKNOWLEDGEMENTS iii
LIST OF TABLES ix
LIST OF FIGURES xi
LIST OF APPENDICES xvii
ABSTRACT xviii
Chapter 1 Introduction 1
1.1 Resource recovery from organic waste streams 1
1.2 Chain elongation for MCCA production 2
1.3 Problem statement and research motivation 4
1.4 Dissertation outline 6
1.5 References 7
Chapter 2 Resource Recovery of Medium Chain Carboxylic Acid from Brewery and Pre-fermented Food Waste Streams: Effect of Microbial Immigration on Chain Elongation 12
2.1 Abstract 12
2.2 Introduction 13
2.3 Materials & Methods 16
2.3.1 Inoculum and Substrate 16
2.3.2 Experimental setup 16
2.3.3 Chemical analyses 18
2.3.4 Microbial analyses 18
2.3.5 Statistical analyses 20
2.4 Results and Discussion 21
2.4.1 MCCAs recovery from brewery and pre-fermented food waste streams 21
2.4.2 MCCAs production correlated with *Clostridiales* and *Pseudoramibacter* activity 24
2.4.3 Effect of pH and SRT on methanogens 26

2.4.4 Influent plays a greater role in shaping the bioreactor microbiome than the inoculum 28
2.4.5 Microbial immigration from influent to downstream, bioreactor microbial community 30
2.5 Conclusions 36
2.6 References 36
Chapter 3 Effect of Methanogenic Inhibitor on Competitive Reactions During Ethanol Chain Elongation 44
3.1 Abstract 44
3.2 Introduction 45
3.3 Materials & Methods 47
3.3.1 Experimental setup and operating conditions 47
3.3.2 Chemical analyses 48
3.3.3 Microbial community analyses 49
3.3.4 Sequencing data processing 49
3.3.5 Statistical analyses 51
3.4 Results and Discussion 51
3.4.1 2-BES temporarily suppressed excessive ethanol oxidation to acetate 51
3.4.2 *Methanobrevibacter* dominates despite addition of methanogenic inhibitor 54
3.4.3 Methanogens develop tolerance towards 2-BES 57
3.4.4 Acetate production in the bioreactor 60
3.4.5 Effect of 2-BES inhibition on the bacterial community and chain elongation 63
3.5 Conclusions 65
3.6 References 66
Chapter 4 Impact of Dynamic Membrane Development on Chain Elongation for Medium Chain Carboxylic Acid Production from Organic Waste Streams 72
4.1 Abstract 72
4.2 Introduction 73
4.3 Materials and Methods 75
4.3.1 Substrate and Inoculum 75
4.3.2 Bioreactor system and operating condition 76
4.3.3 Pertraction system 80
4.3.4 Chemical analyses 80

4.3.5 Microbial analyses 81
4.3.6 Statistical analyses 82
4.4 Results and discussion 83
4.4.1 The dynamic membrane produces high quality permeate despite high bioreactor solids content 83
4.4.2 MLSS concentration and influent solids concentration affect dynamic membrane formation 84
4.4.3 Re-inoculation revived chain elongation activity 86
4.4.4 Integration of extraction unit with the AnDMBR system 90
4.4.5 Dynamic membrane biofilm activity contributes to MCCA production 91
4.5 Conclusions and Future research directions 94
4.6 References 95
Chapter 5 Environmental Life Cycle Assessment of Caproic Acid Recovery from Brewery Waste Streams 101
5.1 Abstract 101
5.2 Introduction 102
5.3 Materials and Method 104
5.3.1 System Boundary and Functional Unit 104
5.3.2 Life Cycle Inventory 107
5.3.3 Life Cycle Impact Assessment 108
5.3.4 Sensitivity Analysis 109
5.4 Results and Discussion 109
5.4.1 Environmental impacts of caproic acid production from brewery waste 109
5.4.2 Comparison of caproic acid production from brewery waste and palm kernel oil 115
5.4.3 Sensitivity Analysis 117
5.5 Conclusions 120
5.6 References 121
Chapter 6 Conclusions, Significance, and Future Research Directions 127
6.1 Overview 127
6.2 Major findings and significance 128
6.2.1 Impact of microbial immigration 128
6.2.2 Controlling competitive reactions during ethanol chain elongation 128

6.2.3 Dynamic membrane biofilm development leads to efficient solids-liquid separation along with enhanced MCCA production 129
6.2.4 MCCA production from brewery waste is environmentally sustainable compared to the conventional palm kernel oil-based method 129
6.3 Future research directions 130
6.4 References 134
APPENDICES 136

LIST OF TABLES

Table 4.1 Summary of AnDMBR experimental phases, operating conditions, and performance 79

Table 5.1 Life cycle assessment results across nine TRACI impact categories calculated per functional unit for BW-CA system for the baseline scenario 110

Table A.1. Chemical characteristics of inoculum and substrates 141

Table A.2. Processes involved in chain elongation 142

Table A.3. Biomass sampling points (days of bioreactor operation) for inoculum, influent, and bioreactor samples 143

Table A.4. Good's coverage values for different samples. The lowest good's coverage value was 97.4% indicating that dominant OTUs were recovered in most of the samples. 144

Table A.5. Average ratio of rRNA and rDNA based on top 15 genera from each sampling point in the bioreactor 145

Table A.6. Comparison of microbial community dissimilarities between influent and bioreactor samples collected on the same day based on Analysis of Similarity (ANOSIM) analysis..... 146

Table A.7. Shared OTUs between influent and bioreactor samples 147

Table A.8. Specific growth rate of populations observed in the chain elongation bioreactor 148

Table A.9. $rDNA_{influent}$/ $rDNA_{reactor}$ and $rRNA_{influent}$/ $rRNA_{reactor}$ values for different genus or family observed in the bioreactor samples. 154

Table B.1 Standard Gibbs free energy (ΔGo) calculated at standard conditions for competitive reactions for acetate production potentially involved during chain elongation. 173

Table B.2. ASVs with significant difference in relative activity due to 2-BES addition as observed with DESEq2 analysis..... 174

Table C.1. Chemical composition of inoculum and substrate 192

Table C.2. Distribution coefficients between aqueous and organic phases for SCCAs and MCCAs with and without TOPO 193

Table C.3. Biomass sampling points (days of reactor operation) from inoculum, bad beer, influent, reactor, and biofilm samples 194

Table D.1 Key process parameters for the production of one kg of caproic acid in the BW-CA system 213

Table D.2. Life cycle inventory of BW-CA for one kg of caproic acid for the baseline scenario. 214

Table D.3. Life cycle inventory of PKO-CA for 1 kg of caproic acid. The inventory data was derived from different literature studies* 215

Table D.4. Life cycle impact data derived from Ecoinvent database for different activities used for BW-CA and PKO-CA systems 216

Table D.5. Alternate scenarios modeled for sensitivity analysis 218

Table D.6. Total life cycle impacts calculated per functional unit for PKO-CA system 219

Table D.7. Comparison of total life cycle impacts of BW-CA including various scenarios and PKO-CA 220

LIST OF FIGURES

Figure 2.1 Volumetric production rate of total MCCAs, caproate, enanthate, and caprylate in the bioreactor over time. The MCCAs volumetric production rate varied cyclically as indicated by a linear regression model (R^2=0.6 with significant sine term, p=8.9E-05). 22

Figure 2.2. Dominant OTUs observed at a relative abundance and activity greater than 1% in at least 50% of the samples (n=14 in DNA and n=13 in RNA group) in the bioreactor samples over time. 25

Figure 2.3. Non-metric multidimensional scaling (NMDS) ordination plot based on the Bray-Curtis dissimilarity index of the microbial community at OTU level using 16S rRNA gene sequencing (a) and 16S rRNA sequencing data (b) and Jaccard index using 16S rRNA gene sequencing (c) and 16S rRNA sequencing data (d) in the rumen inocula, bioreactor, and influent samples. The numbers correspond to sampling time points. 29

Figure 2.4. Comparison of rRNA/rDNA ratio of microbial groups in the bioreactor and influent versus relative abundance (a) and relative activity (b) of the corresponding genus or family in the influent samples and relative abundance (c) and relative activity (d) of the corresponding genus or family in the bioreactor samples. The vertical line is drawn at $[rRNA/rDNA]_{reactor}$:$[rRNA/rDNA]_{influent}$ = 1. The microbial group that falls on the left and right hand sides of the vertical line are more active in the influent ($[rRNA/rDNA]_{reactor}$:$[rRNA/rDNA]_{influent}$ <1) and reactor ($[rRNA/rDNA]_{reactor}$:$[rRNA/rDNA]_{influent}$ > 1), respectively. Genus or family with high relative abundance and relative activity (larger Y-axis values) are colored and labeled. 33

Figure 3.1. Effluent acetate, net acetate, and influent acetate concentrations over time. The dashed lines represent 2-BES additions. 52

Figure 3.2. Net acetate concentration and hydrogen partial pressure (P_{H2}) (a) influent and effluent acetate concentrations and ethanol consumption (b), and theoretical 2-BES concentration profile and net acetate concentration (c) over time in the bioreactor. Ethanol consumption was calculated based on the concentration of ethanol initially present in the influent and that remaining in the effluent. The dashed lines represent 2-BES addition (10 mM in the bioreactor) on Days 230, 246, 259, 269, 278, 287, 296, 305, and 314. 53

Figure 3.3. Relative abundance (a) and activity (b) of methanogens identified to the genus level in the bioreactor samples over time using the ASV based approach. The relative abundance and relative activity were determined as percentages of the total number of 16S rRNA gene sequences and 16S rRNA sequences, respectively. The red dashed lines represent start and end of wasting bioreactor content on Days 20 and 82, respectively, for controlling solids retention time and the black dashed lines represent 2-BES additions. 55

Figure 3.4. Relative abundance (a) and activity (b) of methanogens ASVs in the bioreactor samples over time. The key ASVs discussed in the paper are labeled. The relative abundance and relative activity were determined as percentages normalized to the total number of 16S rRNA gene sequences and 16S rRNA sequences, respectively. The red dashed lines represent start and end of bioreactor content wasting on Days 20 and 82, respectively, for controlling solids retention time (Chapter 2) and the black dashed lines represent 2-BES additions. 59

Figure 3.5. Phylogenetic tree of 16S rRNA gene sequence of most abundant methanogenic ASVs (in red). *Methanopyrus kandleri* was used as the outgroup. The GenBank accession numbers are given in parentheses. The reference sequences are shown in black. Methanogens previously identified as ethanol oxidizers or capable of growth in the presence of ethanol are shown in blue. The numbers at the nodes of the branch indicate bootstrap values. The scale bar of 0.05 represents 5% substitutions per nucleotide base pair. 62

Figure 4.1. Schematic representation of the anaerobic dynamic membrane bioreactor integrated with an in-line MCCA extraction system labeled with different flows in and out of each unit process. 1, 2, 3, and 4 represent system boundaries for the mass balance calculation used in Eq C6 (Appendix C). The ultrafiltration unit was implemented on Day 245 as an additional barrier during instances of sloughing of the dynamic membrane layer. 77

Figure 4.2. Comparison of total suspended solids concentration (TSS) in the permeate and bioreactor over time (a) comparison of TSS in the permeate and influent over time (b). The vertical red dashed line represents a switch to the continuous filtration mode on Day 50 and the vertical black dashed lines represent different experimental phases. 84

Figure 4.3. Volumetric production rate of total MCCAs (a) caproate, enanthate, and caprylate (b) in the bioreactor over time. The vertical black and red dashed line represent re-inoculation with rumen content and adapted chain elongation biomass on Day 175 and integration of AnDMBR with the extraction unit with recirculation on Day 380, respectively. 87

Figure 4.4. Non-metric multidimensional scaling (NMDS) ordination analysis at ASV level based on Bray-Curtis dissimilarity index using 16S rRNA sequencing data in the rumen inoculum, chain elongation inoculum (CE_175), influent, suspended biomass, and biofilm samples. The numbers correspond to sampling time points. 90

Figure 4.5. Comparison of MCCAs concentration in permeate and bioreactor samples over time. MCCAs concentration in the bioreactor was measured starting from Day 259. The vertical dashed lines represent different experimental phases. 92

Figure 4.6. Relative activity of the microbial groups active at relative activity greater than 1% in at least 50% of the samples (n=10 in each group) classified to the genus or family level in the biofilm and suspended biomass samples. 93

Figure 5.1. System boundary and unit processes for BW-CA (a) and PKO-CA (b) systems for production of one kg caproic acid (functional unit). 106

Figure 5.2. Relative contribution of different unit processes to the total life cycle impact of BW-CA (a) and PKO-CA (b) across nine TRACI impact categories during production of one kg of caproic acid. 111

Figure 5.3. Comparison of total life cycle impact of BW-CA and PKO-CA in the Global warming, Acidification, and Eutrophication potential categories during production of one kg of caproic acid. Results for the other six impact categories are given in Table D.7 117

Figure 5.4. Results from the sensitivity analysis for all nine impact categories. Negative and positive values represent percentage reduction and increment in the total life cycle impact, respectively, compared to the baseline scenario. 118

Figure A.1. Hydraulic retention time (HRT) with corresponding organic loading rate (OLR) over time. The vertical lines represent change of HRT on Days 49 and 140. The OLR is a function of soluble chemical oxygen demand (sCOD) of the influent (g sCOD L^{-1}), flow rate of the influent (L d^{-1}), and working volume of the bioreactor (L). MCCAs volumetric production rate was significantly different (p=6.61E-09) between HRTs but there was no particular trend. The longest HRT of 3.7 ± 0.1 days led to lowest average MCCAs volumetric production rate of 3.0 ± 1.1 mmole $L^{-1}d^{-1}$ while the MCCAs production was similar (p=0.48) between HRTs 1.8 ± 0.0 days (4.7 ± 1.5 mmole $L^{-1}d^{-1}$) and 2.9 ± 0.22 days (5.2 ± 1.4 mmole $L^{-1}d^{-1}$)..... 158

Figure A.2. Relative abundance and activity of 15 most abundant microbial groups classified to the genus or family level in rumen inocula and the bioreactor samples over time. The relative abundance and activity were determined as percentages normalized to the total number of 16S rRNA gene sequences and 16S rRNA sequences, respectively. The top 15 microbial groups represented 87.5-95.8% and 84.5-98.3% of the total relative abundance and relative activity, respectively. 159

Figure A.3. Phylogenetic tree of 16S rRNA gene sequence of the dominant bacterial OTUs (in red). The GenBank accession numbers are given in parentheses. The reference sequences are shown in black while the known chain elongating microorganisms are shown in blue. The numbers at the nodes of the branch indicate bootstrap values. The scale bar of 0.10 represents 10% substitutions per nucleotide base pair. 160

Figure A.4. Relative abundance (a) and relative activity (b) of methanogens on OTUs level in the bioreactor samples over time. The relative abundance and relative activity were determined as percentages normalized to the total number of 16S rRNA gene sequences and 16S rRNA sequences, respectively. The dashed lines represent start and end of wasting bioreactor content on Days 20 and 82, respectively, to decrease solids retention time. 162

Figure A.5. Percentage of influent soluble chemical oxygen demand (sCOD) used up in methane production and solids retention time (SRT) over time..... 163

Figure A.6. Alpha diversity indices of the microbial community based on 16S rRNA gene sequencing (a) and 16S rRNA sequencing data (b) between inoculum, influent, and bioreactor samples. 164

Figure A.7. Non-metric multidimensional scaling (NMDS) ordination plot based on Bray-Curtis dissimilarity index of the bacterial community at OTU level using 16S rRNA gene sequencing (a) and 16S rRNA sequencing data (b) and Jaccard index using 16S rRNA gene sequencing (c) and 16S rRNA sequencing data (d) in the rumen inocula, bioreactor, and influent samples. The numbers correspond to sampling time points. 165

Figure A.8. Non-metric multidimensional scaling (NMDS) ordination plot based on Bray-Curtis dissimilarity index of the archaeal community at OTU level using 16S rRNA gene sequencing (a) and 16S rRNA sequencing data (b) and Jaccard index using 16S rRNA gene sequencing (c) and 16S rRNA sequencing data (d) in the rumen inocula, bioreactor, and influent samples. The numbers correspond to sampling time points. 166

Figure A.9. Comparison of community composition at the phylum level based on 16S rRNA gene sequencing (a) 16S rRNA sequencing (b) between influent and bioreactor samples. The data represent averages and error bars represent the standard deviations of data collected at different sampling time points. 167

Figure A.10. Relative abundance and activity of 15 most abundant microbial groups classified to the genus or family level in the influent samples over time. The top 15 microbial groups represented 84.5-96.2% and 86.3-98.2% of the total relative abundance and relative activity, respectively. 168

Figure A.11. Correlation of relative abundance and relative activity of microbial groups identified to the genus level observed in the bioreactor (a) and influent (b) samples. The relative abundance and relative activity were determined as percentages normalized to the total number of 16S rRNA gene sequences and 16S rRNA sequences, respectively. The average values of relative abundance and relative activity corresponding to all sampling time points were used. 169

Figure B.1. Volumetric production rate of total MCCAs, caproate, enanthate, and caprylate (a) acetate and butyrate (b) in the reactor over time. The dashed lines represent 2-BES addition. Chapter 2 reports the data in Figure 2.1a until Day 229. These data are repeated here for clarity. The volumetric production rates were determined by subtracting the influent concentration from the corresponding effluent concentration..... 176

Figure B.2. Gibbs free energy of ethanol oxidation to acetate (EEO) reaction under different pH (H^+ concentration) and temperature conditions assuming 1M of solute (reactant and product) concentration. *conditions used by Grootscholten et al. (2014)..... 177

Figure B.3. Daily production of gas showing its composition after 2-BES addition (represented by the dashed lines). Gas volumes were normalized to standard temperature (273K) and pressure (1 atm) condition. 178

Figure B.4. Alpha diversity indices of the archaeal community based on 16S rRNA gene (a) and 16S rRNA sequencing data (b) and of the bacterial community based on 16S rRNA gene (c) and 16S rRNA sequencing data (d) before (blue) and after (red) the start of 2-BES addition on Day 230. Significant difference is indicated by * ($P<0.05$), ** ($P<0.01$), and *** ($P<0.001$) based on the ANOVA analysis. 179

Figure B.5. Non-metric multidimensional scaling (NMDS) ordination plot based on Bray-Curtis dissimilarity index of the archaeal community at ASV level based on 16S rRNA gene (a) and 16S rRNA sequencing data (b) and of the bacterial community at ASV level based on 16S rRNA gene (c) and 16S rRNA sequencing data (d) before and after the start of 2-BES addition on Day 230. 180

Figure B.6. Relative abundance (a) and activity (b) of methanogens identified to the genus or family level in the reactor samples over time using OTU based clustering approach. The relative abundance and relative activity were determined as percentages normalized to the total number of 16S rRNA gene sequences and 16S rRNA sequences, respectively. The red dashed lines represent start and end of wasting bioreactor content on Days 20 and 82, respectively, for controlling solids retention time and the black dashed lines represent 2-BES additions. 181

Figure B.7. Relative abundance (a) and activity (b) of methanogens OTUs in the reactor samples over time. The key OTUs discussed in the paper are labeled. The relative abundance and relative activity were determined as percentages normalized to the total number of 16S rRNA gene sequences and 16S rRNA sequences, respectively. The red dashed lines represent start and end of bioreactor content wasting on Days 20 and 82, respectively, for controlling solids retention time and the black dashed lines represent 2-BES additions. Chapter 2 report data until Day 229 in Figure S4. 182

Figure B.8. Gibbs free energy changes for hydrogenotrophic methanogenesis (Table B2, Eq B2) and homoacetogenesis (Table B2, Eq B6) reactions. The calculations were done using concentration of respective reactants and products in the reactor and other reactor conditions (pH 5.5, 37^{o}C). The vertical dashed lines represent 2-BES additions. 183

Figure C.1. Hydraulic retention time (HRT) with corresponding organic loading rate (OLR) over time. The vertical dashed lines represent changes in HRT on Days 130, 210, and 364. 195

Figure C.2. Comparison of fraction of caproate, enanthate, and caprylate extracted during liquid-liquid extraction to the solvent (organic phase) with and without extractant TOPO. 196

Figure C.3. Concentration profiles of SCCAs (acetate, propionate, butyrate, and valerate) in the aqueous feed solution (a) and MCCAs (caproate, enanthate, and caprylate) in the stripping solution. The vertical red lines represent addition of MCCAs. 197

Figure C.4. Dynamic membrane formation over time 198

Figure C.5. Total suspended solids (TSS) removal over time. The vertical red dashed line represents a switch to the continuous filtration mode on Day 50 and the vertical black dashed lines represent different experimental phases. 199

Figure C.6. Turbidity measured in the permeate samples over time. The vertical red dashed line represents a switch to the continuous filtration mode on Day 50 and the vertical black dashed lines represent different experimental phases. 200

Figure C.7 Transmembrane pressure (TMP) profiles of the three meshes, F1, F2, and F3 over time versus the TSS concentration in the bioreactor. The TMP dropped whenever the meshes were replaced or flushed with water. The vertical dashed lines represent different experimental phases. 201

Figure C.8. Relative abundance of 15 most abundant microbial groups identified to the genus or family level in the bioreactor samples over time. The relative abundance was determined as percentages normalized to the total number of 16S rRNA gene sequences. The top 15 microbial groups represent 74.6-97.9% of the total relative abundance. 202

Figure C.9. Relative activity of 15 most abundant microbial groups identified to the genus or family level in the bioreactor samples over time. The relative activity was determined as percentages normalized to the total number of 16S rRNA sequences. The top 15 microbial groups represent 76.7-99.5% of the total relative activity. 203

Figure C.10. Non-metric multidimensional scaling (NMDS) ordination analysis at ASV level based on Bray-Curtis dissimilarity index using 16S rRNA gene sequencing data in the rumen inoculum, chain elongation inoculum (CE_175), influent, suspended biomass, and biofilm samples. The numbers correspond to sampling time points. 204

Figure C.11. Relative abundance of the microbial groups present at relative abundance greater than 1% in at least 50% of the samples (n=10 in each group) classified to the genus or family level in the biofilm and suspended biomass samples. 205

Figure D.1. Processes involved in production of one kg of caproic acid from palm kernel oil shown with mass-based allocation 221

LIST OF APPENDICES

APPENDIX A Supplemental Information for Chapter 2 137
APPENDIX B Supplementary Information for Chapter 3 171
APPENDIX C Supplementary Information for Chapter 4 185
APPENDIX D Supplementary Information for Chapter 5 206

ABSTRACT

Innovative approaches to convert organic waste streams into biofuels and biochemicals are gaining attention as they provide substitutes for fossil-fuel based products, address waste management problems, and provide economic return. Chain elongation for medium chain carboxylic acids (MCCAs) production from organic waste streams using anaerobic mixed-culture microbial communities is one such emerging biotechnology. MCCAs are platform chemicals used as building blocks for several industrial and agricultural commodities. This dissertation research focuses on the development and optimization of anaerobic bioreactor systems for efficient MCCA production from complex waste streams by integrating process engineering, microbial ecology, and modeling tools.

We demonstrated that pre-fermented food waste and brewery waste can be used for MCCA production by engineering anaerobic microbiomes. However, excessive ethanol oxidation to acetate, a competing reaction, led to inefficient usage of ethanol present in the brewery waste. Therefore, the competing reaction was suppressed by increasing hydrogen partial pressure through the addition of an inhibitor of hydrogen consuming methanogens, 2-bromoethanesulfonate. While the inhibition initially was successful, it was short-lived as a microbial community resistant to 2-bromoethanesulfonate developed over time. Thus, controlling competing processes is challenging with heterogeneous waste streams and the use of mixed cultures and other strategies need to be developed. Furthermore, the contribution of microbial immigration from the feed to the chain elongation bioreactor was characterized. A significant fraction of the microbial community in the chain elongation bioreactor originated from the influent. However, not all immigrant populations remained active in the bioreactor, while other populations that were present at relatively low relative abundance and activity in the influent contributed significantly towards the chain elongation function.

Given that MCCA recovery with an in-line membrane-based extraction system requires solids removal from the bioreactor effluent to avoid membrane fouling, a lab-scale anaerobic dynamic membrane bioreactor (AnDMBR) was developed. This system contained stainless steel meshes to support the formation of a biological cake layer termed a “dynamic membrane” that provided filtration. The dynamic membrane achieved efficient solid-liquid separation, resulting in higher than 95% suspended solids removal, despite high bioreactor solids concentration, enabling integration of the AnDMBR with the MCCA extraction system. Additionally, the development of the dynamic membrane biofilm led to the enrichment of highly active MCCA producing populations, thus promoting chain elongation activity.

Finally, the environmental life cycle impacts of the production of caproic acid, a six-carbon MCCA, from brewery waste using chain elongation were compared with the environmental impacts of a conventional palm kernel oil approach for caproic acid production using a life cycle assessment tool. The brewery waste based system provided environmental benefits compared to the conventional route on all impact categories assessed. The results also showed that the environmental footprint of the chain elongation system can be further improved by reducing sodium hydroxide addition and using renewable energy sources for heating the system.

As several cities, industries, and organizations are evaluating organic waste diversion through anaerobic bioprocesses, this dissertation research is highly relevant. It addressed knowledge gaps and technological barriers associated with MCCA production from waste streams and suggested strategies to guide future technology development.

Chapter 1

Introduction

1.1 Resource recovery from organic waste streams

The current linear economy has led to unsustainable resource exploitation and vast waste management problems (Esposito et al., 2018). Waste generation across the world is estimated to increase by 22% from 2.01 to 2.59 billion tons from 2016 to 2030 (Kaza et al., 2018). The concept of a circular economy has been proposed as an alternative to the linear economy and is gaining momentum worldwide (Esposito et al., 2018; Schroeder et al., 2019). In recent years, there has been increased interest in developing innovative approaches to repurposing waste streams for the production of bio-based chemicals and fuels (Kehrein et al., 2020; Puyol et al., 2017). Several regulations and policies are being implemented at the local and national levels around the world to reduce, reuse, and recycle waste (Jones et al., 2019; Malinauskaite et al., 2017). Water and wastewater systems account for approximately 3-4% of the total U.S. electricity consumption, which results in the production of almost 45 million tons of greenhouse gases every year (U.S.EPA, 2013). Wastewater treatment plants are also shifting towards the water resource recovery facility model as they are rethinking waste(water) treatment approaches to integrate recovery of resources (water, nutrients, energy, etc.) (Puyol et al., 2017). Integrating resource recovery could help wastewater treatment plants save energy and move towards achieving energy neutrality. Wastewater treatment plants can also generate revenue from tipping fees and earn renewable energy credits (depending on the government energy policies) providing additional incentives for adopting resource recovery approaches from waste streams (Jones et al., 2019).

Current fuel and chemical production methods depend heavily on non-renewable resources. Bioenergy and biochemicals production from organic waste streams provide an alternative to fossil fuel based resources with the additional benefit of providing proper waste treatment (Kehrein et al., 2020; Puyol et al., 2017). This has led to the development of several biotechnologies that harness the metabolisms of microorganisms for diverse applications in the fields of energy and environment, human health, and agriculture. Recent developments in genome sequencing, meta-omics, and computational tools have improved our ability to engineer and control microbial communities for desired outputs (Lawson et al., 2019). Anaerobic microbiomes can be engineered to efficiently convert low-value organic waste streams, despite their complexity and heterogeneity, into high-value chemicals and fuels (Angenent et al., 2016). One of the established anaerobic biotechnologies is the carboxylate platform that involves converting complex feedstocks including waste streams to short-chain carboxylic acids (SCCAs). The SCCAs can be further converted to methane via anaerobic digestion or to higher value platform chemicals such as medium-chain carboxylic acids (MCCAs) via chain elongation (Holtzapple and Granda, 2009; Wu et al., 2019).

1.2 Chain elongation for MCCA production

Chain elongation technology for MCCA production is gaining attention for resource recovery from diverse waste streams. Chain elongation includes oxidation of an electron donor and step-wise elongation of the carbon chain of SCCAs to MCCAs via the reverse β oxidation pathway (Angenent et al., 2016; Wu et al., 2019). Reduced compounds such as ethanol provide reducing equivalents (NADH), carbon in the form of acetyl-CoA, and energy (ATP). The two-carbon acetyl CoA molecule is added to the carbon backbone of the SCCAs leading to sequential carbon chain elongation in two-carbon steps (i.e., acetate (C2) to n-butyrate (C4), n-butyrate to n-caproate (C6), and similarly for odd chain carboxylates) (Angenent et al., 2016). Besides ethanol, other suitable electron donors include lactate, methanol, and propanol (Chen et al., 2016; Coma et al., 2016; Kucek et al., 2016a; Zhu et al., 2015).

MCCAs are carboxylic acids with chain lengths from six to twelve carbons including one carboxyl group (Angenent et al., 2016). MCCAs are platform chemicals with several industrial and agricultural applications. They can be converted into longer chain liquid fuels or used directly as

livestock feed additives, pathogen resistance inducer in plants, a green antimicrobial agent in the pharmaceutical industry, or as a valuable commodity for the production of lubricants, fragrances, and dyes (Angenent et al., 2016; Desbois and Smith, 2010; Hanczakowska, 2017; Scalschi et al., 2013; Takeuchi et al., 2008; Urban et al., 2017). The global MCCA market is expected to reach approximately USD 1.55 billion by 2022, growing at a compound annual growth rate of 12.3% between 2017 and 2022 (Zion Market Research, 2018). MCCAs are currently produced from petrochemical-based methods or extracted from palm kernel oil and coconut oil (Anneken et al., 2012). Palm kernel oil and coconut oil contain a small amount of MCCAs ranging from 0.1-10% by weight (Anneken et al., 2012; Bagby et al., 2004), which increases their market price. Furthermore, the use of plant oils such as palm oil has been associated with severe environmental consequences including greenhouse gas emission, land use changes, and deforestation (Carlson et al., 2012; Petrenko et al., 2016). MCCAs can also be obtained through anaerobic fermentation of waste streams via chain elongation, which has the potential to address the concerns of negative environmental problems and waste management at the same time.

The inputs required for chain elongation, SCCAs and ethanol (or other electron donors), can be present in the waste stream or produced *in situ* during the fermentation of organic waste. Several lab-scale chain elongation studies have demonstrated the use of diverse organic waste streams including yeast fermentation beer, organic fraction of municipal solid waste, food waste, acid whey, wine lees, Chinese liquor making wastewater, and thin stillage (Carvajal-Arroyo et al., 2019; Duber et al., 2018; Ge et al., 2015; Grootscholten et al., 2014; Kucek et al., 2016b; Nzeteu et al., 2018; Zhu et al., 2015).

Chain elongation can be applied for the valorization of waste generated in breweries. The number of breweries, particularly craft breweries, has been growing steadily in the U.S., with a 78% increase from the year 2010 to 2019 (Brewers Association, 2019). However, this growth has brought new challenges related to waste management. There are considerable opportunities to recover resources from the various organic-rich waste fractions generated in breweries. Waste beer, for example, has potential for MCCA production through chain elongation due to its high ethanol content. Waste beer is a waste stream produced as a result of faulty bottling, developing

off-flavors, improper fermentation, improper storage, or beer returned from the market because it is close to or beyond its expiration date (Seluy and Isla, 2014). Currently, this waste is mixed with brewery wastewater and treated onsite or discharged into the sewer system for treatment at a municipal wastewater treatment plant. Utilizing waste beer for MCCA production offers an alternative use for this waste stream. Additionally, a life cycle assessment identified crude ethanol use to have a dominant environmental impact over the life cycle (Chen et al., 2017). Therefore, using ethanol in brewery waste would reduce the operating cost and environmental impact by avoiding the use of crude ethanol in addition to treating brewery waste.

1.3 Problem statement and research motivation

Chain elongation is emerging as a promising biotechnology for the production of high-value platform chemicals such as MCCAs. Commercial-scale production of MCCAs through anaerobic chain elongation has just started in The Netherlands. The first full-scale plant, developed by ChainCraft in The Netherlands, produces caproic acid from food processing waste. A recent startup company called Capro-X (Ithaca, New York) is scaling up MCCA production from acid whey produced during Greek yogurt production. The feasibility of MCCA production from other waste streams has been demonstrated at the lab-scale level by several studies as indicated above. As the options for using waste streams for chain elongation are expanding, it is important to have a better understanding of how to optimize and stabilize the chain elongation process to maximize MCCA production. Research is needed to address several challenges associated with MCCA production from waste streams to successfully scale up this technology for real-world applications.

Chain elongation is facilitated by mixed microbial communities. The efficiency and stability of such microbially mediated processes depend on the concerted activity of microorganisms belonging to different functional groups. Microbial populations are involved in hydrolysis and acidogenesis of the organic substrates to produce MCCA precursors such as SCCAs, ethanol, and lactate, while other community members convert these intermediates into MCCAs. The increased metabolic flexibility and robustness conferred by a diverse range of microbial populations in a mixed culture fermentation process make it possible to use unsterilized, complex, and heterogeneous waste streams. In such a system, the conditions might not be favorable for all

populations in anaerobic microbial communities, but identifying environmental and operational factors that provide ecological advantages to key chain elongating populations is important to enhance MCCA production. This requires understanding the impact of various environmental conditions on the microbial community to develop optimal conditions to steer the production towards MCCA production. Therefore, it is critical to study microbial communities involved in the chain elongation process to successfully engineer and manage microbial communities to maximize MCCA production.

Microbial immigration is ubiquitous in engineered wastewater treatment systems (Mei and Liu, 2019). As these systems are continuously fed with non-sterile waste streams, there is a continuous influx of microbial populations present in the influent to the bioreactor. A previous study found that a significant fraction of immigrant populations was inactive but was mistakenly identified as being important when measured with DNA based sequencing method (Kirkegaard et al., 2017). Excluding inactive populations from process modeling enabled the accurate linkage of process performance with changes in the microbial community (Mei et al., 2019). The importance of immigration in chain elongation has not been studied previously. Microbial populations in an upstream system or in an external substrate/waste stream can influence the function of the chain elongation system. Furthermore, considering previous findings regarding the presence of both active and inactive immigrant populations in the downstream system, it is important to separately identify active and inactive immigrants.

One of the challenges of mixed culture fermentation using waste streams is to produce MCCAs at a sufficiently high titer and yield. Previous studies have shown that MCCA production from complex waste streams is lower than that from easily degradable synthetic substrates (Grootscholten et al., 2014, 2013; Kucek et al., 2016b, 2016c). The temporal variability in the composition of waste streams further increases the complexity. Furthermore, diverse microorganisms with broad metabolic capacity are present in mixed-culture fermentation process such as chain elongation. As a result, competitive reactions such as methanogenesis, excessive ethanol oxidation to acetate (EEO), sulfate reduction to sulfide, carboxylic acid oxidation, and the acrylate pathway (during lactate chain elongation) can co-occur and interfere with the chain

elongation process (Wu et al., 2019). For example, in ethanol driven chain elongation, EEO can lead to inefficient ethanol usage (Roghair et al., 2018). Additionally, EEO also acidifies the system requiring extra base addition thus increasing the operating cost and environmental impacts. Consequently, we need to devise strategies to minimize competitive reactions to favor MCCAs production from the waste stream.

Using waste streams for MCCA production is an attractive alternative from the environmental sustainability perspective compared to the currently used palm kernel oil or petrochemical-based routes. However, with the increasing attention received by chain elongation, it is important to understand the environmental cost and benefits of such new technologies. One promising tool to evaluate the environmental performance of emerging technologies is life cycle assessment (LCA). Such assessment, when used at the early design stages, can highlight areas of improvement for future research to maximize the environmental benefits. Thus, the application of LCA is important to direct chain elongation research and to drive technology development forward.

It is understood that integrating engineering, microbial, and modeling tools will help us improve the chain elongation process and harness the potential of mixed communities for resource recovery from different organic waste streams. This dissertation research integrates bioprocess and chemical engineering, microbial ecology, and LCA modeling, thus taking advantage of knowledge and principles from diverse fields to address the challenges and research gaps discussed above and thus advance our understanding of the chain elongation process.

1.4 Dissertation outline

The overarching goal of this dissertation is to develop and optimize the chain elongation process for efficient MCCA production from complex organic waste, specifically focused on pre-fermented food waste and waste beer. This was achieved by studying the role of immigration of microorganisms from waste streams in chain elongation, devising strategies to inhibit competitive reactions, developing a novel chain elongation bioreactor system, and assessing the environmental performance of the proposed technology.

Chapter 2 investigated the feasibility of using waste beer and pre-fermented food waste for MCCA production using an anaerobic sequencing batch reactor and studied the effect of operational factors such as solids retention time on the bioreactor performance. Furthermore, a combination of a mass balance approach to calculate the specific growth rate of microbial populations and the ratio of relative activity and relative abundance based on 16S rRNA and 16S rRNA gene sequencing (rRNA/rDNA), respectively, was used to identify active and inactive immigrants and thus study their role in chain elongation. Chapter 3 presents results obtained with the same anaerobic sequencing batch reactor and discusses the impact of competitive reactions such as EEO on the chain elongation process. Specifically, this study evaluated the effect of manipulating hydrogen partial pressure in the bioreactor through adding a methanogenic inhibitor of hydrogen consuming methanogens on EEO. The effect of the methanogenic inhibitor on both the archaeal and bacterial community was studied using amplicon sequence variant (ASV) and operational taxonomic unit (OTU) based approaches. Chapter 4 focuses on the development and operation of an anaerobic dynamic membrane bioreactor that allowed the production of a low suspended solids effluent for integration with the downstream MCCA extraction unit. This chapter further compared the microbial community in both the suspended and biofilm biomass providing insights into the role of biofilm microbial community in MCCA production. In Chapter 5, the benefits and burdens of caproic acid production from brewery waste and palm kernel oil were compared from an environmental life cycle perspective. Chapter 6 provides the overall conclusions of the dissertation, discusses the significance of the study, and presents future research directions.

1.5 References

Angenent, L.T., Richter, H., Buckel, W., Spirito, C.M., Steinbusch, K.J.J., Plugge, C.M., Strik, D.P.B.T.B., Grootscholten, T.I.M., Buisman, C.J.N., Hamelers, H.V.M., 2016. Chain Elongation with Reactor Microbiomes: Open-Culture Biotechnology to Produce Biochemicals. Environ. Sci. Technol. 50, 2796–2810. https://doi.org/10.1021/acs.est.5b04847

Anneken, D.J., Both, S., Christoph, R., Fieg, G., Steinberner, U., Westfechtel, A., 2012. Fatty acids:Ullmann's Encyclopedia of Industrial Chemistry. https://doi.org/10.1002/14356007.a10

Bagby, M.O., Johnson, R.W., Daniels, R.W., Contrell, R.R., Sauer, E.T., Keenan, M.J., Krevalis, M.A., 2004. Carboxylic Acids:Kirk-Othmer Encyclopedia of Chemical Technology, John Wiley & Sons, Inc. https://doi.org/10.1016/b978-0-12-388438-1.00008-x

Brewers Association, 2019. Statistics: Number of Breweries [WWW Document]. URL https://www.brewersassociation.org/statistics-and-data/national-beer-stats/ (accessed 5.29.20).

Carlson, K.M., Curran, L.M., Asner, G.P., Pittman, A.M., Trigg, S.N., Adeney, J.M., 2012. Carbon emissions from forest conversion by Kalimantan oil palm plantations. Nat. Clim. Chang. 3, 283–287. https://doi.org/10.1038/nclimate1702

Carvajal-Arroyo, J.M., Candry, P., Andersen, S.J., Props, R., Seviour, T., Ganigué, R., Rabaey, K., 2019. Granular fermentation enables high rate caproic acid production from solid-free thin stillage. Green Chem. 21, 1330–1339. https://doi.org/10.1039/c8gc03648a

Chen, W., Strik, D.P.B.T.B., Buisman, C.J.N., Kroeze, C., 2017. Production of Caproic Acid from Mixed Organic Waste : An Environmental Life Cycle Perspective. Environ. Sci. Technol. 51, 7159–7168. https://doi.org/10.1021/acs.est.6b06220

Chen, W.S., Ye, Y., Steinbusch, K.J.J., Strik, D.P.B.T.B., Buisman, C.J.N., 2016. Methanol as an alternative electron donor in chain elongation for butyrate and caproate formation. Biomass and Bioenergy 93, 201–208. https://doi.org/10.1016/j.biombioe.2016.07.008

Coma, M., Vilchez-Vargas, R., Roume, H., Jauregui, R., Pieper, D.H., Rabaey, K., 2016. Product Diversity Linked to Substrate Usage in Chain Elongation by Mixed-Culture Fermentation. Environ. Sci. Technol. 50, 6467–6476. https://doi.org/10.1021/acs.est.5b06021

Desbois, A.P., Smith, V.J., 2010. Antibacterial free fatty acids: Activities, mechanisms of action and biotechnological potential. Appl. Microbiol. Biotechnol. 85, 1629–1642. https://doi.org/10.1007/s00253-009-2355-3

Duber, A., Jaroszynski, L., Zagrodnik, R., Chwialkowska, J., Juzwa, W., Ciesielski, S., Oleskowicz-popiel, P., 2018. Exploiting the real wastewater potential for resource recovery – n-caproate production from acid whey. Green Chem. https://doi.org/10.1039/c8gc01759j

Esposito, M., Tse, T., Soufani, K., 2018. Introducing a Circular Economy: New Thinking with New Managerial and Policy Implications. Calif. Manage. Rev. 60, 5–19. https://doi.org/10.1177/0008125618764691

Ge, S., Usack, J.G., Spirito, C.M., Angenent, L.T., 2015. Long-Term *n* -Caproic Acid Production from Yeast-Fermentation Beer in an Anaerobic Bioreactor with Continuous Product Extraction. Environ. Sci. Technol. 49, 8012–8021. https://doi.org/10.1021/acs.est.5b00238

Grootscholten, T.I.M., Steinbusch, K.J.J., Hamelers, H.V.M., Buisman, C.J.N., 2013. Improving medium chain fatty acid productivity using chain elongation by reducing the hydraulic retention time in an upflow anaerobic filter. Bioresour. Technol. 136, 735–738. https://doi.org/10.1016/j.biortech.2013.02.114

Grootscholten, T.I.M., Strik, D.P.B.T.B., Steinbusch, K.J.J., Buisman, C.J.N., Hamelers, H.V.M.,

2014. Two-stage medium chain fatty acid (MCFA) production from municipal solid waste and ethanol. Appl. Energy 116, 223–229. https://doi.org/10.1016/j.apenergy.2013.11.061

Hanczakowska, E., 2017. The Use of Medium-Chain Fatty Acids in Piglet Feeding – A Review. Ann. Anim. Sci. 17, 967–977. https://doi.org/10.1515/aoas-2016-0099

Holtzapple, M.T., Granda, C.B., 2009. Carboxylate Platform : The MixAlco Process Part 1 : Comparison of Three Biomass Conversion Platforms. Appl. Biochem. Biotechnol. 156, 95–106. https://doi.org/10.1007/s12010-008-8466-y

Jones, C.A., Coker, C., Kirk, K., Reynolds, L., 2019. Food Waste Co-Digestion at Water Resource Recovery Facilities: Business Case Analysis.

Kaza, S., Yao, L., Bhada-Tata, P., Woerden, and F. Van, 2018. What a waste 2.0: a global snapshot of solid waste management to 2050. The World Bank.

Kehrein, P., Van Loosdrecht, M., Osseweijer, P., Garfí, M., Dewulf, J., Posada, J., 2020. A critical review of resource recovery from municipal wastewater treatment plants-market supply potentials, technologies and bottlenecks. Environ. Sci. Water Res. Technol. 6, 877–910. https://doi.org/10.1039/c9ew00905a

Kirkegaard, R.H., Mcilroy, S.J., Kristensen, J.M., Nierychlo, M., Karst, M., Dueholm, M.S., Albertsen, M., Nielsen, P.H., 2017. The impact of immigration on microbial community composition in full-scale anaerobic digesters. Sci. Rep. 1–11. https://doi.org/10.1038/s41598-017-09303-0

Kucek, L., Nguyen, M., Angenent, L.T., 2016a. Conversion of L-lactate into n-caproate by a continuously fed reactor microbiome. Water Res. 93, 163–171. https://doi.org/10.1016/j.watres.2016.02.018

Kucek, L., Spirito, C.M., Angenent, L.T., 2016b. High n-caprylate productivities and specificities from dilute ethanol and acetate: Chain elongation with microbiomes to upgrade products from syngas fermentation. Energy Environ. Sci. 9, 3482–3494. https://doi.org/10.1039/c6ee01487a

Kucek, L., Xu, J., Nguyen, M., Angenent, L.T., 2016c. Waste conversion into n-caprylate and n-caproate: resource recovery from wine lees using anaerobic reactor microbiomes and in-line extraction. Front. Microbiol. 7, 1–14. https://doi.org/10.3389/fmicb.2016.01892

Lawson, C.E., Harcombe, W.R., Hatzenpichler, R., Lindemann, S.R., Löffler, F.E., O'Malley, M.A., García Martín, H., Pfleger, B.F., Raskin, L., Venturelli, O.S., Weissbrodt, D.G., Noguera, D.R., McMahon, K.D., 2019. Common principles and best practices for engineering microbiomes. Nat. Rev. Microbiol. 17, 725–741. https://doi.org/10.1038/s41579-019-0255-9

Malinauskaite, J., Jouhara, H., Czajczyńska, D., Stanchev, P., Katsou, E., Rostkowski, P., Thorne, R.J., Colón, J., Ponsá, S., Al-Mansour, F., Anguilano, L., Krzyżyńska, R., López, I.C.,

A.Vlasopoulos, Spencer, N., 2017. Municipal solid waste management and waste-to-energy in the context of a circular economy and energy recycling in Europe. Energy 141, 2013–2044. https://doi.org/10.1016/j.energy.2017.11.128

Mei, R., Kim, J., Wilson, F.P., Bocher, B.T.W., Liu, W.T., 2019. Coupling growth kinetics modeling with machine learning reveals microbial immigration impacts and identifies key environmental parameters in a biological wastewater treatment process. Microbiome 7, 1–9. https://doi.org/10.1186/s40168-019-0682-x

Mei, R., Liu, W.T., 2019. Quantifying the contribution of microbial immigration in engineered water systems. Microbiome 7, 1–8. https://doi.org/10.1186/s40168-019-0760-0

Nzeteu, C.O., Trego, A.C., Abram, F., O'Flaherty, V., 2018. Reproducible, high-yielding, biological caproate production from food waste using a single-phase anaerobic reactor system. Biotechnol. Biofuels 11, 108. https://doi.org/10.1186/s13068-018-1101-4

Petrenko, C., Paltseva, J., Searle, S., 2016. Ecological Impacts of Palm Oil Expansion in Indonesia. Washingt. Int. Counc. Clean Transp.

Puyol, D., Batstone, D.J., Hülsen, T., Astals, S., Peces, M., Krömer, J.O., 2017. Resource recovery from wastewater by biological technologies: Opportunities, challenges, and prospects. Front. Microbiol. 7, 1–23. https://doi.org/10.3389/fmicb.2016.02106

Roghair, M., Hoogstad, T., Strik, D.P.B.T.B., Plugge, C.M., Timmers, P.H.A., Weusthuis, R.A., Bruins, M.E., Buisman, C.J.N., 2018. Controlling Ethanol Use in Chain Elongation by CO2 Loading Rate. Environ. Sci. Technol. https://doi.org/10.1021/acs.est.7b04904

Scalschi, L., Vicedo, B., Camañes, G., Fernandez-Crespo, E., Lapeña, L., González-Bosch, C., García-Agustín, P., 2013. Hexanoic acid is a resistance inducer that protects tomato plants against Pseudomonas syringae by priming the jasmonic acid and salicylic acid pathways. Mol. Plant Pathol. 14, 342–355. https://doi.org/10.1111/mpp.12010

Schroeder, P., Anggraeni, K., Weber, U., 2019. The Relevance of Circular Economy Practices to the Sustainable Development Goals. J. Ind. Ecol. 23, 77–95. https://doi.org/10.1111/jiec.12732

Seluy, L.G., Isla, M.A., 2014. A Process To Treat High-Strength Brewery Wastewater via Ethanol Recovery and Vinasse Fermentation. Ind. Eng. Chem. Res. 53, 17043–17050. https://doi.org/10.1021/ie500438j

Takeuchi, H., Sekine, S., Kojima, K., Aoyama, T., 2008. The application of medium-chain fatty acids: Edible oil with a suppressing effect on body fat accumulation. Asia Pac. J. Clin. Nutr. 17, 320–323. https://doi.org/10.6133/apjcn.2008.17.s1.79

U.S.EPA, 2013. Energy Efficiency in Water and Wastewater Facilities, U.S. Environmental Protection Agency.

Urban, C., Xu Jiajie, Strauber Heik, Dantas Tatiane R. dos Santos, Muhlenberg Jana, Hartig Claus, Angenent Largus T. and, Harnisch Falk, 2017. Production of drop-in fuels from biomass at high selectivity by combined microbial and electrochemical conversion. Energy Environ. Sci. 10, 2231–2244. https://doi.org/10.1039/c7ee01303e

Wu, Q., Bao, X., Guo, W., Wang, B., Li, Y., Luo, H., Wang, H., Ren, N., 2019. Medium chain carboxylic acids production from waste biomass: Current advances and perspectives. Biotechnol. Adv. 37, 599–615. https://doi.org/10.1016/j.biotechadv.2019.03.003

Zhu, X., Tao, Y., Liang, C., Li, X., Wei, N., Zhang, W., Zhou, Y., Yang, Y., Bo, T., 2015. The synthesis of n-caproate from lactate: a new efficient process for medium-chain carboxylates production. Sci. Rep. 5, 14360. https://doi.org/10.1038/srep14360

Zion Market Research, 2018. Medium Chain Triglycerides Market (Caproic Acid, Caprylic Acid, Capric Acid, Lauric Acid, Heptanoic Acid and Nonanoic Acid) for Medical, Food, and Other Applications: Global Industry Perspective, Comprehensive Analysis, and Forecast, 2016 – 2022.

Chapter 2

Resource Recovery of Medium Chain Carboxylic Acid from Brewery and Pre-fermented Food Waste Streams: Effect of Microbial Immigration on Chain Elongation

Shilva Shrestha[1], Brittany Colcord[2], Xavier Fonoll[3], Lutgarde Raskin[1]*

[1]Department of Civil and Environmental Engineering, University of Michigan, Ann Arbor, MI 48109, USA

[2]Chevron Corporation, Midland, Texas 79706, USA

[3]Great Lakes Water Authority, Detroit, MI 48226, USA

2.1 Abstract

Chain elongation is an emerging biotechnology for medium chain carboxylic acids (MCCAs) production from diverse waste streams. Organic waste streams such as food and brewery waste were upgraded to MCCAs using mixed-culture microbial communities. A maximum MCCAs volumetric production rate of 9.1 mmole L^{-1} d^{-1} was achieved over a period of 229 days with caproate as the major MCCAs. MCCAs toxicity induced at acidic pH limited MCCAs production. Microbial populations belonging to the *Clostridiales* order and *Pseudoramibacter* genus were dominant and found to be positively correlated to MCCAs production. Furthermore, the impact of microbial immigration on the chain elongation bioreactor was investigated using time-series 16S rRNA gene (rDNA) and 16S rRNA sequencing data. The microbial memberships in the influent

and the bioreactor were similar, but the microbial community structures differed. The ratio of relative activity and relative abundance (rRNA/rDNA) was used to identify active immigrant populations. Some of the most dominant microbial populations in the influent such as *Prevotella* were present at lower activity (low rRNA/rDNA ratio) in the bioreactor. On the other hand, chain elongating microbial groups such as *Clostridiales* order and *Pseudoramibacter* were enriched in the bioreactor even though they were present at low relative abundances and activities in the influent. Since, the rRNA/rDNA did not provide accurate representation for all microbial populations, a mass balance-based approach was used to calculate specific growth rates to differentiate between active populations that contributed to chain elongation and the inactive immigrant populations. Ultimately, identifying active and inactive immigrant populations will enable accurate linkage of process performance with microbial community during process modeling.

2.2 Introduction

Global municipal solid waste generation is expected to increase by 22% from 2.01 to 2.59 billion tons per year from 2016 to 2050, with a concurrent increase in waste management costs and human and environmental health impacts (Kaza et al., 2018). To address this concern, several efforts to divert waste from landfills and reduce anthropogenic methane emissions have been and will continue to be implemented in different parts of the world (Jones et al., 2019; Malinauskaite et al., 2017). Low-cost technologies that can valorize readily available and biodegradable organic waste streams to recover high-value products are urgently needed. Chain elongation of short chain carboxylic acids (SCCAs) using mixed microbial communities for production of medium chain carboxylic acids (MCCAs) from waste streams provides an opportunity to contribute to this need. MCCAs, saturated fatty acids with chain lengths from six to twelve carbons including one carboxyl group, are platform chemicals that are used as livestock feed additives, antimicrobials, commodity chemicals for the manufacturing of pharmaceuticals, fragrances, lubricants, rubbers, and dyes, and liquid biofuels (Angenent et al., 2016; Urban et al., 2017). They are currently produced from plant based oils with considerable environmental impacts (Anneken et al., 2012; Carlson et al., 2012; Petrenko et al., 2016).

Chain elongation involves oxidation of electron donors, such as ethanol, which also serve as a source of carbon, reducing equivalents (NADH), and energy (ATP) in chain elongation. Ethanol chain elongation includes ethanol oxidation to acetyl-CoA and chain elongation of SCCAs via reverse β oxidation (Angenent et al., 2016; Wu et al., 2019). SCCAs and electron donors required for MCCA production can be added from an exogenous source, may be present in the substrate, or can be produced *in situ* as an intermediate during fermentation. Several chain elongation studies have used crude ethanol to mediate chain elongation (Grootscholten et al., 2013a, 2013b, 2013c, 2014; Kucek et al., 2016b; Roghair et al., 2018), while others have utilized waste ethanol such as yeast fermentation beer (Agler et al., 2012; Ge et al., 2015; Urban et al., 2017; Xu et al., 2015), wine lees (Kucek et al., 2016c), and syngas effluent (Gildemyn et al., 2017). Upgrading ethanol-containing brewery waste into MCCAs may be a promising option, given that the increasing number of breweries (Brewers Association, 2019; The Brewers of Europe, 2017) has brought new challenges related to infrastructure and waste management (Brewers Association, 2017a, 2017b). There are considerable opportunities to diversify brewery waste treatment practices and recover resources from the various organic-rich waste streams generated in breweries. Deriving ethanol from brewery waste would not only eliminate the cost and environmental impact of using crude ethanol in chain elongation (Chen et al., 2017), but would also be beneficial for brewery waste treatment.

The efficiency and stability of microbially-mediated processes such as chain elongation depend on the concerted and syntrophic activity of functionally diverse microbial populations. Most chain elongation studies that have used heterogeneous waste streams have focused on studying the bioreactor microbiome only (Andersen et al., 2017; Kucek et al., 2016c; Scarborough et al., 2018). However, when waste streams are used as substrate, microorganisms continuously enter the chain elongation bioreactor as waste streams contain their own microbial communities. Since we rely on optimizing bioreactor conditions to provide ecological advantages to key microorganisms and metabolic pathways, understanding the contributions of the waste stream microbiome is important to optimize process performance (Frigon and Wells, 2019; Mei et al., 2019). The effect of the influent microbiome on the bioreactor microbiome and its function has been studied for anaerobic digesters and activated sludge systems (Kirkegaard et al., 2017; Mei et al., 2019, 2017, 2016; Shin

et al., 2019). These studies identified that a large fraction of the microbial populations originating from the influent were inactive in the downstream system and removing the inactive immigrant populations from the data analysis enabled better prediction of operating parameters that influence process performance. Thus, it is important to identify the microbial immigrants that maintain activity and affect process performance and stability. So far, chain elongation studies have overlooked the impact of these feed associated microbial populations.

Most chain elongation studies have used 16S ribosomal (rRNA) gene sequencing to gain insights into the microbial community governing chain elongation systems (Agler et al., 2012; Andersen et al., 2017, 2015; Gildemyn et al., 2017; Khor et al., 2017; Kucek et al., 2016a, 2016c, 2016b; Liu et al., 2017; Xu et al., 2018). However, this DNA-based technique also targets 16S rRNA genes associated with inactive cells as well as extracellular DNA leading to over-estimation of active cells (Li et al., 2017). The half-life of RNA is much shorter than that of DNA and monitoring the abundance of 16S rRNA of specific microbial populations can be used to infer the overall activity of these populations (Klappenbach et al., 2000), as long as the well-described limitations of this approach are acknowledged (Blazewicz et al., 2013; Poretsky et al., 2014; Větrovský and Baldrian, 2013). Considering the slow decay of DNA and the continuous introduction of dead and inactive cells, in addition to active cells, to the downstream system, it is challenging to characterize microbial immigration only with DNA based methods. Therefore, we used a combination of 16S rRNA and 16S rRNA gene sequencing in this study to compare trends over time and gain insights in microbial immigration.

In this study, we demonstrated that ethanol-rich waste beer and pre-fermented food waste can be used for MCCAs production without exogenous ethanol addition. In addition, we characterized the chain elongating microbial community and investigated the effect of operating parameters on bioreactor performance and its microbial community. Lastly, we studied the role of microbial immigration during chain elongation by calculating the specific growth rate of individual populations to distinguish the inactive immigrant populations from the active ones.

2.3 Materials & Methods

2.3.1 Inoculum and Substrate

The bioreactor was inoculated with rumen content (17.1 ± 1.0 volatile solids (VS) L^{-1}) on the same day it was collected from the rumen of a fistulated cow from a dairy farm at Michigan State University (East Lansing, MI, USA). 5 L of rumen content was added to the bioreactor, which was allowed to degasify for 48 h before starting to feed the bioreactor. On Day 178, 2.5 L of fresh rumen content was added to the bioreactor after an accidental loss of biomass due to a pump error. The bioreactor was fed once a day with a mixture of waste beer and permeate containing high levels (62.1 ± 11.0 mM) of SCCAs produced by an acidogenic bioreactor treating food waste. The chemical characteristics of the inoculum, waste beer, and permeate are summarized in Table A1, Appendix A. Waste beer is a waste stream produced as a result of faulty bottling, development of off-flavors, improper fermentation, improper storage, or beer returned from the market because it is close to or beyond its expiration date (Seluy and Isla, 2014). Three batches of waste beer were collected at different times from Jolly Pumpkin Brewery (Dexter, MI), which produces waste beer at a rate of 2 to 19% of their volumetric beer production (Doug Knox, personal communication). The acidogenic food waste bioreactor was inoculated with rumen content and operated to enhance SCCAs production. Permeate was collected once per week from the acidogenic bioreactor for weekly influent preparation. The SCCAs and ethanol present in permeate and waste beer were considered to determine the ratio of both substrates. The amount of ethanol required for chain elongation of SCCAs was calculated according to the chain elongation stoichiometric equations(Angenent et al., 2016) (4:1 for ethanol:acetate, 2.4:1 for ethanol:propionate, 1.2:1 ethanol:butyrate, and 1.2:1 ethanol:valerate) given in Table A2, Appendix A except during the first three weeks when the ethanol:acetate ratio in the influent was 9:1.

2.3.2 Experimental setup

A 7-L semi-continuous anaerobic sequencing batch reactor (ASBR) with a working volume of 5 L was operated on a 24-h cycle consisting of four steps: i) feeding (8-10 min), ii) continuous mixing and pH adjustment (22 h 40 min), iii) settling (1 h), and iv) decanting for withdrawal of effluent equal to the volume of the influent (8-10 min). The ASBR was controlled remotely by

LabVIEW (National Instruments, Austin, TX) data acquisition software. The bioreactor headspace was connected to a 5-L Tedlar gas bag. The bioreactor was equipped with a water jacket connected to a recirculating bath (Polyscience, Niles, IL, USA) for temperature control and was operated at 40^{o}C until Day 73 and at 37^{o}C for the remainder of the time. The temperature was decreased to 37^{o}C to be closer to the optimal growth temperature of several chain elongating species, such as *Clostridium kluyveri*, *Clostridium* sp. BS-1, *Eubacterium pyruvativorans*, *Eubacterium limosum*, and *Megasphaera elsdenii* (Angenent et al., 2016; Jeon et al., 2010; Weimer and Stevenson, 2012). The bioreactor pH was maintained at slightly acidic conditions (pH 5.5±0.1) to minimize methanogenesis through automatic addition of 3 M NaOH using LabVIEW during the well-mixed react phase. The bioreactor was operated at a hydraulic retention time (HRT) of 2-4 days and an organic loading rate (OLR) of 4.5-34.6 g soluble chemical oxygen demand (sCOD) L^{-1} d^{-1} (Figure A.1, Appendix A). The solids retention time (SRT) was controlled from Days 20-81 by wasting both suspended biomass from the bioreactor (before the settling period) and effluent after the decant phase. Starting from Day 82, the suspended biomass was wasted only once a week to collect biomass samples for microbial analyses. The volatile suspended solids (VSS) concentration in both suspended biomass and effluent were considered for SRT calculation.

In this study, the undissociated carboxylic acid and the corresponding dissociated carboxylate are together referred to as carboxylate. Furthermore, the terms MCCAs and SCCAs, respectively, refer to the sum of caproate (C6), enanthate (C7), and caprylate (C8) and the sum of acetate (C2), propionate (C3), n-butyrate (C4), and n-valerate (C5); the iso-butyrate and iso-valerate were excluded unless stated explicitly. The SCCAs and MCCAs results reported in this study are expressed on a molar basis and are net values calculated after subtracting the concentration of the respective compound in the influent from the gross values. The volumetric production rate (mmole L^{-1} d^{-1}) was determined by dividing the bioreactor effluent concentrations (mmole L^{-1}) with corresponding HRT (d, working volume (L) divided by effluent flow rate (L d^{-1})). The product yield was calculated by dividing soluble oxygen demand (sCOD) of MCCAs produced in the bioreactor by fermentable influent sCOD. The fraction of sCOD contributed by MCCAs already present in the influent was deducted from the fermentable influent sCOD used for the MCCAs yield calculation.

2.3.3 Chemical analyses

We collected samples for various chemical analyses. Inoculum samples were collected at the time of inoculation (Day 0 and Day 178), influent and bioreactor content were sampled once a week, and effluent was collected two to three times a week. Total solids (TS) and VS, total suspended solids (TSS), and VSS analyses were determined as per the procedures outlined in Standard Methods (Eugene et al., 2012). The COD (after filtration with 0.45-µm nylon membrane filters (TISCH Scientific, North Bend, OH, USA)) analysis was performed using Lovibond^{TM} medium-range (0-1500 mg L^{-1}) COD digestion vials (Tintometer, Germany). Gas volume was measured every day with a gas-tight glass syringe, while gas composition (H_2, CO_2, and CH_4) was determined two to three times a week using a Gow-Mac Series gas chromatography (Bethlehem, PA, USA) equipped with a thermal conductivity detector (TCD). The temperature of the column, injector, and detector were set to 104^{o}C, 80^{o}C, and 115^{o}C, respectively, and the current to the TCD was set at 120 mA. Hydrogen was used as the carrier gas to measure nitrogen and methane, while nitrogen was used as the carrier gas for hydrogen measurement. Standard gas samples (ShopCross, Greensboro NC, USA) consisting of varying mixtures of methane, carbon dioxide, and hydrogen were used to calibrate the instrument.

Concentrations of carboxylic acids from C2 to C8, including iso-forms of C4 and C5, and ethanol were determined using an Agilent Technologies 7890B gas chromatograph (Santa Clara, CA) equipped with a stabilwax-DA column (Restex) and a flame ionization detector. The oven temperature was held at 55^{o}C for 1 min, then increased to 205^{o}C at 10^{o}C min^{-1}, and held at 205^{o}C for 8 min. Injector and detector temperatures were set to 250^{o}C and 300^{o}C, respectively, and nitrogen was used as the carrier gas. Prior to injection, the samples were acidified with phosphoric acid, centrifuged, and filtered through 0.45-µm nylon membrane filters (TISCH Scientific, North Bend, OH, USA).

2.3.4 Microbial analyses

Biomass samples were collected from the inoculum and bad beer upon starting the bioreactor and from bioreactor influent and effluent periodically (see Table A3, Appendix A for specific days of biomass sampling). The samples were immediately pelletized by centrifuging at 10,000 x *g* for 10

min, flash-frozen on dry ice, and stored at -80^{o}C until DNA and RNA extractions were performed. DNA was extracted using a CTAB method described by Porebski et al. (1997) with an additional bead-beating step (Mini-Beadbeater-96, BioSpec Products, Bartlesville, OK, USA) for 1.5 min using 0.1-mm diameter zirconium beads. Total RNA was extracted using TRIzol (Invitrogen, CA, USA) following the manufacturer's instructions with some modifications. In the lysis step, 1.5 min bead-beating with 0.1-mm diameter zirconium beads was included for mechanical cell lysis after adding TRIzol reagent to the samples. The RNA precipitation step was slightly modified to include 2.6 M sodium acetate in addition to ice-cold absolute ethanol. Glycoblue was added to visualize the RNA pellets and the RNA samples were stored at -20^{o}C for 24-48 h followed by ethanol washing and resuspension in water. ezDNase (Thermo Scientific, MA, USA) was used to remove residual DNA from RNA extracts following the manufacturer's guidelines. The efficiency of DNA removal was tested by quantifying the abundance of bacterial 16S rRNA genes using bacterial primers(Fierer et al., 2005) by qPCR. A SuperScript® IV VILO cDNA synthesis kit (Invitrogen, Carlsbad, CA) was used to convert RNA into single-stranded complementary DNA (cDNA) according to the manufacturer's instructions. DNA and RNA quantities were determined using a Qubit 2.0 Fluorometer (Invitrogen, Life Technologies, CA, USA).

cDNA and DNA samples were submitted to the Microbial Systems Molecular Biology Laboratory (University of Michigan, Ann Arbor, MI, USA) for 16S rRNA and 16S rRNA gene sequencing, respectively, on the Illumina MiSeq platform (San Diego, CA, USA). Primers F515 and R806(Caporaso et al., 2011) targeting the V4 region of the 16S rRNA gene were modified for dual-index sequencing as described by Kozich et al.(Kozich et al., 2013) A total of 1,636,675 high-quality reads were generated. The sequences were processed using the mothur platform (version 1.42.0) following the MiSeq SOP.(Schloss et al., 2009) The reference SILVA database implemented in mothur was customized to align with the filtered sequences. UCHIME algorithm was used for chimera removal. The Ribosomal Database Project (Version 16) was used for taxonomic classification of sequences to the genus level and sequences were grouped into operational taxonomic units (OTUs) based on the average neighbor algorithm at 3% sequence divergence cutoff. Good's coverage was estimated for each sample (Table A4, Appendix A). OTUs that could not be classified at the genus level were denoted as "unclassified_family name".

16S rRNA gene and 16S rRNA sequencing data were used to study the total and active microbial community, respectively. Singletons were removed for relative abundance and relative activity calculations. The dominant OTUs or genera were defined as OTUs or genera present at a relative abundance or relative activity ≥ 1% in at least 50% of the samples. The ratios of relative abundances ($rDNA_{influent}/rDNA_{reactor}$) and relative activities ($rRNA_{influent}/rRNA_{reactor}$) of different taxa were compared at the genus level in the influent and corresponding bioreactor samples. Furthermore, as an indirect measure of activity, the ratios of relative activity (rRNA) and relative abundance (rDNA) for each genus observed in the bioreactor ($rRNA/rDNA_{reactor}$) and the influent samples ($rRNA/rDNA_{influent}$) were calculated. Genera with increasing rRNA/rDNA ratios are assumed to be active as their ribosome abundance increases more than their genome copy number.(Mueller et al., 2016) The ratios of $[rRNA/rDNA]_{reactor}$:$[rRNA/rDNA]_{influent}$ were used to compare the activities of the different genera in the bioreactor with those in the influent. Lastly, a mass balance approach similar to the one used by Mei et al. (2016) was used to calculate the specific growth rate (μ) for genera observed in both influent and bioreactor samples to study microbial immigration (detailed calculation is given in SI). The specific growth rates were calculated using amount of DNA/RNA recovered from the cell (Method I) and with VSS as an indirect measure of cell concentration (Method II). Representative sequences obtained from mothur, for dominant bacterial OTUs observed in the bioreactor, were used for phylogenetic analysis. The closest relatives of the dominant OTUs were determined using a BLAST analysis and chosen as reference sequences. The 16S rRNA gene sequences of the reference sequences were downloaded from NCBI GenBank Database. MEGA7 (Kumar et al., 2016) was used to align and trim the sequences and compute the evolutionary distances using maximum likelihood analysis.

2.3.5 Statistical analyses

All statistical analyses of microbial community data were performed using R (version 3.6.1) with packages vegan (version 2.5-6) (Oksanen et al., 2019), phyloseq (version 1.30.0) (McMurdie and Holmes, 2013), dplyr (version 0.8.5) (Wickham et al., 2015), and ggplot2 (version 3.3.0) (Wickham et al., 2016). Statistical significance was set at $\alpha \leq 0.05$. Kruskal-Wallis rank sum test

with Benjamini-Hochberg correction for multiple testing (non-parametric one-way ANOVA) was used to test the statistical significance of the difference between groups and conditions for bioreactor performance data. The Pearson correlation coefficient was calculated using the cor.test function in R. Alpha-diversity indices such as observed OTUs for richness, Shannon index, and Pielou's evenness were calculated using the vegan package to compare DNA and RNA community profiles. Beta-diversity analyses included nonmetric multidimensional scaling (NMDS) using the Jaccard (using the binary=TRUE option, community membership-based) and Bray-Curtis (community structure-based) dissimilarity matrices. The statistical difference in microbial community structure and membership among and between the influent and bioreactor samples were tested with analysis of similarities (ANOSIM). The higher the ANOSIM R value, the more dissimilar the groups are. A linear regression model was fitted with MCCAs volumetric production rate (log transformed) as the response variable and HRT, SRT, temperature, and operational days as the explanatory variables. A sinusoidal term was fitted to the "operational days" term in the model to investigate whether the MCCAs production followed a cyclical behavior.

2.4 Results and Discussion

2.4.1 MCCAs recovery from brewery and pre-fermented food waste streams

SCCAs-rich permeate derived from a food waste fermentation process and ethanol containing waste beer were used to produce MCCAs in a chain-elongation ASBR system operated for 229 days. Production of MCCAs, including caproate, enanthate, and octanoate, began within a few days of bioreactor startup as shown in Figure 2.1.

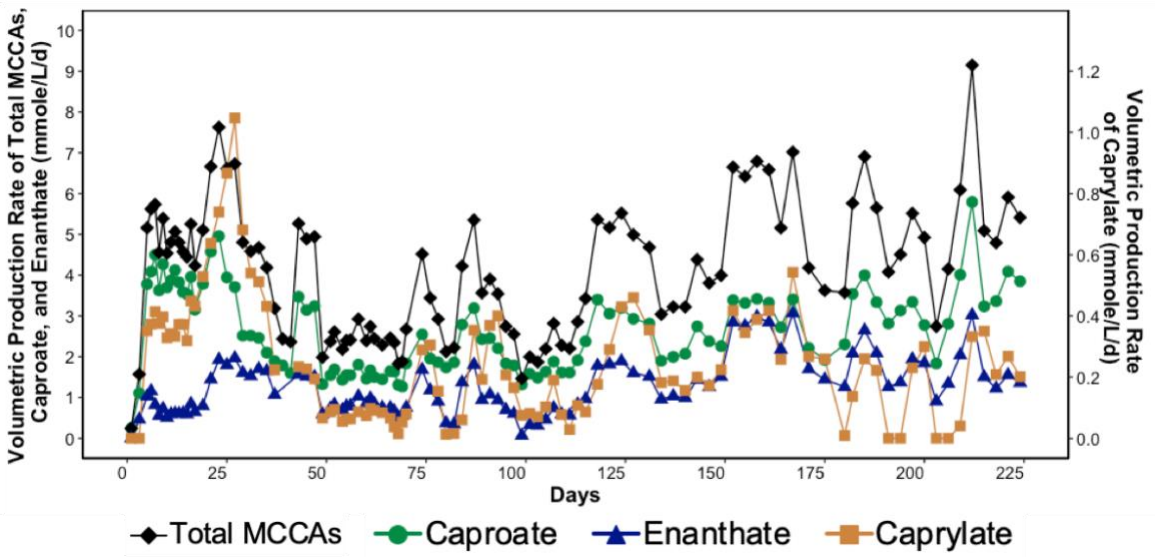

Figure 2.1 Volumetric production rate of total MCCAs, caproate, enanthate, and caprylate in the bioreactor over time. The MCCAs volumetric production rate varied cyclically as indicated by a linear regression model (R^2=0.6 with significant sine term, p=8.9E-05).

The MCCAs volumetric production rate was high in the first four weeks of operation with caprylate reaching a maximum rate of 1.05 mmole L^{-1} d^{-1} on Day 27 (Figure 2.1). The corresponding caprylate to caproate product ratio was 0.4 (on a carbon basis), the highest achieved in this study. The MCCAs volumetric production rate then decreased possibly due to inhibition by undissociated MCCAs and high ethanol concentration. The ethanol concentration in the influent was kept high (73.6 ± 12.9% of the total sCOD) initially to promote MCCAs production since previous studies have shown that higher ethanol loading promotes MCCA production.(Angenent et al., 2016; Kucek et al., 2016b) While ethanol has been shown to be toxic to *C. kluyveri* when in excess of 200-400 mM (Angenent et al., 2016), the ethanol toxicity threshold for an adapted chain elongating microbiome has not been determined. An ethanol concentration in the range of 194.4-602.2 mM was maintained in our bioreactor until Day 27. Since 30.5 ± 7.2% of the ethanol fed was not consumed, the ethanol concentration in the influent was decreased (Figure A.1, Appendix A).

The average MCCAs volumetric production rate was 4.1 ± 1.6 mmole L^{-1} d^{-1} with a maximum of 9.1 mmole L^{-1} d^{-1} observed on Day 212 (Figure 2.1) when 27% of sCOD in the influent was converted to MCCAs. Caproate was the major MCCAs produced comprising on average 62.3 ± 9.8% of the total MCCAs, while enanthate and caprylate constituted 31.2 ± 9.4% and 6.5 ± 4.1% of the total MCCAs produced on a carbon basis, respectively. The maximum MCCAs yield and the MCCAs volumetric production rate (14.5-29.2 mmole L^{-1} d^{-1}) achieved in our study were lower compared to other chain elongation studies that used complex organic waste streams containing ethanol, but they used in-line extraction systems to continuously remove produced MCCAs (Ge et al., 2015; Kucek et al., 2016c; Urban et al., 2017). Roghair et al. (2018) achieved a maximum caproate volumetric production rate of 47.3 mmole L^{-1} d^{-1} in a two-stage system treating food waste and crude ethanol and avoided MCCAs toxicity without an in-line extraction process by maintaining a neutral pH. Furthermore, in our study, most of the sCOD in the influent, including ethanol, was converted into SCCAs, particularly acetate, which was not further elongated into MCCAs despite the availability of sufficient ethanol. Excessive ethanol oxidation to acetate, a competing reaction that took place in the system, is discussed in more detail in Chapter 3.

As indicated above, chain elongation can be a self-limiting process due to the inhibitory effect of MCCAs (Angenent et al., 2016; Ge et al., 2015). A pH of 5.5 was maintained in the bioreactor to minimize methanogenesis, but since this pH value was only slightly above the pKa values of MCCAs (4.8-4.9), a considerable fraction of the MCCAs were present in their undissociated forms. The undissociated forms are more hydrophobic than their corresponding conjugate bases and can diffuse through the membranes of microbial cells decreasing the intracellular pH. The MCCAs volumetric production rate varied cyclically (Figure 2.1). This suggests that MCCAs accumulated to a level inhibitory to chain elongating microorganisms, after which the production decreased, allowing the microbiome to recover. It was calculated that a maximum concentration of undissociated caprylic acid of 0.4 mM occurred on Day 27 after which the MCCAs production decreased drastically suggesting inhibition. Furthermore, the maximum undissociated caproic acid concentration occurred on Day 212 when its concentration was calculated to reach 3.2 mM. The literature reports higher inhibitory concentrations for undissociated caprylic acid and caproic acid. The undissociated caprylic acid was reported to be inhibitory at 0.6 mM at pH 5.2 (Kucek et al.,

2016b), whereas undissociated caproic acid was shown to be inhibitory at concentrations above 7.5 mM at pH 5.5 (Ge et al., 2015). The undissociated MCCAs concentrations in these studies were kept below their inhibitory levels by continuous removal of MCCAs using an in-line extraction unit. The inhibitory MCCA concentrations observed in our study are lower than those reported by other studies as the concentration at which product toxicity occurs depends on the type of bioreactor system (for example, continuous MCCAs removal by in-line extraction unit increases MCCAs production providing selective pressure to the microbiome and thus increasing the inhibition threshold), the undissociated concentration of other carboxylic acids, and the microbial community.

2.4.2 MCCAs production correlated with *Clostridiales* and *Pseudoramibacter* activity

Based on the 16S rRNA gene sequencing data, the dominant OTUs in the bioreactor belonged to *Acidaminococcus*, unclassified *Bacteria, Bifidobacterium,* unclassified *Clostridiales*, unclassified *Erysipelotrichaceae,* unclassified *Lachnospiraceae, Megasphaera, Methanobrevibacter*, *Olsenella*, *Prevotella*, and *Succiniclasticum* (Figure 2.2 andFigure A.2, Appendix A). While the dominant active OTUs, determined by 16S rRNA sequencing, belonged to *Acidaminococcus*, *Bifidobacterium,* unclassified *Clostridiales*, unclassified *Lachnospiraceae*, *Megasphaera*, *Methanobrevibacter*, *Olsenella*, *Prevotella*, and *Pseudoramibacter* (Figure 2.2 andFigure A.2, Appendix A).

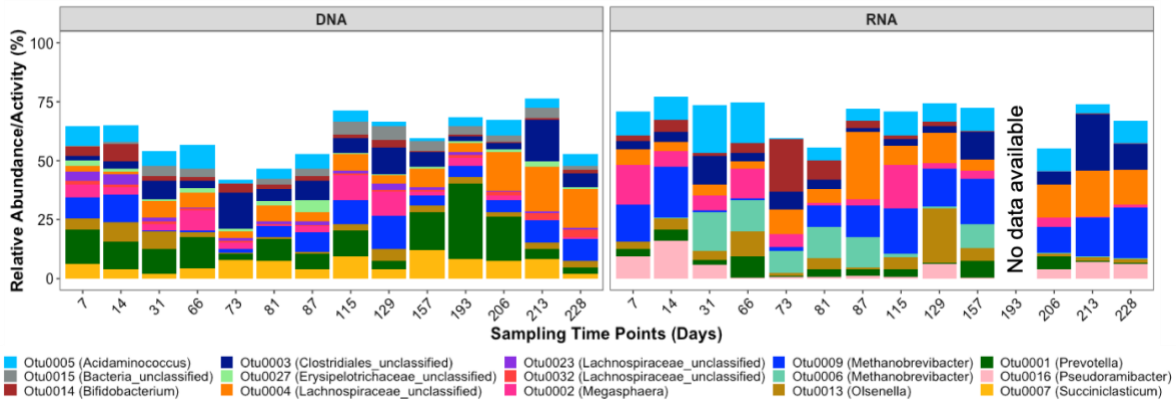

Figure 2.2. Dominant OTUs observed at a relative abundance and activity greater than 1% in at least 50% of the samples (n=14 in DNA and n=13 in RNA group) in the bioreactor samples over time.

The order *Clostridiales* averaged 24.3 ± 8.2% and 26.8 ± 11.9% of the total and active microbial community, respectively, and was comprised of 31 genera, among which *Pseudoramibacter*, unclassified *Lachnospiraceae*, and some unclassified *Clostridiales* were enriched in the bioreactor. Populations within the order *Clostridiales*, especially *C. kluyveri*, have frequently been identified in ethanol chain elongation studies (Agler et al., 2012; Esquivel-elizondo et al., 2018; Kucek et al., 2016c; Wu et al., 2020). Unclassified *Clostridiales* exhibited high relative abundance and relative activity of 8.3 ± 5.1% and 8.0 ± 6.1%, respectively. The dominant *Clostridiales* OTU (OTU 3) clustered with *E. pyruvativorans* (Figure A.3, Appendix A), which has been shown to produce valerate and caproate (Wallace et al., 2003). The relative abundance (correlation coefficient=0.54, p=0.05) and activity (correlation coefficient=0.71, p=0.01) of *Clostridiales* OTU 3 significantly correlated with MCCAs volumetric production rate. It should be made clear that a positive correlation does not imply causation and is just a metric to evaluate the association.

The volumetric production rate of even chained MCCAs (caproate and caprylate) was positively correlated with the relative activity (correlation coefficient=0.55, p=0.05) of *Pseudoramibacter* OTU 16 but it did not correlate significantly with the relative abundance (correlation coefficient=0.35, p=0.22). *Pseudoramibacter* genus had an average rRNA/rDNA ratio of 4.62 ±

3.03 (Table A5, Appendix A), indicating its higher activity in the bioreactor. OTU 16, the most abundant *Pseudoramibacter* OTU (Figure 2.2), was phylogenetically closest to *Pseudoramibacter alactolyticus* (Figure A.3, Appendix A). *P. alactolyticus* has been shown to produce both SCCAs and MCCAs as end products of glucose and sucrose fermentations (Willems and Collins, 1996). It has been previously associated with MCCAs production from lactate in other mixed culture studies (Scarborough et al., 2018; Yang et al., 2018), but its ability to use ethanol for MCCAs production has not been described yet.

Pseudoramibacter was most active in the first month of operation after which its relative activity decreased from 5.9% on Day 31 to 0.22% on Day 66 before increasing again starting from Day 206 (Figure 2.2 andFigure A.2, Appendix A). This decrease in relative activity aligns with the highest caprylate production of 1.05 mmole L^{-1} d^{-1} on Day 27. It is possible that the high caprylate concentration inhibited chain elongating microorganisms and the increase in relative activity afterwards might indicate slow adaptation and reduced product toxicity. The increase in relative abundance and activity of both *Pseudoramibacter* and unclassified *Clostridiales* in the later days also aligns with the maximum volumetric production rate of 9.1 mmole L^{-1} d^{-1} observed on Day 212. The relative activity of *Pseudoramibacter* and unclassified *Clostridiales* increased from 3.8% to 7.2% and 5.5% to 24.1%, respectively, from Day 206 to 213. Besides MCCAs producers, OTUs belonging to *Acidaminococcus* (Rogosa, 1969), *Lachnospiraceae* (Cotta and Forster, 2006), *Megasphaera* (Weimer and Moen, 2013), *Succiniclasticum* (Van Gylswyk, 1995), and *Prevotella* (Emerson and Weimer, 2017), which are generally functionally associated with acidogenesis, were also enriched in the bioreactor (Figure 2.2 andFigure A.2, Appendix A).

2.4.3 Effect of pH and SRT on methanogens

Aceticlastic methanogens can compete with chain elongating microorganisms for acetate, the precursor for MCCAs, while hydrogenotrophic methanogens can affect hydrogen partial pressure and thus the thermodynamics of chain elongation or competitive pathways such as excessive ethanol oxidation to acetate (Wu et al., 2019). Despite maintaining the pH at 5.5 to inhibit methanogenesis, 21.4 ± 5.0% of the active microbial community was comprised of *Euryarchaeota*, the phylum of archaea that contains methanogens. Specifically, hydrogenotrophic methanogens

such as *Methanobrevibacter* and *Methanosphaera* were abundant, while aceticlastic methanogens were not observed (Figure A.4, Appendix A). Thus, aceticlastic methanogens were inhibited by the low bioreactor pH of 5.5, whereas hydrogenotrophic methanogens were not. *Methanobrevibacter* was the most abundant and active methanogen, representing 9.4 ± 3.2% and 19.1 ± 5.6% of the total and active community, respectively (Figure A.4, Appendix A). Even though hydrogenotrophic methanogens were active and abundant, methane levels remained low. On average, 7.4 ± 2.4% of influent COD was used for methane production (Figure A.5, Appendix A).

Decreasing the SRT could be an additional control strategy to suppress methanogenesis. It allows bioreactor operation at neutral pH and thus avoids product toxicity due to high concentrations of undissociated MCCAs under acidic condition. From Days 20-81, a low SRT of 9.7 ± 5.8 days was maintained (Figure A.5, Appendix A), whereas a higher SRT averaging 20.1 ± 13.9 days was maintained from Days 82-229 days. On the OTU level, *Methanobrevibacter* OTU 9 was dominant until Day 14 (Figure A.4, Appendix A). As the SRT was lowered, *Methanobrevibacter* OTU 6 appeared, indicating that OTU 6 had a higher growth rate and was retained during operation with shorter SRT. *Methanobrevibacter* OTU 9 slowly started rising again after the SRT was increased. There was no significant difference in methane production at different SRTs (Figure A.5, Appendix A).

Methanogens have lower growth rates than chain elongating microorganisms (Kenealy and Waselefsky, 1985; Pavlostathis and Gomez, 1991). The maximum growth rates for MCCAs producers such as *C. kluyveri* ATCC 8527 (Kenealy and Waselefsky, 1985) and *M. elsdenii* CECT390 (Soto-cruz et al., 2002) were determined to be 0.287 h^{-1} and 0.20-0.35 h^{-1}, respectively, which are much higher than for aceticlastic methanogens (0.003-0.029 h^{-1}) (Pavlostathis and Gomez, 1991) and slightly higher than for hydrogenotrophic methanogens (0.17 h^{-1}) (Pavlostathis and Gomez, 1991). Theoretically, decreasing the SRT can benefit chain elongation by washing out aceticlastic methanogens. However, manipulating SRT might not control hydrogenotrophic methanogens as shown by our data. The microbial community data also show that the relative abundance and activity of MCCAs producers such as *Pseudoramibacter* decreased for shorter

SRTs. For example, the relative activity of *Pseudoramibacter* decreased from 5.9% on Day 31 to 0.2% on Day 66 when the SRT decreased from 13.6 to 6.0 days. While methanogens are undesirable for chain elongation, MCCA producing microorganisms need to be retained in the system. For selective MCCA production, the bioreactor should be operated at an SRT sufficiently low to promote wash-out of methanogens, but sufficiently high for retention of MCCA producers. Our data indicate that this balance is difficult to accomplish and is made more complicated because of the lack of information on kinetic parameters of chain elongating microorganisms in mixed communities.

2.4.4 Influent plays a greater role in shaping the bioreactor microbiome than the inoculum

Rumen bacteria such as *E. limosum* (Genthner et al., 1981), *E. pyruvativorans* (Wallace et al., 2003), *M. elsdenii* (Weimer and Moen, 2013), and co-cultures of *C. klu*yveri and ruminal cellulolytic bacteria (Weimer et al., 2015) have been reported to produce MCCAs via chain elongation. Moreover, rumen microbial communities exhibit high activity despite the presence of high concentrations of SCCAs in the rumen (Shrestha et al., 2017). Because of these reasons, we inoculated our bioreactor with rumen content. By Day 7 (first biomass sample point after startup), the bioreactor microbial community already had diverged from the inoculum (Figure 2.3,Figure A.7, andFigure A.8, Appendix A). The rumen inoculum was more diverse than the biomass observed in the bioreactor (Figure A.2, Appendix A). The dominant bacterial genera in the rumen inoculum were *Fibrobacter, Prevotella, Ruminobacter*, unclassified *Bacteroidetes,* unclassified *Gammaproteobacteria*, unclassified *Lachnospiraceae*, and *Treponema*. These bacterial populations were either present at a low relative abundance and activity in the bioreactor or undetected except for *Lachnospiraceae* and *Prevotella*. The NMDS analysis (Figure 2.3a and 2.3b) shows that the microbial community composition changed gradually during early bioreactor operation (Day 7 to Day 73), but that there was a substantial change on Day 81. The Day 81 influent sample clustered with the rumen inocula samples (Figure 2.3) likely because the acidogenic food waste bioreactor, the permeate of which was used in this study, was re-inoculated with rumen content a few days before the Day 81 influent was collected. The chain elongation bioreactor was re-inoculated with rumen content on Day 178, but the bioreactor microbial

community structure on Day 193, the first sampling date after re-inoculation, did not appear to be greatly influenced by the rumen inoculum (Figure 2.3,Figure A.7, andFigure A.8, Appendix A).

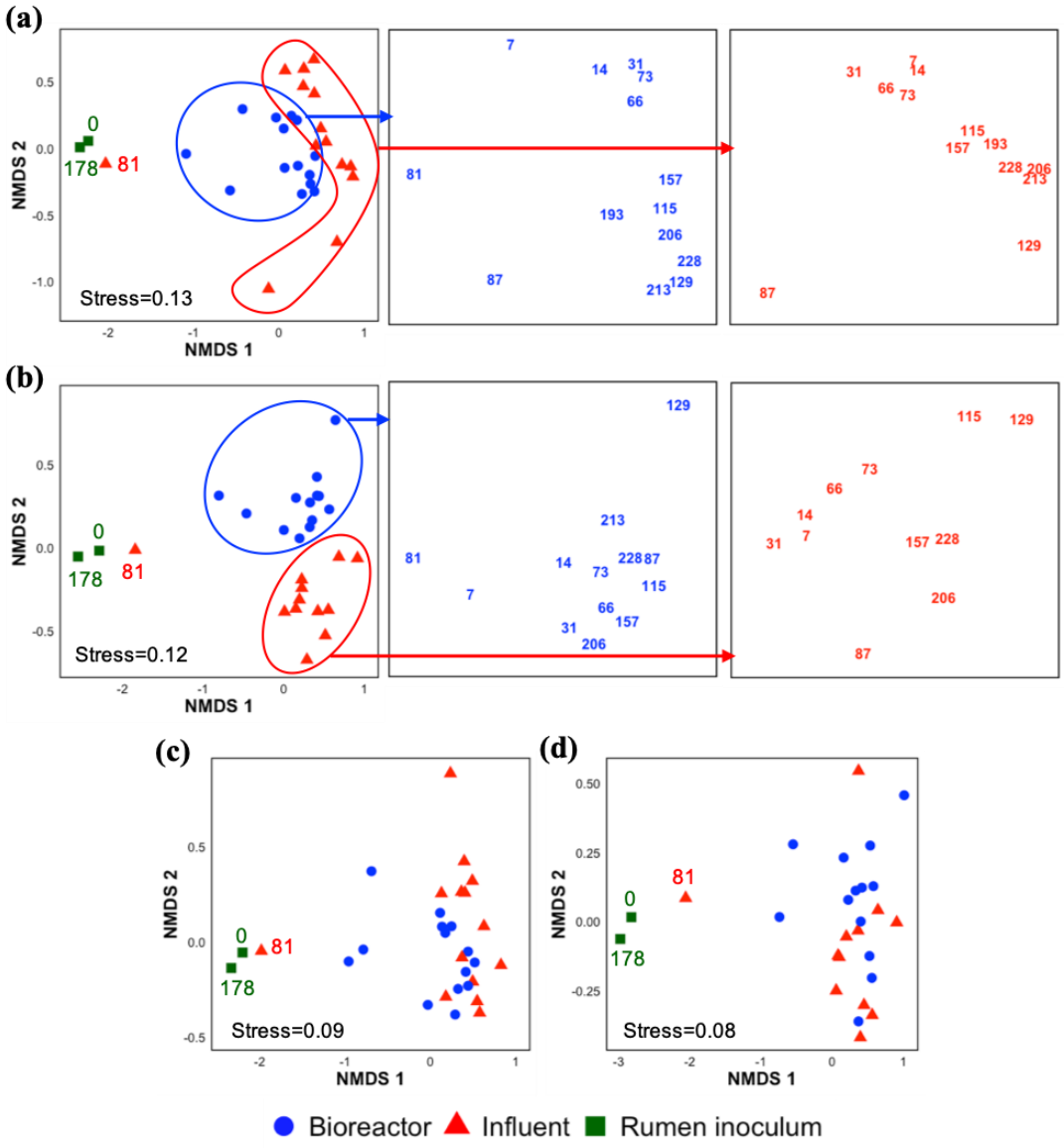

Figure 2.3. Non-metric multidimensional scaling (NMDS) ordination plot based on the Bray-Curtis dissimilarity index of the microbial community at OTU level using 16S rRNA gene sequencing (a) and 16S rRNA sequencing data (b) and Jaccard index using 16S rRNA gene sequencing (c) and 16S rRNA sequencing data (d) in the rumen inocula, bioreactor, and influent samples. The numbers correspond to sampling time points.

Alpha diversity and beta diversity indices were determined to compare the bacterial and archaeal community structure in the inoculum, influent, and bioreactor samples (Figure A.6, Appendix A). The alpha diversity indices were statistically similar between the bioreactor and influent samples. NMDS ordination analysis based on Bray-Curtis dissimilarity (Figure 2.3a) showed that the microbial community structures (OTU memberships and abundance) in the influent and bioreactor samples collected over time were more similar to each other than the community structures in the influent and bioreactor samples collected at the same time point (ANOSIM R value=0.55, p =0.001, Table A.6, Appendix A). A similar observation was made when the 16S rRNA sequencing data were used for the Bray-Curtis dissimilarity analysis (Figure 2.3b, ANOSIM R value=0.67, p =0.001). The NMDS analyses based on the Jaccard index indicated that the influent and bioreactor microbial community compositions (OTU memberships) were similar (Figure 2.3c and 2.3d). This was supported by the ANOSIM analysis based on the Jaccard index (Table A.6, Appendix A), which showed that the R values obtained by comparing influent and bioreactor samples were small (0.13-0.28). These observations suggest that the influent and bioreactor samples collected at the same time were similar based on shared OTUs (Jaccard index), but that they differed when considering relative abundance and activity in addition to membership (Bray-Curtis index). Similar observations were made when bacterial and archaeal communities were compared separately using Bray-Curtis and Jaccard indices (Figure A.7 andFigure A.8, Table A.6, Appendix A). These results suggest that the influent had a greater role in shaping the bioreactor microbiome than the inoculum.

2.4.5 Microbial immigration from influent to downstream, bioreactor microbial community

Microbial community composition and structure in influent and bioreactor samples were compared to identify the immigrating microbial populations and thus study the impact of immigration on overall bioreactor performance. The most abundant and active bacterial phyla in the influent were *Bacteroidetes*, *Firmicutes*, and *Proteobacteria* (Figure A.9, Appendix A). On the other hand, the bioreactor samples were dominated by *Firmicutes* (48.4 ± 6.1%), *Bacteroidetes* (25.1 ± 7.8%), *Euryarchaeota* (10.4 ± 3.3%), and *Actinobacteria* (7.6 ± 3.8%) (Figure A.9a, Appendix A); the relative activity data were similar, except for *Bacteroidetes* (8.6 ± 5.0%) (Figure A.9b, Appendix

A). The OTUs shared between the influent and bioreactor communities accounted for 38.9 ± 8.9% and 41.3 ± 8.2% of the total and active number of OTUs observed in the bioreactor (Table A.7, Appendix A). On average, 44.2 ± 6.3% and 33.0 ± 6.2% of total and active influent OTUs were observed in the bioreactor samples (Table A.7, Appendix A). This indicates that a significant fraction of the OTUs observed in the bioreactor originated from the influent. The presence of OTUs does not necessarily suggest their functional contribution as some of these immigrant OTUs might represent dead or inactive cells.

Two approaches were used to distinguish active microbial populations that immigrated from the influent from inactive populations. One approach used the ratio of rRNA/rDNA in the bioreactor and influent (Figure 2.4) (Mei et al., 2016); the second approach calculated the specific growth rate of individual microbial immigrants (Table A.8, Appendix A) (Mei et al., 2016). Additionally, $rDNA_{influent}/rDNA_{reactor}$ and $rRNA_{influent}/rRNA_{reactor}$ were calculated to compare relative abundances and relative activities, respectively, between influent and bioreactor samples (Table A.9, Appendix A). Bacterial OTUs with a high relative abundance and relative activity in the influent (depicted by large values on the Y axes in Figure 2.4a and 2.4b) were found to be less active in the bioreactor than in the influent, i.e., the $[rRNA/rDNA]_{reactor}$: $[rRNA/rDNA]_{influent} < 1$. This included OTUs belonging to the genus *Prevotella*, *Succiniclasticum*, unclassified *Bacteroidales*, and *Megasphaera.*

Prevotella, the most dominant genus in the influent (38.7 ± 6.2%, Figure A.10, Appendix A), was still abundant in the bioreactor (22.4 ± 7.8%, Figure 2.2) with $rDNA_{influent}/rDNA_{reactor}$ corresponding to 1.7 ± 0.8. However, the relative activity of *Prevotella* in the bioreactor was much lower compared to that in the influent ($rRNA_{influent}/rRNA_{reactor}$=4.5 ± 3.2, Figure A.9, Appendix A) and its $[rRNA/rDNA]_{reactor}$: $[rRNA/rDNA]_{influent}$ was 0.4. The genus *Prevotella* has been mostly associated with fermentation and is commonly found in the rumen (Puniya et al., 2015; Stewart et al., 2018). *Megasphaera* OTU 2, the most dominant *Megasphaera* OTU in the bioreactor (Figure 2.2), was also found in the influent suggesting that it immigrated from the influent. As *Megasphaera* can produce both SCCAs and MCCAs (Scarborough et al., 2018; Weimer and Moen, 2013), its broad fermentative capacity might have supported its growth in both the

acidogenic food waste bioreactor and the chain elongation bioreactor. Other populations that were present at relatively low abundance or activity in the influent that became dominant in the bioreactor (shown by larger Y-axis values in Figure 2.4c and 2.4d) with $rRNA/rDNA]_{reactor}$: $[rRNA/rDNA]_{influent} > 1$ included *Olsenella*, unclassified *Clostridiales*, and unclassified *Lachnospiraceae.* For example, *Clostridiales* OTU 3 was found to be actively involved in MCCAs production in the bioreactor (rRNA/rDNA>1). However, it was present at low relative abundance (0.2 ± 0.3%) and relative activity (0.2 ± 0.2%) in the influent. Similarly, *Pseudoramibacter* OTU 16 that positively correlated to MCCAs production, as discussed above, was enriched in the bioreactor but was only detected in some influent samples ($rDNA_{influent}/rDNA_{reactor}$=0.01 ± 0.01% and $rRNA_{influent}/rRNA_{reactor}$=0.01 ± 0.02%). Feeding ethanol-rich substrate and controlling the bioreactor conditions such as pH seemed to cause a selection for OTUs capable of MCCAs production, even though they were present at low relative abundance and activity in the incoming feed.

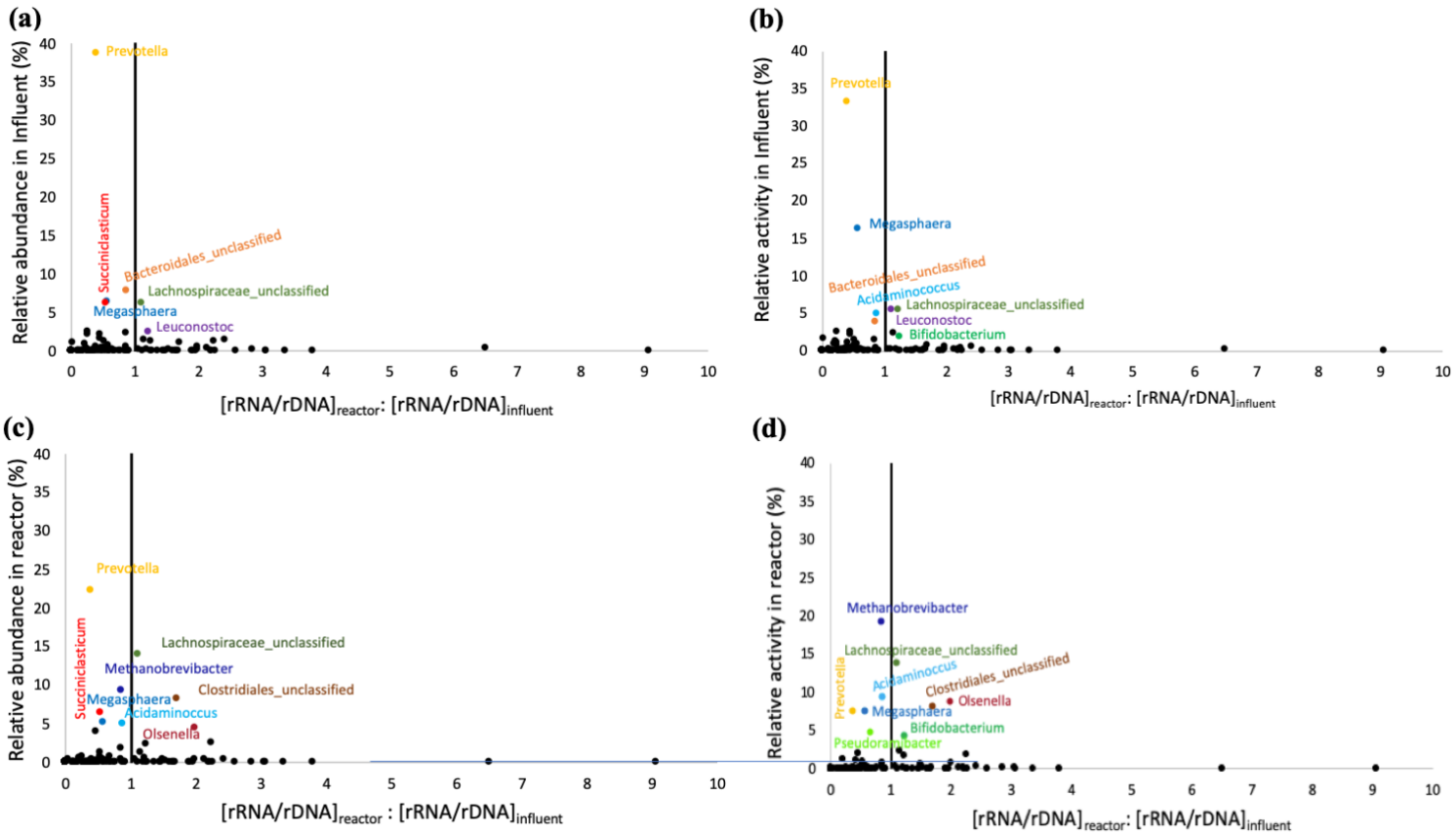

Figure 2.4. Comparison of rRNA/rDNA ratio of microbial groups in the bioreactor and influent versus relative abundance (a) and relative activity (b) of the corresponding genus or family in the influent samples and relative abundance (c) and relative activity (d) of the corresponding genus or family in the bioreactor samples. The vertical line is drawn at $[rRNA/rDNA]_{reactor}$:$[rRNA/rDNA]_{influent}$ = 1. The microbial group that falls on the left and right hand sides of the vertical line are more active in the influent ($[rRNA/rDNA]_{reactor}$:$[rRNA/rDNA]_{influent}$ <1) and reactor ($[rRNA/rDNA]_{reactor}$:$[rRNA/rDNA]_{influent}$ > 1), respectively. Genus or family with high relative abundance and relative activity (larger Y-axis values) are colored and labeled.

Comparing the archaeal microbial communities in influent and bioreactor samples, we observed that the rRNA/rDNA ratio of *Methanobrevibacter* genus was higher in the influent than in the bioreactor ($[rRNA/rDNA]_{reactor}$: $[rRNA/rDNA]_{influent} < 1$), suggesting that *Methanobrevibacter* was less active in the bioreactor compared to the influent. On the contrary, the relative abundance and activity of *Methanobrevibacter* genus were much higher in the bioreactor samples compared to the corresponding influent samples. Similarly, *Pseudoramibacter* was also shown to be less active in the bioreactor compared to the influent as its $rRNA/rDNA]_{reactor}$:$[rRNA/rDNA]_{influent}$ was less than 1. These observations suggest that comparing rRNA/rDNA ratios in the bioreactor and influent is not adequate to identify all the active immigrant populations belonging to different taxa. The relative abundance and activity data were highly correlated to each other in the influent samples (correlation coefficient=0.94), but less so in the bioreactor samples (correlation coefficient=0.78) (Figure A.11, Appendix A). The different correlation between relative activity (rRNA) and relative abundance (rDNA) in the influent compared to that in the bioreactor will introduce bias when calculating the rRNA/rDNA ratio. Some studies have pointed out that sequencing depth and population with different physiologies and growth strategies can distort the interpretation of the rRNA/rDNA ratio (Mei et al., 2016; Steven et al., 2017). Both variable *rrn* gene copy number and sequence variability introduce biases in the relative abundance and relative activity calculations and diversity estimates. The *rrn* gene copy number varies among different microorganism and methanogens on average have a much lower *rrn* gene copy number (1-4) compared to bacteria (1-15) (Stoddard et al., 2015; Sun et al., 2013). Sequence abundance can be underestimated in taxa with low *rrn* gene copy numbers compared to those with high *rrn* gene copy numbers and variation in *rrn* sequences within the same genome increases with increasing copy numbers (Větrovský and Baldrian, 2013).

A mass balance approach was used as an additional tool to identify active influent populations with positive specific growth rate that contributed to the downstream process. *Methanobrevibacter* had a positive specific growth rate of 0.08 d^{-1} using RNA based data, while using the DNA based data resulted in a negative specific growth rate (-0.12 d^{-1}, Method I, Table A.8, Appendix A). *Pseudoramibacter* had positive specific growth rates of 0.07 d^{-1} and 0.10 d^{-1} based on DNA and RNA based data, respectively, suggesting that it was actively growing in the bioreactor. These

specific growth rate values were lower than those obtained by the Method II (using VSS to approximate cell concentration) i.e 0.32 d^{-1} and 0.35 d^{-1} for *Methanobrevibacter* and *Pseudoramibacter*, respectively (Method II, Table A.8, Appendix A). As VSS measures all suspended organic matter in the bioreactor including live and dead microbial cells and other microbial components such as extracellular polymeric substance, Method II might overestimate cell concentration and skew the specific growth calculation.

The impact of immigration can vary with how different the upstream and the downstream systems are. Some of the dominant influent OTUs were washed out, were found to be inactive or decreased in relative abundance and activity in the bioreactor whereas some low-abundant/low-activity influent OTUs played an important role in the bioreactor. The low similarity in microbial community structure due to the difference in the dominant and active OTUs between the influent and the bioreactor suggest that the community assembly in the bioreactor was dominated by selection. Community assembly theory predicts that immigration is important in structuring bioreactor communities when competitive selection is weak, and when population sizes are small, alpha diversity is low and environmental conditions are dynamic (Frigon and Wells, 2019). The similar growth (anaerobic) environments, availability of resources, and functional redundancy of some microorganisms between the upstream and downstream processes possibly allowed some immigrants to survive and flourish in the chain elongation bioreactor. For example, due to the broad metabolic capacity of fermenters, the fermentative bacteria present in the influent can also degrade the residual organics in the chain elongation bioreactor. One study reported a marginal impact of immigration from an upflow anaerobic sludge blanket bioreactor to a downstream activated sludge bioreactor due to a major change in environmental conditions (i.e., from anaerobic to aerobic condition) (Mei et al., 2019). Mei et al. (2017) observed that a majority of the immigrant populations in full-scale anaerobic digesters treating sludge from a municipal wastewater treatment system consisted of inactive aerobes and facultative anaerobes. These aerobic and facultative anaerobic immigrants derived from the upstream activated sludge process were not directly involved in the downstream anaerobic metabolism. Therefore, the bioreactor conditions like temperature, pH, presence of oxygen, substrate pretreatment, and metabolic flexibility of the

microorganisms play important roles in determining the impact of the influent on the downstream system.

2.5 Conclusions

This study demonstrated that MCCAs can be produced using waste ethanol and pre-fermented food waste using mixed-culture microbial communities. However, the toxicity induced by undissociated MCCAs present at low pH negatively affected MCCAs production. Waste chain elongation bioreactors that are continuously seeded by the upstream microbial community are impacted by microbial immigration. The influent microbial community was found to play a greater role in shaping the chain elongation microbiome than the inoculum microbial community. While a significant fraction of the chain elongation microbial community originated from the influent, not all immigrating populations were active. Moreover, microbial OTUs that were not abundant in the influent such as *Clostridiales* and *Pseudoramibacter* OTUs positively correlated with MCCAs production and played an important role in the chain elongation function. Our study highlighted the application of the mass balance model to determine the specific growth rate of individual microbial populations coupled with the rRNA/rDNA approach in differentiating potentially active and inactive immigrant populations. The mass balance model relied on relative abundance and relative activity data to estimate the total number of cells entering and exiting the system. Future studies should look into using absolute abundance by quantifying cell count using flow cytometry or quantitative PCR.

2.6 References

Agler, M.T., Spirito, C.M., Usack, J.G., Werner, J.J., Angenent, L.T., 2012. Chain elongation with reactor microbiomes: upgrading dilute ethanol to medium-chain carboxylates. Energy Environ. Sci. 5, 8189. https://doi.org/10.1039/c2ee22101b

Andersen, S.J., Candry, P., Basadre, T., Khor, W.C., Roume, H., Hernandez-Sanabria, E., Coma, M., Rabaey, K., 2015. Electrolytic extraction drives volatile fatty acid chain elongation through lactic acid and replaces chemical pH control in thin stillage fermentation. Biotechnol. Biofuels 8, 221. https://doi.org/10.1186/s13068-015-0396-7

Andersen, S.J., De Groof, V., Khor, W.C., Roume, H., Props, R., Coma, M., Rabaey, K., 2017. A Clostridium Group IV Species Dominates and Suppresses a Mixed Culture Fermentation by

Tolerance to Medium Chain Fatty Acids Products. Front. Bioeng. Biotechnol. 5, 1–10. https://doi.org/10.3389/fbioe.2017.00008

Angenent, L.T., Richter, H., Buckel, W., Spirito, C.M., Steinbusch, K.J.J., Plugge, C.M., Strik, D.P.B.T.B., Grootscholten, T.I.M., Buisman, C.J.N., Hamelers, H.V.M., 2016. Chain Elongation with Reactor Microbiomes: Open-Culture Biotechnology to Produce Biochemicals. Environ. Sci. Technol. 50, 2796–2810. https://doi.org/10.1021/acs.est.5b04847

Anneken, D.J., Both, S., Christoph, R., Fieg, G., Steinberner, U., Westfechtel, A., 2012. Fatty acids:Ullmann's Encyclopedia of Industrial Chemistry. https://doi.org/10.1002/14356007.a10

Blazewicz, S.J., Barnard, R.L., Daly, R.A., Firestone, M.K., 2013. Evaluating rRNA as an indicator of microbial activity in environmental communities: limitations and uses. ISME J. 7, 2061–2068. https://doi.org/10.1038/ismej.2013.102

Brewers Association, 2019. Statistics: Number of Breweries [WWW Document]. URL https://www.brewersassociation.org/statistics-and-data/national-beer-stats/ (accessed 5.29.20).

Brewers Association, 2017a. Wastewater Management Guidance Manual.

Brewers Association, 2017b. Water and Wastewater : Treatment / Volume Reduction Manual.

Caporaso, J.G., Lauber, C.L., Walters, W.A., Berg-Lyons, D., Lozupone, C.A., Turnbaugh, P.J., Fierer, N., Knight, R., 2011. Global patterns of 16S rRNA diversity at a depth of millions of sequences per sample. Proc. Natl. Acad. Sci. U. S. A. 108 Suppl, 4516–22. https://doi.org/10.1073/pnas.1000080107

Carlson, K.M., Curran, L.M., Asner, G.P., Pittman, A.M., Trigg, S.N., Adeney, J.M., 2012. Carbon emissions from forest conversion by Kalimantan oil palm plantations. Nat. Clim. Chang. 3, 283–287. https://doi.org/10.1038/nclimate1702

Chen, W., Strik, D.P.B.T.B., Buisman, C.J.N., Kroeze, C., 2017. Production of Caproic Acid from Mixed Organic Waste : An Environmental Life Cycle Perspective. Environ. Sci. Technol. 51, 7159–7168. https://doi.org/10.1021/acs.est.6b06220

Cotta, M., Forster, R., 2006. The Family Lachnospiraceae, Including the Genera Butyrivibrio, Lachnospira and Roseburia, The prokaryotes: a handbook on the biology of bacteria: Bacteria: Firmicutes, Cyanobacteria. Springer, New York, NY. https://doi.org/10.1007/0-387-30744-3_32

Emerson, E.L., Weimer, P.J., 2017. Fermentation of model hemicelluloses by Prevotella strains and Butyrivibrio fibrisolvens in pure culture and in ruminal enrichment cultures. Appl. Microb. cell Physiol. 110, 4269–4278. https://doi.org/10.1007/s00253-017-8150-7

Esquivel-elizondo, S., Krajmalnik-brown, R., Miceli, J., Cesar, I.I.I., 2018. Impact of carbon monoxide partial pressures on methanogenesis and medium chain fatty acids production during

ethanol fermentation 341–350. https://doi.org/10.1002/bit.26471

Eugene, W.R., Rodger, B.B., Andrew, D.E., Lenore, S.C., 2012. Standard Methods for the Examination of Water and Wastewater, American Public Health Association, American Water Works Association, Water environment federation.

Fierer, N., Jackson, J.A., Vilgalys, R., Jackson, R.B., 2005. Assessment of soil microbial community structure by use of taxon-specific quantitative PCR assays. Appl. Environ. Microbiol. 71, 4117–4120. https://doi.org/10.1128/AEM.71.7.4117-4120.2005

Frigon, D., Wells, G., 2019. Microbial immigration in wastewater treatment systems: analytical considerations and process implications. Curr. Opin. Biotechnol. 57, 151–159. https://doi.org/10.1016/j.copbio.2019.02.021

Ge, S., Usack, J.G., Spirito, C.M., Angenent, L.T., 2015. Long-Term *n* -Caproic Acid Production from Yeast-Fermentation Beer in an Anaerobic Bioreactor with Continuous Product Extraction. Environ. Sci. Technol. 49, 8012–8021. https://doi.org/10.1021/acs.est.5b00238

Genthner, B.R.S., Davis, C.L., Bryant, M.P., 1981. Features of rumen and sewage sludge strains of *Eubacterium limosum*, a methanol-utilizing and H2-CO2-utilizing species. Appl. Environ. Microbiol. 42, 12–19.

Gildemyn, S., Molitor, B., Usack, J.G., Nguyen, M., Rabaey, K., Angenent, L.T., 2017. Upgrading syngas fermentation effluent using Clostridium kluyveri in a continuous fermentation. Biotechnol. Biofuels 10, 83. https://doi.org/10.1186/s13068-017-0764-6

Grootscholten, T.I.M., Steinbusch, K.J.J., Hamelers, H.V.M., Buisman, C.J.N., 2013a. Chain elongation of acetate and ethanol in an upflow anaerobic filter for high rate MCFA production. Bioresour. Technol. 135, 440–445. https://doi.org/10.1016/j.biortech.2012.10.165

Grootscholten, T.I.M., Steinbusch, K.J.J., Hamelers, H.V.M., Buisman, C.J.N., 2013b. Improving medium chain fatty acid productivity using chain elongation by reducing the hydraulic retention time in an upflow anaerobic filter. Bioresour. Technol. 136, 735–738. https://doi.org/10.1016/j.biortech.2013.02.114

Grootscholten, T.I.M., Steinbusch, K.J.J., Hamelers, H.V.M., Buisman, C.J.N., 2013c. High rate heptanoate production from propionate and ethanol using chain elongation. Bioresour. Technol. 136, 715–718. https://doi.org/10.1016/j.biortech.2013.02.085

Grootscholten, T.I.M., Strik, D.P.B.T.B., Steinbusch, K.J.J., Buisman, C.J.N., Hamelers, H.V.M., 2014. Two-stage medium chain fatty acid (MCFA) production from municipal solid waste and ethanol. Appl. Energy 116, 223–229. https://doi.org/10.1016/j.apenergy.2013.11.061

Jeon, B.S., Kim, B.C., Um, Y., Sang, B.I., 2010. Production of hexanoic acid from d-galactitol by a newly isolated Clostridium sp. BS-1. Appl. Microbiol. Biotechnol. 88, 1161–1167.

https://doi.org/10.1007/s00253-010-2827-5

Jones, C.A., Coker, C., Kirk, K., Reynolds, L., 2019. Food Waste Co-Digestion at Water Resource Recovery Facilities: Business Case Analysis.

Kaza, S., Yao, L., Bhada-Tata, P., Woerden, and F. Van, 2018. What a waste 2.0: a global snapshot of solid waste management to 2050. The World Bank.

Kenealy, W.R., Waselefsky, D.M., 1985. Studies on the substrate range of Clostridium kluyveri; the use of propanol and succinate *. Arch. Microbiol. 141, 187–194. https://doi.org/10.3747/pdi.2011.00058

Khor, W.C., Andersen, S., Vervaeren, H., Rabaey, K., 2017. Electricity - assisted production of caproic acid from grass. Biotechnol. Biofuels 10, 1–11. https://doi.org/10.1186/s13068-017-0863-4

Kirkegaard, R.H., Mcilroy, S.J., Kristensen, J.M., Nierychlo, M., Karst, M., Dueholm, M.S., Albertsen, M., Nielsen, P.H., 2017. The impact of immigration on microbial community composition in full-scale anaerobic digesters. Sci. Rep. 1–11. https://doi.org/10.1038/s41598-017-09303-0

Klappenbach, J.A., Dunbar, J.M., Schmidt, T.M., 2000. rRNA operon copy number reflects ecological strategies of bacteria. Appl. Environ. Microbiol. 66, 1328–1333. https://doi.org/10.1128/AEM.66.4.1328-1333.2000

Kozich, J.J., Westcott, S.L., Baxter, N.T., Highlander, S.K., Schloss, P.D., 2013. Development of a dual-index sequencing strategy and curation pipeline for analyzing amplicon sequence data on the miseq illumina sequencing platform. Appl. Environ. Microbiol. 79, 5112–5120. https://doi.org/10.1128/AEM.01043-13

Kucek, L., Nguyen, M., Angenent, L.T., 2016a. Conversion of L-lactate into n-caproate by a continuously fed reactor microbiome. Water Res. 93, 163–171. https://doi.org/10.1016/j.watres.2016.02.018

Kucek, L., Spirito, C.M., Angenent, L.T., 2016b. High n-caprylate productivities and specificities from dilute ethanol and acetate: Chain elongation with microbiomes to upgrade products from syngas fermentation. Energy Environ. Sci. 9, 3482–3494. https://doi.org/10.1039/c6ee01487a

Kucek, L., Xu, J., Nguyen, M., Angenent, L.T., 2016c. Waste conversion into n-caprylate and n-caproate: resource recovery from wine lees using anaerobic reactor microbiomes and in-line extraction. Front. Microbiol. 7, 1–14. https://doi.org/10.3389/fmicb.2016.01892

Kumar, S., Stecher, G., Tamura, K., 2016. MEGA7: Molecular Evolutionary Genetics Analysis Version 7.0 for Bigger Datasets. Mol. Biol. Evol. 33, 1870–1874. https://doi.org/10.1093/molbev/msw054

Li, R., Tun, H.M., Jahan, M., Zhang, Z., Kumar, A., Fernando, D., Farenhorst, A., Khafipour, E., 2017. Comparison of DNA-, PMA-, and RNA-based 16S rRNA Illumina sequencing for detection of live bacteria in water. Sci. Rep. 7, 1–11. https://doi.org/10.1038/s41598-017-02516-3

Liu, Y., He, P., Shao, L., Zhang, H., Lü, F., 2017. Significant enhancement by biochar of caproate production via chain elongation. Water Res. 119, 150–159. https://doi.org/10.1016/j.watres.2017.04.050

Malinauskaite, J., Jouhara, H., Czajczyńska, D., Stanchev, P., Katsou, E., Rostkowski, P., Thorne, R.J., Colón, J., Ponsá, S., Al-Mansour, F., Anguilano, L., Krzyżyńska, R., López, I.C., A.Vlasopoulos, Spencer, N., 2017. Municipal solid waste management and waste-to-energy in the context of a circular economy and energy recycling in Europe. Energy 141, 2013–2044. https://doi.org/10.1016/j.energy.2017.11.128

McMurdie, P.J., Holmes, S., 2013. Phyloseq: An R Package for Reproducible Interactive Analysis and Graphics of Microbiome Census Data. PLoS One 8. https://doi.org/10.1371/journal.pone.0061217

Mei, R., Kim, J., Wilson, F.P., Bocher, B.T.W., Liu, W.T., 2019. Coupling growth kinetics modeling with machine learning reveals microbial immigration impacts and identifies key environmental parameters in a biological wastewater treatment process. Microbiome 7, 1–9. https://doi.org/10.1186/s40168-019-0682-x

Mei, R., Narihiro, T., Nobu, M.K., Kuroda, K., Liu, W.T., 2016. Evaluating digestion efficiency in full-scale anaerobic digesters by identifying active microbial populations through the lens of microbial activity. Sci. Rep. 6, 1–10. https://doi.org/10.1038/srep34090

Mei, R., Nobu, M.K., Narihiro, T., Kuroda, K., Muñoz Sierra, J., Wu, Z., Ye, L., Lee, P.K.H., Lee, P.H., van Lier, J.B., McInerney, M.J., Kamagata, Y., Liu, W.T., 2017. Operation-driven heterogeneity and overlooked feed-associated populations in global anaerobic digester microbiome. Water Res. 124, 77–84. https://doi.org/10.1016/j.watres.2017.07.050

Mueller, R.C., Gallegos-Graves, L., Zak, D.R., Kuske, C.R., 2016. Assembly of Active Bacterial and Fungal Communities Along a Natural Environmental Gradient. Microb. Ecol. 71, 57–67. https://doi.org/10.1007/s00248-015-0655-y

Oksanen, J., Blanchet, F.G., Friendly, M., Kindt, R., Legendre, P., McGlinn, D., Minchin, P.R., O'Hara, R.B., Simpson, G.L., Solymos, P., Stevens, M.H.H., Szoecs, E., Wagner, H., 2019. Package 'vegan': Community Ecology Package. R Packag. version 2.5-6.

Pavlostathis, S.G., Gomez, E.G., 1991. Kinetics of anaerobic treatment : A critical review. Crit. Rev. Environ. Sci. Technol. 21, 411–490. https://doi.org/10.1080/10643389109388424

Petrenko, C., Paltseva, J., Searle, S., 2016. Ecological Impacts of Palm Oil Expansion in Indonesia. Washingt. Int. Counc. Clean Transp.

Porebski, S., Bailey, L.G., Baum, B.R., 1997. Modification of a CTAB DNA Extraction Protocol for Plants Containing High Polysaccharide and Polyphenol Components 15, 8–15.

Poretsky, R., Rodriguez-r, L.M., Luo, C., Tsementzi, D., Konstantinidis, K.T., 2014. Strengths and Limitations of 16S rRNA Gene Amplicon Sequencing in Revealing Temporal Microbial Community Dynamics 9. https://doi.org/10.1371/journal.pone.0093827

Puniya, A.K., Singh, R., Kamra, D.N., 2015. Rumen Microbiology : From Evolution to Revolution. Springer.

Roghair, M., Liu, Y., Strik, D.P.B.T.B., Weusthuis, R.A., Bruins, M.E., Buisman, and C.J.N., 2018. Development of an Effective Chain Elongation Process From Acidified Food Waste and Ethanol Into n-Caproate. Front. Bioeng. Biotechnol. 6, 1–11. https://doi.org/10.3389/fbioe.2018.00050

Rogosa, M., 1969. Acidaminococcus gen. n., Acidaminococcus fermentans sp. n., Anaerobic Gram-negative Diplococci Using Amino Acids as the Sole Energy Source for Growth. J. Bacteriol. 98, 756–766.

Scarborough, M.J., Lynch, G., Dickson, M., Mcgee, M., Donohue, T.J., Noguera, D.R., 2018. Increasing the economic value of lignocellulosic stillage through medium - chain fatty acid production. Biotechnol. Biofuels 1–17. https://doi.org/10.1186/s13068-018-1193-x

Schloss, P.D., Westcott, S.L., Ryabin, T., Hall, J.R., Hartmann, M., Hollister, E.B., Lesniewski, R.A., Oakley, B.B., Parks, D.H., Robinson, C.J., Sahl, J.W., Stres, B., Thallinger, G.G., Van Horn, D.J., Weber, C.F., 2009. Introducing mothur: Open-source, platform-independent, community-supported software for describing and comparing microbial communities. Appl. Environ. Microbiol. 75, 7537–7541. https://doi.org/10.1128/AEM.01541-09

Seluy, L.G., Isla, M.A., 2014. A Process To Treat High-Strength Brewery Wastewater via Ethanol Recovery and Vinasse Fermentation. Ind. Eng. Chem. Res. 53, 17043–17050. https://doi.org/10.1021/ie500438j

Shin, J., Cho, S.K., Lee, J., Hwang, K., Chung, J.W., Jang, H.N., Shin, S.G., 2019. Performance and microbial community dynamics in anaerobic digestion of waste activated sludge: Impact of immigration. Energies 12, 1–15. https://doi.org/10.3390/en12030573

Shrestha, S., Fonoll, X., Kumar, S., Raskin, L., 2017. Biological strategies for enhanced hydrolysis of lignocellulosic biomass during anaerobic digestion : Current status and future perspectives. Bioresour. Technol. 245, 1245–1257. https://doi.org/10.1016/j.biortech.2017.08.089

Soto-cruz, O., Favela-torres, E., Saucedo-Castañeda, G., 2002. Modeling of Growth , Lactate Consumption , and Volatile Fatty Acid Complex Media. Biotechnol. Prog. 18, 193–200.

Steven, B., Hesse, C., Soghigian, J., Gallegos-Graves, L.V., Dunbar, J., 2017. Simulated

rRNA/DNA ratios show potential to misclassify active populations as dormant. Appl. Environ. Microbiol. 83, 1–11. https://doi.org/10.1128/AEM.00696-17

Stewart, R.D., Auffret, M.D., Warr, A., Wiser, A.H., Press, M.O., Langford, K.W., Liachko, I., Snelling, T.J., Dewhurst, R.J., Walker, A.W., Roehe, R., Watson, M., 2018. Assembly of 913 microbial genomes from metagenomic sequencing of the cow rumen. Nat. Commun. 9, 1–11. https://doi.org/10.1038/s41467-018-03317-6

Stoddard, S.F., Smith, B.J., Hein, R., Roller, B.R.K., Schmidt, T.M., 2015. rrnDB: Improved tools for interpreting rRNA gene abundance in bacteria and archaea and a new foundation for future development. Nucleic Acids Res. 43, D593–D598. https://doi.org/10.1093/nar/gku1201

Sun, D.L., Jiang, X., Wu, Q.L., Zhou, N.Y., 2013. Intragenomic heterogeneity of 16S rRNA genes causes overestimation of prokaryotic diversity. Appl. Environ. Microbiol. 79, 5962–5969. https://doi.org/10.1128/AEM.01282-13

The Brewers of Europe, 2017. Brewers statistics 2017 edition.

Urban, C., Xu Jiajie, Strauber Heik, Dantas Tatiane R. dos Santos, Muhlenberg Jana, Hartig Claus, Angenent Largus T. and, Harnisch Falk, 2017. Production of drop-in fuels from biomass at high selectivity by combined microbial and electrochemical conversion. Energy Environ. Sci. 10, 2231–2244. https://doi.org/10.1039/c7ee01303e

Van Gylswyk, N.O., 1995. Succiniclasticum ruminis gen . nov ., sp . nov ., a Ruminal Bacterium Converting Succinate to Propionate as the Sole Energy-Yielding Mechanism. Int. J. Syst. Evol. Microbiol. 45, 297–300.

Větrovský, T., Baldrian, P., 2013. The Variability of the 16S rRNA Gene in Bacterial Genomes and Its Consequences for Bacterial Community Analyses. PLoS One 8, 1–10. https://doi.org/10.1371/journal.pone.0057923

Wallace, R.J., McKain, N., McEwan, N.R., Miyagawa, E., Chaudhary, L.C., King, T.P., Walker, N.D., Apajalahti, J.H.A., Newbold, C.J., 2003. Eubacterium pyruvativorans sp. nov., a novel non-saccharolytic anaerobe from the rumen that ferments pyruvate and amino acids, forms caproate and utilizes acetate and propionate. Int. J. Syst. Evol. Microbiol. 53, 965–970. https://doi.org/10.1099/ijs.0.02110-0

Weimer, P.J., Moen, G.N., 2013. Quantitative analysis of growth and volatile fatty acid production by the anaerobic ruminal bacterium Megasphaera elsdenii T81. Appl. Microb. cell Physiol. 4075–4081. https://doi.org/10.1007/s00253-012-4645-4

Weimer, P.J., Nerdahl, M., Brandl, D.J., 2015. Production of medium-chain volatile fatty acids by mixed ruminal microorganisms is enhanced by ethanol in co-culture with Clostridium kluyveri. Bioresour. Technol. 175, 97–101. https://doi.org/10.1016/j.biortech.2014.10.054

Weimer, P.J., Stevenson, D.M., 2012. Isolation, characterization, and quantification of Clostridium kluyveri from the bovine rumen. Appl. Microbiol. Biotechnol. 94, 461–466. https://doi.org/10.1007/s00253-011-3751-z

Wickham, H., Chang, W., Henry, L., Pedersen, T.L., Takahashi, K., Wilke, C., Woo, K., Yutani, H., Dunnington, D., 2016. ggplot2: Create Elegant Data Visualisations Using the Grammar of Graphics version 3.3.0.

Wickham, H., Francois, R., Henry, L., Müller, K., 2015. dplyr: A Grammar of Data Manipulation version 0.8.5.

Willems, A., Collins, M.D., 1996. Phylogenetic relationships of the genera Acetobacterium and Eubacterium sensu stricto and reclassification of Eubacterium alactolyticum as Pseudoramibacter alactolyticus gen. nov., comb. nov. Int. J. Syst. Bacteriol. 46, 1083–1087. https://doi.org/10.1099/00207713-46-4-1083

Wu, Q., Bao, X., Guo, W., Wang, B., Li, Y., Luo, H., Wang, H., Ren, N., 2019. Medium chain carboxylic acids production from waste biomass: Current advances and perspectives. Biotechnol. Adv. 37, 599–615. https://doi.org/10.1016/j.biotechadv.2019.03.003

Wu, S.L., Sun, J., Chen, X., Wei, W., Song, L., Dai, X., Ni, B.J., 2020. Unveiling the mechanisms of medium-chain fatty acid production from waste activated sludge alkaline fermentation liquor through physiological, thermodynamic and metagenomic investigations. Water Res. 169, 115218. https://doi.org/10.1016/j.watres.2019.115218

Xu, J., Guzman, J.J.L., Andersen, S.J., Rabaey, K., Angenent, L.T., 2015. In-line and selective phase separation of medium-chain carboxylic acids using membrane electrolysis. Chem. Commun. 51, 6847–6850. https://doi.org/10.1039/C5CC01897H

Xu, J., Hao, J., Juan, J.L., Spirito, C.M., Harroff, L.A., Largus, T., Xu, J., Hao, J., Guzman, J.J.L., Spirito, C.M., Harroff, L.A., 2018. Temperature-Phased Conversion of Acid Whey Waste Into Medium-Chain Carboxylic Acids via Lactic Acid : No External e-Donor. Joule 1–16. https://doi.org/10.1016/j.joule.2017.11.008

Yang, P., Leng, L., Tan, G.Y.A., Dong, C., Leu, S.Y., Chen, W.H., Lee, P.H., 2018. Upgrading lignocellulosic ethanol for caproate production via chain elongation fermentation. Int. Biodeterior. Biodegrad. 135, 103–109. https://doi.org/10.1016/j.ibiod.2018.09.011

Chapter 3

Effect of Methanogenic Inhibitor on Competitive Reactions During Ethanol Chain Elongation

Shilva Shrestha, Siqi Xue, Lutgarde Raskin

Department of Civil and Environmental Engineering, University of Michigan, Ann Arbor, Michigan 48109, USA

3.1 Abstract

Organic waste streams can be converted into high value platform chemicals such as medium chain carboxylic acids (MCCAs) using mixed microbial communities via chain elongation. However, the heterogeneity of waste streams and the use of complex microbial communities can lead to undesirable reactions thus decreasing process efficiency. Our previous work demonstrated the feasibility of producing MCCAs by combining pre-treated food waste with high concentrations of short chain carboxylic acids and brewery waste containing ethanol. However, we observed substantial undesirable ethanol oxidation to acetate. In the current study, we explored suppressing excessive ethanol oxidation to acetate (EEO) by increasing the hydrogen partial pressure (P_{H2}) through inhibition of hydrogenotrophic methanogens by adding the methanogen inhibitor, 2-bromoethylsulfonate (2-BES). While 2-BES addition initially reduced EEO, some methanogens (*Methanobrevibacter* spp.) persisted and resistant populations were selected over time. Besides changing the methanogenic community structure, 2-BES also changed the bacterial community structure mostly due to its impact on the P_{H2}, thus affecting the bacterial populations involved in EEO. While we demonstrated that P_{H2} can be manipulated using 2-BES to control EEO, methods

that do not require the addition of a chemical inhibitor should be explored to maintain optimum P_{H2} for long-term suppression of EEO.

3.2 Introduction

Chain elongation of short chain carboxylic acids (SCCAs) is an emerging anaerobic biotechnology for the production of medium chain carboxylic acids (MCCAs). It involves the stepwise elongation of the carbon chain of SCCAs to MCCAs by two carbons via the reverse β oxidation pathway (Angenent et al., 2016). The two-carbon acetyl group added to SCCAs is derived from ethanol, lactate, or other reduced compounds. MCCAs are saturated fatty acids with chain lengths from six to twelve carbons and include one carboxyl group. MCCAs have many industrial and agricultural applications. MCCAs can be converted into longer chain liquid fuels or used directly as livestock feed additives, antimicrobial agents, corrosion inhibitors, and plant growth promoters, or as building blocks for the production of lubricants, fragrances, and dyes (Angenent et al., 2016).

The field of waste management has been preparing for a paradigm shift involving a transitioning from landfill disposal and incineration to utilizing sustainable biotechnologies to recover biofuels and biochemicals from waste streams. The production of MCCAs from waste streams using mixed microbial communities via chain elongation has been demonstrated by several studies (Duber et al., 2018; Ge et al., 2015; Grootscholten et al., 2014; Kucek et al., 2016b; Roghair et al., 2018b; Xu et al., 2018). One of the challenges of mixed culture fermentation of waste streams is to control competing biochemical pathways that have the potential to take place due to the high diversity of the microbial communities, their broad metabolic capacity, and the heterogeneity of most waste streams. Methanogenesis, sulfate reduction to sulfide, excessive ethanol oxidation to acetate, carboxylic acids oxidation, and the acrylate pathway (i.e., propionate formation from lactate during lactate mediated chain elongation) are some of the competing pathways that can affect chain elongation efficiency (Kucek et al., 2016a; Roghair et al., 2018a; Wu et al., 2019). In the ethanol-driven chain elongation process, for every six molecules of ethanol, one molecule of ethanol is anaerobically oxidized into acetate to harvest one ATP via substrate level phosphorylation (Angenent et al., 2016). Oxidation of ethanol to acetate at a proportion higher than one out of six molecules can occur along with the chain elongation process and has been termed excessive

ethanol oxidation (EEO) (Roghair et al., 2018a). It is important to suppress EEO to ensure efficient use of ethanol, especially if costly synthetic ethanol is used. Diversion of ethanol towards EEO can reduce the amount of acetyl-CoA available for chain elongation of SCCAs. Furthermore, acetate produced through EEO acidifies the medium leading to higher consumption of alkalinity. EEO can be beneficial when the acetate produced via EEO is subsequently used in chain elongation and is referred to as ethanol upgrading (Roghair et al., 2018a). However, ethanol upgrading leads to an inefficient use of ethanol (Roghair et al., 2018a). For example, ethanol upgrading to MCCAs via EEO consumes three moles of ethanol for every mole of caproate produced, whereas the reverse β oxidation pathway requires 2.4 moles of ethanol to elongate acetate to one mole of caproate.

EEO has been identified in several studies as an undesirable reaction (Grootscholten et al., 2014; Roghair et al., 2018a, 2018b), but an adequate control strategy has not been developed. Anaerobic ethanol oxidation to acetate has a positive standard Gibbs free energy of 49.6 kJ/mole reaction (Table B1, Eq B1, Appendix B). This reaction is energetically feasible only when the partial pressure of hydrogen (P_{H2}) is low. The need for hydrogen removal results in a syntrophic association between the hydrogen-producing ethanol oxidizers and hydrogenotrophic methanogens (Table B1, Eqs B1, B2, and B3, Appendix B) or other hydrogen consumers (Kirstine and Galbally, 2012). Some studies have limited EEO by controlling the CO_2 loading rate, a strategy that indirectly controls lowering of the P_{H2} via hydrogenotrophic methanogenesis by limiting CO_2 availability (Grootscholten et al., 2014; Roghair et al., 2018a). Another way to control EEO is to inhibit hydrogenotrophic methanogenesis by adding methanogenic inhibitors. The most widely used methanogenic inhibitor in a variety of applications is 2-bromoethanesulfonate (2-BES) (Liu et al., 2011), a structural analog of coenzyme M (CoM), the methyl carrier in the final step of methanogenesis. 2-BES and other methanogenic inhibitors have been used in previous chain elongation studies (Ganigué et al., 2016; Han et al., 2018; Liu et al., 2017, 2016; Lonkar et al., 2016; Steinbusch et al., 2011; Wu et al., 2018). However, these studies focused on the effect of such inhibitors on the suppression of methane production from acetate, thus preventing consumption of this MCCA precursor and giving a competitive advantage to chain elongating microorganisms. As 2-BES also inhibits hydrogenotrophic methanogenesis, it can influence

metabolic pathways affected by the P_{H2}. For example, a study conducted to investigate the effects of 2-BES and chloroform on anaerobic bacterial communities showed that the use of 2-BES affected the growth of syntrophic bacteria (e.g., *Syntrophomonas* and *Syntrophobacter*) and homoacetogenic bacteria (e.g., *Moorella*) due to accumulation of H_2 (Xu et al., 2010b). Similarly, it can be expected that EEO can be altered by 2-BES addition due to its inhibition of hydrogenotrophic methanogens and the subsequent thermodynamic inhibition caused by high P_{H2}.

This study evaluated the long-term effect of 2-BES addition on inhibiting EEO during chain elongation with pre-treated food waste and brewery waste as the substrates in a semi-continuous anaerobic bioreactor. The high cost of chemical additives could most likely increase the operating cost of MCCAs production making the addition of methanogenic inhibitors difficult to scale up, however, 2-BES was primarily added to evaluate the effect of P_{H2} on the EEO process in this study. The inhibition was evaluated by monitoring methane production, P_{H2}, ethanol consumption, and acetate production as well as evaluating changes in bacterial and archaeal population dynamics.

3.3 Materials & Methods

3.3.1 Experimental setup and operating conditions

A 7-L lab scale bioreactor with working volume of 5 L was operated semi-continuously as an anaerobic sequencing batch reactor (ASBR) on a 24-h cycle for 339 days. The bioreactor was temperature controlled at 40 ± 0.5 ^{o}C until Day 73 and at 37 ± 0.5 ^{o}C for the rest of the time period. The bioreactor pH was controlled at 5.5 ± 0.1 by automatic addition of 3-M NaOH (only during the react phase) with the help of LabVIEW. The biogas was collected in a 5-L Tedlar gas bag. Rumen content (17.1 ± 1.0 g volatile solids (VS) L^{-1}) collected from a fistulated cow from a dairy farm at Michigan State University (East Lansing, MI, USA) was used as an inoculum. The ASBR operational details are described in Chapter 2. A mixture of permeate extracted from an acidogenic bioreactor treating food waste (Fonoll et al., 2019) and waste beer containing ethanol was fed to the ASBR once a day. The influent was prepared once a week. Waste beer was obtained from Jolly Pumpkin Brewery (Dexter, MI), where it represents 2-19% of the total volumetric beer production (Doug Knox, personal communication). The sodium salt of 2-BES (Sigma Aldrich, St. Louis, MO)

was added to the bioreactor roughly every two weeks the first two times and every ten days (equivalent to three hydraulic retentions time (3 days)) after that on Days 230, 246, 259, 269, 278, 287, 296, 305, and 314 to reach a bioreactor concentration of 10 mM immediately after each addition. The 2-BES dose was selected based on literature values (Webster et al., 2016; Zhang et al., 2013). The change in 2-BES concentration over time was estimated using the initial concentration added, the volume of effluent wasted per day, and the bioreactor working volume. Thermodynamic calculations were performed to evaluate the feasibility of different reactions during the period 2-BES was added (details given in Appendix B, Section B1).

3.3.2 Chemical analyses

Samples for various chemical analyses were collected from the influent and bioreactor content once a week, and from the effluent two to three times a week. Soluble chemical oxygen demand (sCOD, measured after filtration with 0.45-µm nylon membrane filters (TISCH Scientific, North Bend, OH, USA)) analyses were conducted using Lovibond^{TM} medium-range (0-1500 mg L^{-1}) COD digestion vials (Tintometer, Germany). Gas volume was measured every day with a 0.1-L gas-tight glass syringe. Gas composition (H_2, CO_2, and CH_4) was determined two to three times a week using a Gow-Mac Series gas chromatography (Bethlehem, PA, USA) equipped with a thermal conductivity detector. P_{H2} was calculated by considering the hydrogen percentages in the gas and assuming that the headspace in the bioreactor was at atmospheric pressure. Carboxylic acids (C2 to C8, including iso-forms of C4 and C5) and ethanol concentrations were determined by Agilent Technologies 7890B gas chromatograph (Santa Clara, CA) equipped with a stabilwax-DA column (Restex) and a flame ionization detector (GC-FID). The samples were acidified with phosphoric acid, centrifuged, and filtered through the 0.45-µm nylon membrane filters before running them on the GC-FID. Detailed information on the gas chromatograph operating conditions and methods are given Chapter 2. The concentrations of SCCAs and MCCAs are reported as the sum of undissociated carboxylic acids and the dissociated carboxylates, even though we refer to them with their dissociated carboxylate names for simplicity. The concentrations of SCCAs (including acetate, propionate, n-butyrate, and n-valerate) and MCCAs (including caproate, enanthate, and caprylate) are expressed on a molar basis. To determine net acetate concentrations, the influent concentrations were subtracted from the corresponding effluent concentrations.

3.3.3 Microbial community analyses

Samples for biomass analyses were collected from the bioreactor effluent periodically for the specific days of biomass collection), pelletized, flash frozen on dry ice, and stored at -80^{o}C until DNA and RNA extractions. DNA extraction was carried out by using a CTAB method following the procedure outlined in Porebski et al. (1997) with an additional 1.5 min bead beating step (Mini-Beadbeater-96, BioSpec Products, Bartlesville, OK, USA) using 0.1-mm diameter zirconium beads. RNA extraction was done using TRIzol reagent (Invitrogen, CA, USA) following the manufacturer's instructions with some modifications described in Chapter 2. RNA was converted to single stranded complementary DNA (cDNA) using the SuperScript® IV VILO cDNA synthesis kit (Invitrogen, Carlsbad, CA) according to the manufacturer's instructions. DNA and RNA were quantified using a Qubit 2.0 Fluorometer (Invitrogen, Life Technologies, CA, USA). The samples were submitted to the Microbial Systems Molecular Biology Laboratory (University of Michigan, Ann Arbor, MI, USA) for amplicon sequencing of V4 hypervariable region of the 16S rRNA gene. The PCR amplification was done using primers F515 and R806 (Caporaso et al., 2011) with the dual-index sequencing strategy (Kozich et al., 2013). Multiplexed amplicons were sequenced using the MiSeq Reagent Kit V2 (500 cycles) on the Illumina MiSeq platform (San Diego, CA, USA).

3.3.4 Sequencing data processing

The 16S rRNA and 16S rRNA gene sequences were processed with DADA2 v1.16 (Callahan et al., 2016) in R following the online tutorial (amplicon sequence variant (ASV) approach) and with mothur (version 1.42.0) (Schloss et al., 2009) following the MiSeq SOP (operational taxonomic unit (OTU) approach). For the ASV approach, quality filtering was done by trimming the forward and reverse reads to 240 and 200 bp, respectively, based on the read quality profiles. A maximum expected error of 2 was used to remove low-quality reads by setting truncQ to 2 followed by generating an error model for the data. Core sample inference algorithm was applied to infer true biological sequences with the pool=TRUE option to increase sensitivity to distinguish between sequencing error and real biological variation in the amplicon sequences that may be present at very low read counts across multiple samples thus allowing detection of rare taxa. The paired-end

reads were merged and non-target length sequences were removed from the sequence table followed by removal of chimeras. Finally, the sequences were taxonomically classified with the naïve Bayesian Classifier method against the Ribosomal Database Project (RDP, Version 16) database. A total of 1,323,208 reads and 3,480 ASVs were generated.

For the OTU approach, a total of 1,299,839 high quality reads and 7,229 OTUs were generated. The SILVA database (Release 132) was customized to align with the resulting set of sequences. The UCHIME algorithm was used to check for the presence of chimeras. The sequences were taxonomically classified to genus level using RDP database (Version 16) and clustered into OTUs using the average neighbor algorithm at 97% sequence similarity. The total and active microbial community were studied using 16S rRNA gene and 16S rRNA sequencing data, respectively. Singletons were removed for relative abundance and activity calculations using the OTU approach.

For phylogenetic analyses, representative 16S rRNA gene sequences obtained from DADA2, for the major methanogenic ASVs observed in the bioreactor, such as *Methanobrevibacter* ASVs 5, 12, 20, and 29 were used. The closest relatives of the *Methanobrevibacter* ASVs given by the BLAST query search were chosen as reference sequences. This also included 16S rRNA genes of methanogens previously identified to be involved in ethanol metabolism such as *Methanobrevibacter* sp. AbM4 (Weimar et al., 2017), *Methanofollis ethanolicus* (Imachi et al., 2009), *Methanogenium organophilum* (Widdel, 1986), and *Methanosphaera* sp. WGK6 (Hoedt et al., 2016). The 16S rRNA gene sequences of the reference sequences were downloaded from NCBI GenBank Database. The sequences were aligned and trimmed to have equal length by removing the overhangs on either side using MEGA7 (Kumar et al., 2016). The evolutionary distances were computed in MEGA7 using a maximum likelihood analysis of the aligned sequences. Bootstrap testing with 1,000 replicates was used to generate the final tree. The microbial data presented below are based on the ASV based approach unless stated otherwise; most of the OTU based results are provided in the SI.

3.3.5 Statistical analyses

Statistical analyses of microbial community data were performed using packages vegan (v.2.5-6) (Oksanen et al., 2019), phyloseq (v.1.30.0) (McMurdie and Holmes, 2013) dplyr (0.8.5) (Wickham et al., 2015), and ggplot2 (v.3.3.0) (Wickham et al., 2016) in R (v.3.6.1). Statistical significance between groups were identified using the Kruskal-Wallis test with Benjamini-Hochberg correction for multiple testing. The Pearson correlation coefficient was calculated to determine the correlation between the microbial populations and various carboxylates. DESeq2 (v.1.26.0) (Love et al., 2014) using the wald significance test was used to test differential abundance of ASVs between the bioreactor microbial community before and after 2-BES addition. Observed ASVs for richness, Shannon diversity index, and Pielou's evenness were calculated as alpha-diversity estimates using the vegan package in R. Nonmetric multidimensional scaling (NMDS) plots were made using Bray-Curtis dissimilarity matrix as implemented in the vegan package. The statistical difference in microbial community structure before and after 2-BES addition was tested with analysis of similarities (ANOSIM) with 999 permutations. The contribution of individual ASVs to overall community dissimilarity due to 2-BES addition was determined using SIMPER as implemented in vegan.

3.4 Results and Discussion

3.4.1 2-BES temporarily suppressed excessive ethanol oxidation to acetate

The bioreactor performance is described in detail in Chapter 2. On average, MCCAs were produced at a rate of 4.4 ± 1.6 mmole L^{-1} d^{-1} with a maximum volumetric production rate of 9.1 mmole L^{-1} d^{-1} (Figure B.1, Appendix B). Caproate was the major MCCAs produced comprising 62.7 ± 8.7 % (on a carbon basis) of the total MCCAs, while enanthate and caprylate constituted on average 30.5 ± 8.5 % and 6.8 ± 3.7 % of the total MCCAs produced, respectively. Neither ethanol nor SCCAs were completely consumed suggesting that their concentrations were not limiting. Ethanol, constituting on average 75% of the total influent COD, was oxidized to acetate, which accumulated in the system reaching a maximum concentration of 156.6 mM on Day 9 (Figure 3.1). Acetate was not further elongated into MCCAs despite sufficient ethanol remaining in the system.

Roghair et al. (2018a) demonstrated that acetate derived from EEO can be involved in chain elongation, so it is unclear why acetate continued to accumulate in the current study.

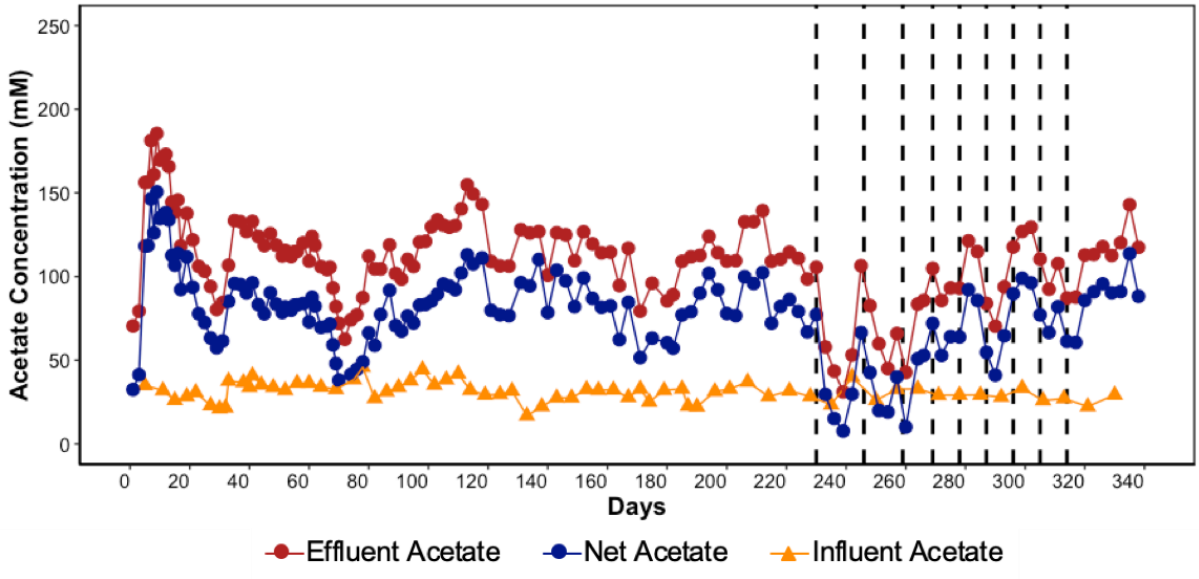

Figure 3.1. Effluent acetate, net acetate, and influent acetate concentrations over time. The dashed lines represent 2-BES additions.

Since EEO becomes thermodynamically unfavorable at high P_{H2} (Grootscholten et al., 2014), 2-BES was added in an attempt to suppress hydrogen consuming methanogens and thus inhibit ethanol oxidation. P_{H2} in the bioreactor headspace averaged 2.7E-03 ± 2.9E-03 atm from Days 0-229 (before 2-BES addition). This P_{H2} is still higher than the P_{H2} required for SCCAs (1.45 E-04 atm for acetate, 6.65E-06 atm for butyrate) and MCCAs (2.52E-06 for caproate) oxidation via β oxidation (Ge et al., 2015). The observed increase in P_{H2} to levels as high as 0.44 atm on Day 251 (Figure 3.2a) after 2-BES addition suggested that hydrogen consumption by hydrogenotrophic methanogens was inhibited. This increase in P_{H2} made EEO thermodynamically unfavorable leading to a decrease in acetate concentrations and a decrease in the amount of ethanol consumed (Figure 3.2a and b). MCCAs were consistently produced and their production did not appear to be affected negatively by these high P_{H2} (Figure B.1, Appendix B). These results demonstrated that chain elongation still happened at a P_{H2} sufficiently high to suppress EEO and that maintaining a certain P_{H2} in a chain elongation system may be an effective EEO control strategy.

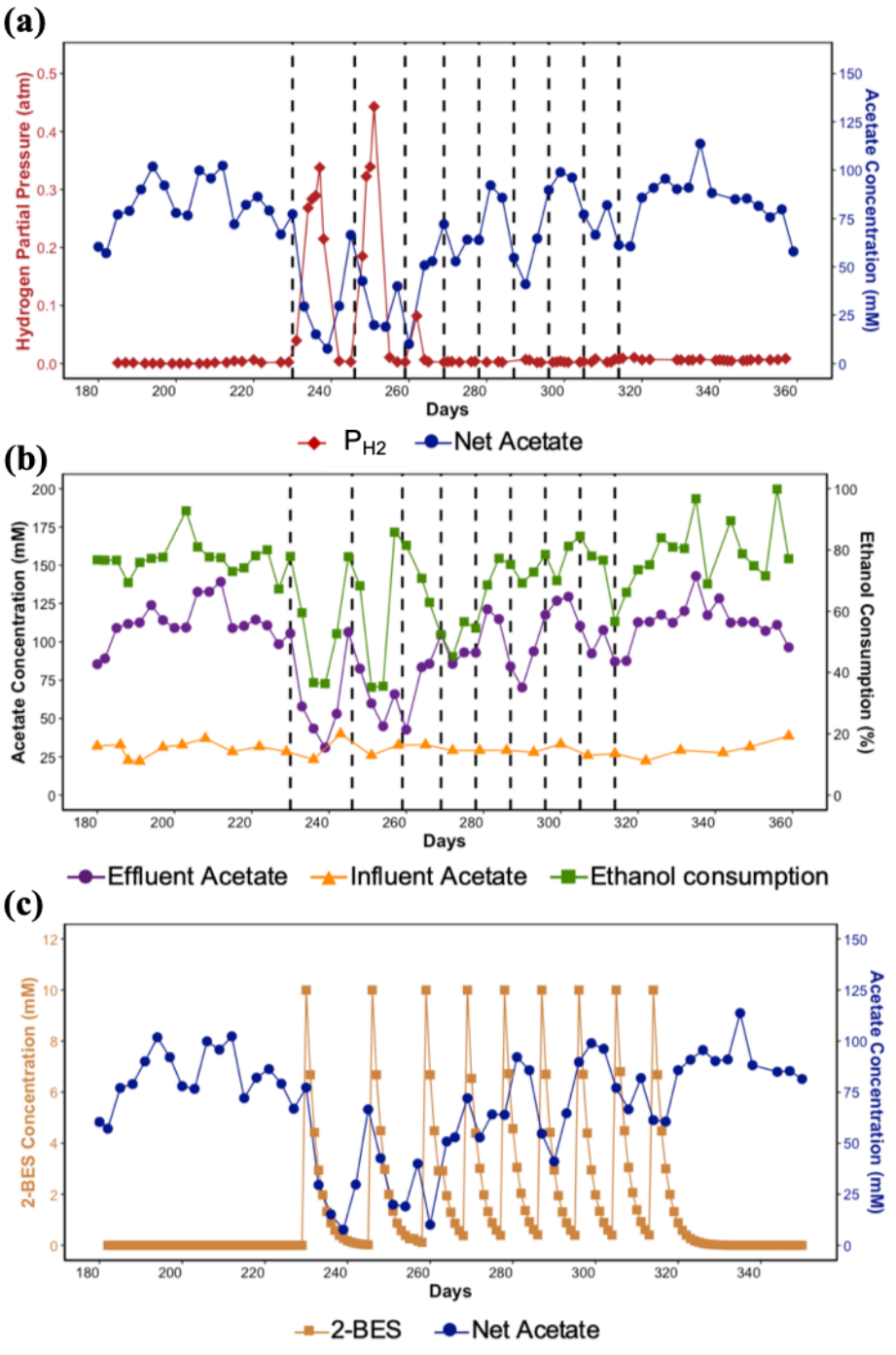

Figure 3.2. Net acetate concentration and hydrogen partial pressure (P_{H2}) (a) influent and effluent acetate concentrations and ethanol consumption (b), and theoretical 2-BES concentration profile and net acetate concentration (c) over time in the bioreactor. Ethanol consumption was calculated based on the concentration of ethanol initially present in the influent and that remaining in the

effluent. The dashed lines represent 2-BES addition (10 mM in the bioreactor) on Days 230, 246, 259, 269, 278, 287, 296, 305, and 314.

As 2-BES gradually washed out of the system (Figure 3.2c), the P_{H2} decreased and the net acetate concentration increased (Figure 3.2a) indicating reduced inhibition. The P_{H2} again increased after additional 2-BES was added with a corresponding reduction in the net acetate concentration. This trend continued until Day 268 after which the P_{H2} decreased despite six more 2-BES additions indicating that the 2-BES induced inhibition was short-lived. The P_{H2} significantly decreased ($p=6.78E-05$) from average values of 0.16 ± 0.15 atm from Days 230 to 268 to $4.6E-03 \pm 2.3E-03$ atm from Days 269 to 339. The corresponding net acetate concentrations also increased averaging 35.5 ± 21.9 mM and 78.3 ± 17.8 mM, respectively. While the average P_{H2} from Days 269 to 339 was slightly higher than the average P_{H2} before 2-BES addition had started, the P_{H2} was not high enough to suppress EEO. While Grootscholten et al. (2014) reported that a P_{H2} above 0.03 atm was sufficient to suppress EEO, our experimental results suggested that a P_{H2} higher than 0.02 atm was needed to prevent EEO. Besides P_{H2}, the thermodynamic feasibility of the EEO reaction is also affected by in-situ conditions such as pH and temperature. Theoretical thermodynamic calculations show that the higher pH of 6.5-7.0 used by Grootscholten et al. (2014), may explain the higher P_{H2} required for EEO inhibition in their study, compared to our study, which used a pH of 5.5; the small difference in temperature between the two studies did not have an impact (Figure B.2, Appendix B). There is little information available on the microorganisms responsible for EEO during chain elongation, so further work is needed to study how metabolic triggers for EEO play out for different populations.

3.4.2 *Methanobrevibacter* dominates despite addition of methanogenic inhibitor

More than one fifth ($22.0 \pm 5.2\%$) of the active microbial community was comprised of the phylum *Euryarchaeota* and was dominated by hydrogenotrophic methanogens. Aceticlastic methanogens were not detected indicating that they were inhibited by the low bioreactor pH of 5.5. Other studies have also shown that aceticlastic methanogens are more sensitive towards lower pH than hydrogenotrophic methanogens and may be inhibited to a greater extent by undissociated SCCAs and MCCAs (Ge et al., 2015). Results from both the 16S rRNA and 16S rRNA gene sequencing

indicated that *Methanobrevibacter* was the dominant methanogenic genus at each sampling time point (Figure 3.3). The relative activity of methanogens was higher than their relative abundance for each time point. Over the period from Day 0 to Day 229, i.e., before 2-BES addition, the relative abundance of *Methanobrevibacter* spp. averaged 9.6 ± 3.4% according to the 16S rRNA gene sequencing data, while their relative activity averaged 19.7 ± 5.7% as determined by 16S rRNA sequencing results. We used the RNA based approach to study the short-term changes in microbial activity induced by 2-BES. Even though using 16S rRNA sequence data to estimate activity has substantial biases (Blazewicz et al., 2013), our use of both 16S rRNA and 16S rRNA gene sequence data and comparing trends over time has provided insights into the microbial community responses to 2-BES additions.

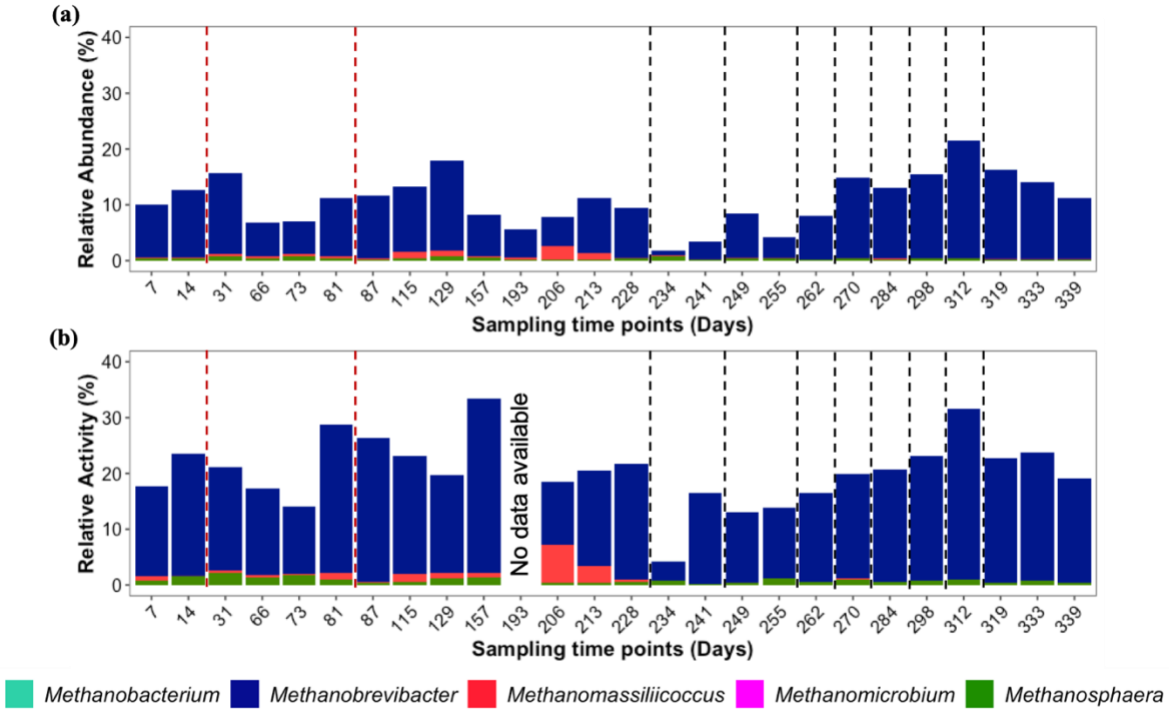

Figure 3.3. Relative abundance (a) and activity (b) of methanogens identified to the genus level in the bioreactor samples over time using the ASV based approach. The relative abundance and relative activity were determined as percentages of the total number of 16S rRNA gene sequences and 16S rRNA sequences, respectively. The red dashed lines represent start and end of wasting bioreactor content on Days 20 and 82, respectively, for controlling solids retention time and the black dashed lines represent 2-BES additions.

After the first 2-BES addition on Day 230, the relative abundance of methanogens decreased from 9.5% on Day 228 to 1.9% on Day 234 (Figure 3.3a). The decrease in relative activity was even more pronounced (from 21.8% on Day 228 to 4.1% on Day 234, Figure 3.3b). Similarly, the methane production decreased after 2-BES addition (Figure B.3, Appendix B). The average methane yield decreased significantly from 7.4 ± 2.4% to 5.3 ± 3.3% of the total sCOD fed (p=1.8E-03) after 2-BES addition (data not shown). The relative abundance of methanogens remained low for several weeks, but the relative activity of the methanogens increased substantially soon after the first 2-BES addition. These microbial data confirm that 2-BES was ineffective in inhibiting methanogens over time as suggested by the decrease in P_{H2} levels (Figure 3.2). These long-term trends are further supported by the finding that there was no significant change in the average relative abundance (p=0.744) and relative activity (p=0.23) of methanogens before and after the start of 2-BES addition on Day 230.

The archaeal diversity (both Shannon index and Pielou's evenness) and richness (observed ASVs) were compared before and after the start of 2-BES addition (Figure B4, Appendix B). The mean number of archaeal ASVs decreased significantly (p=1.6E-06) from 23 ± 5 to 12 ± 3 after 2-BES addition and a similar decrease was observed for the active archaeal ASVs (p=1.9E-02). The mean Shannon index and Pielou's evenness of the total and active archaeal community also consistently decreased after 2-BES addition, but the decrease was not always statistically significant. The archaeal community structures based on both 16S rRNA gene and 16S rRNA sequencing distinctly differed before and after 2-BES addition as shown by the Bray-Curtis dissimilarity analysis (Figure B5, Appendix B; 78% and 71% dissimilarity, respectively). High ANOSIM R values of 0.69 (p=0.001) and 0.47 (p=0.001) also indicated significant changes in archaeal community structures due to 2-BES addition.

Regardless of the effectiveness of 2-BES addition, it could be argued that inhibiting methanogens may not be sufficient to control the P_{H2} as there are other hydrogen sinks besides hydrogenotrophic methanogenesis in anaerobic processes. For example, hydrogen can be used by sulfate-reducing microorganisms or for acetate production by homoacetogens. While sulfate was not detected in the influent (data not reported), the sulfonate moiety of 2-BES can also serve as an electron

acceptor for sulfate-reducing bacteria and thus can support their growth (Lie et al., 1999). However, sulfate-reducing bacteria (e.g., *Desulfovibrio* spp.) were present at a relative abundance and activity of less than 0.1% both before and after 2-BES addition. Similarly, homoacetogenesis was not observed in the bioreactor (discussed in detail below). Since the P_{H2} increased with a simultaneous decrease in methane production (Figure B.3, Appendix B) and relative abundance and activity of methanogens (Figure 3.3) after the first few 2-BES additions, methanogenesis appeared to be the major pathway for hydrogen consumption and directly affected EEO. As 2-BES inhibition was short-lived, the low P_{H2} in the bioreactor in the later days again favored EEO.

3.4.3 Methanogens develop tolerance towards 2-BES

The effective inhibitory concentration of 2-BES can differ for different methanogens and environmental conditions (Liu et al., 2011). For example, aceticlastic methanogens are more susceptible to 2-BES inhibition than hydrogenotrophic methanogens (Webster et al., 2016; Xu et al., 2010a). Several studies have reported the presence of methanogens after the addition of 2-BES (Han et al., 2018; Liu et al., 2017), which may be due to differences in cell envelopes resulting in varying ability to uptake inhibitors as well as differences in CoM transport rates (Liu et al., 2011). Some methanogens can become adapted to 2-BES through a loss of cell permeability to 2-BES and selection of 2-BES resistant strains (Smith, 1983).

2-BES is a structural analog of CoM, the methyl carrier in the final step of methanogenesis, which catalyzes the reduction of the methyl group to methane by methyl CoM reductase (Liu et al., 2011). Methanogens that are able to synthesize CoM do not depend on external CoM and likely are more resistant to 2-BES (Balch and Wolfe, 1979). *Methanobrevibacter ruminantium* M1 requires an external source of CoM for growth, while *Methanobrevibacter smithii* can synthesize CoM (Stewart et al., 1975; Ungerfeld et al., 2004). 16S rRNA gene and 16S rRNA sequencing results showed that *Methanobrevibacter* spp. represented the highest fraction of the total and active archaeal community throughout the period with 2-BES addition (Figure 3.3), which suggests that they were able to synthesize CoM making them resistant to 2-BES.

As discussed in Chapter 2 and shown in Figure 3.4, different *Methanobrevibacter* populations were prevalent during periods with different solids retention times (SRTs). Specifically, *Methanobrevibacter* ASV 5 became more prevalent after the SRT was reduced on Day 20, while the relative abundance and activity of *Methanobrevibacter* ASV 20 and *Methanobrevibacter* ASV 12 dropped (Figure 3.4). These results suggest that ASV 5 has a higher growth rate than other *Methanobrevibacter* populations, allowing its growth and retention in the system when operated at a short SRT. ASV 5 was replaced by ASV 12 and ASV 20 when the SRT was increased again on Day 82. ASV 5 reappeared after 2-BES was added (Figure 3.4) suggesting that the higher growth rate of this population combined with the likely ability to synthesize CoM conferred resistance towards 2-BES and allowed its growth, while ASV 12 and ASV 20 were inhibited. In addition to ASV 5, *Methanobrevibacter* ASV 29 appeared to be resistant to 2-BES (Figure 3.4). ASV 29, which was not detected or observed at a very low relative abundance (<1%) and activity (<0.1%) before 2-BES addition, started appearing after Day 230 when 2-BES addition started. The relative abundance and activity of ASV 29 increased from $0.8 \pm 0.6\%$ and $1.9 \pm 1.5\%$ during Days 234-262 to $6.9 \pm 2.8\%$ and $4.7 \pm 1.0\%$ during Days 270-339, respectively. This increase in relative abundance and activity of ASV 29 aligns with the observation that P_{H2} remained low despite frequent 2-BES additions (Figure 3.2) showing decreased inhibition of some methanogens. The SIMPER analysis also shows that ASVs 5, 12, 20, and 29 contributed to most of the differences (>63%) observed between the active archaeal community before and after 2-BES addition (Figure B.5b, Appendix B). Therefore, periodic addition of 2-BES likely provided a selective pressure to allow a 2-BES resistant strain of *Methanobrevibacter* to become abundant over time.

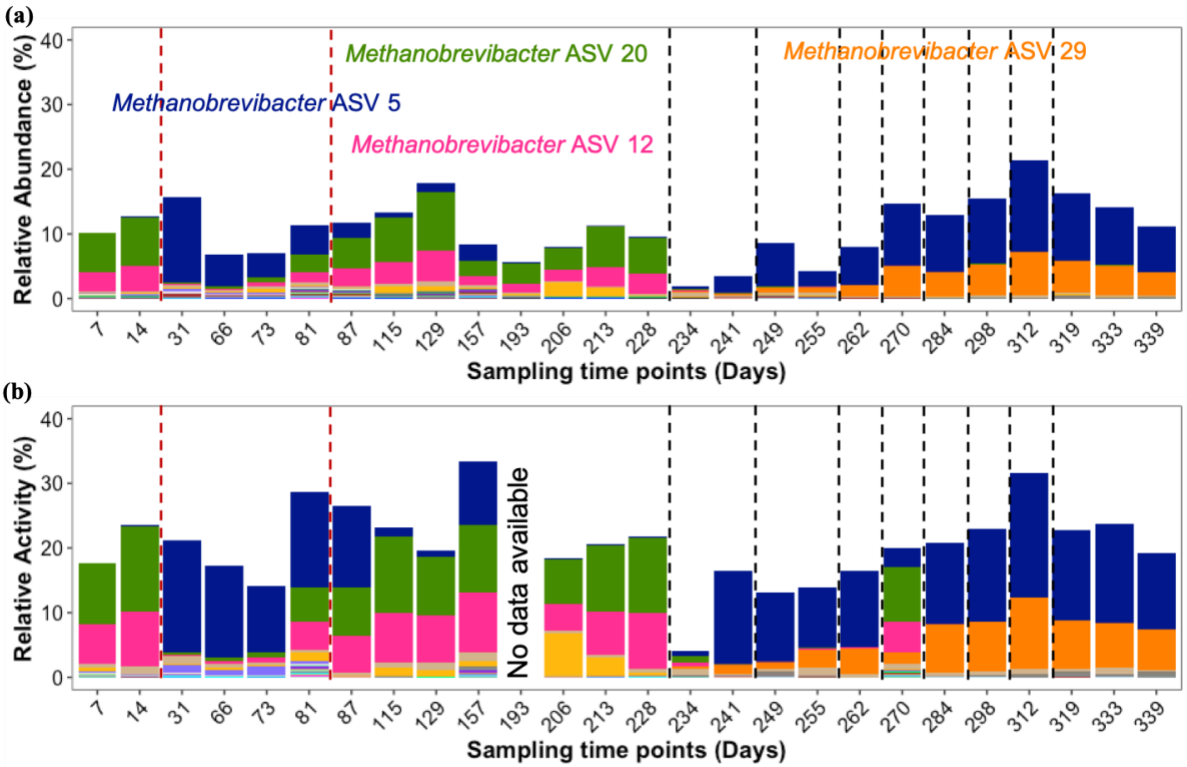

Figure 3.4. Relative abundance (a) and activity (b) of methanogens ASVs in the bioreactor samples over time. The key ASVs discussed in the paper are labeled. The relative abundance and relative activity were determined as percentages normalized to the total number of 16S rRNA gene sequences and 16S rRNA sequences, respectively. The red dashed lines represent start and end of bioreactor content wasting on Days 20 and 82, respectively, for controlling solids retention time (Chapter 2) and the black dashed lines represent 2-BES additions.

The sequence data were also analyzed with an OTU based approach using mothur (Figure B.6 and Figure B.7, Appendix B). Both OTU and ASV based approaches produced similar results for relative abundance and relative activity (Figure 3.3 vs. Figure B.6 and Figure 3.4 vs. Figure B.7, Appendix B). However, the OTU method indicated that *Methanobrevibacter* OTU 6 was the primary population able to grow in the presence of 2-BES and was also dominant during the shorter SRT period (Days 20-81) (Figure B.7, Appendix B), in contrast to the ASV method, which indicated that two major *Methanobrevibacter* populations (ASVs 5 and 29) became dominant after 2-BES addition. The comparison of the two methods confirms that the ASV method is better suited for differentiating sequence variants down to a single nucleotide difference, thus providing improved taxonomic resolution (Callahan et al., 2017). The OTU approach clusters 16S rRNA

gene sequences with 97% similarity into the same OTU and representative OTU sequences are compared with sequences in a reference database for taxonomic identification. The increased resolution provided by the ASV based approach captured changes in methanogen community in response to the 2-BES inhibition not picked up by the OTU based approach. At the same time, the ASV method has some disadvantages, including the inability to effectively discriminate between PCR bias or sequencing error and real biological variation. Moreover, many microorganisms harbor multiple *rrn* operons and the 16S rRNA gene sequence diversity increases with increasing *rrn* operon copy numbers (Větrovský and Baldrian, 2013). In the case of intragenomic heterogeneity, multiple ASVs can arise from a single population harboring multiple rRNA gene copies leading to more ASVs than populations present in a community (Callahan et al., 2017; Sun et al., 2013). *Methanobrevibacter* spp. have two or three 16S rRNA gene copies and intragenomic sequence variation could lead to multiple ASVs from the same *Methanobrevibacter* population (Klappenbach et al., 2001). So, it is possible that DADA2 assigned divergent copies of the 16S rRNA gene that belonged to one *Methanobrevibacter* population into ASV 5 and ASV 29. Comparing metagenomes before and after 2-BES addition would resolve this uncertainty, but this analysis is beyond the scope of this study.

3.4.4 Acetate production in the bioreactor

The high relative abundance and activity of *Methanobrevibacter* populations indicated that a favorable ecological niche was created that supported their growth and activity even at low pH and during exposure to 2-BES. Some studies have pointed towards the versatility of methanogens in substrate utilization for methanogenesis. For example, alcohols such as ethanol can be utilized for growth and methane production (Berk and Thauer, 1997; Metje and Frenzel, 2005; Poehlein et al., 2018). Bryant et al. (1967) found a syntrophic association between a H_2 producing ethanol oxidizer and a H_2 utilizing microorganism, such that ethanol oxidation was coupled with interspecies hydrogen transfer for methane production. Some studies have reported that species of methanogens such as *M. ethanolicus* and *M. organophilum* can directly convert ethanol to methane and acetate (Imachi et al., 2009; Widdel, 1986). Two moles of ethanol were oxidized to two moles of acetate for every moles of methane formed (Table B.1, Eq B4, Appendix B).

A phylogenetic analysis showed that the dominant *Methanobrevibacter* populations, ASVs 5 and 29 clustered with *Methanobrevibacter wolinii* strain SH, ASV 20 with *Methanobrevibacter boviskoreani* JH1, and ASV 12 with *Methanobrevibacter* sp. AbM4 (Figure 3.5). *Methanobrevibacter* strains such as *M. wolinii* strain DSM 11976^T and *M. boviskoreani* strain DSM 25824^T have been shown to have the genes to utilize ethanol for methanogenesis (Poehlein et al., 2018). ASV 12 clustered with *Methanobrevibacter* sp. AbM4, which has been reported to be capable of growth without H_2 but in presence of methanol/ethanol (Weimar et al., 2017). Figure 3.5 shows that *Methanobrevibacter* ASVs were also phylogenetically closely related to *Methanosphaera* sp. WGK6, ethanol oxidizers found in macropodids (Hoedt et al., 2016). While these results suggest involvement of methanogens in ethanol metabolism, we have no direct evidence to verify the role of *Methanobrevibacter* in EEO observed in our bioreactor. Future research should focus on using quantitative PCR and/or multi-omics tools to retrieve genome-level information to confirm the presence of specific genes involved in the EEO metabolic pathway.

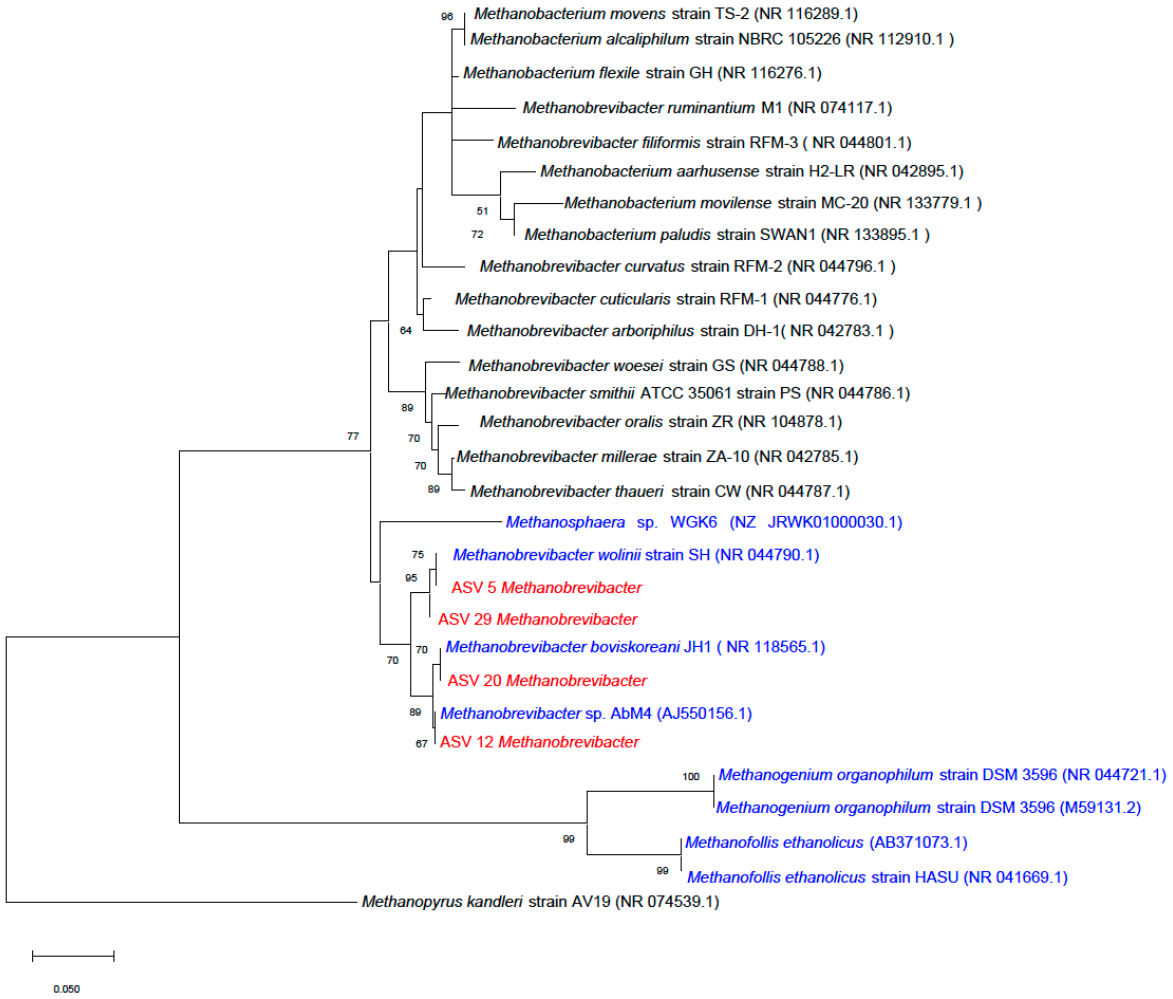

Figure 3.5. Phylogenetic tree of 16S rRNA gene sequence of most abundant methanogenic ASVs (in red). *Methanopyrus kandleri* was used as the outgroup. The GenBank accession numbers are given in parentheses. The reference sequences are shown in black. Methanogens previously identified as ethanol oxidizers or capable of growth in the presence of ethanol are shown in blue. The numbers at the nodes of the branch indicate bootstrap values. The scale bar of 0.05 represents 5% substitutions per nucleotide base pair.

Acetogens can also carry out ethanol oxidation by using CO_2 as an electron acceptor with no thermodynamic restriction (Table B.1, Eq B5, Appendix B). ASVs belonging to the genus *Acetobacter* were consistently present throughout bioreactor operation but at a low relative abundance (1.4 ± 1.2%) and relative activity (1.4 ± 1.4%). *Acetobacter* is a typical acetic acid bacteria characterized by its ability to convert ethanol to acetate in the presence of oxygen (Ghommidh et al., 1982). Acetic acid bacteria such as *Acetobacter* are thought to be strict aerobes,

however, their ability to use electron acceptors other than oxygen suggests that they may still show limited metabolic activity under anaerobic conditions (Jackson, 2008). Furthermore, the relative abundance and activity of *Acetobacter* was not significantly correlated to acetate production in the bioreactor, which further indicates the involvement of other microbial populations in EEO.

Homoacetogens can also produce acetate from CO_2 and H_2 (Table B.1, Eq B6, Appendix B), however, methanogens generally have a higher affinity for H_2 than homoacetogens making H_2 consumption by methanogenesis more competitive than reductive homoacetogeneis (Kotsyurbenko et al., 2001). Unclassified *Eubacteriaceae* ASV that shared 98% similarity with *Eubacterium aggregans*, a homoacetogenic bacterium (Mechichi et al., 1998), was observed at a very low relative abundance and relative activity of less than 0.01%. Other homoacetogens such as *Acetobacterium (A. carbinolicum* (Eichler and Schink, 1984)) that can combine ethanol oxidation to acetate with concomitant formation of acetate from carbon dioxide, were not observed in the bioreactor. Furthermore, the actual Gibbs free energy of hydrogenotrophic methanogenesis was exergonic over the bioreactor operating period, whereas homoacetogenesis was endergonic for part of the operating time (Figure B.8, Appendix B). Moreover, hydrogenotrophic methanogenesis was thermodynamically more favorable than H_2 oxidation by homoacetogens for the complete operating period (Figure B8, Appendix B), which explains the low relative abundance and activity of homoacetogens. If 2-BES had favored homoacetogens, the acetate yield should have been improved. However, net acetate production decreased after 2-BES addition showing that acetate production via homoacetogenesis was not feasible under the bioreactor conditions. These observations confirm that syntrophic ethanol oxidation to acetate (Table B.1, Eq B3, Appendix B), which is suppressed when H_2 is not consumed by methanogen, was the most favorable pathway for acetate production under the bioreactor conditions. However, identifying the microbial groups responsible for EEO was not possible within the scope of this study.

3.4.5 Effect of 2-BES inhibition on the bacterial community and chain elongation

Most of the methanogenic inhibitors are considered methanogen-specific, but some studies have provided evidence for bacterial community shifts during the use of inhibitors such as 2-BES (Webster et al., 2016; Xu et al., 2010b, 2010a). In a mixed culture system, inhibition of one group

can affect another metabolically associated group. The inhibition of hydrogenotrophic methanogens with 2-BES can lead to higher P_{H2}. Bacteria affected by P_{H2}, such as syntrophs, homoacetogens, and ethanol oxidizers, can thus indirectly be influenced by the use of methanogenic inhibitors. The use of 2-BES can affect the activity of syntrophs as H_2 consumption, for example, by methanogens make syntrophic reactions energetically favorable. However, commonly found syntrophs such as *Syntrophobacter*, *Syntrophomonas*, *Smithella* were not observed in the bioreactor. Homoacetogens have a competitive advantage at higher hydrogen concentration than methanogens. Therefore, H_2 accumulation due to inhibition of hydrogen consuming methanogen by 2-BES can favor reductive homoacetogenesis. ASVs belonging to unclassified *Eubacteriaceae,* with a functional role in homoacetogenesis started appearing after 2-BES addition, however, its relative abundance and relative activity were lower than 0.01%.

The total MCCAs production rate increased significantly from 4.6 ± 1.8 mmole L^{-1} d^{-1} to 5.5 ± 1.2 mmole L^{-1} d^{-1} after 2-BES addition (p=5.8E-03, Figure B.1, Appendix B). Specifically, chain elongation of even chain SCCAs was affected with significant increases in caproate and caprylate production rates. In contrast, chain elongation of odd chain SCCAs was not affected and the enanthate production was not significantly different before and after 2-BES addition. As reported in Chapter 2, the relative abundance and activity of OTUs belonging to *Pseudoramibacter* and *Clostridiales*_unclassified correlated positively with caproate (correlation coefficient=0.50, p=0.01) and heptanoate production (correlation coefficient=0.49, p=0.01). The relative abundance and relative activity of both *Pseudoramibacter* (p=9.0E-04 and p=3.5E-02) and *Clostridiales*_unclassified (p=6.7E-04 and p=6.5E-03) significantly increased after 2-BES addition. Members belonging to order *Clostridiales* and *Pseudoramibacter* have been associated with MCCAs production in some ethanol- and lactate-driven chain elongation studies (Agler et al., 2012; Kucek et al., 2016b; Scarborough et al., 2018). The ethanol consumption decreased (Figure 3.2b) after the addition of 2-BES led to inhibition of EEO. As ethanol was diverted from EEO, the higher availability of ethanol might have favored higher MCCAs production. At the same time, it is also possible that the microbial community got adapted to the MCCAs toxicity leading to higher MCCAs production over time.

The observed number of ASVs in the active bacterial community were similar (p=0.93) before and after 2-BES addition, however, the richness in the total bacterial community decreased significantly (p=3.1E-03) after 2-BES addition (Figure B.4c and B.4d, Appendix B). Furthermore, there was no significant difference in the diversity (Shannon diversity index) and evenness (Pielou's evenness) of the bacterial community due to 2-BES addition except for Pielou's evenness of the total bacterial community (p=1.2E-05, Figure B.4c and B.4d, Appendix B). The NMDS analysis based on both 16S rRNA gene (62% dissimilarity, Figure B.5c, Appendix B) and 16S rRNA sequencing (64% dissimilarity, Figure B.5d, Appendix B) data shows that the samples collected after 2-BES addition clustered closer to each other compared with the samples before 2-BES addition (ANOSIM R value=0.52, p=0.001 for DNA based data and ANOSIM R value=0.47, p=0.001 for RNA based data). The similarity of the bacterial community in terms of alpha diversity indicates similarity in community structure i.e similar number and abundance of taxa before and after 2-BES addition. The beta diversity analysis, however, shows differences in the bacterial community due to 2-BES addition, indicating a change in bacterial community composition. Differential abundance analysis using DESeq2 indicated that 139 and 76 bacterial ASVs showed a significant difference in relative abundance and activity (Table B.2, Appendix B), respectively, after 2-BES addition. Moreover, there was a distinct shift in some bacterial populations on the ASV level. For example, a shift to a different ASV belonging to *Acidaminococcus*, which is known to utilize amino acids forming acetate and butyrate (Rogosa, 1969), was observed after 2-BES addition. The relative abundance and activity of *Acidaminococcus* ASV 26 increased from 0.4 ± 1.0% and 0.7 ± 1.8% to 2.1 ± 1.0% and 4.3 ± 3.9%, respectively, after 2-BES addition, replacing *Acidaminococcus* ASV 9 (relative abundance and activity decreased from 3.0 ± 2.3% and 7.1 ± 5.7% to 0.2 ± 0.2% and 0.5 ± 0.5%, respectively). Therefore, 2-BES can have direct or indirect effects on the bacterial community.

3.5 Conclusions

While controlling competing metabolic processes such as EEO is challenging when heterogeneous waste streams are fed to a mixed community bioreactor, it is important to limit inefficient substrate usage and optimize MCCAs yield and selectivity. Hydrogenotrophic methanogenesis was the key

process leading to H_2 consumption as other H_2 sinks such as homoacetogenesis and sulfate reduction were limited under the bioreactor condition. The addition of the methanogenic inhibitor 2-BES limited the activity of hydrogen consuming methanogens and minimized EEO due to thermodynamic inhibition caused by high P_{H2}. We observed that EEO was limited under P_{H2} higher than 0.02 atm. However, the addition of the methanogenic inhibitor 2-BES did not provide long term-EEO suppression. The microbial community developed tolerance making 2-BES inhibition ineffective. *Methanobrevibacter* was dominant throughout the operational period, even under 2-BES inhibited condition. Future studies should evaluate the role of methanogens such as *Methanobrevibacter* during chain elongation. Lastly, future research is required to identify microbial populations involved in EEO and study its growth characteristics to devise alternate operational strategies to control EEO.

3.6 References

Agler, M.T., Spirito, C.M., Usack, J.G., Werner, J.J., Angenent, L.T., 2012. Chain elongation with reactor microbiomes: upgrading dilute ethanol to medium-chain carboxylates. Energy Environ. Sci. 5, 8189. https://doi.org/10.1039/c2ee22101b

Angenent, L.T., Richter, H., Buckel, W., Spirito, C.M., Steinbusch, K.J.J., Plugge, C.M., Strik, D.P.B.T.B., Grootscholten, T.I.M., Buisman, C.J.N., Hamelers, H.V.M., 2016. Chain Elongation with Reactor Microbiomes: Open-Culture Biotechnology to Produce Biochemicals. Environ. Sci. Technol. 50, 2796–2810. https://doi.org/10.1021/acs.est.5b04847

Balch, W.., Wolfe, R.., 1979. Transport of Coenzyme M (2-Mercaptoethanesulfomc Acid) in Methanobacterium ruminantium. J. Bacteriol. 137, 264–273.

Berk, H., Thauer, R.K., 1997. Function of coenzyme F 420 -dependent NADP reductase in methanogenic archaea containing an NADP-dependent alcohol dehydrogenase. Arch Microbiol 168, 396–402.

Blazewicz, S.J., Barnard, R.L., Daly, R.A., Firestone, M.K., 2013. Evaluating rRNA as an indicator of microbial activity in environmental communities: limitations and uses. ISME J. 7, 2061–2068. https://doi.org/10.1038/ismej.2013.102

Bryant, M.., Wolin, E.., Wolin, M.., Wolfe, R.., 1967. Methanobacillus omelianskii, a Symbiotic Association of Two Species of Bacteria*. Arch. ifir Mikrobiol. 59, 20–31.

Callahan, B.J., Mcmurdie, P.J., Holmes, S.P., 2017. Exact sequence variants should replace operational taxonomic units in marker-gene data analysis 11, 2639–2643.

https://doi.org/10.1038/ismej.2017.119

Callahan, B.J., McMurdie, P.J., Rosen, M.J., Han, A.W., Johnson, A.J.A., Holmes, S.P., 2016. DADA2: High-resolution sample inference from Illumina amplicon data. Nat. Methods 13, 581–583. https://doi.org/10.1038/nmeth.3869

Caporaso, J.G., Lauber, C.L., Walters, W.A., Berg-Lyons, D., Lozupone, C.A., Turnbaugh, P.J., Fierer, N., Knight, R., 2011. Global patterns of 16S rRNA diversity at a depth of millions of sequences per sample. Proc. Natl. Acad. Sci. U. S. A. 108 Suppl, 4516–22. https://doi.org/10.1073/pnas.1000080107

Duber, A., Jaroszynski, L., Zagrodnik, R., Chwialkowska, J., Juzwa, W., Ciesielski, S., Oleskowicz-Popiel, P., 2018. Exploiting the real wastewater potential for resource recovery-: N -caproate production from acid whey. Green Chem. 20, 3790–3803. https://doi.org/10.1039/c8gc01759j

Eichler, B., Schink, B., 1984. Oxidation of primary aliphatic alcohols by Acetobacterium carbinolicum sp. nov., a homoacetogenic anaerobe. Arch. Microbiol. 140, 147–152. https://doi.org/10.1007/BF00454917

Fonoll, X., Meuwissen, T., Aley, L., Shrestha, S., Raskin, L., 2019. The rumen membrane bioreactor: Transforming food waste into volatile fatty acids at the small scale, in: IWA 16th World Congress on Anaerobic Digestion.

Ganigué, R., Sánchez-Paredes, P., Bañeras, L., Colprim, J., 2016. Low fermentation pH is a trigger to alcohol production, but a killer to chain elongation. Front. Microbiol. 7, 1–11. https://doi.org/10.3389/fmicb.2016.00702

Ge, S., Usack, J.G., Spirito, C.M., Angenent, L.T., 2015. Long-Term *n* -Caproic Acid Production from Yeast-Fermentation Beer in an Anaerobic Bioreactor with Continuous Product Extraction. Environ. Sci. Technol. 49, 8012–8021. https://doi.org/10.1021/acs.est.5b00238

Ghommidh, C., Navarro, J.M., Durand, G., 1982. A study of acetic acid production by immobilized Acetobacter cells: Product inhibition effects. Biotechnol. Bioeng. 24, 605–617. https://doi.org/10.1002/bit.260240907

Grootscholten, T.I.M., Strik, D.P.B.T.B., Steinbusch, K.J.J., Buisman, C.J.N., Hamelers, H.V.M., 2014. Two-stage medium chain fatty acid (MCFA) production from municipal solid waste and ethanol. Appl. Energy 116, 223–229. https://doi.org/10.1016/j.apenergy.2013.11.061

Han, W., He, P.I. of a C.E.M., Shao, L., Lü, F., 2018. Metabolic Interactions of a Chain Elongation Microbiome. Appl. Environ. Microbiol. https://doi.org/10.1128/AEM.01614-18

Hoedt, E.C., Cuív, P., Evans, P.N., Smith, W.J.M., McSweeney, C.S., Denman, S.E., Morrison, M., 2016. Differences down-under: Alcohol-fueled methanogenesis by archaea present in

Australian macropodids. ISME J. 10, 2376–2388. https://doi.org/10.1038/ismej.2016.41

Imachi, H., Sakai, S., Nagai, H., Yamaguchi, T., Takai, K., 2009. Methanofollis ethanolicus sp. nov., an ethanol- utilizing methanogen isolated from a lotus field Hiroyuki. Int. J. Syst. Evol. Microbiol. 800–805. https://doi.org/10.1099/ijs.0.003731-0

Jackson, R., 2008. Postfermentation Treatments and Related Topics – Stabilization and Clarification, Wine Science Principles and Applications. https://doi.org/10.1016/B978-0-12-373646-8.50011-1

Kirstine, W. V, Galbally, I.E., 2012. Ethanol in the Environment : A Critical Review of Its Roles as a Natural Product , a Biofuel , and a Potential Environmental Pollutant Ethanol. Crit. Rev. Environ. Sci. Technol. 3389. https://doi.org/10.1080/10643389.2011.569874

Klappenbach, J.A., Saxman, P.R., Cole, J.R., Schmidt, T.M., 2001. rrndb: the Ribosomal RNA Operon Copy Number Database. Nucleic Acids Res. 29, 181–184. https://doi.org/10.1093/nar/29.1.181

Kotsyurbenko, O.R., Glagolev, M. V, Nozhevnikova, A.N., Y, R.C., 2001. Competition between homoacetogenic bacteria and methanogenic archaea for hydrogen at low temperature. FEMS Microbiol. Ecol. 38, 153–159.

Kozich, J.J., Westcott, S.L., Baxter, N.T., Highlander, S.K., Schloss, P.D., 2013. Development of a dual-index sequencing strategy and curation pipeline for analyzing amplicon sequence data on the miseq illumina sequencing platform. Appl. Environ. Microbiol. 79, 5112–5120. https://doi.org/10.1128/AEM.01043-13

Kucek, L., Nguyen, M., Angenent, L.T., 2016a. Conversion of L-lactate into n-caproate by a continuously fed reactor microbiome. Water Res. 93, 163–171. https://doi.org/10.1016/j.watres.2016.02.018

Kucek, L., Xu, J., Nguyen, M., Angenent, L.T., 2016b. Waste conversion into n-caprylate and n-caproate: resource recovery from wine lees using anaerobic reactor microbiomes and in-line extraction. Front. Microbiol. 7, 1–14. https://doi.org/10.3389/fmicb.2016.01892

Kumar, S., Stecher, G., Tamura, K., 2016. MEGA7: Molecular Evolutionary Genetics Analysis Version 7.0 for Bigger Datasets. Mol. Biol. Evol. 33, 1870–1874. https://doi.org/10.1093/molbev/msw054

Lie, T.J., Godchaux, W., Leadbetter, E.R., 1999. Sulfonates as terminal electron acceptors for growth of sulfite-reducing bacteria (Desulfitobacterium spp.) and sulfate-reducing bacteria: Effects of inhibitors of sulfidogenesis. Appl. Environ. Microbiol. 65, 4611–4617. https://doi.org/10.1128/AEM.66.6.2693-2693.2000

Liu, H., Wang, J., Wang, A., Chen, J., 2011. Chemical inhibitors of methanogenesis and putative

applications. Appl. Microbiol Biotechnol. 1333–1340. https://doi.org/10.1007/s00253-010-3066-5

Liu, Y., He, P., Shao, L., Zhang, H., Lü, F., 2017. Significant enhancement by biochar of caproate production via chain elongation. Water Res. 119, 150–159. https://doi.org/10.1016/j.watres.2017.04.050

Liu, Y., Lü, F., Shao, L., He, P., 2016. Alcohol-to-acid ratio and substrate concentration affect product structure in chain elongation reactions initiated by unacclimatized inoculum 218, 1140–1150. https://doi.org/10.1016/j.biortech.2016.07.067

Lonkar, S., Fu, Z., Holtzapple, M., 2016. Optimum alcohol concentration for chain elongation in mixed-culture fermentation of cellulosic substrate. Biotechnol. Bioeng. 113, 2597–2604. https://doi.org/10.1002/bit.26024

Love, M.I., Huber, W., Anders, S., 2014. Moderated estimation of fold change and dispersion for RNA-seq data with DESeq2. Genome Biol. 15, 1–21. https://doi.org/10.1186/s13059-014-0550-8

McMurdie, P.J., Holmes, S., 2013. Phyloseq: An R Package for Reproducible Interactive Analysis and Graphics of Microbiome Census Data. PLoS One 8. https://doi.org/10.1371/journal.pone.0061217

Mechichi, T., Labat, M., Woo, T.H.S., Thomas, P., Garcia, J.L., Patel, B.K.C., 1998. Eubacterium aggregans sp. nov., a new homoacetogenic bacterium from olive mill wastewater treatment digestor. Anaerobe 4, 283–291. https://doi.org/10.1006/anae.1998.0179

Metje, M., Frenzel, P., 2005. Effect of temperature on anaerobic ethanol oxidation and methanogenesis in acidic peat from a Northern Wetland. Appl. Environ. Microbiol. 71, 8191–8200. https://doi.org/10.1128/AEM.71.12.8191-8200.2005

Oksanen, J., Blanchet, F.G., Friendly, M., Kindt, R., Legendre, P., McGlinn, D., Minchin, P.R., O'Hara, R.B., Simpson, G.L., Solymos, P., Stevens, M.H.H., Szoecs, E., Wagner, H., 2019. Package 'vegan': Community Ecology Package. R Packag. version 2.5-6.

Poehlein, A., Schneider, D., Soh, M., Daniel, R., Seedorf, H., 2018. Comparative Genomic Analysis of Members of the Genera Methanosphaera and Methanobrevibacter Reveals Distinct Clades with Specific Potential Metabolic Functions 2018.

Porebski, S., Bailey, L.G., Baum, B.R., 1997. Modification of a CTAB DNA Extraction Protocol for Plants Containing High Polysaccharide and Polyphenol Components 15, 8–15.

Roghair, M., Hoogstad, T., Strik, D.P.B.T.B., Plugge, C.M., Timmers, P.H.A., Weusthuis, R.A., Bruins, M.E., Buisman, C.J.N., 2018a. Controlling Ethanol Use in Chain Elongation by CO2 Loading Rate. Environ. Sci. Technol. https://doi.org/10.1021/acs.est.7b04904

Roghair, M., Liu, Y., Strik, D.P.B.T.B., Weusthuis, R.A., Bruins, M.E., Buisman, and C.J.N., 2018b. Development of an Effective Chain Elongation Process From Acidified Food Waste and Ethanol Into n-Caproate. Front. Bioeng. Biotechnol. 6, 1–11. https://doi.org/10.3389/fbioe.2018.00050

Rogosa, M., 1969. Acidaminococcus gen. n., Acidaminococcus fermentans sp. n., Anaerobic Gram-negative Diplococci Using Amino Acids as the Sole Energy Source for Growth. J. Bacteriol. 98, 756–766.

Scarborough, M.J., Lynch, G., Dickson, M., McGee, M., Donohue, T.J., Noguera, D.R., 2018. Increasing the economic value of lignocellulosic stillage through medium-chain fatty acid production. Biotechnol. Biofuels 11, 1–17. https://doi.org/10.1186/s13068-018-1193-x

Schloss, P.D., Westcott, S.L., Ryabin, T., Hall, J.R., Hartmann, M., Hollister, E.B., Lesniewski, R.A., Oakley, B.B., Parks, D.H., Robinson, C.J., Sahl, J.W., Stres, B., Thallinger, G.G., Van Horn, D.J., Weber, C.F., 2009. Introducing mothur: Open-source, platform-independent, community-supported software for describing and comparing microbial communities. Appl. Environ. Microbiol. 75, 7537–7541. https://doi.org/10.1128/AEM.01541-09

Smith, M.R., 1983. Reversal of 2-Bromoethanesulfonate Inhibition of Methanogenesis in Methanosarcina sp . J. Bacteriol. 156, 516–523.

Steinbusch, K.J.J., Hamelers, H.V.M., Plugge, C.M., Buisman, C.J.N., 2011. Biological formation of caproate and caprylate from acetate: fuel and chemical production from low grade biomass. Energy Environ. Sci. 4, 216. https://doi.org/10.1039/c0ee00282h

Stewart, C.S., Flint, H.J., Bryant, M.P., 1975. The Rumen bacteria, The rumen microbial ecosystem. https://doi.org/10.1146/annurev.es.06.110175.000351

Sun, D.L., Jiang, X., Wu, Q.L., Zhou, N.Y., 2013. Intragenomic heterogeneity of 16S rRNA genes causes overestimation of prokaryotic diversity. Appl. Environ. Microbiol. 79, 5962–5969. https://doi.org/10.1128/AEM.01282-13

Ungerfeld, E.M., Rust, S.R., Boone, D.R., Liu, Y., 2004. Effects of several inhibitors on pure cultures of ruminal methanogens * 520–526. https://doi.org/10.1111/j.1365-2672.2004.02330.x

Větrovský, T., Baldrian, P., 2013. The Variability of the 16S rRNA Gene in Bacterial Genomes and Its Consequences for Bacterial Community Analyses. PLoS One 8, 1–10. https://doi.org/10.1371/journal.pone.0057923

Webster, T.M., Smith, A.L., Reddy, R.R., Pinto, A.J., Hayes, K.F., Raskin, L., 2016. Anaerobic microbial community response to methanogenic bromoethanesulfonate and propynoic acid. Microbiologyopen 537–550. https://doi.org/10.1002/mbo3.349

Weimar, M.R., Cheung, J., Dey, D., McSweeney, C., Morrison, M., Kobayashi, Y., Whitman,

W.B., Carbone, V., Schofield, L.R., Ronimus, R.S., Cooka, G.M., 2017. Development of multiwell-plate methods using pure cultures of methanogens to identify new inhibitors for suppressing ruminant methane emissions. Appl. Environ. Microbiol. 83, 1–8. https://doi.org/10.1128/AEM.00396-17

Wickham, H., Chang, W., Henry, L., Pedersen, T.L., Takahashi, K., Wilke, C., Woo, K., Yutani, H., Dunnington, D., 2016. ggplot2: Create Elegant Data Visualisations Using the Grammar of Graphics version 3.3.0.

Wickham, H., Francois, R., Henry, L., Müller, K., 2015. dplyr: A Grammar of Data Manipulation version 0.8.5.

Widdel, F., 1986. Growth of methanogenic bacteria in pure culture with 2-propanol and other alcohols as hydrogen donors. Appl. Environ. Microbiol. 51, 1056–1062. https://doi.org/10.1128/aem.51.5.1056-1062.1986

Wu, Q., Bao, X., Guo, W., Wang, B., Li, Y., Luo, H., Wang, H., 2019. Medium chain carboxylic acids production from waste biomass : Current advances and perspectives. Biotechnol. Adv. 1–17. https://doi.org/10.1016/j.biotechadv.2019.03.003

Wu, Q., Guo, W., Bao, X., Meng, X., Yin, R., Du, J., Zheng, H., Feng, X., Luo, H., Ren, N., 2018. Upgrading liquor-making wastewater into medium chain fatty acid: Insights into co-electron donors, key microflora, and energy harvest. Water Res. 145, 650–659. https://doi.org/10.1016/j.watres.2018.08.046

Xu, J., Hao, J., Juan, J.L., Spirito, C.M., Harroff, L.A., Largus, T., Xu, J., Hao, J., Guzman, J.J.L., Spirito, C.M., Harroff, L.A., 2018. Temperature-Phased Conversion of Acid Whey Waste Into Medium-Chain Carboxylic Acids via Lactic Acid : No External e-Donor. Joule 1–16. https://doi.org/10.1016/j.joule.2017.11.008

Xu, K., Liu, H., Chen, J., 2010a. Effect of classic methanogenic inhibitors on the quantity and diversity of archaeal community and the reductive homoacetogenic activity during the process of anaerobic sludge digestion. Bioresour. Technol. 101, 2600–2607. https://doi.org/10.1016/j.biortech.2009.10.059

Xu, K., Liu, H., Li, X., Chen, J., Wang, A., 2010b. Typical methanogenic inhibitors can considerably alter bacterial populations and affect the interaction between fatty acid degraders and homoacetogens 2267–2279. https://doi.org/10.1007/s00253-010-2708-y

Zhang, F., Ding, J., Zhang, Y., Chen, M., Ding, Z.W., van Loosdrecht, M.C.M., Zeng, R.J., 2013. Fatty acids production from hydrogen and carbon dioxide by mixed culture in the membrane biofilm reactor. Water Res. 47, 6122–6129. https://doi.org/10.1016/j.watres.2013.07.033

Chapter 4

Impact of Dynamic Membrane Development on Chain Elongation for Medium Chain Carboxylic Acid Production from Organic Waste Streams

Shilva Shrestha[1], Siqi Xue[1], Dianna Kitt[1], Hang Song[1], Caro Truyers[2], Maxim Muermans[2], Ilse Smets[2], Lutgarde Raskin[1]

[1]Department of Civil and Environmental Engineering, University of Michigan, Ann Arbor, Michigan, USA

[2]Department of Chemical Engineering, KU Leuven, Leuven, Belgium

4.1 Abstract

Medium chain carboxylic acids (MCCAs) can be produced from waste streams via chain elongation in mixed-culture bioreactors. A product recovery system is needed to recover MCCAs from the bioreactor effluent. Membrane based liquid-liquid extraction, the most commonly used approach, requires suspended solids removal from the bioreactor effluent to avoid membrane fouling. An anaerobic dynamic membrane bioreactor (AnDMBR) was developed to evaluate MCCA production from ethanol-rich brewery waste and pre-fermented food waste and to produce a permeate with low suspended solids. The AnDMBR system employed an inexpensive stainless-steel mesh as the support material for the development of a biological cake layer or dynamic membrane that accomplished solid-liquid separation. The AnDMBR produced a good permeate quality (mean ± standard deviation of 0.12 ± 0.06 g total suspended solids (TSS) L^{-1}), with a TSS concentration as low as 0.037 g L^{-1}. The average bioreactor TSS concentration during this period was two orders of magnitude higher (21.6 ± 9.9 g L^{-1}) than the permeate TSS. A maximum solids

removal efficiency of ≥ 99% was achieved and good permeate quality was sustained for over 200 days without fouling control and cleaning the support material. The relative activity, as determined by 16S rRNA sequencing, of unclassified *Clostridiales*, which correlated with MCCA production, was significantly higher in the biofilm than in the suspended biomass. This was consistent with MCCA performance data as the MCCA concentrations in the permeate were significantly higher than in the suspended bioreactor samples (p=8.2E-05), suggesting that the dynamic membrane biofilm contributed to chain elongation.

4.2 Introduction

Chain elongation is gaining increased attention due to its potential to convert diverse organic waste streams into high value products such as medium chain carboxylic acids (MCCAs) (Andersen et al., 2017; Angenent et al., 2016; Ge et al., 2015; Kucek et al., 2016c; Xu et al., 2018). MCCAs are platform chemicals that can be used in the production of lubricants, fragrances, dyes, and fuels, or directly used as livestock feed additives or antimicrobial agents (Angenent et al., 2016). Chain elongation involves step-wise elongation of the carbon chain of short chain carboxylic acids (SCCAs, C1-C5) into longer chain MCCAs (C6-C12), such as caproic acid (C6), enanthic acid (C7), and caprylic acid (C8) (Angenent et al., 2016). While mixed-culture chain elongation can be used to produce MCCAs, this process often also yields unconsumed precursors such as SCCAs and other soluble products that need to be removed. A product recovery system is thus required to obtain MCCAs in a useful form. When the bioreactor is operated under acidic conditions, most of the MCCAs are present in the undissociated form, resulting in inhibitory conditions for microorganisms (Angenent et al., 2016). Therefore, extracting MCCAs also helps to alleviate product toxicity. Since toxicity increases with MCCA carbon-chain length, continuous MCCA removal provides a selective advantage for the formation of the longest possible MCCAs (Angenent et al., 2018). Lastly, continuous removal of acidic products like MCCAs from the bioreactor reduces the amount of base needed for buffering.

Membrane-based liquid-liquid extraction (LLX, i.e., pertraction) is the most commonly used extraction approach in chain elongation studies (Ge et al., 2015; Kucek et al., 2016b, 2016a, 2016c; Urban et al., 2017; Xu et al., 2018). It is important to remove solids from the bioreactor effluent

prior to downstream extraction to avoid fouling of the membrane extraction system. Membrane fouling also increases mass transfer resistance and decreases extraction efficiency, as shown by Sitter et al. (2018). Most chain elongation systems use multiple external filters before the extraction step for solid-liquid separation (Kucek et al., 2016b, 2016a, 2016c; Urban et al., 2017; Xu et al., 2018). The use of external filtration steps leads to biomass loss from the chain elongation bioreactor and increases capital and operating costs. The use of a membrane bioreactor for MCCA production and simultaneous solids removal would make it possible to directly integrate MCCA production with downstream separation processes. Anaerobic membrane bioreactors (AnMBRs) using microfiltration or ultrafiltration membranes have been widely applied in wastewater treatment processes. However, they have several disadvantages, including low flux, high capital and operating costs, rapid membrane fouling, and high energy and chemical consumption for membrane cleaning (Ozgun et al., 2013; Smith et al., 2012). Anaerobic dynamic membrane bioreactors (AnDMBRs) have the potential to address some of these shortcomings. Operation of an AnDMBR depends on the in-situ formation of a biological cake layer, also referred to as a "dynamic membrane," layer, on a support surface to provide effective filtration (Ersahin et al., 2012; Hu et al., 2018; Zhang et al., 2014). Materials such as stainless steel meshes as well as woven and non-woven fabrics, with pore sizes typically ranging from 5-200 um, serve as the support for the development of the dynamic membrane. The dynamic membrane has a lower porosity than the support material, providing improved filtration (Ersahin et al., 2012; Hu et al., 2018). Low cost, high flux, ease of fouling control, and low energy requirements make AnDMBR a promising technology (Ersahin et al., 2012; Hu et al., 2018).

The versatility of AnDMBR systems has been demonstrated previously with diverse waste streams, including domestic wastewater, food waste, cheese whey wastewater, and landfill leachate, resulting in the production of biogas, lactic acid, and SCCAs (Cayetano et al., 2019; Liu et al., 2016; Paçal et al., 2019; Tang et al., 2017; Xie et al., 2014). Previous studies have demonstrated that AnDMBRs are able to produce permeate quality with total suspended solids (TSS) less than 10 mg L^{-1} (Ersahin et al., 2014, 2016a). With such efficient solids-liquid separation, AnDMBRs can produce a low particulate containing permeate that can be sent directly to a membrane-based extraction system, thus avoiding external filtration steps. The integration of

AnDMBRs with downstream extraction systems is expected to reduce cost and environmental impacts, as well as to decrease the physical footprint of current chain elongation bioreactor systems. Furthermore, biomass retention has been shown to result in a high conversion rate for MCCA production due to high microbial density as well as high resilience towards upsets (Carvajal-Arroyo et al., 2019; Roghair et al., 2016; Q. Wu et al., 2020). Biomass retention in chain elongation systems so far has been mediated by the use of granular sludge-based processes and cell immobilization on carrier materials in up-flow anaerobic filters (Carvajal-Arroyo et al., 2019; Grootscholten et al., 2013a, 2013b; Kucek et al., 2016b; Roghair et al., 2016; Q. Wu et al., 2020). The potential of AnDMBR for MCCA production with simultaneous suspended solids removal has not yet been explored.

A bench-scale AnDMBR equipped with flat sheet stainless steel meshes was developed to promote dynamic membrane formation for solids-liquid separation and for biomass retention. The bioreactor was operated with SCCA-rich permeate from a bioreactor treating food waste and ethanol-rich waste beer. The objectives of this study were to develop and evaluate the applicability of AnDMBR technology for MCCA production and effective solids-liquid separation. We evaluated the factors affecting its performance and characterized the contribution of the dynamic membrane biofilm in MCCA production.

4.3 Materials and Methods

4.3.1 Substrate and Inoculum

The bioreactor was inoculated with 5 L of rumen content (14.0 g volatile solids (VS) L^{-1}) collected from a fistulated cow at the Michigan State University dairy farm (East Lansing, MI, USA). The bioreactor influent was composed of waste beer and a SCCA-rich permeate collected from an acidogenic bioreactor treating food waste (Fonoll et al., 2019). The SCCA-rich permeate was left to settle overnight and the supernatant was used to prepare the influent in this study. Waste beer is a waste stream produced in breweries as a result of failure to meet quality standards, development of off flavors, improper fermentation or storage, and includes beer past its expiration date (Seluy and Isla, 2014). The waste beer contained 4-6% ethanol and was collected in three batches from the Jolly Pumpkin Brewery (Dexter, MI). In the influent, the ratio of SCCA-rich permeate to

ethanol-rich waste beer was determined by using the stoichiometric equations for chain elongation (4:1 for ethanol:acetate, 2.4:1 for ethanol:propionate, 1.2:1 ethanol:butyrate, and 1.2:1 ethanol:valerate) (Angenent et al., 2016). The characteristics of the inoculum, waste beer, and SCCA-rich permeate are provided in Table C.1, Appendix C. A mixture of 1.2 L of rumen content and 1.2 L of biomass (referred to as adapted chain elongation inoculum) from the chain elongation bioreactor operated in Chapter 2 was added on Day 175 to re-inoculate the bioreactor with the goal of recovering chain elongation activity. Malfunctioning of the base pump led to a high pH on Day 179. To address this potential concern, 0.3 L of rumen content and 0.3 L of biomass from the same chain elongation bioreactor were added to maintain bioreactor performance.

4.3.2 Bioreactor system and operating condition

A 7-L AnDMBR was equipped with three submerged rectangular membrane modules. Each module contained two flat sheet stainless steel meshes (TWP, Berkeley, CA) with an area of 0.0163 m^2 each resulting in a total effective filtration area of 0.0978 m^2. The bioreactor system included peristaltic pumps for feeding and permeation, which were remotely controlled using LabVIEW (National Instruments, Austin, TX) data acquisition software. The bioreactor was continually fed from a well-mixed and refrigerated influent reservoir. The bioreactor working volume was maintained at 4.8 L using a LabVIEW-controlled level sensor (Grainger, Lake Forest, Illinois) and the bioreactor contents were continuously stirred with an overhead impeller (Scilogex, Rocky Hill, CT). A 5-L Tedlar gas bag was connected to the bioreactor headspace for gas collection. The transmembrane pressure (TMP) of each membrane module was continuously recorded starting from Day 282 using pressure sensors (Ashcroft, Stratford, CT) and the LabVIEW data acquisition software. A schematic representation of the AnDMBR bioreactor is shown in Figure 4.1.

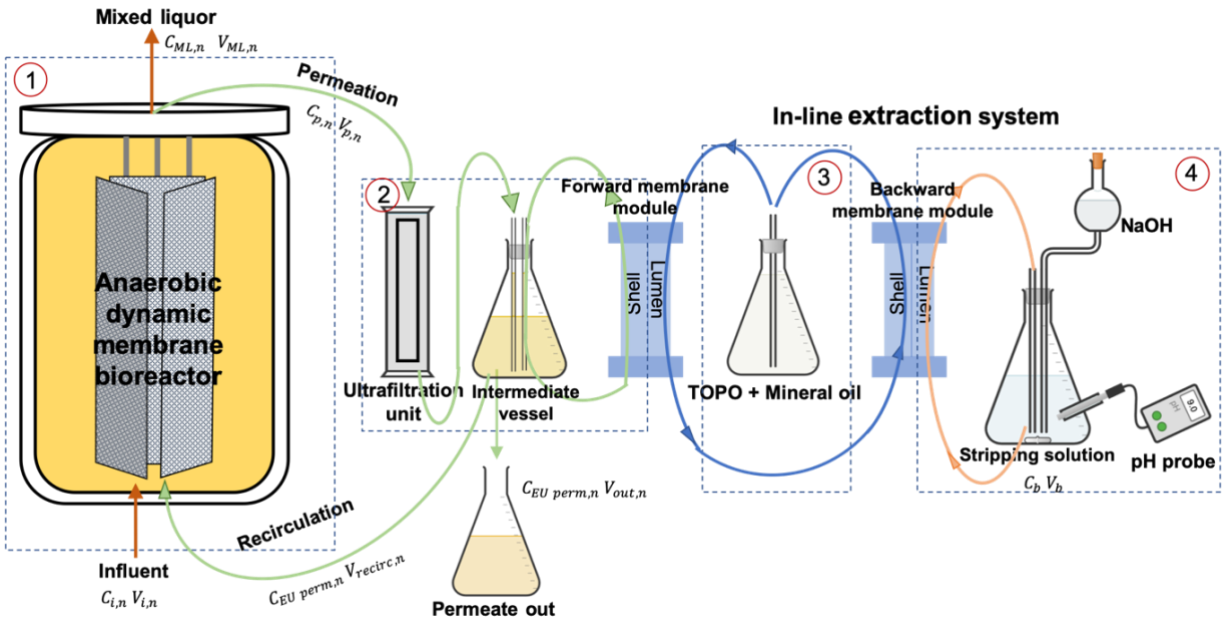

Figure 4.1. Schematic representation of the anaerobic dynamic membrane bioreactor integrated with an in-line MCCA extraction system labeled with different flows in and out of each unit process. 1, 2, 3, and 4 represent system boundaries for the mass balance calculation used in Eq C6 (Appendix C). The ultrafiltration unit was implemented on Day 245 as an additional barrier during instances of sloughing of the dynamic membrane layer.

The bioreactor was operated at 37°C and a pH of 5.5 was maintained by addition of 3 M NaOH controlled with LabVIEW. The hydraulic retention time (HRT) was maintained between 3 to 5 days and the organic loading rate (OLR) varied from 2.7 to 18.0 g soluble chemical oxygen demand (sCOD) L^{-1} d^{-1} over the course of the experiment (Figure C.1, Appendix C). The solids retention time (SRT) was calculated by considering the amount of biomass wasted through measuring the volatile suspended solids (VSS) in bioreactor samples (without considering attached biomass) and permeate.

The AnDMBR experimental time was divided into four phases based on operational changes (Table 4.1). In Phase 1 (Days 1-284), stainless steel meshes with a pore size of 25 µm were used as the support material with no fouling control until Day 274. The filtration mode was semi-continuous until Day 49 (Phase 1A, Days 1-49) with frequent backwashing after which it was switched to continuous filtration without backwashing (Phase 1B, Days 50-233). The TSS

concentration in the influent increased starting on Day 234 (Phase 1C, Days 234-284) due to an increase in the TSS concentration of the SCCAs-rich permeate. The meshes were removed from the bioreactor for chemical cleaning with 1 M NaOH solution on Day 274, but this did not recover membrane permeability indicating severe pore blockage of the meshes. Consequently, the 25-μm meshes were replaced with a new set of meshes in Phase 2 (Days 285-334). As the AnDMBR permeate TSS was still high, starting on Day 313 (Phase 2B, Days 313-334), the SCCA-rich permeate was centrifuged (10,000 x g for 10 min) and the supernatant was used to prepare the AnDMBR influent. To evaluate the effect of lower influent TSS with unfouled meshes, a new set of 25-μm meshes were used in Phase 3 (Days 335-364). In Phase 4 (Days 365-435), 5-μm meshes were incorporated in the membrane modules to compare performance for different mesh pore sizes. In the later part of Phase 4 (Phase 4B, Days 394-435), non-centrifuged SCCA-rich permeate was mixed with the supernatant of centrifuged SCCA-rich permeate at a ratio (v:v) of 30:70 (Days 393–421) and 15:85 (Days 422–435) to increase the TSS concentration in the influent.

Table 4.1 Summary of AnDMBR experimental phases, operating conditions, and performance

Phases	Phase 1			Phase 2		Phase 3	Phase 4	
	Phase 1A	Phase 1B	Phase 1C	Phase 2A	Phase 2B		Phase 4A	Phase 4B
Filtration mode	semi-continuous	continuous		continuous		continuous	continuous	
Mesh pore size		25 μm		25 μm		25 μm	5 μm	
Flux (L m^{-2} h^{-1})	N.A.	0.47 ± 0.07	0.62 ± 0.05	0.65 ± 0.05	0.62 ± 0.08	0.65 ± 0.05	0.55 ± 0.07	0.44 ± 0.15
Influent change			solids concentration increased		Centrifuged			Centrifuged+ non-centrifuged
Influent TSS (g L^{-1})	1.60 ± 0.51	3.08 ± 2.20	9.73 ± 2.72	10.23 ± 0.91	1.73 ± 0.86	1.50 ± 0.40	1.33 ± 0.39	3.29 ± 0.87
Reactor TSS (g L^{-1})	6.22 ± 3.39	18.17 ± 7.23	35.87 ± 3.86	29.67 ± 5.14	26.78 ± 8.70	12.17 ± 2.45	11.68 ± 1.85	19.13 ± 4.65
Permeate TSS (g L^{-1})	0.81 ± 0.52	0.11 ± 0.06	0.22 ± 0.15	0.41 ± 0.45	0.20 ± 0.15	0.85 ± 0.38	0.47 ± 0.14	0.17 ± 0.08
Permeate Turbidity (NTU)	554.17 ± 401.25	42.34 ± 62.85	80.75 ± 95.46	275.53 ± 681.14	36.15 ± 13.98	1693.90 ± 981.49	953.29 ± 978.23	73.06 ± 146.00
TSS removal (%)	55.8 ± 23.9	93.9 ± 5.7	97.8 ± 1.3	96.1 ± 4.3	85.0 ± 13.1	42.5 ± 31.7	61.8 ± 12.4	94.2 ± 2.7
Days	1 to 49	50-233	234-284	285-312	313-334		365-393	394-435
	1-284			285-334		335-364	365-435	

N.A. stands for not available

4.3.3 Pertraction system

The pertraction system consisted of two hollow-fiber, hydrophobic membrane contactors (Liqui-Cel EXF 2.5*8, X40) from 3M (Charlotte, NC, USA). The bioreactor permeate was passed through an ultrafiltration membrane (GE healthcare, PA, USA, 0.03 μm pore size, 0.53 m^2 membrane area), collected in an intermediate vessel, and recirculated through the shell side of the forward membrane contactor. The intermediate vessel (Figure 4.1) enabled permeate recirculation through the forward membrane at a higher flow rate of 140 L d^{-1} independent of the AnDMBR permeate flow rate from the AnDMBR side. A hydrophobic solvent consisting of mineral oil (Sigma Aldrich, St. Louis, MO, USA) and 30 g L^{-1} trioctylphosphine oxide (TOPO) was recirculated continuously through the lumen of the forward and backward membrane modules to selectively extract MCCAs. An alkaline stripping solution made up of sodium tetraborate and boric acid was used to back extract MCCAs from the hydrophobic solvent. The in-line extraction system was integrated with the bioreactor and operated from Days 245-270, Days 314-334, and Days 380-435 with some interruptions due to technical difficulties. During Days 380-435 of Phase 4, the bioreactor permeate was recirculated continuously at a flow rate of 3.6 ± 1.0 mL min^{-1} between the bioreactor and intermediate vessel while the permeate left the system at a flow rate of 0.8 ± 0.1 mL min^{-1} (Figure 4.1). Prior to integration with the AnDMBR system, pertraction system trials were run with a synthet.ic mixture of ethanol, SCCAs, and MCCAs to simulate operation with the real AnDMBR permeate. The trials included evaluating the extraction performance with and without TOPO in mineral oil (Section C1.1, Figure C.2, Table C.2, Appendix C) and the effectiveness of the LLX unit for MCCA recovery (Section C1.2, Figure C.3, Appendix C). Detailed information on the pertraction system and the trials is provided in Section C1 (Appendix C).

4.3.4 Chemical analyses

TSS, VSS, sCOD, and carboxylic acid, lactate, and ethanol concentrations were determined to evaluate the AnDMBR performance. The bioreactor permeate was sampled every three days and the bioreactor content (before filtration) and influent were sampled weekly. Inocula samples were collected at each inoculation event. We sampled the intermediate vessel permeate and alkaline

stripping solution on the same day of permeate sampling. TSS and VSS were determined according to Standard Methods (Eugene et al., 2012). Prior to analyses, liquid samples were pretreated with phosphoric acid for carboxylic acids measurements, with sodium hydroxide for lactate measurements, and with sulfuric acid for sCOD analysis, centrifuged, and filtered through 0.45-µm nylon membrane filters (TISCH Scientific, North Bend, OH, USA). sCOD analysis was performed using Lovibond^{TM} medium-range (0-1500 mg L^{-1}) COD digestion vials (Tintometer, Germany). Turbidity was measured with a turbidimeter (Hach 2100N, Loveland, CO, USA). Gas volume was measured daily with a gas-tight glass syringe. Gas composition was determined using a Gow-Mac Series gas chromatograph (Bethlehem, PA, USA) equipped with a thermal conductivity detector (TCD), as described in Chapter 2. Carboxylic acid concentrations from C2 to C8 (including iso-forms of C4 and C5) and ethanol were determined using an Agilent Technologies 7890B gas chromatograph (Santa Clara, CA) equipped with a stabilwax-DA column (Restex) and a flame ionization detector (Chapter 2). Lactate concentration was measured using an ion chromatograph (ICS-1600, Dionex, Sunnyvale, CA) equipped with a Dionex DX 100 conductivity detector. Carboxylic acid values are reported as total carboxylate (sum of dissociated carboxylate and undissociated carboxylic acids) unless stated otherwise.

4.3.5 Microbial analyses

Biomass samples were collected from the inoculum immediately before each inoculation event and from the influent, the bioreactor, and the biofilm at various points throughout the experimental period (Table C.3, Appendix C) for microbial analyses. Biofilm samples were taken by removing the membrane module from the bioreactor and scraping biofilm from the mesh surface using a sterile spatula. The biomass samples were centrifuged (10,000 x g for 10 min at 4^{o}C) and the pellet was flash frozen using ethanol and dry ice and stored at -80^{o}C. The cetyl trimethylammonium bromide (CTAB) method was used for DNA extraction as described by Porebski et al. (1997) with minor modifications (Chapter 2). RNA extraction was carried out using TRIzol reagent (Invitrogen, CA, USA) following the manufacturer's instructions with some modifications to include an RNA precipitation step using sodium acetate and ethanol (Chapter 2). Extracted DNA and RNA concentrations were determined using a Qubit 2.0 Fluorometer (Invitrogen, Life Technologies, CA, USA). RNA extracts were treated with DNAse followed by cDNA synthesis

as described in Chapter 2. cDNA and DNA samples were submitted for 16S rRNA and 16S rRNA gene sequencing, respectively, to the Microbial Systems Molecular Biology Laboratory (University of Michigan, Ann Arbor, MI, USA). The V4 region of the 16S rRNA gene was amplified using the primers set F515 and R806 (Caporaso et al., 2011), which were modified for dual-index sequencing as described by Kozich et al. (2013). The sequencing was performed on the Illumina MiSeq platform (San Diego, CA, USA) using the MiSeq Reagent Kit V2 500 cycles. The sequences were processed with DADA2 v1.16 (Callahan et al., 2016) in R (version 3.6.1) according to the online pipeline tutorial (Section C3, Appendix C3). A total of 2,741,368 high-quality reads were generated, which were assigned to 3,064 ASVs. The dominant ASVs or genera were defined as those ASVs or genera that were present at a relative abundance or relative activity of ≥ 1% in at least 50% of the samples.

4.3.6 Statistical analyses

Statistical analyses of bioreactor performance and microbial community data were performed in R (v.3.6.1) using the vegan (v.2.5.6) (Oksanen et al., 2019), phyloseq (v.1.30.0) (McMurdie and Holmes, 2013), dplyr (v.0.8.5) (Wickham et al., 2015), DESeq2 (v.1.26.0) (Love et al., 2014), and ggplot (v.3.3.0) packages (Wickham et al., 2016). Statistically significant differences between conditions for bioreactor performance data were identified with the Kruskal-Wallis test with Benjamini-Hochberg correction. Pearson correlation coefficients were calculated to determine the correlation between the relative abundance/activity of different microbial ASVs and MCCAs production. Nonmetric multidimensional scaling (NMDS) plots were generated using Bray-Curtis distances as implemented in the vegan package to compare microbial community composition among inocula, influent, bioreactor, and biofilm samples using both DNA and RNA datasets. Analysis of similarities (ANOSIM) was used to determine whether the observed clusters in the NMDS were significantly different. An ANOSIM R-value close to 1 indicates a complete separation between groups and an R-value near 0 indicates no difference between groups. DESeq2 using the Wald significance test was used to test differential abundance of ASVs read counts between the suspended biomass and corresponding biofilm samples and DNA and RNA microbial data.

4.4 Results and discussion

4.4.1 The dynamic membrane produces high quality permeate despite high bioreactor solids content

The permeate TSS concentration was high (0.81 ± 0.52 g L^{-1}, Figure 4.2) in Phase 1A when the AnDMBR was operated in a semi-continuous filtration mode indicating insufficient development of the dynamic membrane. Visual inspection on Day 41 confirmed nonuniform distribution of cake layer on the supporting meshes (Figure C.4). The permeate TSS decreased drastically from 0.82 g L^{-1} on Day 48 to 0.17 g L^{-1} on Day 51 after switching to continuous filtration mode (Phase 1B), as shown in Figure 4.2. The TSS removal also improved from 56.3% on Day 48 to 74.3% on Day 51 (Figure C.5, Appendix C). Upon visual observation during biomass sampling on Day 89, the cake layer was uniformly distributed on the supporting meshes (Figure C.4, Appendix C). These observations indicate that formation of a uniform dynamic membrane resulted in effective filtration. The permeate TSS concentration remained below 0.12 g L^{-1} and averaged 0.08 ± 0.04 g L^{-1} from Day 50 to 114 with the lowest TSS concentration of 0.04 g L^{-1} achieved on Day 69. Similarly, the permeate turbidity remained low with values as low as 7.61 NTU during Phase 1B (Figure C.6, Appendix C).

The average mixed liquor suspended solids (MLSS) concentration in the bioreactor was 10.19 ± 2.71 g L^{-1} from Days 50-114, which was almost two orders of magnitude higher (Figure 4.2a) than the permeate TSS. Given the influent TSS concentration averaged 2.71 ± 2.01 g TSS L^{-1}, a high TSS removal efficiency averaging 91.5 ± 8.5% was achieved despite a high TSS concentration in the bioreactor. The ratio of SRT to HRT was 21.0 ± 5.2, indicating that the AnDMBR was capable of decoupling SRT and HRT and successfully retained biomass.

Some studies have shown that AnDMBRs can produce permeate with TSS concentration below 10 mg L^{-1} (or turbidity <20 NTU) when treating low solids feedstocks and for MLSS concentrations of 5-8.1 g L^{-1} (Ersahin et al., 2016a, 2014; Siddiqui et al., 2019). However, when high solids waste streams such as food waste were treated with high MLSS concentrations of 20-45 g L^{-1}, a much higher permeate TSS concentration (~0.8-2.8 g TSS L^{-1}) was observed (Cayetano

et al., 2019; Tang et al., 2017). Therefore, careful control of operating conditions to produce permeate with low TSS for an extended period (e.g, Phase 1B) is necessary for the optimal operation of the downstream extraction unit.

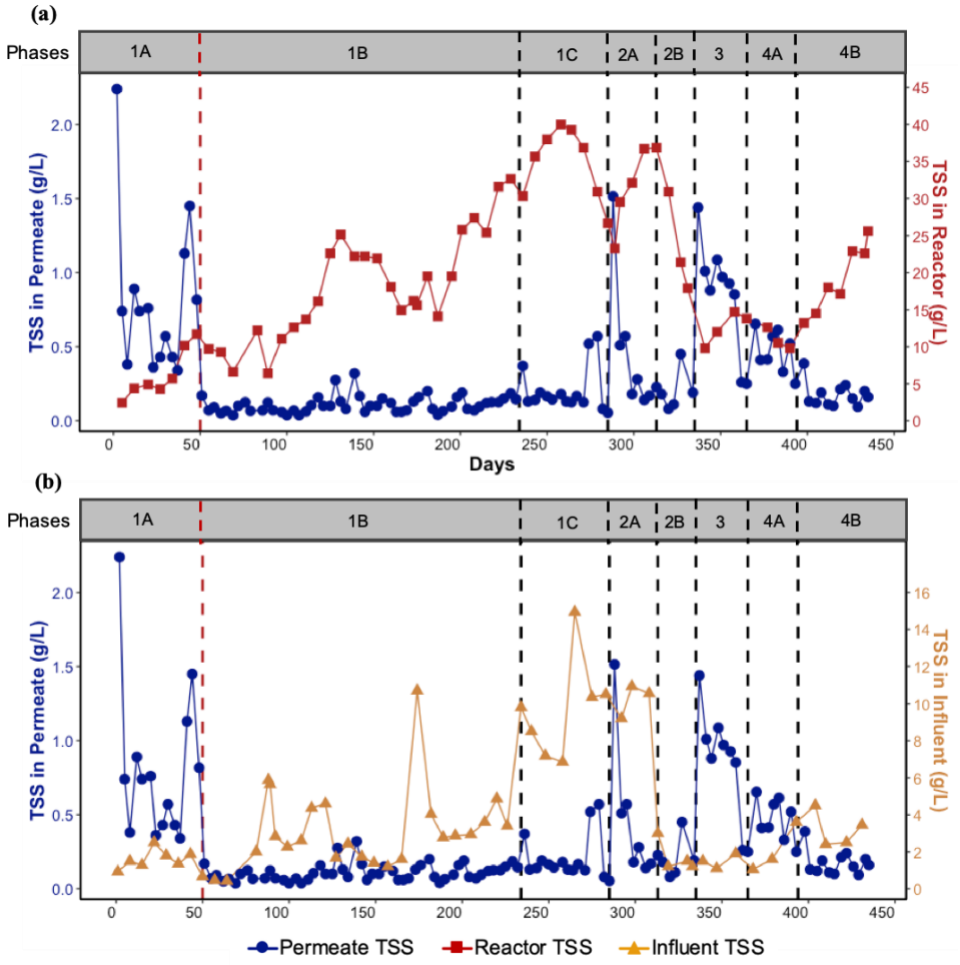

Figure 4.2. Comparison of total suspended solids concentration (TSS) in the permeate and bioreactor over time (a) comparison of TSS in the permeate and influent over time (b). The vertical red dashed line represents a switch to the continuous filtration mode on Day 50 and the vertical black dashed lines represent different experimental phases.

4.4.2 MLSS concentration and influent solids concentration affect dynamic membrane formation

A mature and stable dynamic membrane is essential to consistently achieve high quality permeate (Ersahin et al., 2014), but controlling the dynamic membrane thickness is important to limit

filtration resistance. Our AnDMBR was operated continuously without removing the dynamic membrane or cleaning the supporting meshes until Day 274. Over this time period, the dynamic membrane likely increased in thickness and compactness. Guan et al. (2018) showed that a compact dynamic membrane can push the biomass into the pores of the support mesh due to compression, leading to breakdown and dissociation of particles into the permeate. Consistent with this, the permeate TSS concentration started increasing slowly and stayed above 0.12 g L^{-1} after Day 114. At the same time, the bioreactor MLSS kept increasing with the MLSS concentration reaching a maximum of 40.00 ± 0.35 g TSS L^{-1} on Day 258 (Figure 4.2a). A previous study showed that higher MLSS concentrations increased the rate of fouling, thus reducing filtration flux and subsequently decreasing the permeate quality (Saleem et al., 2017). To alleviate these concerns, the volume and frequency of wasting bioreactor content were increased starting from Day 138. Despite this change, the permeate quality did not improve. An unintentional rise in influent TSS concentration (Phase 1C) further increased the MLSS concentration despite frequent biomass wasting (Figure 4.2).

The meshes were replaced with a new set of 25-µm pore size meshes in Phase 2, but the TMP values continued to increase to 40-50 kPa (Figure C.7, Appendix C) indicating membrane clogging and the permeate TSS concentration remained high (0.35 ± 0.38 g L^{-1}). Because these modifications failed to improve the permeate quality, the influent TSS concentration was decreased from 10.23 ± 0.91 g L^{-1} (Days 285-312) to 1.73 ± 0.86 g L^{-1} (Days 313-334) (Table 4.1) during Phase 2B (Days 313-334). Changing the meshes again in Phase 3 to evaluate the effect of feeding a low TSS influent still resulted in poor permeate quality (0.85 ± 0.38 g TSS L^{-1} and 1693.90 ± 981.49 NTU) (Table 4.1, Figure 4.2 andFigure C.6, Appendix C). Consistent with this, visual inspection showed that the dynamic membrane was not well-formed (Figure C.4, Appendix C). Centrifugation of the influent during Phase 2B likely had a negative effect on bioreactor performance, as centrifugation presumably removed large suspended particles and left mostly particles smaller than the pore size of the support mesh, which had a negative impact on dynamic membrane formation. Additional studies would be necessary to confirm this hypothesis and further determine the impact of influent particle size distribution on dynamic membrane formation.

Moreover, frequently wasting bioreactor content and feeding a low solids influent led to a decrease in MLSS concentration, with a minimum MLSS concentration of 9.8 g L^{-1} reached on Day 390 (Figure 4.2a). The dynamic membrane can take a longer time to form at a lower MLSS concentration as shown by Siddiqui et al. (2019).

The pore size of the support material can affect dynamic membrane formation rate, permeate quality, and flux (Cai et al., 2018; Ersahin et al., 2012; Paçal et al., 2019; Saleem et al., 2017). The decrease in mesh pore size from 25 μm to 5 μm during Phase 4 resulted in improved permeate quality compared to Phase 3. However, the permeate TSS concentration remained higher (0.47 ± 0.14 g L^{-1}) than in Phases 1 and 2, indicating insufficient development of the dynamic membrane. Mesh pore size impacts permeate quality before the formation of the dynamic membrane and after the dynamic membrane is cleaned, otherwise permeate quality is primarily determined by the dynamic membrane (Cai et al., 2018). Salerno et al. (2017) showed that decreasing mesh pore size increased the rate of stable dynamic membrane formation. However, this phenomenon was not observed in our study, as a thick and stable dynamic membrane was not formed until Phase 4B (Table 4.1). The transition to higher solids containing influent in Phase 4B resulted in an increase in the TSS removal efficiency, and a decrease in the permeate TSS concentration and turbidity (Table 4.1). It should be noted that the influent TSS concentration during Phase 4B was still lower than that during Phases 1C and 2A when the permeate quality began to deteriorate. As influent solids characteristics affect MLSS concentration, both high (>9 g L^{-1}) and low (<1.3 g L^{-1}) influent solids concentration proved detrimental to the AnDMBR performance. Additionally, the MLSS concentration also affected the dynamic membrane formation, which suggests the need to control MLSS within a certain range to optimize AnDMBR performance. The role of mesh pore size was less evident.

4.4.3 Re-inoculation revived chain elongation activity

The AnDMBR system was evaluated for MCCAs production from ethanol rich brewery waste and SCCAs rich permeate produced by an anaerobic bioreactor treating food waste, for a total of 435 days. The MCCAs volumetric production rate was high during the first two weeks of operation, with the volumetric production rate reaching up to 4.23 mmole L^{-1} d^{-1} on Day 14, however, the

production started decreasing thereafter and stayed low until Day 175 (Figure 4.3). The bioreactor was re-inoculated on Day 175, after which the MCCAs production recovered immediately as shown in Figure 4.3.

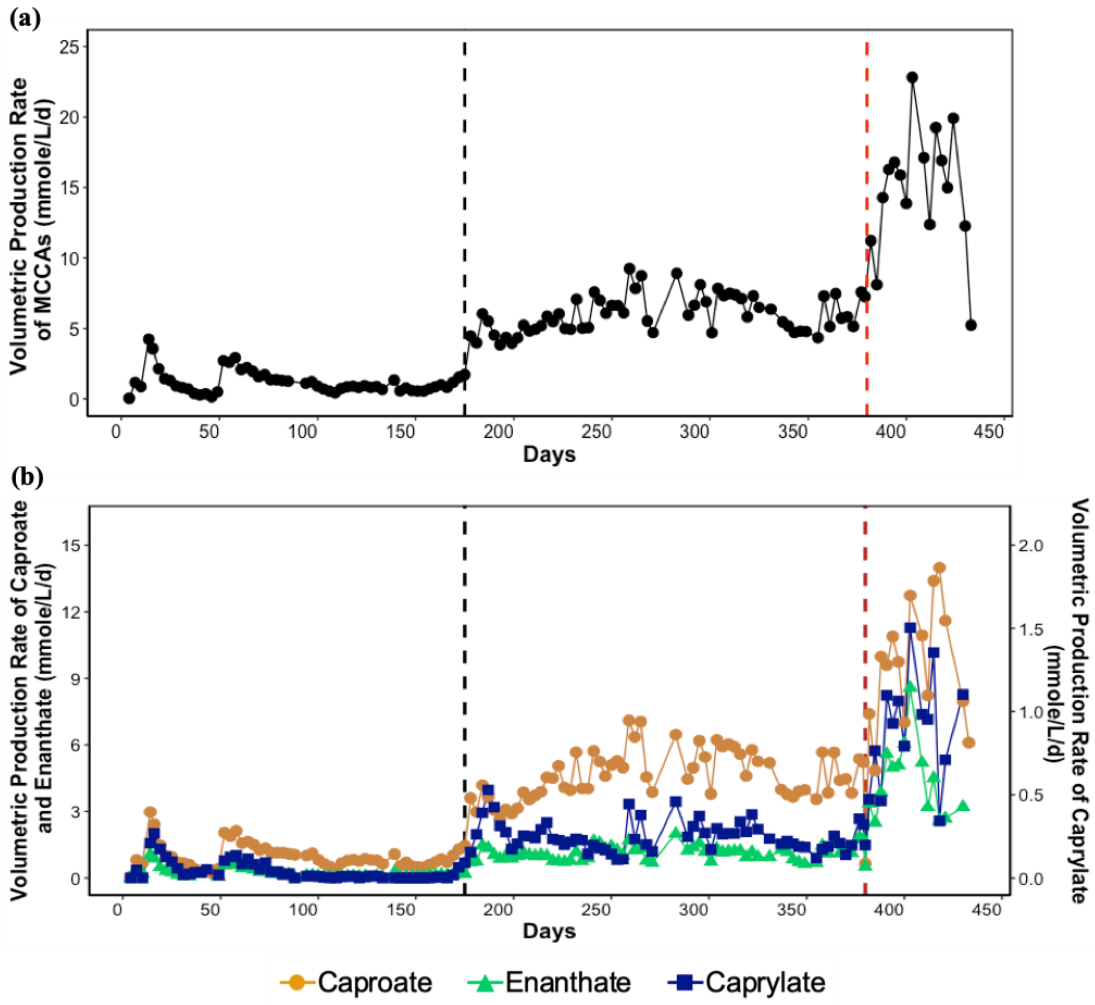

Figure 4.3. Volumetric production rate of total MCCAs (a) caproate, enanthate, and caprylate (b) in the bioreactor over time. The vertical black and red dashed line represent re-inoculation with rumen content and adapted chain elongation biomass on Day 175 and integration of AnDMBR with the extraction unit with recirculation on Day 380, respectively.

The microbial community in the suspended biomass was more diverse at the start of bioreactor operation and was dominated by a few microbial groups as bioreactor operation progressed (Figure C.8 and Figure C.9, Appendix C). A shift in microbial community was observed after the re-inoculation event on Day 175. Starting from Day 181, the active microbial community was mostly

dominated by *Methanobrevibacter, Pseudoramibacter, Lactobacillus,* and *Clostridiales*_unclassified. The relative activity of *Clostridiales*_unclassified (correlation coefficient=0.54, p=0.02) and *Pseudoramibacter* (correlation coefficient=0.45, p=0.04) was significantly correlated with volumetric production rate of MCCAs in the bioreactor. The relative abundance and activity of *Clostridiales*_unclassified on Day 12 was 13.7% and 15.1%, respectively (Figure C.8 and Figure C.9, Appendix C), which corresponded with the high MCCAs production observed in the first two weeks of operation (Figure 4.3). The relative abundance and relative activity decreased to 0.5 ± 0.5% and 0.3 ± 0.3% starting from Day 27 which aligned with the decrease in the MCCAs production thereafter until re-inoculation. *Clostridium sensu stricto* ASV 132 shared 100% similarity with *Clostridium kluyveri*, a model chain elongating bacterium. It was active on Day 12 with a relative activity of 5.9% but it was either absent in other sampling time points or detected at much lower relative abundance and activity (<1%). Similarly, *Pseudoramibacter* was also active at the beginning of bioreactor operation when the MCCAs production was high after which its relative activity decreased from 8.4% on Day 27 to 1.3% on Day 41 before increasing again after re-inoculation.

Clostridiales and *Pseudoramibacter* were either undetected or detected at low relative abundance and activity in a few influent samples collected over the course of the bioreactor operational period. On the other hand, *Clostridiales*_unclassified was present and active in both the adapted chain elongation and rumen inocula, but it was observed at a higher relative abundance (10.0%) and activity (14.5%) in the adapted chain elongation inoculum than in the rumen inoculum (relative abundance and activity of 2.0% and 2.1%, respectively). *Pseudoramibacter* was not detected in the rumen inocula but was observed at a relative abundance and activity of 0.7% and 0.7%, respectively, in the adapted chain elongation inoculum.

*Clostridiales*_unclassified ASV 7, the dominant ASV in the suspended biomass samples, was present and active in the adapted chain elongation inoculum but had a very low relative activity of 0.005% in the rumen inoculum. The NCBI BLAST (Altschul et al., 1990) analysis showed that ASV 7 was most closely related to *Eubacterium pyruvativorans* (91% identity), previously known to be involved in chain elongation (Wallace et al., 2003). *Pseudoramibacter* was reported in

MCCAs production from lactate in other mixed culture studies (Liu et al., 2020; Scarborough et al., 2018). *Clostridiales* and *Pseudoramibacter* were found to be involved in MCCAs production in our previous study using waste beer and pre-fermented food waste (Chapter 2). Therefore, re-inoculation helped in seeding the reactor with MCCAs producers such as *Clostridiales* and *Pseudoramibacter*.

A distinct microbial community developed over time in the bioreactor independent of the rumen inoculum community as shown by the beta-diversity analysis (Figure 4.4 and Figure C.10, Appendix C). The NMDS ordination plot in Figure 4.4 (Figure C.10, Appendix C) also shows that the bioreactor microbiome in the suspended biomass was more similar to the adapted chain elongation inoculum than either of the rumen inocula. Seeding with adapted chain elongation inoculum appeared more important in establishing a stable and active chain elongation community in the AnDMBR. The inoculum was derived from an ethanol-fed chain elongation bioreactor which was possibly enriched with microbial community for MCCAs production. Several chain elongation studies have used acclimated biomass from a previously operating chain elongation bioreactor as an inoculum (Agler et al., 2012; Grootscholten et al., 2013a, 2013b; Kucek et al., 2016a, 2016c; Roghair et al., 2016; Xu et al., 2018). Using inoculum from a well-functioning and similar system ensures faster start-up and shorter acclimation period leading to more stable bioreactor performance (Oz et al., 2012). It is also possible that seeding with a mixture of diverse inoculum sources (as was done during the re-inoculation on Day 175) led to better performance when compared to seeding with a single inoculum (as was done at the beginning of the study). Further investigation on the effect of inoculum type on chain elongation is needed to make a stronger conclusion.

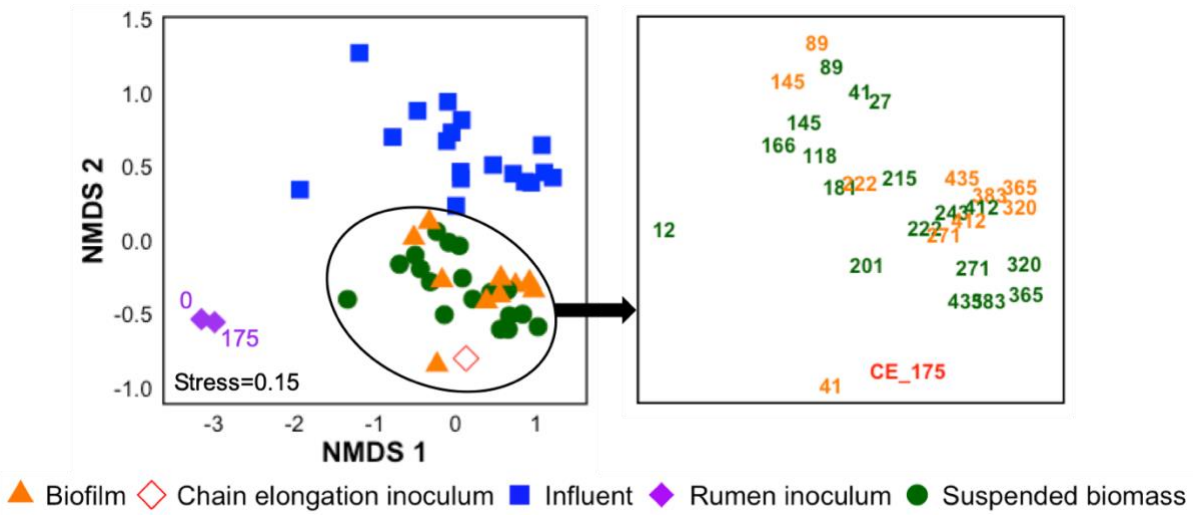

Figure 4.4. Non-metric multidimensional scaling (NMDS) ordination analysis at ASV level based on Bray-Curtis dissimilarity index using 16S rRNA sequencing data in the rumen inoculum, chain elongation inoculum (CE_175), influent, suspended biomass, and biofilm samples. The numbers correspond to sampling time points.

4.4.4 Integration of extraction unit with the AnDMBR system

The LLX unit was integrated with the AnDMBR after the experimental trials showed that the LLX method could selectively and effectively separate MCCAs from a mixture of SCCAs and MCCAs (Section C1.2, Figure C.3, Appendix C). Once the LLX unit was integrated with the AnDMBR, the extraction efficiencies were on average 36.1 ± 27.3% and 39.7 ± 33.6%, from Days 245-270 and Days 314-334, respectively, which increased to 52.0 ± 23.2% from Days 380-435 when the extraction unit was operated with the recirculation mode (Figure 4.1). The extraction efficiency depends on the initial acid concentration in the bioreactor (Saboe et al., 2018). The extraction efficiencies were lower compared to the other studies probably due to the lower MCCAs concentration in this study (Ge et al., 2015; Kucek et al., 2016b). The AnDMBR produced low suspended solids permeate during Phase 1B (Figure 4.2) that could have been sent to the downstream LLX unit. However, when we were ready to connect the LLX unit to the AnDMBR, the permeate quality started deteriorating (Phase 1C). Several changes were made as discussed above in an attempt to achieve stable performance, but the permeate quality remained poor. Therefore, an ultrafiltration unit was installed between the AnDMBR and the LLX unit on Day 245 (Figure 4.1) as an extra protection for the in-line membrane contactors.

The MCCAs volumetric production rate increased from average values of 6.01 ± 1.45 mmole $L^{-1}d^{-1}$ on Days 175-379 to 14.04 ± 5.37 mmole $L^{-1}d^{-1}$ on Days 380-435 after extraction unit integration with the recirculation mode (Figure 4.3). Overall, the major MCCA produced was caproate, constituting 76.6 ± 8.5 % of the total MCCAs based on mmoles of carbon produced while enanthate and caprylate accounted for 18.9 ± 6.5% and 4.5 ± 2.7%, respectively. There was a continuous recirculation of AnDMBR permeate between the AnDMBR and UF unit during this time period that allowed more time for the unconsumed MCCAs precursors like ethanol and acetate present in the permeate to react in the bioreactor. Furthermore, the AnDMBR system was operated at slightly acidic condition under which condition the inhibitory effect of MCCAs increases as the fraction of undissociated MCCAs, which is more toxic, increases. Therefore, the continuous removal of MCCAs from the bioreactor possibly decreased MCCAs toxicity on the microbial community hence explaining the increase in MCCAs volumetric production rate. Other chain elongation studies have also demonstrated increase in MCCAs production due to reduced inhibition after integration with in-line MCCAs extraction system (Ge et al., 2015; Kucek et al., 2016c, 2016b).

4.4.5 Dynamic membrane biofilm activity contributes to MCCA production

The concentration of MCCAs was determined in both the bioreactor and permeate samples starting from Day 259. The MCCAs concentration in the permeate was consistently higher than in the bioreactor (p=1.14E-09) through Day 333 (Figure 4.5). This suggests that the dynamic membrane was contributing to MCCA production. Similarly, Alibardi et al. (2016) reported significant contribution of the dynamic membrane to COD removal during the treatment of high-strength municipal wastewater. In an aerobic dynamic membrane bioreactor, ammonium (NH_4^+-N) concentrations were elevated in the permeate compared to the suspended bioreactor liquid and was attributed to degradation of organic nitrogen in the dynamic membrane (Wu et al., 2005).

While the permeate MCCAs concentration was higher than the corresponding bioreactor concentration for a considerable amount of time, this trend was not consistent starting from Day 334 (Figure 4.5). The difference in MCCAs concentration in the permeate and the bioreactor samples aligned with the changes observed in the dynamic membrane formation (Figure C.4,

Appendix C). The MCCAs concentrations in the bioreactor and permeate were similar from Days 334 to 399 (p=0.91) when the dynamic membrane was not properly formed on the meshes. A higher MCCAs concentration in the permeate than the corresponding bioreactor samples was again observed starting from Day 400 (Figure 4.5) during which time a well-formed dynamic membrane was observed. Although there was a difference in MCCAs concentration between the permeate and bioreactor samples during this period, it was not statistically significant (p=0.11).

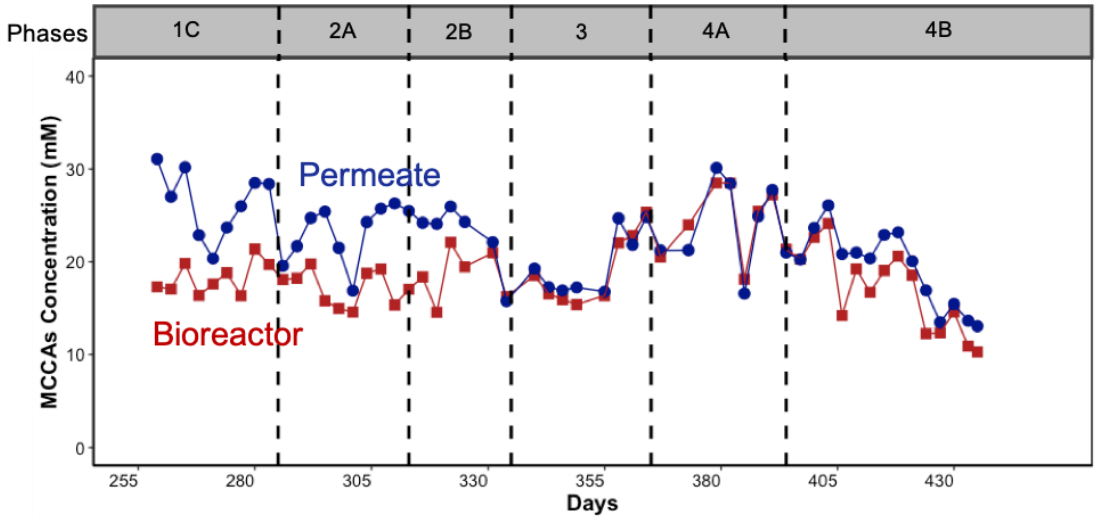

Figure 4.5. Comparison of MCCAs concentration in permeate and bioreactor samples over time. MCCAs concentration in the bioreactor was measured starting from Day 259. The vertical dashed lines represent different experimental phases.

The microbial community in the biofilm was also characterized and compared to that in the suspended biomass samples. A few dominant microbial groups such as *Methanobrevibacter* (56.9%), *Pseudoramibacter* (15.8%), and unclassified *Bacteria* (6.1%) represented the majority of the active microbial community in the biofilm on Day 41. The active microbial community composition of the biofilm was distinct from that in the suspended biomass on Day 41 (Figure 4.4 andFigure 4.6), however, this was less evident from the 16S rRNA gene sequencing data (Figure C.11, Appendix C). There was a shift in the active microbial community on Day 89 (Figure 4.4 andFigure 4.6) which corresponded to Phase 1B when continuous mode of filtration led to enhanced dynamic membrane formation. Similar to the suspended microbial community, the active biofilm microbial community composition again changed on Day 222 corresponding to the re-inoculation event on Day 175. Furthermore, *Lactobacillus* was active in the biofilm samples

throughout with varying relative abundance (0.6-11.2%) and activity (0.4-45.0%) and particularly made up a significant fraction of the active biofilm community (22.7-53.4%) starting from Day 383 after changing the mesh from 25-µm to 5-µm. *Lactobacillus* produces extracellular polymeric substances (EPS) as a metabolic product of carbohydrate degradation (Badel et al., 2011). As EPS plays an important role in microbial biofilm formation by promoting cell aggregation and adhesion in the dynamic membrane (Czaczyk and Myszka, 2007; Ersahin et al., 2016b; Siddiqui et al., 2019), the enrichment of *Lactobacillus* possibly facilitated the development of the dynamic membrane.

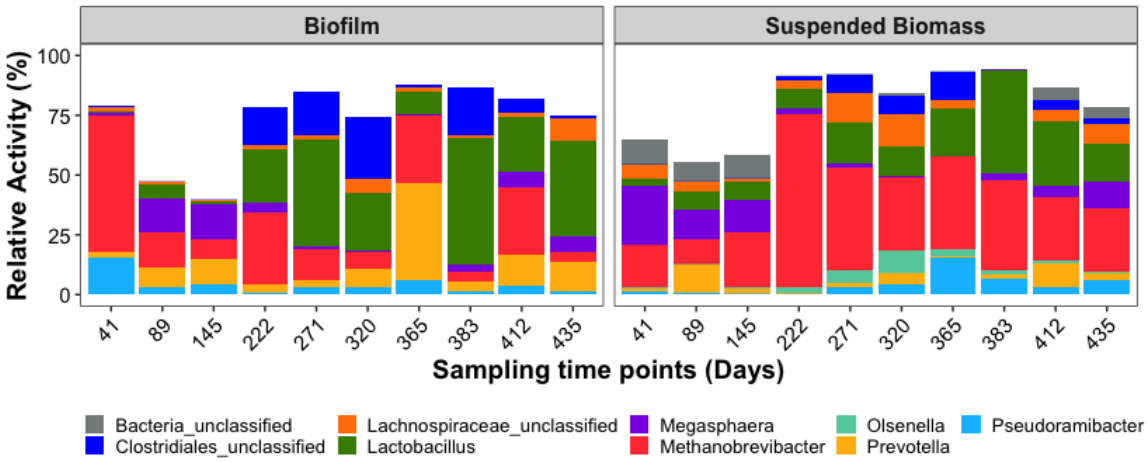

Figure 4.6. Relative activity of the microbial groups active at relative activity greater than 1% in at least 50% of the samples (n=10 in each group) classified to the genus or family level in the biofilm and suspended biomass samples.

The beta diversity results represented by the NMDS plot (Figure 4.4) showed that the active biofilm and suspended biomass communities were different at the beginning until Day 41. However, the microbial community in the suspended biomass and the biofilm samples became more similar to each other with time (ANOSIM R=0.11, p=0.06). Although the microbial community structures of the suspended and biofilm samples were similar, the relative activity of *Clostridiales*_unclassified, which was positively correlated to MCCAs production, differed greatly between the suspended biomass and biofilm samples, particularly during the period when permeate MCCAs concentration was significantly higher than the corresponding bioreactor concentration. *Clostridiales*_unclassified was found at a higher relative activity of 20.0 ± 4.9% from Days 222-

320 in the biofilm samples compared to 5.2 ± 2.7% of relative activity in the suspended biomass samples (Figure 4.6), thus corroborating the chemical data. These observations indicate that the dynamic membrane biofilm formation not only improved permeate quality but also played a significant role in MCCAs production. Other AnDMBR studies have also reported differences in microbial community composition between suspended biomass and dynamic membrane (Ersahin et al., 2016b; Quek et al., 2017), however, these inferences were based on a single sample of the dynamic membrane. High spatial organization and different environmental conditions in the dynamic membrane can lead to niche differentiation providing favorable conditions to one microbial population over another. On the other hand, Zhang et al. (2011) found that the microbial activity in the dynamic membrane was lower than that in the suspended biomass due to the suppressed mass transfer in the compact fouling layer that limits substrate and nutrient availability in the dynamic membrane. Nevertheless, the microbial data in our study suggests that AnDMBR potentially contributed towards chain elongation by enriching MCCAs producing populations. However, further investigation is needed to confirm the underlying mechanism responsible for higher MCCAs production due to the dynamic membrane.

4.5 Conclusions and Future research directions

The dynamic membrane formation led to high solid retention resulting in low permeate TSS concentration for integration with the downstream LLX extraction unit. Directly integrating an AnDMBR with the extraction unit can decrease the environmental footprint and cost compared to other chain elongation systems by eliminating the use of multiple external filters. While the AnDMBR achieved stable performance for a considerable amount of time without cleaning the dynamic membrane or cleaning or replacing the supporting meshes, the meshes clogged when the dynamic membrane became denser. Therefore, adopting some form of cleaning to control the dynamic membrane thickness would be beneficial in a long-term run. Our results show that high (>9 g L^{-1}) influent solids concentration, which consequently affected MLSS concentration, negatively influenced dynamic membrane formation. Additionally, the AnDMBR dynamic membrane was enriched in highly active MCCAs producing microbial populations such as *Clostridiales*. These observations were consistent with higher concentrations of MCCAs in the

permeate compared to the bioreactor samples and suggest that chain elongation activity was promoted in the dynamic membrane biofilm. The characterization of biofilm morphology and composition needs to be done to get a detailed understanding of the microbial interaction and its role in MCCAs production. Lastly, the AnDMBR was operated at low flux thus hindering the scale-up of this technology. Downstream extraction unit also requires constant and higher flux for better extraction efficiency. Therefore, the AnDMBR needs to be optimized further to operate at higher flux in order to expand its practical application.

4.6 References

Agler, M.T., Spirito, C.M., Usack, J.G., Werner, J.J., Angenent, L.T., 2012. Chain elongation with reactor microbiomes: upgrading dilute ethanol to medium-chain carboxylates. Energy Environ. Sci. 5, 8189. https://doi.org/10.1039/c2ee22101b

Alibardi, L., Bernava, N., Cossu, R., Spagni, A., 2016. Anaerobic dynamic membrane bioreactor for wastewater treatment at ambient temperature. Chem. Eng. J. 284, 130–138. https://doi.org/10.1016/j.cej.2015.08.111

Altschul, S.F., Gish, W., Miller, W., Myers, E.W., Lipman, D.J., 1990. Basic Local Alignment Search Tool. J. Mol. Biol. 215, 403–410. https://doi.org/10.1016/S0022-2836(05)80360-2

Andersen, S.J., De Groof, V., Khor, W.C., Roume, H., Props, R., Coma, M., Rabaey, K., 2017. A Clostridium Group IV Species Dominates and Suppresses a Mixed Culture Fermentation by Tolerance to Medium Chain Fatty Acids Products. Front. Bioeng. Biotechnol. 5, 1–10. https://doi.org/10.3389/fbioe.2017.00008

Angenent, L.T., Richter, H., Buckel, W., Spirito, C.M., Steinbusch, K.J.J., Plugge, C.M., Strik, D.P.B.T.B., Grootscholten, T.I.M., Buisman, C.J.N., Hamelers, H.V.M., 2016. Chain Elongation with Reactor Microbiomes: Open-Culture Biotechnology to Produce Biochemicals. Environ. Sci. Technol. 50, 2796–2810. https://doi.org/10.1021/acs.est.5b04847

Angenent, L.T., Usack, J.G., Xu, J., Hafenbradl, D., Posmanik, R., Tester, W., 2018. Integrating electrochemical , biological , physical , and thermochemical process units to expand the applicability of anaerobic digestion. Bioresour. Technol. 247, 1085–1094. https://doi.org/10.1016/j.biortech.2017.09.104

Badel, S., Bernardi, T., Michaud, P., 2011. New perspectives for Lactobacilli exopolysaccharides. Biotechnol. Adv. 29, 54–66. https://doi.org/10.1016/j.biotechadv.2010.08.011

Cai, D., Huang, J., Liu, G., Li, M., Yu, Y., Meng, F., 2018. Effect of support material pore size on the filtration behavior of dynamic membrane bioreactor. Bioresour. Technol. 255, 359–363.

https://doi.org/10.1016/j.biortech.2018.02.007

Callahan, B.J., McMurdie, P.J., Rosen, M.J., Han, A.W., Johnson, A.J.A., Holmes, S.P., 2016. DADA2: High-resolution sample inference from Illumina amplicon data. Nat. Methods 13, 581–583. https://doi.org/10.1038/nmeth.3869

Caporaso, J.G., Lauber, C.L., Walters, W.A., Berg-Lyons, D., Lozupone, C.A., Turnbaugh, P.J., Fierer, N., Knight, R., 2011. Global patterns of 16S rRNA diversity at a depth of millions of sequences per sample. Proc. Natl. Acad. Sci. U. S. A. 108 Suppl, 4516–22. https://doi.org/10.1073/pnas.1000080107

Carvajal-Arroyo, J.M., Candry, P., Andersen, S.J., Props, R., Seviour, T., Ganigué, R., Rabaey, K., 2019. Granular fermentation enables high rate caproic acid production from solid-free thin stillage. Green Chem. 21, 1330–1339. https://doi.org/10.1039/c8gc03648a

Cayetano, R.D.A., Park, J.H., Kang, S., Kim, S.H., 2019. Food waste treatment in an anaerobic dynamic membrane bioreactor (AnDMBR): Performance monitoring and microbial community analysis. Bioresour. Technol. 280, 158–164. https://doi.org/10.1016/j.biortech.2019.02.025

Czaczyk, K., Myszka, K., 2007. Biosynthesis of extracellular polymeric substances (EPS) and its role in microbial biofilm formation. Polish J. Environ. Stud. 16, 799–806.

Ersahin, M.E., Gimenez, J.B., Ozgun, H., Tao, Y., Spanjers, H., van Lier, J.B., 2016a. Gas-lift anaerobic dynamic membrane bioreactors for high strength synthetic wastewater treatment: Effect of biogas sparging velocity and HRT on treatment performance. Chem. Eng. J. 305, 46–53. https://doi.org/10.1016/j.cej.2016.02.003

Ersahin, M.E., Ozgun, H., Dereli, R.K., Ozturk, I., Roest, K., van Lier, J.B., 2012. A review on dynamic membrane filtration: Materials, applications and future perspectives. Bioresour. Technol. 122, 196–206. https://doi.org/10.1016/j.biortech.2012.03.086

Ersahin, M.E., Ozgun, H., Tao, Y., van Lier, J.B., 2014. Applicability of dynamic membrane technology in anaerobic membrane bioreactors. Water Res. 48, 420–429. https://doi.org/10.1016/j.watres.2013.09.054

Ersahin, M.E., Tao, Y., Ozgun, H., Spanjers, H., van Lier, J.B., 2016b. Characteristics and role of dynamic membrane layer in anaerobic membrane bioreactors. Biotechnol. Bioeng. 113, 761–771. https://doi.org/10.1002/bit.25841

Eugene, W.R., Rodger, B.B., Andrew, D.E., Lenore, S.C., 2012. Standard Methods for the Examination of Water and Wastewater, American Public Health Association, American Water Works Association, Water environment federation.

Fonoll, X., Meuwissen, T., Aley, L., Shrestha, S., Raskin, L., 2019. The rumen membrane bioreactor: Transforming food waste into volatile fatty acids at the small scale, in: IWA 16th World

Congress on Anaerobic Digestion.

Ge, S., Usack, J.G., Spirito, C.M., Angenent, L.T., 2015. Long-Term *n* -Caproic Acid Production from Yeast-Fermentation Beer in an Anaerobic Bioreactor with Continuous Product Extraction. Environ. Sci. Technol. 49, 8012–8021. https://doi.org/10.1021/acs.est.5b00238

Grootscholten, T.I.M., Steinbusch, K.J.J., Hamelers, H.V.M., Buisman, C.J.N., 2013a. Chain elongation of acetate and ethanol in an upflow anaerobic filter for high rate MCFA production. Bioresour. Technol. 135, 440–445. https://doi.org/10.1016/j.biortech.2012.10.165

Grootscholten, T.I.M., Steinbusch, K.J.J., Hamelers, H.V.M., Buisman, C.J.N., 2013b. High rate heptanoate production from propionate and ethanol using chain elongation. Bioresour. Technol. 136, 715–718. https://doi.org/10.1016/j.biortech.2013.02.085

Guan, D., Dai, J., Watanabe, Y., Chen, G., 2018. Changes in the physical properties of the dynamic layer and its correlation with permeate quality in a self-forming dynamic membrane bioreactor. Water Res. 140, 67–76. https://doi.org/10.1016/j.watres.2018.04.041

Hu, Y., Wang, X.C., Ngo, H.H., Sun, Q., Yang, Y., 2018. Anaerobic dynamic membrane bioreactor (AnDMBR) for wastewater treatment: A review. Bioresour. Technol. 247, 1107–1118. https://doi.org/10.1016/j.biortech.2017.09.101

Kozich, J.J., Westcott, S.L., Baxter, N.T., Highlander, S.K., Schloss, P.D., 2013. Development of a dual-index sequencing strategy and curation pipeline for analyzing amplicon sequence data on the miseq illumina sequencing platform. Appl. Environ. Microbiol. 79, 5112–5120. https://doi.org/10.1128/AEM.01043-13

Kucek, L., Nguyen, M., Angenent, L.T., 2016a. Conversion of L-lactate into n-caproate by a continuously fed reactor microbiome. Water Res. 93, 163–171. https://doi.org/10.1016/j.watres.2016.02.018

Kucek, L., Spirito, C.M., Angenent, L.T., 2016b. High n-caprylate productivities and specificities from dilute ethanol and acetate: Chain elongation with microbiomes to upgrade products from syngas fermentation. Energy Environ. Sci. 9, 3482–3494. https://doi.org/10.1039/c6ee01487a

Kucek, L., Xu, J., Nguyen, M., Angenent, L.T., 2016c. Waste conversion into n-caprylate and n-caproate: resource recovery from wine lees using anaerobic reactor microbiomes and in-line extraction. Front. Microbiol. 7, 1–14. https://doi.org/10.3389/fmicb.2016.01892

Liu, B., Kleinsteuber, S., Centler, F., Harms, H., Sträuber, H., 2020. Competition Between Butyrate Fermenters and Chain-Elongating Bacteria Limits the Efficiency of Medium-Chain Carboxylate Production. Front. Microbiol. 11, 1–13. https://doi.org/10.3389/fmicb.2020.00336

Liu, Hongbo, Wang, Y., Yin, B., Zhu, Y., Fu, B., Liu, He, 2016. Improving volatile fatty acid yield from sludge anaerobic fermentation through self-forming dynamic membrane separation.

Bioresour. Technol. 218, 92–100. https://doi.org/10.1016/j.biortech.2016.06.077

Love, M.I., Huber, W., Anders, S., 2014. Moderated estimation of fold change and dispersion for RNA-seq data with DESeq2. Genome Biol. 15, 1–21. https://doi.org/10.1186/s13059-014-0550-8

McMurdie, P.J., Holmes, S., 2013. Phyloseq: An R Package for Reproducible Interactive Analysis and Graphics of Microbiome Census Data. PLoS One 8. https://doi.org/10.1371/journal.pone.0061217

Oksanen, J., Blanchet, F.G., Friendly, M., Kindt, R., Legendre, P., McGlinn, D., Minchin, P.R., O'Hara, R.B., Simpson, G.L., Solymos, P., Stevens, M.H.H., Szoecs, E., Wagner, H., 2019. Package 'vegan': Community Ecology Package. R Packag. version 2.5-6.

Oz, N.A., Ince, O., Turker, G., Ince, B.K., 2012. Effect of seed sludge microbial community and activity on the performance of anaerobic reactors during the start-up period. World J. Microbiol. Biotechnol. 28, 637–647. https://doi.org/10.1007/s11274-011-0857-5

Ozgun, H., Dereli, R.K., Ersahin, M.E., Kinaci, C., Spanjers, H., Van Lier, J.B., 2013. A review of anaerobic membrane bioreactors for municipal wastewater treatment: Integration options, limitations and expectations. Sep. Purif. Technol. 118, 89–104. https://doi.org/10.1016/j.seppur.2013.06.036

Paçal, M., Semerci, N., Çallı, B., 2019. Treatment of synthetic wastewater and cheese whey by the anaerobic dynamic membrane bioreactor. Environ. Sci. Pollut. Res. 32942–32956. https://doi.org/10.1007/s11356-019-06397-z

Porebski, S., Bailey, L.G., Baum, B.R., 1997. Modification of a CTAB DNA Extraction Protocol for Plants Containing High Polysaccharide and Polyphenol Components 15, 8–15.

Quek, P.J., Yeap, T.S., Ng, H.Y., 2017. Applicability of upflow anaerobic sludge blanket and dynamic membrane-coupled process for the treatment of municipal wastewater. Appl. Microbiol. Biotechnol. 101, 6531–6540. https://doi.org/10.1007/s00253-017-8358-6

Roghair, M., Strik, D.P.B.T.B., Steinbusch, K.J.J., Weusthuis, R.A., Bruins, M.E., Buisman, C.J.N., 2016. Granular sludge formation and characterization in a chain elongation process. Process Biochem. 51, 1594–1598. https://doi.org/10.1016/j.procbio.2016.06.012

Saboe, P.O., Manker, L.P., Michener, W.E., Peterson, D.J., Brandner, D.G., Deutch, S.P., Kumar, M., Cywar, R.M., Beckham, T., Karp, E.M., 2018. In situ recovery of bio-based carboxylic acids. Green Chem. 20, 1791–1804. https://doi.org/10.1039/c7gc03747c

Saleem, M., Alibardi, L., Cossu, R., Cristina, M., Spagni, A., 2017. Analysis of fouling development under dynamic membrane filtration operation. Chem. Eng. J. 312, 136–143. https://doi.org/10.1016/j.cej.2016.11.123

Salerno, C., Vergine, P., Berardi, G., Pollice, A., 2017. Influence of air scouring on the performance of a Self Forming Dynamic Membrane BioReactor (SFD MBR) for municipal wastewater treatment. Bioresour. Technol. 223, 301–306. https://doi.org/10.1016/j.biortech.2016.10.054

Scarborough, M.J., Lawson, C.E., Hamilton, J.J., Donohue, T.J., Noguera, D.R., 2018. Metatranscriptomic and Thermodynamic Insights into Medium-Chain Fatty Acid Production Using an Anaerobic Microbiome. mSystems 3, 1–21. https://doi.org/10.1128/mSystems.00221-18

Seluy, L.G., Isla, M.A., 2014. A Process To Treat High-Strength Brewery Wastewater via Ethanol Recovery and Vinasse Fermentation. Ind. Eng. Chem. Res. 53, 17043–17050. https://doi.org/10.1021/ie500438j

Siddiqui, M.A., Dai, J., Guan, D., Chen, G., 2019. Exploration of the formation of self-forming dynamic membrane in an upflow anaerobic sludge blanket reactor. Sep. Purif. Technol. 212, 757–766. https://doi.org/10.1016/j.seppur.2018.11.065

Sitter, K. De, Garcia-gonzalez, L., Matassa, C., Bertin, L., 2018. The use of membrane based reactive extraction for the recovery of carboxylic acids from thin stillage. Sep. Purif. Technol. 206, 177–185. https://doi.org/10.1016/j.seppur.2018.06.001

Smith, A.L., Stadler, L.B., Love, N.G., Skerlos, S.J., Raskin, L., 2012. Perspectives on anaerobic membrane bioreactor treatment of domestic wastewater: A critical review. Bioresour. Technol. 122, 149–159. https://doi.org/10.1016/j.biortech.2012.04.055

Tang, J., Wang, X.C., Hu, Y., Hao, H., Li, Y., 2017. Dynamic membrane-assisted fermentation of food wastes for enhancing lactic acid production. Bioresour. Technol. 234, 40–47. https://doi.org/10.1016/j.biortech.2017.03.019

Urban, C., Xu Jiajie, Strauber Heik, Dantas Tatiane R. dos Santos, Muhlenberg Jana, Hartig Claus, Angenent Largus T. and, Harnisch Falk, 2017. Production of drop-in fuels from biomass at high selectivity by combined microbial and electrochemical conversion. Energy Environ. Sci. 10, 2231–2244. https://doi.org/10.1039/c7ee01303e

Wallace, R.J., McKain, N., McEwan, N.R., Miyagawa, E., Chaudhary, L.C., King, T.P., Walker, N.D., Apajalahti, J.H.A., Newbold, C.J., 2003. Eubacterium pyruvativorans sp. nov., a novel non-saccharolytic anaerobe from the rumen that ferments pyruvate and amino acids, forms caproate and utilizes acetate and propionate. Int. J. Syst. Evol. Microbiol. 53, 965–970. https://doi.org/10.1099/ijs.0.02110-0

Wickham, H., Chang, W., Henry, L., Pedersen, T.L., Takahashi, K., Wilke, C., Woo, K., Yutani, H., Dunnington, D., 2016. ggplot2: Create Elegant Data Visualisations Using the Grammar of Graphics version 3.3.0.

Wickham, H., Francois, R., Henry, L., Müller, K., 2015. dplyr: A Grammar of Data Manipulation

version 0.8.5.

Wu, Q., Feng, X., Guo, W., Bao, X., Ren, N., 2020. Long-term medium chain carboxylic acids production from liquor-making wastewater: parameters optimization and toxicity mitigation. Chem. Eng. J. 124218. https://doi.org/10.1016/j.cej.2020.124218

Wu, Y., Huang, X., Wen, X., Chen, F., 2005. Function of dynamic membrane in self-forming dynamic membrane coupled bioreactor. Water Sci. Technol. 51, 107–114. https://doi.org/10.2166/wst.2005.0628

Xie, Z., Wang, Z., Wang, Q., Zhu, C., Wu, Z., 2014. An anaerobic dynamic membrane bioreactor (AnDMBR) for landfill leachate treatment: Performance and microbial community identification. Bioresour. Technol. 161, 29–39. https://doi.org/10.1016/j.biortech.2014.03.014

Xu, J., Hao, J., Juan, J.L., Spirito, C.M., Harroff, L.A., Largus, T., Xu, J., Hao, J., Guzman, J.J.L., Spirito, C.M., Harroff, L.A., 2018. Temperature-Phased Conversion of Acid Whey Waste Into Medium-Chain Carboxylic Acids via Lactic Acid : No External e-Donor. Joule 1–16. https://doi.org/10.1016/j.joule.2017.11.008

Zhang, X., Wang, Z., Wu, Z., Wei, T., Lu, F., Tong, J., Mai, S., 2011. Membrane fouling in an anaerobic dynamic membrane bioreactor (AnDMBR) for municipal wastewater treatment : Characteristics of membrane foulants and bulk sludge. Process Biochem. 46, 1538–1544. https://doi.org/10.1016/j.procbio.2011.04.002

Zhang, Y., Zhao, Y., Chu, H., Dong, B., Zhou, X., 2014. Characteristics of dynamic membrane filtration: Structure, operation mechanisms, and cost analysis. Chinese Sci. Bull. 59, 247–260. https://doi.org/10.1007/s11434-013-0048-x

Chapter 5

Environmental Life Cycle Assessment of Caproic Acid Recovery from Brewery Waste Streams

Shilva Shrestha[1], Muhammad Abdullah[2], Lutgarde Raskin[1], Steve Skerlos[1,2]

[1]Department of Civil and Environmental Engineering, University of Michigan, Ann Arbor, Michigan 48109, USA

[2]Department of Mechanical Engineering, University of Michigan, Ann Arbor, Michigan 48109, USA

5.1 Abstract

Bio-based production of medium chain carboxylic acids such as caproic acid from waste streams has the potential to replace conventional caproic acid production from plant oils such as palm kernel oil. Given the growth in the number of breweries along with the waste streams they generate, we evaluated the environmental impacts of diverting brewery waste into caproic acid. An environmental life cycle assessment was conducted and critical factors affecting environmental footprint during the production of one kilogram caproic acid (functional unit) from brewery waste streams (BW-CA) were identified. The environmental performance of BW-CA can be further improved by decreasing sodium hydroxide addition and using renewable energy to meet heating demands. Despite key areas for improvement identified for the future, BW-CA offered environmental benefits compared to caproic acid production from palm kernel oil (PKO-CA) in all impact categories. The total global warming life cycle of BW-CA was almost 21 times lower than PKO-CA. For the reference PKO-CA system, the use of mineral fertilizer during palm oil

cultivation had the highest contribution to global warming potential and other impact categories. Therefore, caproic acid production from brewery waste is attractive from an environmental perspective.

5.2 Introduction

Medium chain carboxylic acids (MCCAs), carboxylic acids with six to twelve carbons, are platform chemicals with diverse industrial and agricultural applications. MCCAs such as caproic acid (C6), enanthic acid (C7), and caprylic acid (C8) serve as building blocks for a variety of compounds. They can be used directly as livestock feed additives (Hanczakowska, 2017), antimicrobial agents (Desbois and Smith, 2010), plant growth promoters (Scalschi et al., 2013), food additives (Takeuchi et al., 2008), or as valuable commodities for production of lubricants, fragrances, and dyes (Angenent et al., 2016). They can also be converted into longer chain liquid fuels (alcohols and alkanes) and then used as drop-in fuels (Urban et al., 2017). The global consumption of caproic acid increased from 8.6E+06 kg in 2013 to 1.0E+07 kg in 2017 and is predicted to reach 1.3E+7 kg by 2024 (360 Research Reports, 2020). Due to their versatility, the global MCCAs market is expected to reach USD 1.25 billion by 2020, with a compound annual growth rate of 12.3% between 2017 and 2022 (Zion Market Research, 2018).

Currently, MCCAs are produced through extraction from plant oils including palm kernel oil (PKO) and coconut oil. These oils contain small amounts of caproic acid and caprylic acid, leading to significant consumption of plant oil and also high prices of the final product (Anneken et al., 2012). For example, PKO consist of 0.5% by weight of caproic acid (Anneken et al., 2012). There is an increasing global demand for palm oil due to an increase in demand for food, feedstock for chemicals, and diesel production. Indonesia and Malaysia lead the world's production and export of palm oil, meeting approximately 90% of the total global demand (United States Department of Agriculture, 2020). However, there is growing environmental concern about the rapidly expanding palm oil industry. Palm oil production has been shown to have negative environmental consequences such as land-use changes, resource depletion, and increased air pollution (Carlson et al., 2012; Goodman and Mulik, 2015; Petrenko et al., 2016). The land-use change such as destruction of humid tropical forest, draining of peatlands, and clearing agricultural land using fire

for oil palm cultivation has been reported to cause wildfire affecting air quality, biodiversity loss, and animal habitat destruction (Carlson et al., 2012; Goodman and Mulik, 2015; Petrenko et al., 2016). Due to the low concentration of caproic acid in PKO and the undesirable environmental effects associated with palm oil production, there exists an unmet environmental need to produce these high-value chemicals from other resources without incurring high environmental costs.

A shift to sustainable bio-based caproic acid production is needed to reduce our dependence on plant oils and address the concern of the high environmental footprint of conventional caproic acid production methods. Caproic acid can be produced by mixed-culture microbial communities during a process called chain elongation using organic rich waste streams as substrates (Angenent et al., 2016). The carbon backbone of short chain carboxylic acids (SCCAs) such as acetate gets elongated into caproic acid in two carbon step by the addition of an electron donor such as ethanol (Angenent et al., 2016). Caproic acid production has been studied extensively at the lab-scale with diverse waste streams ranging from yeast fermentation beer (Agler et al., 2012a; Ge et al., 2015), the organic fraction of municipal solid waste (Grootscholten et al., 2014), food waste (Nzeteu et al., 2018), acid whey from Greek yogurt production (Xu et al., 2018), wine lees (Kucek et al., 2016), effluent from syngas fermenter (Vasudevan et al., 2014), lignocellulosic biomass such as pretreated corn fiber (Agler et al., 2012b), and waste beer (Chapters 2 and 4). There have been efforts to scale up this process to pilot- and full-scale in a few places (Angenent et al., 2016; “Capro-X”., “ChainCraft”) The first full-scale system developed by ChainCraft converts the organic fraction of municipal solid waste and waste from food industries into MCCAs (“ChainCraft”). As the feasibility of MCCA production from other waste streams has been demonstrated at the lab-scale, it is important to assess the environmental performance of such emerging technologies at an early stage to maximize environmental performance during scale-up.

Chain elongation can be applied for the valorization of brewery waste. Waste beer, for example, has potential for caproic acid production through chain elongation due to its high ethanol content. An environmental life cycle assessment (LCA) of caproic acid production from crude ethanol and food waste identified ethanol addition to have a dominant environmental impact over the life cycle (Chen et al., 2017). Deriving ethanol needed for the chain elongation process from waste streams

would reduce the operating cost and environmental impact otherwise caused by the addition of an external electron donor. Besides ethanol, there are considerable opportunities to recover untapped resources from other organic rich brewery waste streams such as spent grain. The lignocellulose component in the spent grain can be hydrolyzed for the production of SCCAs, the precursors for MCCAs (Liang and Wan, 2015). The use of brewery waste for resource recovery will also address the increasing waste management problems due to the increase in the number of breweries (Brewers Association, 2019; The Brewers of Europe, 2017). While caproic acid production from brewery waste appears attractive, this resource recovery technology should be evaluated to avoid unintended environmental consequences. Moreover, as the technology is still evolving, it is important to identify factors that contribute the most to the environmental emissions thus highlighting the areas of intervention to improve the environmental performance. Thus, a proper assessment of the environmental consequences of caproic acid production from brewery waste is necessary.

The objective of this paper was to quantify environmental life-cycle impacts of caproic acid production from brewery waste (BW-CA) and to identify sensitive parameters that affect environmental impacts, thus highlighting areas for improvement. Furthermore, this study also focuses on the comparative assessment of BW-CA technology relative to the life cycle environmental impacts of caproic acid production from PKO (PKO-CA).

5.3 Materials and Method

5.3.1 System Boundary and Functional Unit

The process flow diagram and unit processes of the BW-CA and PKO-CA (reference) systems with all the components and flows within the scope of the LCA system boundary are shown in Figure 5.1. The details of the process parameters, unit processes, and material, chemical, and energy consumption are given in Table D.1 and sections 1-3 of the Appendix D. The functional unit was defined as the production of one kg of caproic acid. A gate-to-gate life cycle of material flows was evaluated for BW-CA. The BW-CA plant is assumed to be situated in Jolly Pumpkin Brewery (Dexter, MI, USA) and thus transportation of brewery waste was excluded. The BW-CA system begins with the digestion of brewery waste streams at the brewery and ends with the

recovery of caproic acid and leaving the boundary for use offsite. The caproic acid produced can be sold as it is or converted into other high-value products or fuels, but the end-of-life of caproic acid was not included within the system boundary. The route of caproic acid use can affect the overall sustainability of both BW-CA and PKO-CA systems. The BW-CA system boundary includes acidogenic and chain elongation digesters, caproic acid extraction via liquid-liquid extraction (LLX) and separation via distillation, digestate disposal, and wastewater treatment (Figure 5.1a). As waste beer and spent grain are produced independent of whether caproic acid is produced, the additional environmental impact of managing these brewery waste streams were also included in the model. The reference PKO-CA system assumes that caproic acid was extracted from the PKO, the byproduct of crude palm oil. A cradle-to-gate approach was used for PKO-CA. The system boundary included the production of palm oil seedling and palm fresh fruit bunch at the oil palm nursery and plantation, respectively, palm kernels production during crude palm oil production at the palm oil mill, PKO extraction at the kernel crushing plant, and distillation for caproic acid recovery (Figure 5.1b).

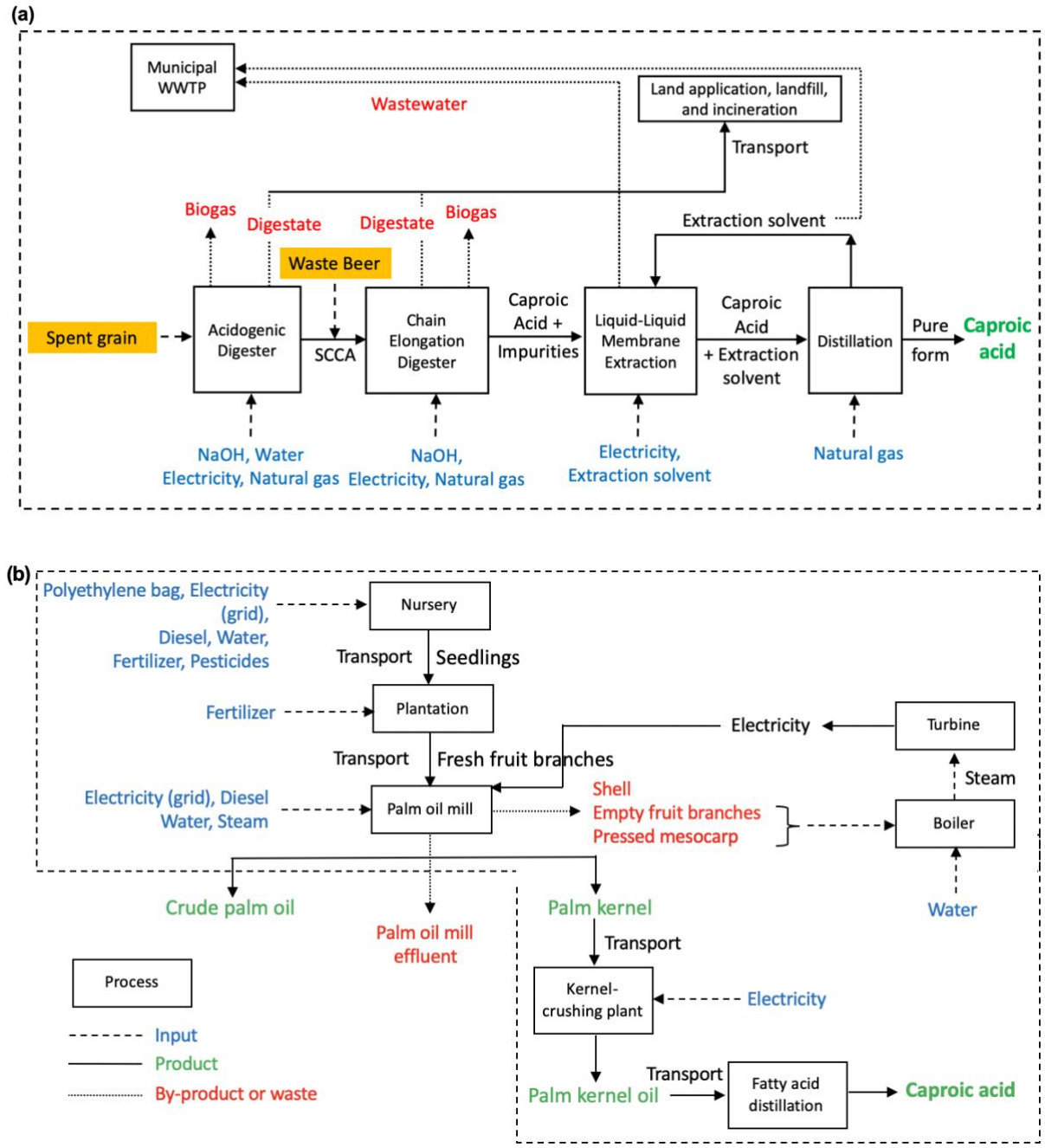

Figure 5.1. System boundary and unit processes for BW-CA (a) and PKO-CA (b) systems for production of one kg caproic acid (functional unit).

5.3.2 Life Cycle Inventory

The life cycle inventory (LCI) for BW-CA was built with data based on lab-scale experiments, literature values, and communication with industrial personnel (Doug Knox, the Sustainability Director at Jolly Pumpkin Brewery) and vendors. The LCI input and output data are summarized in Table D.2, Appendix D. The two-phase digesters (acidogenic (Fonoll et al., 2019) and chain elongation (Chapter 5) reactors) were modeled based on the lab-scale systems operated at the University of Michigan. The BW-CA system used brewery spent grain as input to the acidogenic digester and ethanol rich waste beer (60 g L^{-1}) in the chain elongation digester.. The lifetime of the system was assumed to be 10 years. It was assumed that the composition of inflows to both systems remains the same throughout the period of 10 years. Membrane-based LLX unit was used for caproic acid recovery from the chain elongation digester permeate and was modeled using both our lab-scale and literature data (Saboe et al., 2018). Caproic acid was extracted from the extraction solvent via vacuum distillation (Saboe et al., 2018) while the extraction solvent was recycled back to the LLX unit. The solid waste (digestate) from the digesters was disposed of using the average U.S. sludge disposal practice (25% landfill, 55% land application, and 20% incineration) (Beecher et al., 2007). The digestate was assumed to be thickened via centrifuge dewatering with polymer addition before disposal. Digestate transportation and diesel consumption during land application were accounted for within the system boundary.

The life cycle inventory for the PKO-CA was built from a series of peer-reviewed LCA studies conducted by the Malaysian Palm Oil Board (MPOB, Table D.3, Appendix D) (Choo et al., 2011; Muhammad et al., 2010; Subramaniam et al., 2010a, 2010b; Zulkifli et al., 2010). Detailed description of the processes involved in the production of caproic acid from PKO is given in section 3 of Appendix D. The environmental impact due to import of caproic acid from Malaysia to the U.S., was also considered. Some of the processes produce more than one product. For example, palm kernel and crude palm oil are considered as co-products of the palm oil milling process. Mass-based allocation was used to partition emissions to different products as shown in Figure D.1 (Appendix D). It should be noted that the choice of allocation (energy-based or economic value) influence the results.

5.3.3 Life Cycle Impact Assessment

The life cycle impact assessment (LCIA) data of all the materials and processes was obtained from Ecoinvent Database (Frischknecht et al., 2005) (v 3.3) using Umberto NXT Universal 7.1 (Table D.4, Appendix D) and imported to Excel to develop a full comparative LCI. The Tools for the Reduction and Assessment of Chemical and Other Environmental Impacts (TRACI 2.1) developed by U.S. EPA was used as the impact characterization methodology (Bare et al., 2002). The environmental impact categories evaluated included global warming potential (GWP, kg CO_2 equivalent (eq)), eutrophication potential (kg N eq), acidification potential (moles of H^+ eq), ecotoxicity (kg 2,4-D eq), ozone depletion (kg CFC-11 eq), smog (kg NO_x eq), carcinogens (kg benzene eq), non-carcinogens (kg toluene eq), and respiratory effects (kg PM 2.5 eq). The impact values reported in this study are expressed per functional unit i.e per one kg of caproic acid produced.

The environmental impact of the production of brewery waste was excluded, given that caproic acid production does not interfere with beer production and assumed that caproic acid is not a motivation for beer production. The wastewater generated from the BW-CA system was treated using the impact data included in the Ecoinvent Database. The biogas produced from both digesters was flared and the resulting CO_2 was excluded as biogenic CO_2 from the impact assessment. Previous LCA studies have shown that the construction phase environmental impacts are negligible compared to life cycle impacts (Ioannou-ttofa et al., 2016; Renou et al., 2008), thus only use-phase impacts were included in this study. Digester and LLX membranes lifetime were assumed to be 2.5 and 5 years, respectively. Membranes material and water and chemicals needed for membrane cleaning was included in the system boundary. The offset due to the substitution of mineral N and P fertilizers by digestate use for the land application was included. The impact data derived from Ecoinvent was primarily for global (GLO) geography with uses of Rest-of-World (RoW) for some activities if GLO data was not available (Table D.4, Appendix D). The electricity mix for BW-CA was based on Midwest (MRO) electricity grid. The electricity impact data for PKO-CA was based on Malaysia's electricity generation [MY] data available in the Ecoinvent database. The impact data information on other activities in the PKO-CA such as fertilizers,

pesticides, chemicals, and diesel used was based on the global data [GLO] as country specific data was not available in the Ecoinvent database.

5.3.4 Sensitivity Analysis

Based on the initial results and contribution of different parameters to the overall environmental impacts of the BW-CA system, a sensitivity analysis was performed using the parameters listed in Table D.5 (Appendix D). The baseline scenario was defined as the production of one kg of caproic acid from spent grain and waste beer in the BW-CA system with aggregate U.S. digestate disposal practice (25% landfill, 55% land application, and 20% incineration), and no biogas capture. Several scenarios were modeled and evaluated: biogas capture for heating, 100% land application for digestate disposal, and alternate data for NaOH addition. Detailed descriptions of all scenarios are provided in section 4 of Appendix D.

5.4 Results and Discussion

5.4.1 Environmental impacts of caproic acid production from brewery waste

The environmental impacts of the BW-CA system across the nine TRACI impact categories are shown in Table 5.1. All nine TRACI impact categories considered showed a negative environmental impact (Table 5.1). BW-CA achieved a positive environmental benefit from the eutrophication perspective only. The dominant factors causing significant environmental impact in all impact categories were assessed. This led to the identification of two major contributor to the environmental loads; NaOH use and brewery waste treatment (Figure 5.2). These two activities were the primary contributors in all the impact categories assessed except for the eutrophication impact category, for which wastewater treatment also had a significant impact.

Table 5.1 Life cycle assessment results across nine TRACI impact categories calculated per functional unit for BW-CA system for the baseline scenario

Unit Process	Global warming	Acidification	Carcinogenics	Non-Carcinogenics	Respiratory effects	Eutrophication	Ozone depletion	Ecotoxicity	Photochemical oxidation
	kg CO_2-eq	moles of H^+-eq	kg benzene-eq	kg toluene-eq	kg PM2.5-eq	kg N	kg CFC-11-eq	kg 2,4-D eq	kg NO_x-Eq
Water	6.0E-02	1.7E-02	1.9E-04	3.5E-01	1.6E-04	1.0E-05	1.6E-08	2.1E-02	1.4E-03
Electricity	1.3E-01	2.5E-02	1.2E-04	2.7E-01	5.7E-04	9.9E-06	1.7E-09	6.1E-02	1.8E-04
NaOH	1.7	4.9E-01	6.0E-03	1.4E+01	4.3E-03	3.9E-04	9.4E-07	6.9E-01	4.1E-03
Extraction solvent	9.7E-03	2.7E-04	6.6E-06	1.2E-02	1.4E-06	3.9E-06	6.1E-11	5.4E-04	4.4E-06
Membrane	2.8E-01	7.5E-02	1.0E-03	2.1	5.9E-04	1.0E-04	1.1E-08	1.7E-01	6.0E-04
Wastewater treatment	3.4E-02	1.4E-02	2.3E-04	2.4	7.4E-05	1.8E-03	1.9E-09	6.2E-01	1.2E-04
Digestate handling	1.2E-02	-1.1E-03	-3.7E-05	-3.0E-01	2.3E-05	-8.0E-03	7.3E-10	-1.1E-04	2.3E-05
Heating	7.0E-01	1.6E-01	3.3E-04	1.9	7.8E-04	3.4E-05	6.8E-08	4.0E-02	4.1E-04
Brewery waste	1.5	1.7	6.1E-03	9.9E+01	1.6E-03	9.8E-03	8.3E-08	6.7	6.8E-03
Total	4.5	2.4	1.4E-03	1.2E+02	8.1E-03	4.1E-03	1.1E-06	8.3	1.4E-02

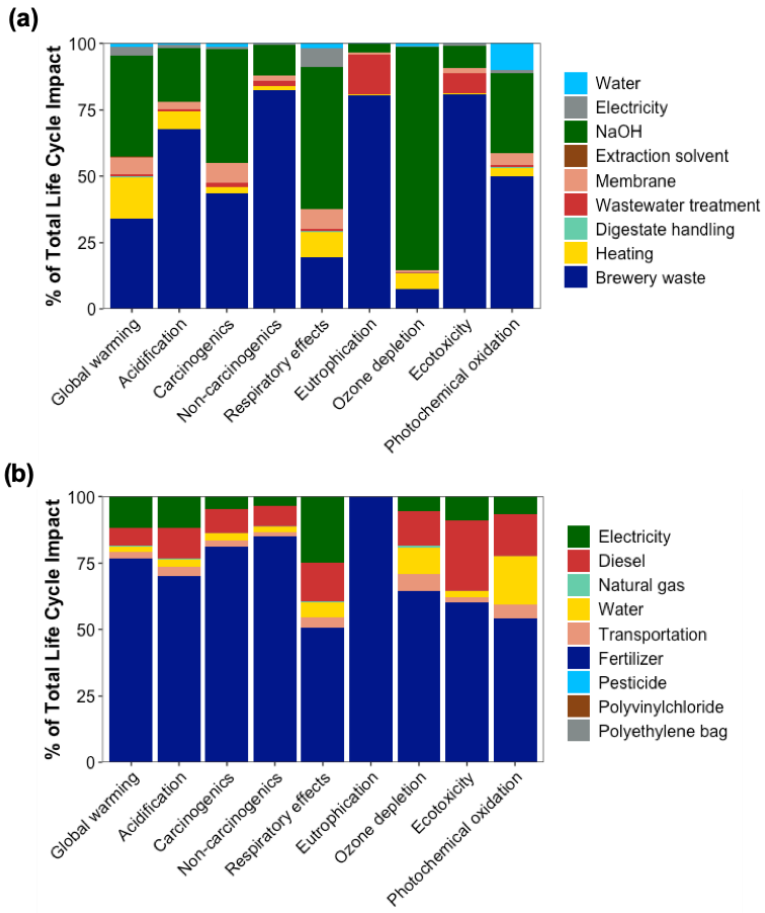

Figure 5.2. Relative contribution of different unit processes to the total life cycle impact of BW-CA (a) and PKO-CA (b) across nine TRACI impact categories during production of one kg of caproic acid.

NaOH consumption created a significant impact on the environmental loads of the BW-CA system. It was estimated that 1.25 kg of NaOH was required per kg of caproic acid produced in the first and second phase digesters for pH adjustment and 0.05 kg of NaOH per kg of caproic acid for LLX membrane cleaning (Table D.2, Appendix D). It is important to maintain slightly acidic conditions to favor SCCAs and caproic acid production in the acidogenic and chain elongation digesters, respectively. The NaOH use is the major source of GWP and is responsible for 1.71 kg CO_2 eq, which accounts for 38.3% of the total life-cycle GWP (Table 5.1, Figure 5.2). The environmental impact of NaOH production is mostly due to raw salt production and a large amount of electricity used during electrolysis and brine extraction (Hong et al., 2014; Thannimalay et al.,

2013). The environmental burden of NaOH heavily depends on the method of electricity generation during the production process (Hong et al., 2014). Additionally, the ecotoxicity, carcinogenics, and non-carcinogenics impacts are associated with the release of heavy metals and organochlorine compounds during NaOH production.

The environmental burden of brewery waste management i.e waste beer treatment and re-purposing spent grain as a substrate in the first phase digester instead of animal feed was also considered in the BW-CA system boundary. Waste beer is often combined with other brewery wastewater and either treated onsite or sent to the local wastewater treatment plant for further treatment. As waste beer comprises a small fraction (<1%) of the total brewery wastewater generated, the additional environmental impact due to waste beer treatment had small contribution (0.7-1.7%) to the total life cycle impact of the BW-CA system except in the eutrophication (13%) and ecotoxicity (6.6%) impact categories. However, spent grain use was the second biggest contributor to the total life-cycle GWP (33.3%) after NaOH while it was the leading contributor to impact categories such as eutrophication (67.6%), ecotoxicity (74.1%), acidification (67.3%), smog (49.3%), and non-carcinogenics (80.7%). Most of the breweries, including Jolly Pumpkin Brewery, send their spent grain to local farms to be used as animal feed due to its high protein and fiber content (Mussatto et al., 2006). Using spent grain as animal feed offsets the emissions from the carbon-intensive process of growing grains for animal feed production (Mogensen et al., 2014), thus providing environmental benefits of 14.6 kg of spent grain was used per kg of caproic acid produced in the BW-CA system. The environmental impacts from delivering the same amount of animal feed from another source led to emission of 1.5 kg CO_2 eq, 1.6 moles of H^+ eq, 9.7E+01 kg toluene eq, and 6.1 kg 2,4-D eq per functional unit. On the other hand, some places lack large-sized cattle farms, which can create problems in handling the huge amount of spent grain produced by some breweries. Moreover, pick-up and transportation of spent grain from the brewery to farms might not always be straightforward in urban settings with traffic, narrow streets, and parking problems. In such scenarios, diverting spent grain into a biological process such as chain elongation for resource recovery as proposed in this study seems to be an alternative strategy.

Energy use (electricity, diesel used in agricultural machinery during digestate spreading, and natural gas) was the third leading factor contributing to the total life-cycle GWP impact of the BW-CA system. Electricity is primarily produced from fossil fuel sources (coal, petroleum, and natural gas) in the midwest region of the U.S, which leads to detrimental environmental impact (U.S. Department of Energy, 2016). A major fraction (93.1%) of the total energy consumed during the BW-CA operation was attributed to the heating needs of the digesters (66.9%) and the distillation step (26.2%). The use of non-renewable natural gas for heating led to GWP of 0.70 kg CO_2-eq, contributing to 15.8% of the total life cycle GWP impact of the BW-CA system. Wastewater treatment, water consumption, and membrane use also led to some detrimental environmental consequences (Figure 5.2). The eutrophication and ecotoxicity impacts due to wastewater treatment are mostly associated with the remaining nutrients and other micropollutants in the wastewater, which are released to the water bodies after wastewater treatment. Water production and use had varying contribution ranging from 0.3-10.1% of the total life cycle impact across the nine impact categories. It was responsible for the second highest contribution (10.1%) to the total life cycle impact in terms of photochemical oxidation impacts, after NaOH use and brewery waste management. 35.6 L of water was required per functional unit (Table D.2, Appendix D), of which 94.2% was used for spent grain dilution in the acidogenic digester. 60.2 L wastewater was generated from the BW-CA system which can be used as dilution water, displacing the water use. Membrane material and cleaning had varying contribution in the range of 0.9-7.3% of the total life cycle impact in all categories.

Digestate handling showed environmental benefit in five impact categories (acidification, eutrophication, ecotoxicity, carcinogenics, and non-carcinogenics, Table 5.1). The positive environmental impact was associated with the fraction of digestate that was diverted into land application as it avoids an equivalent amount of mineral fertilizer depending on the nutrient concentration in the digestate. However, the environmental benefits of mineral fertilizer substitution were not large enough to completely offset the impacts in the other four impact categories (GWP, respiratory effects, ozone depletion, and photochemical oxidation categories). Among the three digestate disposal methods (25% landfill, 55% land application, and 20% incineration), landfilling was the biggest contributor to the GWP emissions (57.9%) due to

digestate handling, even though only one-fourth of the total digestate produced was landfilled. Improper land application practices can lead to over-fertilization and nutrient runoff causing negative environmental impacts (Nkoa, 2014).

In the Chen et al. (2017) study using crude ethanol and food waste, the total life-cycle GWP was in the range of 8.7-14.9 kg CO_2 per kg of caproic acid produced, which was almost two times higher compared to our study (4.5 kg CO_2-eq). They identified crude ethanol use, extraction solvent, and NaOH addition as the main contributors to the total life cycle impact. The addition of crude ethanol accounted for at least 20% of the total life-cycle impacts for all impact categories (Chen et al., 2017). In the BW-CA system, brewery waste served as the source of ethanol displacing crude ethanol use. 3.2 kg of ethanol present in the brewery waste was consumed per kg of caproic acid produced in the BW-CA system. If waste beer is replaced with crude ethanol in the BW-CA system, the environmental impacts, in particular GWP, will increase. The magnitude of GWP increase depends on the source of crude ethanol. For example, the highest impact was incurred when ethanol produced from corn was used compared to other sources of ethanol such as ethylene or lignocellulosic biomass, which was also pointed out by the Chen et al. (2017) study. There was a 206.2% (13.7 kg CO_2-eq), 84.0% (8.2 kg CO_2-eq), and 75.6% (7.8 kg CO_2-eq) increase in GWP compared to the baseline scenario when corn ethanol, ethylene, and lignocellulosic ethanol, respectively, were used instead of brewery waste. The higher life cycle impact using corn ethanol is associated with intensive agricultural practices during corn cultivation (González-García et al., 2013). Furthermore, the Chen et al. (2017) study employed two step extraction (forward and backward extraction) followed by acidification with HCl and distillation for recovery. Backward extraction requires an additional membrane unit and more chemical use (NaOH, HCl, and sodium borate solution). Furthermore, this step leads to the formation of sodium salt of the caproic acid which requires an additional post-stripping salt-breaking step to recover free acid product, for example, by acidification using HCl followed by a dewatering step. The double distillation step (extraction solvent and caproic acid distillation) developed by Saboe et al. (2018) and implemented in this study directly recovers caproic acid from the extraction solvent after the forward extraction, avoiding the backward extraction and acidification steps. The solvent distillation also recovers the stripped extraction solvent for subsequent reuse in the extraction step.

However, the distillation can be energy-intensive depending on the number of distillation columns used. Further investigation is needed to compare the economics of both approaches. Finally, it should be noted that a direct comparison cannot be made between the two studies due to the difference in the system boundary and the unit processes, and the different assumptions made.

5.4.2 Comparison of caproic acid production from brewery waste and palm kernel oil

The environmental impacts due to caproic acid production from the palm kernel oil route (PKO-CA) were modeled and compared with caproic acid production from brewery waste i.e BW-CA. The total life cycle impacts of PKO-CA system and relative contributions of various activities to the total life cycle impact are given in Table D.6 (Appendix D) and Figure 5.2, respectively. The nursery and plantation phases for the cultivation of palm oil fruit had the greatest impact on the life cycle of caproic acid production from palm kernel oil. This was primarily due to the use of mineral fertilizer (Figure 5.2). In the GWP category, fertilizer use was the main contributor (76.8%) followed by the consumption of electricity (11.6%), diesel for agricultural machinery (6.9%), transportation (2.2%), and water (2.1%). Fertilizer application was also the largest contributor in all other impact categories (Figure 5.2). The negative impacts of fertilizer are related to the energy-intensive production process and emissions during and after field application (Basosi et al., 2014; International Fertilizer Industry Association, 1998). The excess nutrients lost from fertilizer can be released to the environment via volatilization, leaching to groundwater, and surface runoff. Fertilizer use accounted for 99.9% of the total eutrophication impact, which is related to nitrogen and phosphorus emissions. Replacing mineral fertilizers with organic sources can possibly reduce environmental emissions of PKO-CA. Palm oil mill effluent (POME), the liquid waste produced during crude palm oil production, can be anaerobically digested to capture biogas, while the digested POME can be used as a fertilizer substitute (Aziz et al., 2020). Empty fruit branches, branches after stripping the fruits, or nutrient-rich slurry from the POME treatment ponds can also be used as a fertilizer (Chiew and Shimada, 2013).

Consumption of diesel for agricultural machinery, water, and electricity and the transportation phase also attributed to the total environmental loads of the PKO-CA system. The electricity produced on-site in the palm oil mill displaced 89.8% of the electricity use from the grid. The

impact due to deriving remaining electricity (2.5 kWh per functional unit) from the grid still contributed 11.6%, 11.7%, 25.0%, and 8.8% of the overall life cycle in the GWP, acidification, respiratory effects, and ecotoxicity, respectively (Figure 5.2). The fossil fuel (natural gas, coal, and crude oil) dependent electricity generation in Malaysia (Samsudina et al., 2016) contributed to these negative environmental consequences. Alternate to the literature data from the MPOB study, impact data for the production of palm kernel oil and fatty acid production from vegetable oil (data for caproic acid was not available in Ecoinvent database) was directly taken from the Ecoinvent database. The LCIA results derived from the Ecoinvent data predicted much higher environmental impacts compared to the MPOB study. For example, the GWP was 1.7 times higher (105.4 kg CO_2 eq) compared to the MPOB study (63.1 kg CO_2 eq). This difference might be due to the use of renewable electricity generated on-site by the MPOB study. This highlights the impact of renewable energy sources on the total life cycle impact of PKO-CA.

PKO-CA showed significantly higher environmental impacts relative to BW-CA (Table D.6, Appendix D, Figure 5.3). PKO-CA performed much worse from the GWP perspective than the BW-CA, with almost 14 times higher impact in the GWP category. The net increase in GWP impact from the BW-CA to PKO-CA was 58.7 kg CO_2 eq per kg of caproic acid produced, which is equivalent to avoiding CO_2 emission from 29.3 kg of coal burned (US EPA, 2020). 1.0E+07 kg of caproic acid was consumed globally in 2017 (360 Research Reports, 2020) which translates to 3.1E+08 kg of coal burned. Similarly, the LCIA results of PKO-CA for other impact categories were similar significantly higher compared to the BW-CA system (Table D.6, Appendix D, Figure 5.3). A significant fraction (51.0-99.9% across the nine impact categories) of the total life cycle impacts come from the raw material i.e palm oil cultivation in the PKO-CA system versus using waste streams as feedstock in the BW-CA system, which is otherwise disposed of and does not add to the environmental burden of the system.

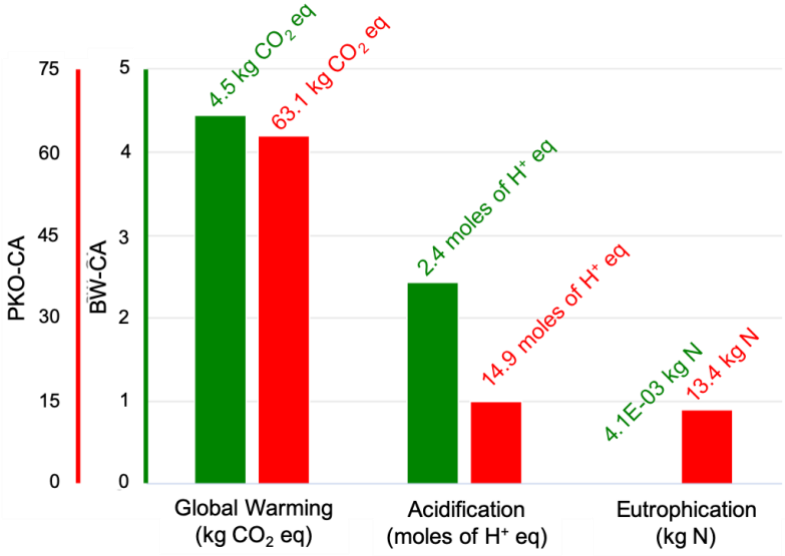

Figure 5.3. Comparison of total life cycle impact of BW-CA and PKO-CA in the Global warming, Acidification, and Eutrophication potential categories during production of one kg of caproic acid. Results for the other six impact categories are given in Table D.7

5.4.3 Sensitivity Analysis

A few alternative scenarios (Table D.5, Appendix D) were examined to evaluate their impact on the environmental footprint of the BW-CA system and identify areas for potential improvement. The percentage differences in total life cycle impact due to different changes compared to the baseline scenario are shown in Figure 5.4 and Table D.7 (Appendix D).

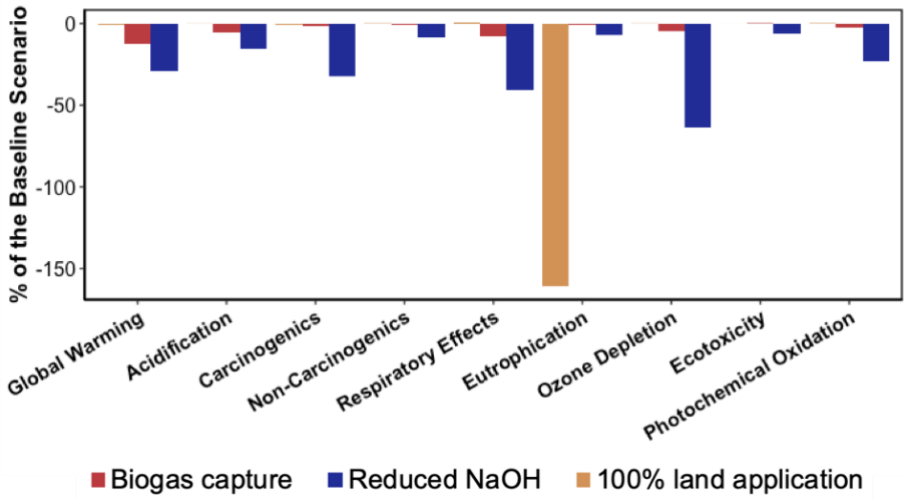

Figure 5.4. Results from the sensitivity analysis for all nine impact categories. Negative and positive values represent percentage reduction and increment in the total life cycle impact, respectively, compared to the baseline scenario.

The use of NaOH for pH control during the operation phase of BW-CA was the leading factor responsible for the environmental loads of BW-CA from GWP standpoint. Excessive ethanol oxidation to acetate (EEO), a competitive reaction during ethanol-based chain elongation, leads to production of acidic products like acetic acid. Controlling EEO can thus decrease the NaOH addition (Roghair et al., 2018b). Previous studies have shown that manipulating hydrogen partial pressure (Chapter 3), controlling CO_2 loading (Roghair et al., 2018a), and longer hydraulic retention time (Roghair et al., 2018b) can reduce EEO. Roghair et al. (2018b) reduced NaOH consumption from 0.67 kg NaOH per kg of caproic acid at HRT 1 day to 0.32 kg NaOH per kg of caproic acid at HRT of 4 days. In the current LCA model, 1.6 kg of acetic acid was produced per functional unit due to EEO. Acetic acid has several applications and can be used as carbon source for nitrogen and phosphorus removal, solvent in the production of dimethyl terephthalate and terephthalic acid, raw materials for several industrial products such as polymers, resins, paints, and adhesives (Pal and Nayak, 2017; Strazzera et al., 2018). However, the high hydrophilicity of acetic acid can make separation and purification difficult. The acetic acid remains in the permeate and was wasted, and its use was not included in this study. In the sensitivity analysis, the lower NaOH addition (0.32 kg NaOH per kg of caproic acid produced taken from Roghair et al. (2018b)) decreased the total GWP life-cycle impact by almost 28.9%, with changes of similar magnitude in

other impact categories (Figure 5.4, Table D.7, Appendix D). The contribution of NaOH to total GWP life cycle impact decreased from 38.3% (1.7 kg CO_2 eq per kg of caproic acid) in the baseline scenario to 13.2% (0.4 kg CO_2 eq per kg of caproic acid) due to lower NaOH addition, making brewery waste management the leading factor over NaOH. Other impact categories that were affected were acidification potential, carcinogenics, respiratory effects, ozone depletion, and photochemical oxidation, with 15.3%, 32.5%, 40.4%, 63.3%, and 22.7% impact reduction compared to the baseline scenario (Figure 5.4). However, operation at longer HRT as modeled in the alternative scenario will increase the footprint of the system and needs to be evaluated in the future studies. Another approach to avoid NaOH addition is to implement membrane electrochemical extraction. Electrolytic extraction has been applied to recover MCCAs and simultaneously control pH (due to OH^- production) (Andersen et al., 2015; Khor et al., 2017). However, this approach has often been associated with high electricity consumption and membrane material use. Therefore, the environmental impacts of electrolytic extraction should be evaluated to assess whether the advantage of avoiding NaOH addition will outweigh the added environmental loads from the electrochemical electrolytic system.

The environmental impact of using biogas on-site for heating, which was otherwise flared in the baseline scenario, was assessed in the sensitivity analysis. Both digesters were operated at slightly acidic condition to primarily produce carboxylic acids, as a result of which only a small fraction of the organics fed was used in biogas production. In total, biogas combustion produced 2.0 kWh per kg of caproic acid, which displaced approximately 77.9% of the total natural gas derived heating of the BW-CA system. Biogas leakage was ignored in this analysis. Comparing it with the baseline scenario, there was a 12.3% reduction in the GWP impact when substituting natural gas derived heating with biogas heating (Figure 5.4). Brewery wastewater temperature can affect the energy balance due to its impact on the heating requirement of the digesters. Studies have reported a wide range of brewery wastewater temperatures, from 25°C to 42°C (Chaitanyakumar et al., 2011). Retrofitting existing biogas plants to produce both caproic acid and biogas would also open new possibilities. The quantity and quality of biogas generated will also determine the practicality of energy recovery from biogas generated in chain elongation plants. These factors must be

considered in future studies to determine the feasibility of biogas capture and its impact on the environmental sustainability and cost-effectiveness of caproic acid production.

Digestate landfilling (25%) and incineration (20%), as proposed in the baseline scenario, were replaced with 100% land application in the sensitivity analysis. This resulted in a marginal reduction in total life cycle impact in all impact categories, except eutrophication (161.2%) and non-carcinogenics (1.5%), while there was a minor increase in the respiratory effects (0.7%) compared to the baseline scenario (Figure 5.4). This might be due to small environmental impacts attributed to digestate handling compared to other activities in the BW-CA system (Figure 5.2). The environmental benefits of the 100% land application were large enough to completely offset the total eutrophication life cycle impacts of BW-CA (-2.5E-03 kg N per kg of caproic acid, Table D.7, Appendix D).

Thus, the digestate handling method (100% land application vs 25% landfill, 55% land application, and 20% incineration) made least difference in total life cycle impact except in the eutrophication category compared to the biogas capture and reduction in NaOH addition. The greatest differences in impact results were observed due to lower NaOH addition, which decreased the GWP by 28.9% compared to the baseline. The best-case scenario, i.e with biogas capture, lower NaOH consumption, and 100% digestate land application led to total life cycle impact reduction in the range of 6.6-47.1% across the nine impact categories. Future research should also prioritize improving the caproic acid yield from waste streams as it affects both the environmental sustainability and economics of the system.

5.5 Conclusions

This study identified NaOH consumption and natural gas heating as the major contributors to the environmental burdens within the proposed system boundary of the BW-CA system. BW-CA system produced 4.5 kg CO_2-eq, of which 1.7 kg CO_2-eq resulted from NaOH use. However, PKO-CA approach was more detrimental than the BW-CA technology from all the TRACI impact categories standpoint. Assessing the environmental performance of emerging technologies such as chain elongation using the LCA method can be challenging due to lack of data. There is still a lot

of potential for improvement for BW-CA system as caproic acid production from waste streams gets optimized and chain elongation technology progresses towards full scale implementation. Particularly, if the NaOH addition can be reduced or avoided, the BW-CA system will become even more competitive from the environmental perspective for production of caproic acid. The outcome of this study can be used in decision making during the implementation, process design, and commercialization stages of the chain elongation technology. An economic life cycle costing analysis was beyond the scope of our study but would be useful to assess the economic viability and likelihood of market adoption and thus direct efforts to make chain elongation cost efficient.

5.6 References

360 Research Reports, 2020. Hexanoic Acid Market 2020 : Top Countries Data, Market Size with Global Demand Analysis and Business Opportunities Outlook 2024 [WWW Document]. URL https://www.marketwatch.com/press-release/hexanoic-acid-market-2020-top-countries-data-market-size-with-global-demand-analysis-and-business-opportunities-outlook-2024-2020-08-11 (accessed 10.28.20).

Agler, M.T., Spirito, C.M., Usack, J.G., Werner, J.J., Angenent, L.T., 2012a. Chain elongation with reactor microbiomes: upgrading dilute ethanol to medium-chain carboxylates. Energy Environ. Sci. 5, 8189. https://doi.org/10.1039/c2ee22101b

Agler, M.T., Werner, J.J., Iten, L.B., Dekker, A., Cotta, M.A., Dien, B.S., Angenent, L.T., 2012b. Shaping reactor microbiomes to produce the fuel precursor n-butyrate from pretreated cellulosic hydrolysates. Environmental Science & Technology, 46(. Environ. Sci. Technol. 46, 10229–38. https://doi.org/10.1021/es302352c

Andersen, S.J., Candry, P., Basadre, T., Khor, W.C., Roume, H., Hernandez-Sanabria, E., Coma, M., Rabaey, K., 2015. Electrolytic extraction drives volatile fatty acid chain elongation through lactic acid and replaces chemical pH control in thin stillage fermentation. Biotechnol. Biofuels 8, 221. https://doi.org/10.1186/s13068-015-0396-7

Angenent, L.T., Richter, H., Buckel, W., Spirito, C.M., Steinbusch, K.J.J., Plugge, C.M., Strik, D.P.B.T.B., Grootscholten, T.I.M., Buisman, C.J.N., Hamelers, H.V.M., 2016. Chain Elongation with Reactor Microbiomes: Open-Culture Biotechnology to Produce Biochemicals. Environ. Sci. Technol. 50, 2796–2810. https://doi.org/10.1021/acs.est.5b04847

Anneken, D.J., Both, S., Christoph, R., Fieg, G., Steinberner, U., Westfechtel, A., 2012. Fatty acids:Ullmann's Encyclopedia of Industrial Chemistry. https://doi.org/10.1002/14356007.a10

Aziz, N.I.H.A., Hanafiah, M.M., Gheewala, S.H., Ismail, H., 2020. Bioenergy for a cleaner future: A case study of sustainable biogas supply chain in the Malaysian Energy Sector. Sustain. 12. https://doi.org/10.3390/SU12083213

Bare, J.C., Norris, G.A., Pennington, D.W., McKone, T., 2002. The Tool for the Reduction and Assessment Impacts. J. Ind. Ecol. 6, 49–78. https://doi.org/10.1162/108819802766269539

Basosi, R., Spinelli, D., Fierro, A., Jez, S., 2014. Mineral nitrogen fertilizers: Environmental impact of production and use, Fertilizers: Components, Uses in Agriculture and Environmental Impacts. Nova science publishers.

Beecher, N., Crawford, K., Goldstein, N., Kester, G., Lono-Batura, M., Dziezyk, E., 2007. A national biosolids regulation, quality, end use, and disposal survey, North East Biosolids and Residuals Association (NEBRA).

Brewers Association, 2019. Statistics: Number of Breweries [WWW Document]. URL https://www.brewersassociation.org/statistics-and-data/national-beer-stats/ (accessed 5.29.20).

Capro-X [WWW Document], n.d. URL http://capro-x.com/ (accessed 10.12.20).

Carlson, K.M., Curran, L.M., Asner, G.P., Pittman, A.M., Trigg, S.N., Adeney, J.M., 2012. Carbon emissions from forest conversion by Kalimantan oil palm plantations. Nat. Clim. Chang. 3, 283–287. https://doi.org/10.1038/nclimate1702

ChainCraft [WWW Document], n.d. URL https://www.chaincraft.nl/ (accessed 10.12.20).

Chaitanyakumar, D., Unnisa, S.A., Rao, B., Kumar, G.V., 2011. Efficiency Assessment of Combined Treatment Technologies : A Case Study of Charminar Brewery Wastewater Treatment Plant 1, 138–145.

Chen, W., Strik, D.P.B.T.B., Buisman, C.J.N., Kroeze, C., 2017. Production of Caproic Acid from Mixed Organic Waste : An Environmental Life Cycle Perspective. Environ. Sci. Technol. 51, 7159–7168. https://doi.org/10.1021/acs.est.6b06220

Chiew, Y.L., Shimada, S., 2013. Current state and environmental impact assessment for utilizing oil palm empty fruit bunches for fuel, fiber and fertilizer - A case study of Malaysia. Biomass and Bioenergy 51, 109–124. https://doi.org/10.1016/j.biombioe.2013.01.012

Choo, Y.M., Muhamad, H., Hashim, Z., Subramaniam, V., Puah, C.W., Tan, Y., 2011. Determination of GHG contributions by subsystems in the oil palm supply chain using the LCA approach. Int. J. Life Cycle Assess. 16, 669–681. https://doi.org/10.1007/s11367-011-0303-9

Desbois, A.P., Smith, V.J., 2010. Antibacterial free fatty acids: Activities, mechanisms of action and biotechnological potential. Appl. Microbiol. Biotechnol. 85, 1629–1642. https://doi.org/10.1007/s00253-009-2355-3

Frischknecht, R., Jungbluth, N., Althaus, H., Doka, G., Dones, R., Heck, T., Hellweg, S., Hischier, R., Nemecek, T., Rebitzer, G., Spielmann, M., 2005. The ecoinvent Database : Overview and Methodological Framework. Int. J. Life Cycle Assess. 10, 3–9.

Ge, S., Usack, J.G., Spirito, C.M., Angenent, L.T., 2015. Long-Term *n* -Caproic Acid Production from Yeast-Fermentation Beer in an Anaerobic Bioreactor with Continuous Product Extraction. Environ. Sci. Technol. 49, 8012–8021. https://doi.org/10.1021/acs.est.5b00238

González-García, S., Bacenetti, J., Negri, M., Fiala, M., Arroja, L., 2013. Comparative environmental performance of three different annual energy crops for biogas production in Northern Italy. J. Clean. Prod. 43, 71–83. https://doi.org/10.1016/j.jclepro.2012.12.017

Goodman, L.K., Mulik, K., 2015. Clearing the air: Palm oil, peat destruction, and air pollution, Union of Concerned Scientists. https://doi.org/10.1177/0740277512443805

Grootscholten, T.I.M., Strik, D.P.B.T.B., Steinbusch, K.J.J., Buisman, C.J.N., Hamelers, H.V.M., 2014. Two-stage medium chain fatty acid (MCFA) production from municipal solid waste and ethanol. Appl. Energy 116, 223–229. https://doi.org/10.1016/j.apenergy.2013.11.061

Hanczakowska, E., 2017. The Use of Medium-Chain Fatty Acids in Piglet Feeding – A Review. Ann. Anim. Sci. 17, 967–977. https://doi.org/10.1515/aoas-2016-0099

Hong, J., Chen, W., Wang, Y., Xu, C., Xu, X., 2014. Life cycle assessment of caustic soda production: A case study in China. J. Clean. Prod. 66, 113–120. https://doi.org/10.1016/j.jclepro.2013.10.009

International Fertilizer Industry Association, 1998. Mineral Fertilizer Use and the Environment, United Nations Environment Programme.

Ioannou-ttofa, L., Foteinis, S., Chatzisymeon, E., Fatta-kassinos, D., 2016. The environmental footprint of a membrane bioreactor treatment process through Life Cycle Analysis. Sci. Total Environ. 568, 306–318. https://doi.org/10.1016/j.scitotenv.2016.06.032

Khor, W.C., Andersen, S., Vervaeren, H., Rabaey, K., 2017. Electricity - assisted production of caproic acid from grass. Biotechnol. Biofuels 10, 1–11. https://doi.org/10.1186/s13068-017-0863-4

Kucek, L., Xu, J., Nguyen, M., Angenent, L.T., 2016. Waste conversion into n-caprylate and n-caproate: resource recovery from wine lees using anaerobic reactor microbiomes and in-line extraction. Front. Microbiol. 7, 1–14. https://doi.org/10.3389/fmicb.2016.01892

Liang, S., Wan, C., 2015. Carboxylic acid production from Brewer's spent grain via mixed culture fermentation. Bioresour. Technol. 182, 179–183. https://doi.org/10.1016/j.biortech.2015.01.082

Mogensen, L., Kristensen, T., Nguyen, T.L.T., Knudsen, M.T., Hermansen, J.E., 2014. Method for calculating carbon footprint of cattle feeds - Including contribution from soil carbon changes and use of cattle manure. J. Clean. Prod. 73, 40–51. https://doi.org/10.1016/j.jclepro.2014.02.023

Muhammad, H., Hashim, Z., Subramaniam, V., Tan, Y.A., Wei, P.C., Let, C.C., May, C.Y., 2010. Life cycle assessment of oil palm seedling production (part 1). J. Oil Palm Res. 22, 878–886.

Mussatto, S.I., Dragone, G., Roberto, I.C., 2006. Brewers ' spent grain : generation , characteristics and potential applications. J. Cereal Sci. 43, 1–14. https://doi.org/10.1016/j.jcs.2005.06.001

Nkoa, R., 2014. Agricultural benefits and environmental risks of soil fertilization with anaerobic digestates: A review. Agron. Sustain. Dev. 34, 473–492. https://doi.org/10.1007/s13593-013-0196-z

Nzeteu, C.O., Trego, A.C., Abram, F., O'Flaherty, V., 2018. Reproducible, high-yielding, biological caproate production from food waste using a single-phase anaerobic reactor system. Biotechnol. Biofuels 11, 108. https://doi.org/10.1186/s13068-018-1101-4

Pal, P., Nayak, J., 2017. Acetic Acid Production and Purification: Critical Review Towards Process Intensification. Sep. Purif. Rev. 46, 44–61. https://doi.org/10.1080/15422119.2016.1185017

Petrenko, C., Paltseva, J., Searle, S., 2016. Ecological Impacts of Palm Oil Expansion in Indonesia. Washingt. Int. Counc. Clean Transp.

Renou, S., Thomas, J.S., Aoustin, E., Pons, M.N., 2008. Influence of impact assessment methods in wastewater treatment LCA. J. Clean. Prod. 16, 1098–1105. https://doi.org/10.1016/j.jclepro.2007.06.003

Roghair, M., Hoogstad, T., Strik, D.P.B.T.B., Plugge, C.M., Timmers, P.H.A., Weusthuis, R.A., Bruins, M.E., Buisman, C.J.N., 2018a. Controlling Ethanol Use in Chain Elongation by CO2 Loading Rate. Environ. Sci. Technol. https://doi.org/10.1021/acs.est.7b04904

Roghair, M., Liu, Y., Strik, D.P.B.T.B., Weusthuis, R.A., Bruins, M.E., Buisman, and C.J.N., 2018b. Development of an Effective Chain Elongation Process From Acidified Food Waste and Ethanol Into n-Caproate. Front. Bioeng. Biotechnol. 6, 1–11. https://doi.org/10.3389/fbioe.2018.00050

Saboe, P.O., Manker, L.P., Michener, W.E., Peterson, D.J., Brandner, D.G., Deutch, S.P., Kumar, M., Cywar, R.M., Beckham, T., Karp, E.M., 2018. In situ recovery of bio-based carboxylic acids. Green Chem. 20, 1791–1804. https://doi.org/10.1039/c7gc03747c

Samsudina, M.S.N., Rahman, M.M., Wahid, M.A., 2016. Power Generation Sources in Malaysia : Status and Prospects for Sustainable Development. J. Adv. Rev. Sci. Res. 25, 11–28.

Scalschi, L., Vicedo, B., Camañes, G., Fernandez-Crespo, E., Lapeña, L., González-Bosch, C., García-Agustín, P., 2013. Hexanoic acid is a resistance inducer that protects tomato plants against Pseudomonas syringae by priming the jasmonic acid and salicylic acid pathways. Mol. Plant Pathol. 14, 342–355. https://doi.org/10.1111/mpp.12010

Strazzera, G., Battista, F., Garcia, N.H., Frison, N., Bolzonella, D., 2018. Volatile fatty acids production from food wastes for biorefinery platforms: A review. J. Environ. Manage. 226, 278–288. https://doi.org/10.1016/j.jenvman.2018.08.039

Subramaniam, V., May, C.Y., Muhammad, H., Hashim, Z., Tan, Y.A., Wei, P.C., 2010a. Life cycle assessment of the production of crude palm oil (part 3). J. Oil Palm Res. 22, 895–903.

Subramaniam, V., May, C.Y., Muhammad, H., Hashim, Z., Tan, Y.A., Wei, P.C., 2010b. Life cycle assessment of the production of crude palm kernel oil (part 3a). J. Oil Palm Res. 22, 904–912.

Takeuchi, H., Sekine, S., Kojima, K., Aoyama, T., 2008. The application of medium-chain fatty acids: Edible oil with a suppressing effect on body fat accumulation. Asia Pac. J. Clin. Nutr. 17, 320–323. https://doi.org/10.6133/apjcn.2008.17.s1.79

Thannimalay, L., Yusoff, S., Zawawi, N.Z., 2013. Life Cycle Assessment of Sodium Hydroxide. Aust. J. Basic Appl. Sci. 7, 421–431.

The Brewers of Europe, 2017. Brewers statistics 2017 edition.

U.S. Department of Energy, 2016. Midwest Region Energy Sector Risk Profile. https://doi.org/10.1097/00152192-198803000-00015

United States Department of Agriculture, 2020. Oilseeds: World Markets and Trade.

Urban, C., Xu Jiajie, Strauber Heik, Dantas Tatiane R. dos Santos, Muhlenberg Jana, Hartig Claus, Angenent Largus T. and, Harnisch Falk, 2017. Production of drop-in fuels from biomass at high selectivity by combined microbial and electrochemical conversion. Energy Environ. Sci. 10, 2231–2244. https://doi.org/10.1039/c7ee01303e

US EPA, 2020. Greenhouse gas equivalencies calculator [WWW Document]. URL www.epa.gov/energy/greenhouse-gas-equivalencies-calculator (accessed 10.28.20).

Vasudevan, D., Richter, H., Angenent, L.T., 2014. Upgrading dilute ethanol from syngas fermentation to n-caproate with reactor microbiomes. Bioresour. Technol. 151, 378–382. https://doi.org/10.1016/j.biortech.2013.09.105

Xu, J., Hao, J., Juan, J.L., Spirito, C.M., Harroff, L.A., Largus, T., Xu, J., Hao, J., Guzman, J.J.L., Spirito, C.M., Harroff, L.A., 2018. Temperature-Phased Conversion of Acid Whey Waste Into

Medium-Chain Carboxylic Acids via Lactic Acid : No External e-Donor. Joule 1–16. https://doi.org/10.1016/j.joule.2017.11.008

Zion Market Research, 2018. Medium Chain Triglycerides Market (Caproic Acid, Caprylic Acid, Capric Acid, Lauric Acid, Heptanoic Acid and Nonanoic Acid) for Medical, Food, and Other Applications: Global Industry Perspective, Comprehensive Analysis, and Forecast, 2016 – 2022.

Zulkifli, H., Halimah, M., Chan, K.W., Choo, Y.M., Mohd Basri, W., 2010. Life cycle assessment for oil palm fresh fruit bunch production from continued land use for oil palm planted on mineral soil (part 2). J. Oil Palm Res. 22, 887–894.

Chapter 6

Conclusions, Significance, and Future Research Directions

6.1 Overview

Implementing chain elongation biotechnology to recover resources from waste streams is an attractive option that can reduce environmental impacts through waste treatment and reduce the use of plant oil based medium chain carboxylic acid (MCCA) production, and provide opportunities for revenue generation. Wastewater treatment plants are moving beyond traditional treatment methods and are investing in sustainable approaches to recover water, energy, and nutrients. Furthermore, as the number of breweries has been increasing and municipal wastewater treatment infrastructure has been strained, breweries have become interested in innovative solutions for waste management. Other food processing and chemical industries are also considering expanding on-site waste management. In this context, this dissertation research is highly relevant as it explores development of novel resource recovery technologies.

In this dissertation research, the diverse metabolic capacity of anaerobic microbiomes was leveraged to produce MCCAs from organic waste streams such as pre-fermented food waste and brewery waste streams. This work advanced our fundamental knowledge about chain elongation, assisted in technology development, and addressed several challenges that would otherwise limit the application of MCCA production from waste streams. Specifically, we assessed the impact of microbial immigration on the chain elongation microbiome (Chapter 2), employed strategies to control undesirable reactions during ethanol chain elongation (Chapter 3), developed an innovative bioreactor system to facilitate integration with downstream MCCA extraction (Chapter 4), and

evaluated environmental performance of the technology with life cycle assessment modeling (Chapter 5). Additionally, we demonstrated that applying microbial and modeling information in bioprocess engineering and technology development is crucial to inform engineering decisions to make the chain elongation system efficient and stable.

6.2 Major findings and significance

6.2.1 Impact of microbial immigration

Chapter 2 presented new insights into the role of microbial immigration in shaping the chain elongation microbiome. It is challenging to evaluate the contribution of microbial immigration to the microbial diversity and function of the bioreactor system as it can introduce both active and inactive microbial populations. This dissertation research combined a mass balance approach to calculate the specific growth rate of individual microbial populations with the ratio of relative activity and relative abundance based on 16S rRNA and 16S rRNA gene sequencing (rRNA/rDNA), respectively. This enabled us to distinguish populations actively contributing to the chain elongation process from the ones not or minimally influencing function. Such approaches, when incorporated into future studies, will avoid potential bias introduced by including inactive yet dominant populations in process modeling, improving our ability to identify environmental parameters that influence the active fraction of the microbial community and thus process performance. Future research should consider determining absolute abundances by using quantitative approaches such as flow cytometry and quantitative PCR in contrast to using relative abundance and activity data to calculate the specific growth rate.

6.2.2 Controlling competitive reactions during ethanol chain elongation

Chapter 3 focused on improving the chain elongation process by inhibiting competitive pathways. Excessive ethanol oxidation to acetate (EEO) was identified as one of the major competitive reactions during the ethanol chain elongation process. Our findings in Chapter 3 indicated that maintaining high hydrogen partial pressure (P_{H2}) in the bioreactor by suppressing the activity of hydrogenotrophic methanogens can limit EEO. This elucidates how the metabolism of one population can affect the metabolic activity of another, highlighting the need to understand the

interaction between different functional guilds in mixed microbial communities. Furthermore, understanding the impact of different operational parameters, P_{H2} in this case, on the bioprocess of interest, including inhibiting competitive reactions, is important. This further highlights the fact that operational parameters can serve as tools to engineer anaerobic microbiomes for desired outputs. Hydrogenotrophic methanogenesis was inhibited by adding 2-bromoethanesulfonate (2-BES), a methanogenic inhibitor. However, the results showed that the inhibition was short-lived and an environment that selected for the growth of microbial populations resistant to 2-BES was created. These findings further indicated that evaluating the long-term efficacy of such methanogenic inhibitors is important to determine their potential applications in the field. Lastly, using both amplicon sequence variant (ASV) and operational taxonomic unit (OTU) based approaches were instrumental in gaining detailed insights into the inhibitor-induced changes.

6.2.3 Dynamic membrane biofilm development leads to efficient solids-liquid separation along with enhanced MCCA production

The anaerobic dynamic membrane bioreactor (AnDMBR) developed in Chapter 4 combined the chain elongation bioprocess with solids-liquid separation through dynamic membrane biofilm development. This research suggests that developing an integrated system that directly couples the chain elongation bioreactor with downstream processing, avoiding multiple external filtration steps, is possible. In terms of cost and environmental impacts, this integrated approach is likely advantageous compared to other MCCA systems (Kucek et al., 2016b, 2016c, 2016a). Additionally, the dynamic membrane involved in efficient solids-liquid separation also played a significant role in MCCA production. The development of the dynamic membrane biofilm led to a specialized microbial community enriched in highly active MCCAs producing microorganisms, thus promoting chain elongation activity. The results presented in Chapter 4 open up the possibility to use a biofilm enhanced anaerobic system to improve MCCA production.

6.2.4 MCCA production from brewery waste is environmentally sustainable compared to the conventional palm kernel oil-based method

As demonstrated by the life cycle assessment (LCA) in Chapter 5, repurposing brewery waste streams into MCCA production showed great potential to address environmental concerns

associated with MCCA production from the traditional palm kernel oil-based route. The total life cycle environmental impacts of caproic acid production from brewery waste were significantly lower than those associated with the palm kernel oil production. The environmental LCA modeling highlighted activities such as sodium hydroxide use and energy consumption for heating as major contributors to the environmental impacts. As sodium hydroxide limited the potential environmental benefits, an alternate source for pH control with a smaller environmental footprint or strategies to reduce sodium hydroxide consumption need to be explored. Furthermore, there is an opportunity to reduce the energy requirement of the system by capturing biogas produced on-site to meet the heating demand of the system. These outcomes can be used to improve the environmental sustainability of the technology. Recovering caproic acid from waste streams may also have economic benefits. An economic life cycle costing analysis was beyond the scope of our study but would be useful to support the further development and implementation of this technology. Therefore, future studies should integrate environmental LCA with economic LCA to identify undesirable environmental and economic consequences.

6.3 Future research directions

This study has raised additional research questions and opened up several possibilities for future work. First, alternate strategies need to be developed for long term suppression of competing processes such as EEO to reduce inefficient usage of ethanol and thus increase the product selectivity and yield. 2-BES was added every ten days (equivalent to three hydraulic retentions times in this study) to control EEO. This resulted in short-term inhibition of hydrogenotrophic methanogens and hence the EEO pathway. It would be valuable to assess the impact of continuous addition of 2-BES on EEO and the response of the microbial community to inhibitor addition. This approach will still not address the sustainability issue related to using a chemical inhibitor but can be used to verify whether controlling P_{H2} is a reliable operational strategy to ensure long term inhibition of EEO. Furthermore, the microorganisms involved in EEO are still unidentified. Therefore, a better understanding of the ethanol oxidizers and their physiology could assist in developing strategies to suppress their metabolism during chain elongation.

The AnDMBR is a relatively new technology for waste(water) treatment. While conventional membrane bioreactors have been widely implemented and tested at various scales for waste(water) treatment, AnDMBRs need further optimization before they can be successfully deployed at full scale. For example, the AnDMBR developed in Chapter 4 was operated at a flux around 0.5-0.7 L m^{-2} h^{-1}. Efficient integration of the AnDMBR with the downstream extraction unit would require much higher fluxes as the operating flux directly influences the extraction efficiency as shown by Kucek et al. (2016c). AnDMBRs for treatment of domestic wastewater, a waste stream containing much lower levels of organic compounds and suspended solids than the waste streams considered here, have been evaluated with a flux as high as 65 L m^{-2} h^{-1} (Zhang et al., 2010). The AnDMBR was continuously operated without cleaning the dynamic membrane and the support material for more than 200 days, after which the permeate quality started deteriorating. In general, the reduced energy and chemical need and ease of fouling control provide a great benefit compared to the conventional membrane bioreactors using polymeric or ceramic membranes (Ersahin et al., 2012; Hu et al., 2018). However, integrating a minimal cleaning scheme into the AnDMBR operation to control the thickness of the dynamic membrane and to prevent fouling of the support material would be beneficial to ensure stable performance for an extended time and to enable operation at high flux. Some of the commonly used cleaning methods employed by other AnDMBRs studies include backwashing, biogas recirculation, intermittent operation, and relaxation (Hu et al., 2018).

The AnDMBR system exhibited a long start-up period during which the MCCA production was low after inoculation with rumen content. Chain elongation activity was enhanced once the bioreactor was re-seeded with an adapted inoculum consisting of a mixture of rumen content and bioreactor biomass from a functional chain elongating bioreactor. Microbial analysis showed that re-inoculation with the adapted inoculum introduced key chain elongating populations. Future research should also explore other start-up strategies, such as a gradual increase in organic loading rate, to shorten the acclimation period.

In Chapter 4, we hypothesized that the higher MCCA concentrations in the permeate samples compared to the bioreactor samples were due to high microbial activity in the dynamic membrane formed in the AnDMBR. Several studies have highlighted the role of biofilm microbial activity in

promoting organics removal in anaerobic systems (Alibardi et al., 2016; Smith et al., 2015). Future research should focus on an in-depth characterization of the biofilm morphology and composition including the composition of extracellular polymeric substances (EPS). Relevant methods for such work include scanning electron microscopy (SEM), optical coherence tomography (OCT), confocal laser scanning microscopy (CLSM), and fluorescence in-situ hybridization (FISH) (Guan et al., 2018; Lin et al., 2010). The in-situ visualization and identification of microbial populations, for example, using species-specific oligonucleotide probes using FISH will help to understand the spatial organization of different microorganisms in the biofilm providing information to help elucidate syntrophic or other interspecies interactions. This will assist in understanding the underlying mechanisms for enhanced MCCA producing activity in the dynamic membrane biofilm. EPS plays an important role in dynamic membrane formation and greatly contributes to its characteristics, thereby affecting the performance of the system (Ersahin et al., 2016; Lin et al., 2010; Zhang et al., 2010). Furthermore, EPS has been found to protect against external stress and also influences surface charge and membrane fouling. Therefore, EPS characterization can shed light on its effect on microbial interaction and function and can also help in devising EPS control strategies to promote dynamic membrane formation and fouling mitigation.

Methanobrevibacter was consistently observed at high relative abundance and activity in the chain elongation bioreactors operated in this dissertation, even after adding a methanogenic inhibitor (Chapter 3). Several studies have demonstrated that methanogens, such as *Methanobrevibacter* spp., are capable of utilizing alcohol for growth and methane production (Berk and Thauer, 1997; Imachi et al., 2009; Metje and Frenzel, 2005; Poehlein et al., 2018; Widdel, 1986). It remains unclear whether *Methanobrevibacter* contributed to ethanol utilization in our study. Thus, an important hypothesis to test is whether *Methanobrevibacter* is involved in ethanol metabolism such as EEO during the chain elongation process. The bioreactor samples collected during this dissertation research during periods with high relative abundance and activity of *Methanobrevibacter* could be used for metagenomic and metatranscriptomic sequencing to study the metabolic potential and functional role of *Methanobrevibacter* spp. in chain elongation and specifically identify possible genes involved in ethanol metabolism.

There is limited information on the microorganisms capable of chain elongation. We need to improve our understanding of interspecies interactions and metabolic diversity required for stable MCCA production. It is challenging to establish the identity of microorganisms and their (multiple) roles in a mixed culture environmental system as complex as the one needed for chain elongation using diverse waste streams as substrates. The microbial data reported in this dissertation (Chapters 2-4) are based on partial 16S rRNA gene and 16S rRNA amplicon sequencing and only provide limited taxonomic information. While the rRNA gene remains the most commonly used marker in chain elongation studies, targeting core protein-coding genes can provide important insights into community composition and function not obtainable through rRNA based analyses. Furthermore, a stable isotope probing (SIP) approach integrated with DNA or RNA sequencing would allow linkage of individual taxa with their function (Coyotzi et al., 2016; Lueders et al., 2016). SIP experiments were conducted in our lab in serum bottles by incubating AnDMBR biomass with ^{13}C-ethanol and ^{13}C-propionate. The long-term goal of the effort initiated with the SIP experiments is to build a comprehensive metabolic model using the SIP-omics microbial data, bioreactor results, and stoichiometric, thermodynamic, and kinetic information. This will provide metabolic and genomic insights into chain elongating microbial communities.

Downstream processing can be a bottleneck during the scale-up of a biochemical process as it typically significantly contributes to the total capital and operating costs and environmental impacts (Biddy et al., 2016; Chen et al., 2017). Therefore, it is necessary to develop an efficient and cost-effective MCCA recovery system. During the first two years of this dissertation research, we collaborated with TDA Research Inc., a company focused on developing chemical technologies, to create a novel extractant-supported hollow fiber membrane for MCCA extraction. In contrast to commonly used two-step, liquid-liquid extraction systems (Chapter 4), TDA developed a single-step membrane system. This configuration is expected to reduce capital and operating costs and environmental impacts due to lower energy and solvent usage and reduced membrane need. Future research should continue to explore strategies for optimizing the downstream process to make the chain elongation system more sustainable and feasible for scale-up.

Taken together, this dissertation research contributed significantly to the current state of knowledge on chain elongation. It further provides information to guide future research and make strategic decisions for technology development.

6.4 References

Alibardi, L., Bernava, N., Cossu, R., Spagni, A., 2016. Anaerobic dynamic membrane bioreactor for wastewater treatment at ambient temperature. Chem. Eng. J. 284, 130–138. https://doi.org/10.1016/j.cej.2015.08.111

Berk, H., Thauer, R.K., 1997. Function of coenzyme F 420 -dependent NADP reductase in methanogenic archaea containing an NADP-dependent alcohol dehydrogenase. Arch Microbiol 168, 396–402.

Biddy, M.J., Davis, R., Humbird, D., Tao, L., Dowe, N., Guarnieri, M.T., Linger, J.G., Karp, E.M., Salvachúa, D., Vardon, D.R., Beckham, G.T., 2016. The Techno-Economic Basis for Coproduct Manufacturing to Enable Hydrocarbon Fuel Production from Lignocellulosic Biomass. ACS Sustain. Chem. Eng. 4, 3196–3211. https://doi.org/10.1021/acssuschemeng.6b00243

Chen, W., Strik, D.P.B.T.B., Buisman, C.J.N., Kroeze, C., 2017. Production of Caproic Acid from Mixed Organic Waste : An Environmental Life Cycle Perspective. Environ. Sci. Technol. 51, 7159–7168. https://doi.org/10.1021/acs.est.6b06220

Coyotzi, S., Pratscher, J., Murrell, J.C., Neufeld, J.D., 2016. Targeted metagenomics of active microbial populations with stable-isotope probing. Curr. Opin. Biotechnol. 41, 1–8. https://doi.org/10.1016/j.copbio.2016.02.017

Ersahin, M.E., Ozgun, H., Dereli, R.K., Ozturk, I., Roest, K., van Lier, J.B., 2012. A review on dynamic membrane filtration: Materials, applications and future perspectives. Bioresour. Technol. 122, 196–206. https://doi.org/10.1016/j.biortech.2012.03.086

Ersahin, M.E., Tao, Y., Ozgun, H., Spanjers, H., van Lier, J.B., 2016. Characteristics and role of dynamic membrane layer in anaerobic membrane bioreactors. Biotechnol. Bioeng. 113, 761–771. https://doi.org/10.1002/bit.25841

Guan, D., Dai, J., Watanabe, Y., Chen, G., 2018. Changes in the physical properties of the dynamic layer and its correlation with permeate quality in a self-forming dynamic membrane bioreactor. Water Res. 140, 67–76. https://doi.org/10.1016/j.watres.2018.04.041

Hu, Y., Wang, X.C., Ngo, H.H., Sun, Q., Yang, Y., 2018. Anaerobic dynamic membrane bioreactor (AnDMBR) for wastewater treatment: A review. Bioresour. Technol. 247, 1107–1118. https://doi.org/10.1016/j.biortech.2017.09.101

Imachi, H., Sakai, S., Nagai, H., Yamaguchi, T., Takai, K., 2009. Methanofollis ethanolicus sp.

nov., an ethanol- utilizing methanogen isolated from a lotus field Hiroyuki. Int. J. Syst. Evol. Microbiol. 800–805. https://doi.org/10.1099/ijs.0.003731-0

Kucek, L., Nguyen, M., Angenent, L.T., 2016a. Conversion of L-lactate into n-caproate by a continuously fed reactor microbiome. Water Res. 93, 163–171. https://doi.org/10.1016/j.watres.2016.02.018

Kucek, L., Spirito, C.M., Angenent, L.T., 2016b. High n-caprylate productivities and specificities from dilute ethanol and acetate: Chain elongation with microbiomes to upgrade products from syngas fermentation. Energy Environ. Sci. 9, 3482–3494. https://doi.org/10.1039/c6ee01487a

Kucek, L., Xu, J., Nguyen, M., Angenent, L.T., 2016c. Waste conversion into n-caprylate and n-caproate: resource recovery from wine lees using anaerobic reactor microbiomes and in-line extraction. Front. Microbiol. 7, 1–14. https://doi.org/10.3389/fmicb.2016.01892

Lin, H.J., Xie, K., Mahendran, B., Bagley, D.M., Leung, K.T., Liss, S.N., Liao, B.Q., 2010. Factors affecting sludge cake formation in a submerged anaerobic membrane bioreactor. J. Memb. Sci. 361, 126–134. https://doi.org/10.1016/j.memsci.2010.05.062

Lueders, T., Dumont, M.G., Bradford, L., Manefield, M., 2016. RNA-stable isotope probing: From carbon flow within key microbiota to targeted transcriptomes. Curr. Opin. Biotechnol. 41, 83–89. https://doi.org/10.1016/j.copbio.2016.05.001

Metje, M., Frenzel, P., 2005. Effect of temperature on anaerobic ethanol oxidation and methanogenesis in acidic peat from a Northern Wetland. Appl. Environ. Microbiol. 71, 8191–8200. https://doi.org/10.1128/AEM.71.12.8191-8200.2005

Poehlein, A., Schneider, D., Soh, M., Daniel, R., Seedorf, H., 2018. Comparative Genomic Analysis of Members of the Genera Methanosphaera and Methanobrevibacter Reveals Distinct Clades with Specific Potential Metabolic Functions 2018.

Smith, M. biofilm development improves C. removal in anaerobic membrane bioreactor wastewater treatmentAdam L., Skerlos, S.J., Raskin, L., 2015. Membrane biofilm development improves COD removal in anaerobic membrane bioreactor wastewater treatment. Microb. Biotechnol. 8, 883–894. https://doi.org/10.1111/1751-7915.12311

Widdel, F., 1986. Growth of methanogenic bacteria in pure culture with 2-propanol and other alcohols as hydrogen donors. Appl. Environ. Microbiol. 51, 1056–1062. https://doi.org/10.1128/aem.51.5.1056-1062.1986

Zhang, X., Wang, Z., Wu, Z., Lu, F., Tong, J., Zang, L., 2010. Formation of dynamic membrane in an anaerobic membrane bioreactor for municipal wastewater treatment. Chem. Eng. J. 165, 175–183. https://doi.org/10.1016/j.cej.2010.09.013

APPENDICES

APPENDIX A

Supplemental Information for Chapter 2

Resource Recovery of Medium Chain Carboxylic Acids from Brewery and Pre-Fermented Food Waste Streams: Effect of Microbial Immigration on Chain Elongation

A.1 Materials and Methods

A.1.1 Mass balance calculation:

The following equation was used to calculate specific growth rate of microbial population x:

Change = Influent – Effluent + Growth

$$\frac{d(N_{x,re})}{dt} = n_{x,in} - n_{x,out} + \mu_x \times N_{x,re}$$

where:

$N_{x,re}$ is the absolute number of microorganism x in the bioreactor

$n_{x,in}$ = number microorganism x in the influent entering the bioreactor per day [d^{-1}]

$n_{x,out}$ = number microorganism x in the effluent leaving the bioreactor per day [d^{-1}]

μ_x = net specific growth rate of microorganism x [d^{-1}]

Assuming steady state ($\frac{d(N_{x,re})}{dt} = 0$):

$$\mu_x = \frac{n_{x,out} - n_{x,in}}{N_{x,re}}$$

$n_{x,out}$ and $n_{x,in}$ were calculated separately using both relative abundance and activity data derived from the 16S rRNA gene and 16S rRNA sequencing, respectively.

$n_{x,out}$ was calculated by multiplying the relative abundance (or relative activity) of microorganism x in the effluent ($r_{x,out}$) with the total number of cells leaving the bioreactor per day (n_{out}).

$n_{x,in}$ was calculated by multiplying the relative abundance (or relative activity) of microorganism x in the influent ($r_{x,in}$) with the total number of cells entering the bioreactor per day (n_{in}).

$N_{x,re}$ was calculated by multiplying the relative abundance (or relative activity) of microorganism x in the bioreactor ($r_{x,re}$) with the total number of cells in the bioreactor (N_{re}).

$$\mu_x = \frac{r_{x,out}n_{out} - r_{x,in}n_{in}}{r_{x,re}N_{re}}$$

n_{out} was calculated by multiplying the volume of effluent wasted per day (Q_{out}, L d^{-1}) with the total cell concentration in the effluent (C_{out}, cells L^{-1})

n_{in} was calculated by multiplying volume of influent fed per day (Q_{in}, L d^{-1}) with the total cell concentration in the influent (C_{in}, cells L^{-1})

N_{re} was calculated by multiplying working volume of the bioreactor (V_{re}, L) with total cell concentration in the bioreactor (C_{re}, cells L^{-1})

$$\mu_x = \frac{r_{x,out} \times Q_{out} \times C_{out} - r_{x,in} \times Q_{in} \times C_{in}}{r_{x,re} \times V_{re} \times C_{re}}$$

The relative abundance and relative activity of x in effluent was assumed to be equal to the relative abundance and relative activity of x in bioreactor ($r_{x,out} = r_{x,re}$), respectively, a reasonable assumption given that the bioreactor was well mixed.

$$\mu_x = \frac{r_{x,out} \times Q_{out} \times C_{out} - r_{x,in} \times Q_{in} \times C_{in}}{r_{x,out} \times V_{re} \times C_{re}}$$

We describe below two approaches to calculate cell concentration in the bioreactor, effluent, and influent (C_{re}, C_{out}, and C_{in}).

Method I:

The first approach used was modified from Mei et al. (2016). The amount of DNA or RNA recovered per cell and g volatile suspended solids (VSS) equivalent to the amount of biomass used for extraction were used to approximate cell concentration in respective samples. Volume of influent (Q_{in}) and effluent (Q_{out}) per day were expressed in terms of gVSS fed per day [$gVSS_{in}\ d^{-1}$] and gVSS wasted per day [$gVSS_{out}\ d^{-1}$], respectively.

Total cell concentration in the effluent was assumed to be equal to total cell concentration in the bioreactor ($C_{out} = C_{re}$). Total cell concentration in the influent (C_{in}) and the effluent (bioreactor, C_{re}) were expressed as a ratio of number of cells per gVSS in the influent [$cells_{in}\ gVSS_{in}^{-1}$] and number of cells per gVSS in the effluent [$cells_{out}\ gVSS_{out}^{-1}$], respectively. gVSS refers to amount of VSS equivalent to the amount of biomass (μg) used for DNA or RNA extraction. Extraction efficiency was assumed to be 100%.

$$\mu_x = \frac{r_{x,out} \times \frac{\mathrm{gVSS}_{out}}{\mathrm{d}} \times \frac{\mathrm{cells}_{out}}{\mathrm{gVSS}_{out}} - r_{x,in} \times \frac{\mathrm{gVSS}_{in}}{\mathrm{d}} \times \frac{\mathrm{cells}_{in}}{\mathrm{gVSS}_{in}}}{r_{x,out} \times gVSS_{out} \times \frac{\mathrm{cells}_{out}}{\mathrm{gVSS}_{out}}}$$

The number of cells ($cells_{in}$ and $cells_{out}$) was calculated separately for influent and effluent by determining the amount of DNA (or RNA, μg) recovered and assuming that one cell (6 Mbp genome size) contains 9 fg of DNA (or 60 fg RNA) (Milo, Ron and Phillips, 2015). The amount

of DNA (or RNA) was determined by multiplying DNA (or RNA) concentration (μg μL^{-1}) with the extraction elution volume (μL).

For example,

$$cells = \frac{amount\ of\ DNA\ or\ RNA\ recoverd\ (\mu g)}{9\ fg\ DNA\ or\ 60\ fg\ RNA\ per\ cell\ \times\ 10^{-9}}$$

$$= \frac{DNA\ or\ RNA\ concentration\ \left(\frac{\mu g}{\mu L}\right) \times\ \text{elution volume}\ (\mu L)}{9\ fg\ DNA\ or\ 60\ fg\ RNA\ per\ cell\ \times\ 10^{-9}}$$

Method II:

The second approach used was similar to that used by Mei et al.(Mei et al., 2016) where VSS of influent (VSS_{in}), effluent (VSS_{out}), and bioreactor (VSS_{re}) were used to approximate cell concentration in respective samples.

$$\mu_x = \frac{r_{x,out} \times Q_{out} \times VSS_{out} - r_{x,in} \times Q_{in} \times VSS_{in}}{r_{x,out} \times V_{re} \times VSS_{re}}$$

A.1 Tables

Table A.1. Chemical characteristics of inoculum and substrates

Parameter	Unit	Rumen (Day 0)	Rumen (Day 178)	Waste beer (Batch 1)	Waste beer (Batch 2)	Permeate
TS	g/L	24.9 ± 1.1	19.2 ± 0.0	35.5 ± 0.2	30.0 ± 0.2	8.7 ± 1.2
VS	g/L	17.1 ± 1.0	10.7 ± 0.0	33.8 ± 0.5	27.8 ± 0.1	5.2 ± 1.0
TSS	g/L	17.2 ± 0.3	10.9 ± 0.0	0.9 ± 0.1	1.3 ± 0.1	3.1 ± 1.9
VSS	g/L	13.4 ± 0.3	8.7 ± 0.3	0.9 ± 0.1	1.2 ± 0.1	2.7 ± 1.7
sCOD	g/L	17.8 ± 0.4	N.D.	191.0 ± 1.9	130.2 ± 0.1	13.4 ± 6.6
Ethanol	mM	0.0 ± 0.0	0.0 ± 0.0	1745.5 ± 1.0	1024.2 ± 4.6	1.9 ± 2.3
SCCAs	mM	172.5 ± 0.4	83.9 ± 0.1	0.0 ± 0.0	0.0 ± 0.0	63.1 ± 10.5
MCCAs	mM	0.0 ± 0.0	0.0 ± 0.0	0.0 ± 0.0	0.0 ± 0.0	1.1 ± 1.0
Lactate	mM	N.D.	N.D.	N.D.	N.D.	N.D.

Values are reported as means with standard deviations of technical triplicates. Permeate values are averages with standard deviations over 229 days. SCCAs include n-acetate, n-propionate, n- and iso-butyrate, n- and iso-valerate. MCCAs include n-caproate, n-enanthate, n-caprylate. Waste beer batch 1 and 2 were used from Days 1-180 and Days 181-230, respectively. N.D. stands for not determined.

Table A.2. Processes involved in chain elongation

Process	Equation
Reverse *β* oxidation	
1) Ethanol oxidation for ATP generation	$C_2H_5OH + H_2O \rightarrow CH_3COO^- + H^+ + 2\,H_2$
2) Chain elongation	$C_xH_{2x-1}O_2^- + C_2H_5OH \rightarrow C_{x+2}H_{2x+3}O_2^- + H_2O$
a) Acetate chain elongation	$CH_3COO^- + C_2H_5OH \rightarrow C_3H_7COO^- + H_2O$
b) Butyrate chain elongation	$C_3H_7COO^- + C_2H_5OH \rightarrow C_5H_{11}COO^- + H_2O$
c) Caproate chain elongation	$C_5H_{11}COO^- + C_2H_5OH \rightarrow C_7H_{15}COO^- + H_2O$
3) Overall chain elongation by reverse *β* oxidation:	$5\,C_xH_{2x-1}O_2^- + 6\,C_2H_5OH \rightarrow 5\,C_{x+2}H_{2x+3}O_2^- + CH_3COO^- + H^+ + 4\,H_2O + 2\,H_2$

Table A.3. Biomass sampling points (days of bioreactor operation) for inoculum, influent, and bioreactor samples

Samples	DNA	RNA
Rumen inoculum	0, 178	0, 178
Influent	7, 14, 31, 66, 73, 81, 87, 115, 129, 157, 193, 206, 213, 228	7, 14, 31, 66, 73, 81, 87, 115, 129, 157, 206, 228
Bioreactor	7, 14, 31, 66, 73, 81, 87, 115, 129, 157, 193, 206, 213, 228	7, 14, 31, 66, 73, 81, 87, 115, 129, 157, 206, 213, 228

Influent biomass samples consist of mixture of waste beer and SCCAs rich permeate.

Table A.4. Good's coverage values for different samples. The lowest good's coverage value was 97.4% indicating that dominant OTUs were recovered in most of the samples.

Sample	No of sequences	Coverage	Sample	No of sequences	Coverage
RumenI_DNA	38651	0.987	RumenI_RNA	18648	0.976
RumenII_DNA	25651	0.977	RumenII_RNA	19257	0.974
InfDay7_DNA	29092	0.997	InfDay7_RNA	18634	0.995
InfDay14_DNA	32704	0.998	InfDay14_RNA	17941	0.994
InfDay31_DNA	31707	0.997	InfDay31_RNA	18336	0.995
InfDay66_DNA	26867	0.997	InfDay66_RNA	24217	0.997
InfDay73_DNA	20331	0.996	InfDay73_RNA	20906	0.997
InfDay81_DNA	32271	0.987	InfDay81_RNA	25160	0.986
InfDay87_DNA	25723	0.997	InfDay87_RNA	30181	0.997
InfDay115_DNA	32666	0.998	InfDay115_RNA	30550	0.998
InfDay129_DNA	35208	0.997	InfDay129_RNA	27545	0.998
InfDay157_DNA	39833	0.998	InfDay157_RNA	23085	0.995
InfDay193_DNA	34687	0.997			
InfDay206_DNA	41152	0.997	InfDay206_RNA	16743	0.994
InfDay213_DNA	45086	0.997			
InfDay228_DNA	32885	0.997	InfDay228_RNA	17364	0.995
MLDay7_DNA	42733	0.995	MLDay7_RNA	18002	0.990
MLDay14_DNA	47564	0.997	MLDay14_RNA	17555	0.996
MLDay31_DNA	33899	0.997	MLDay31_RNA	23530	0.997
MLDay66_DNA	28345	0.997	MLDay66_RNA	26169	0.998
MLDay73_DNA	31418	0.997	MLDay73_RNA	25564	0.998
MLDay81_DNA	34841	0.991	MLDay81_RNA	22733	0.991
MLDay87_DNA	34923	0.993	MLDay87_RNA	7501	0.995
MLDay115_DNA	38289	0.998	MLDay115_RNA	12604	0.998
MLDay129_DNA	42549	0.998	MLDay129_RNA	5071	0.994
MLDay157_DNA	40774	0.997	MLDay157_RNA	30378	0.997
MLDay193_DNA	32778	0.995			
MLDay206_DNA	37740	0.997	MLDay206_RNA	22115	0.996
MLDay213_DNA	41536	0.997	MLDay213_RNA	16897	0.994
MLDay228_DNA	29516	0.997	MLDay228_RNA	19389	0.996

Table A.5. Average ratio of rRNA and rDNA based on top 15 genera from each sampling point in the bioreactor

Genus	**$[rRNA/rDNA]_{reactor}>1$**
Acetobacter	1.23 ± 1.06
Acidaminococcus	1.89 ± 2.37
Bifidobacterium	1.28 ± 2.13
*Burkholderiales*_unclassified	1.93 ± 1.9
*Clostridiales*_unclassified	1.07 ± 1.42
Lactobacillus	1.78 ± 1.59
Leuconostoc	5.21 ± 3.7
Megasphaera	1.52 ± 1.6
Methanobrevibacter	1.85 ± 1.26
Methanosphaera	17.17 ± 4.53
Olsenella	1.37 ± 2.38
Pseudoclavibacter	1.89 ± 1.3
Pseudoramibacter	4.62 ± 3.03
Sharpea	1.8 ± 1.8
Snodgrassella	1.26 ± 1.24
*Thermoplasmata*_unclassified	3.47 ± 2.79
Genus	**$[rRNA/rDNA]_{reactor}<1$**
*Acetobacteraceae*_unclassified	0.62 ± 0.58
*Bacteria*_unclassified	0.53 ± 1.07
*Bacteroidales*_unclassified	0.28 ± 0.44
*Bacteroidetes*_unclassified	0.58 ± 0.96
*Betaproteobacteria*_unclassified	0.93 ± 0.91
*Erysipelotrichaceae*_unclassified	0.92 ± 0.73
*Lachnospiraceae*_unclassified	0.94 ± 1.49
Lactococcus	0.9 ± 0.79
Prevotella	0.31 ± 0.55
Pseudomonas	0.81 ± 0.88
Succiniclasticum	0.06 ± 0.17

*Values are reported as means with standard deviations of time series data.

Table A.6. Comparison of microbial community dissimilarities between influent and bioreactor samples collected on the same day based on Analysis of Similarity (ANOSIM) analysis.

Sample	Bray-Curtis		Jaccard	
	R	p value	R	p value
DNA_total	0.55	0.001	0.14	0.003
RNA_total	0.67	0.001	0.28	0.001
DNA_Bacteria	0.50	0.001	0.13	0.01
RNA_Bacteria	0.63	0.001	0.27	0.001
DNA_Archaea	0.86	0.001	0.20	0.002
RNA_Archaea	0.65	0.01	0.13	0.016

Table A.7. Shared OTUs between influent and bioreactor samples

Day	No of OTUs observed in the influent		No of OTUs observed in the bioreactor		No of shared OTUs		% of influent OTUs		% of bioreactor OTUs	
	DNA	RNA	DNA	RNA	DNA	RNA	DNA	RNA	DNA	RNA
7	265	285	586	381	121	87	45.7	30.5	20.6	22.8
14	280	275	346	204	130	82	46.4	29.8	37.6	40.2
31	329	296	317	246	149	108	45.3	36.5	47.0	43.9
66	300	256	308	201	127	97	42.3	37.9	41.2	48.3
73	253	215	314	189	132	86	52.2	40.0	42.0	45.5
81	1406	962	922	521	427	199	30.4	20.7	46.3	38.2
87	271	222	625	149	121	62	44.6	27.9	19.4	41.6
115	224	187	321	128	121	70	54.0	37.4	37.7	54.7
129	271	159	300	129	110	40	40.6	25.2	36.7	31.0
157	346	339	390	264	179	124	51.7	36.6	45.9	47.0
193	384		481		173		45.1		36.0	
206	355	311	323	303	144	126	40.6	40.5	44.6	41.6
213	421		345	241	150		35.6		43.5	
228	339	282	323	229	149	94	44.0	33.3	46.1	41.0
Average:	388.8 ± 297.8	315.8 ± 210.2	421.5 ± 178.6	245 ± 108.7	159.5 ± 79.5	97.9 ± 40.2	44.2 ± 6.3	33.0 ± 6.2	38.9 ± 8.9	41.3 ± 8.2

Table A.8. Specific growth rate of populations observed in the chain elongation bioreactor

Genus	Method I		Method II	
	DNA (d^{-1})	RNA (d^{-1})	DNA (d^{-1})	RNA (d^{-1})
Acetobacter	-0.01 ± 0.29	0.07 ± 0.1	0.33 ± 0.12	0.3 ± 0.23
*Acetobacteraceae*_unclassified	0.06 ± 0.14	0.09 ± 0.05	0.34 ± 0.12	0.34 ± 0.11
*Acidaminococcaceae*_unclassified	-0.48 ± 0.58		0.04 ± 0.36	
Acidaminococcus	-1.47 ± 2.91	-0.4 ± 1.37	0.03 ± 0.31	-0.29 ± 1.45
Acinetobacter	-39.42 ± 94.96	-9.19 ± 14.6	-8.17 ± 13.9	-17.98 ± 16.86
Actinomyces	0.07 ± 0.03		0.41 ± 0.19	
*Actinomycetales*_unclassified	0.08 ± 0.03		0.3 ± 0.04	
Aeromonas	-2.9 ± 2.69		-1.29 ± 1.39	
*Alcaligenaceae*_unclassified	-0.51 ± 1.23	0.05 ± 0.04	0 ± 0.58	0.07 ± 0.37
Alcaligenes	-0.27 ± 0.57		0.21 ± 0.08	
Allisonella	-2.13 ± 5.71	0.05 ± 0.07	-0.32 ± 1.02	0.11 ± 0.41
*Alphaproteobacteria*_unclassified	-0.82 ± 0		-2.06 ± 0	
Altererythrobacter		0.05 ± 0		0.27 ± 0
Anaerocella	-21.34 ± 52.82	-3.36 ± 3.89	-3.14 ± 6.27	-18.8 ± 17.9
Anaerofilum	0.08 ± 0		0.33 ± 0	
*Anaerolineaceae*_unclassified	0.07 ± 0.05	-0.52 ± 1.07	0.28 ± 0.22	-0.27 ± 1.26
Anaeroplasma	0.1 ± 0	0.1 ± 0	0.54 ± 0	0.54 ± 0
Anaerosalibacter	0.1 ± 0.01	0.1 ± 0	0.34 ± 0.02	0.35 ± 0.02
Anaerovibrio	-1.3 ± 2.67	-0.32 ± 0.47	-0.15 ± 0.48	-0.2 ± 0.53
Aquabacterium		0.05 ± 0		0.27 ± 0
Arcobacter	-27.29 ± 50.95	-21.28 ± 41.44	-7.75 ± 8.15	-82.97 ± 127.17
Asteroleplasma	-0.12 ± 0.24		0.25 ± 0.03	
Azoarcus	-1.03 ± 0		-0.4 ± 0	
Azospira	-8.56 ± 0		-2.09 ± 0	
*Bacillales*_unclassified	0.11 ± 0.02	0.06 ± 0.15	0.22 ± 0.07	0.18 ± 0.16
*Bacteria*_unclassified	-3.62 ± 10.71	-0.26 ± 0.6	-0.07 ± 0.78	-1.31 ± 3.44
*Bacteroidales*_unclassified	-21.59 ± 62.81	-4.78 ± 9.25	-2.26 ± 2.31	-7.02 ± 7.79
Bacteroides	-16.72 ± 50.02	-3.95 ± 5.02	-1.63 ± 1.86	-8.1 ± 11.81
*Bacteroidetes*_unclassified	-15.58 ± 45.02	-0.28 ± 0.66	-1.61 ± 2.9	-0.78 ± 1.28
Barnesiella	-0.07 ± 0.19		-0.15 ± 0.59	
*Betaproteobacteria*_unclassified	-2.45 ± 6.86	-0.22 ± 0.42	-0.05 ± 0.28	-0.58 ± 1.15
*Bifidobacteriaceae*_unclassified	-0.08 ± 0.31	0.08 ± 0	0.21 ± 0.19	0.33 ± 0

Bifidobacterium	-1.15 ± 2.46	-0.08 ± 0.31	0.09 ± 0.15	0.03 ± 0.44
Bilophila	-1.43 ± 1.14	-0.1 ± 0.37	-0.38 ± 0.39	0.06 ± 0.43
Brachybacterium		0.06 ± 0		0.36 ± 0
Brevibacillus	0.06 ± 0		0.27 ± 0	
Brevundimonas		0.05 ± 0		0.27 ± 0
*Brucellaceae*_unclassified	-2.6 ± 2.63		-0.53 ± 0.15	
Bulleidia	0.08 ± 0		0.33 ± 0	
*Burkholderiales*_unclassified	-3.4 ± 10.63	-0.21 ± 0.58	-0.01 ± 0.45	-1.67 ± 3.67
Butyricicoccus	-1.84 ± 0		-0.03 ± 0	
Butyrivibrio	-13.47 ± 33.43	-0.27 ± 0	-1.59 ± 1.29	-2.62 ± 0
Camelimonas	-5 ± 0		-0.53 ± 0	
*Candidatus_Endomicrobium*_unclassified	-0.42 ± 0.59		-0.13 ± 0.2	
*Candidatus_Saccharibacteria*_unclassified	0.06 ± 0		0.27 ± 0	
Catabacter		0.09 ± 0		0.36 ± 0
Cellulomonas	0.06 ± 0.01		0.3 ± 0.05	
Cellulosilyticum	-1.64 ± 0	-0.35 ± 0	-0.52 ± 0	-3.27 ± 0
*Chloroflexi*_unclassified	-0.97 ± 1.17		-0.23 ± 0.45	
Christensenella	0.06 ± 0		0.36 ± 0	
Chryseobacterium	-0.25 ± 0.53		0.15 ± 0.25	
Cloacibacillus	-16.39 ± 42.94	-0.3 ± 0.51	-0.89 ± 1.36	-0.73 ± 1.32
*Clostridia*_unclassified	0.08 ± 0.1	0.13 ± 0.06	0.25 ± 0.29	0.33 ± 0.03
*Clostridiaceae_1*_unclassified	0.17 ± 0		0.28 ± 0	
*Clostridiales_Incertae_Sedis_XI*_unclassified	0.11 ± 0		0.34 ± 0	
*Clostridiales_Incertae_Sedis_XIII*_unclassified	-1.43 ± 2.53		-0.52 ± 1.21	
*Clostridiales*_unclassified	-0.25 ± 0.63	0.08 ± 0.04	0.26 ± 0.12	0.31 ± 0.09
Clostridium_IV	-7.98 ± 11.44	0.06 ± 0	-2.02 ± 3.33	0.09 ± 0
Clostridium_sensu_stricto	-2.62 ± 2.96	-0.76 ± 1.7	-1.21 ± 1.84	-2.21 ± 4.63
Clostridium_XI	0.11 ± 0		0.34 ± 0	
Clostridium_XlVa	-3.87 ± 5.81	-0.67 ± 0	-1.16 ± 1.3	-6.27 ± 0
*Comamonadaceae*_unclassified	0.06 ± 0.07	0.07 ± 0.02	0.33 ± 0.05	0.32 ± 0.04
Comamonas	-6.53 ± 10.15	0.03 ± 0.06	-1.57 ± 3.03	-0.07 ± 0.57
Coprococcus	0.05 ± 0.12	0.14 ± 0.05	0.27 ± 0.11	0.31 ± 0.05
*Coriobacteriaceae*_unclassified	-2.21 ± 5.94	0.09 ± 0.06	0.09 ± 0.49	0.36 ± 0.12
Corynebacterium	-0.54 ± 1.23	-0.16 ± 0.41	0.04 ± 0.62	0.13 ± 0.27
Deinococcus		0.05 ± 0		0.27 ± 0
Denitrobacterium		0.14 ± 0		0.27 ± 0
Desulfovibrio	-3.53 ± 7.61	-1.4 ± 1.39	-0.32 ± 0.42	-3.5 ± 2.54
*Desulfovibrionaceae*_unclassified	0.06 ± 0		0.27 ± 0	

Dialister	-3.34 ± 8.1	-0.07 ± 0.2	-0.14 ± 0.49	-0.17 ± 0.54
Dietzia		0.05 ± 0		0.27 ± 0
Dysgonomonas	-0.98 ± 1.2		-0.28 ± 0.61	
Eggerthella	-13.87 ± 45.33	0.08 ± 0.05	-0.79 ± 1.76	0.3 ± 0.12
Elusimicrobium	-0.94 ± 1.41		-2.24 ± 3.55	
Empedobacter	-2.79 ± 3.72	-0.02 ± 0	-1.47 ± 2.45	-0.61 ± 0
Enhydrobacter	-5.06 ± 7.39	0.05 ± 0	-1.17 ± 2.05	0.27 ± 0
*Enterobacteriaceae*_unclassified	-2.21 ± 4.39	0.11 ± 0.06	-0.52 ± 1.11	0.28 ± 0.04
Enterococcus	-1.4 ± 1.42	0.06 ± 0.07	-0.5 ± 0.72	0.09 ± 0.28
*Erysipelotrichaceae*_unclassified	-1.31 ± 3.71	0.05 ± 0.05	0.1 ± 0.18	0.16 ± 0.24
*Eubacteriaceae*_unclassified	-1.02 ± 0.99	0.01 ± 0.11	-0.56 ± 0.58	-0.06 ± 0.49
Eubacterium	-1.55 ± 2.95	-0.1 ± 0.17	-0.1 ± 0.38	-0.3 ± 0.66
*Euryarchaeota*_unclassified		0.08 ± 0		0.33 ± 0
Faecalibacterium	-0.78 ± 1.47	0.05 ± 0	0.26 ± 0.35	0.27 ± 0
Firmicutes_unclassified	-1.5 ± 3.85	-0.09 ± 0.29	0.02 ± 0.33	0.12 ± 0.36
*Flavobacteriaceae*_unclassified	-0.08 ± 0.24		0.19 ± 0.21	
Flavobacterium		0.05 ± 0		0.27 ± 0
*Gammaproteobacteria*_unclassified	-19.8 ± 61.6	-0.47 ± 1.26	-1.35 ± 2.05	-0.41 ± 1.34
Gordonia	0.05 ± 0	0.05 ± 0	0.27 ± 0	0.27 ± 0
Hathewaya	-7.2 ± 2.73	-0.19 ± 0.34	-4.29 ± 2.1	-1.06 ± 1.46
Herbiconiux		0.05 ± 0		0.27 ± 0
Holdemania	0.11 ± 0.08		0.32 ± 0.06	
*Hyphomicrobiaceae*_unclassified		0.1 ± 0		0.54 ± 0
Ignatzschineria	0.13 ± 0		0.27 ± 0	
Ilumatobacter		0.05 ± 0		0.27 ± 0
Intestinimonas	-14.5 ± 36.29	-0.67 ± 0.62	-2.02 ± 1.78	-2.93 ± 3.11
Kurthia	-1508.81 ± 0	-4.31 ± 0	-54.65 ± 0	-51.89 ± 0
Lachnospira	-0.17 ± 0.33		-0.39 ± 0.93	
*Lachnospiraceae*_unclassified	-1.44 ± 3.94	-0.01 ± 0.13	0.11 ± 0.14	0.02 ± 0.32
*Lactobacillaceae*_unclassified	0.19 ± 0	-0.21 ± 0.54	0.31 ± 0	-0.89 ± 2.75
*Lactobacillales*_unclassified	-1.01 ± 2.24	-0.11 ± 0.18	0.13 ± 0.48	-0.36 ± 0.16
Lactobacillus	-1.46 ± 1.53	-0.16 ± 0.24	-0.37 ± 0.7	-0.14 ± 0.43
Lactococcus	-1.57 ± 2.1	-0.03 ± 0.14	-0.51 ± 1.5	-0.08 ± 0.44
Leuconostoc	-5.83 ± 10.08	-0.98 ± 0.92	-1.19 ± 0.91	-1.51 ± 1.33
*Marinilabiliaceae*_unclassified	0.06 ± 0		0.27 ± 0	
Massilia		0.05 ± 0		0.27 ± 0
Megasphaera	-2.13 ± 3.85	-0.71 ± 1.34	-0.34 ± 0.73	-1.13 ± 1.97
*Methanobacteriaceae*_unclassified		0.07 ± 0		0.52 ± 0

Methanobacterium	0.06 ± 0	0.13 ± 0.1	0.36 ± 0	0.33 ± 0.04
Methanobrevibacter	-0.12 ± 0.58	0.08 ± 0.03	0.32 ± 0.09	0.32 ± 0.1
Methanomassiliicoccus	-0.44 ± 0.76	-0.19 ± 0.48	0.03 ± 0.52	0.08 ± 0.65
Methanosphaera	-0.83 ± 2.17	-0.1 ± 0.18	0.16 ± 0.12	-0.05 ± 0.33
Methylobacterium		0.05 ± 0		0.27 ± 0
*Microbacteriaceae*_unclassified	-0.05 ± 0.26	-0.04 ± 0.19	0.26 ± 0.15	0 ± 0.61
*Micrococcaceae*_unclassified		0.1 ± 0		0.33 ± 0
Microvirgula	-5.46 ± 9.76	-1.31 ± 0.35	-0.63 ± 1.4	-2.24 ± 1.84
Mitsuokella	-0.62 ± 0		-0.92 ± 0	
Mogibacterium	-1.91 ± 3.19	-0.4 ± 0.32	-0.17 ± 0.34	-0.99 ± 0.98
*Neisseriaceae*_unclassified	0.06 ± 0		0.36 ± 0	
Nitrospirillum	-94.99 ± 164.44	-0.19 ± 0.17	-3.12 ± 5.85	-2.03 ± 2.99
Nocardioides		0.05 ± 0		0.27 ± 0
Nocardiopsis	-0.28 ± 0.46		0.03 ± 0.34	
Oligella	0.05 ± 0		0.27 ± 0	
Oligosphaera	-0.21 ± 0		-0.58 ± 0	
Olsenella	-0.15 ± 0.47	0.08 ± 0.06	0.29 ± 0.09	0.31 ± 0.11
Oribacterium	0.1 ± 0		0.33 ± 0	
Oscillibacter	-3.34 ± 3.8	-0.22 ± 0.41	-1.56 ± 1.57	-2.13 ± 3.49
*Oxalobacteraceae*_unclassified		0.09 ± 0		0.36 ± 0
Paenibacillus		0.14 ± 0		0.27 ± 0
Pandoraea	-0.7 ± 0.62		-0.09 ± 0.39	
Paraprevotella	-0.93 ± 1.84	-1.82 ± 2	-0.67 ± 1.6	-15.98 ± 19.46
Pectinatus	0.09 ± 0.05	-0.02 ± 0.23	0.31 ± 0.07	-0.03 ± 0.43
Pedobacter		0.1 ± 0.07		0.27 ± 0
Peptoniphilus		0.06 ± 0		0.27 ± 0
Peptostreptococcus		0.08 ± 0		0.33 ± 0
Phascolarctobacterium		0.06 ± 0		0.36 ± 0
*Planctomycetaceae*_unclassified	0.11 ± 0.06		0.29 ± 0.18	
Pleomorphomonas		0.06 ± 0		0.36 ± 0
*Porphyromonadaceae*_unclassified	-0.04 ± 0.24	-0.03 ± 0	0.08 ± 0.74	0.09 ± 0
Prevotella	-6.01 ± 15.28	-1.25 ± 1.96	-0.64 ± 0.67	-2.24 ± 2.08
*Prevotellaceae*_unclassified	-33.75 ± 100.2	-0.23 ± 0.29	-2.23 ± 3.65	-0.71 ± 1.16
Proteiniphilum	0.09 ± 0.01	0.09 ± 0	0.35 ± 0.02	0.36 ± 0
*Proteobacteria*_unclassified	-7.7 ± 15.98	-0.06 ± 0.24	-0.7 ± 1.28	0.21 ± 0.47
Proteus	-0.91 ± 1.59	0.09 ± 0	-0.05 ± 0.29	0.36 ± 0
Pseudobutyrivibrio	0.06 ± 0		0.27 ± 0	
Pseudoclavibacter	-0.68 ± 2.45	0.08 ± 0.08	0.07 ± 0.7	0.17 ± 0.37

*Pseudomonadaceae*_unclassified	-1.73 ± 0	0.05 ± 0	-0.57 ± 0	0.27 ± 0
Pseudomonas	-321.86 ± 0	-2.6 ± 5.85	-11.23 ± 0	-31.12 ± 70.06
Pseudoramibacter	0.07 ± 0.07	0.1 ± 0.05	0.35 ± 0.1	0.35 ± 0.1
Pseudoscardovia	-0.52 ± 0.55	0.03 ± 0.14	-0.01 ± 0.32	-0.01 ± 0.62
Psychrobacter		0.05 ± 0		0.27 ± 0
Pyramidobacter	-0.88 ± 1.33	-1.26 ± 1.74	-0.25 ± 0.87	-3.15 ± 5.04
*Rhizobiaceae*_unclassified	0.09 ± 0.05	0.06 ± 0	0.31 ± 0.07	0.36 ± 0
*Rhodobacteraceae*_unclassified	-29.07 ± 71.06	0.1 ± 0.09	-1.45 ± 2.54	0.25 ± 0.07
Rhodococcus	-0.11 ± 0.35	-0.14 ± 0.27	0.27 ± 0.09	0.19 ± 0.16
*Rhodocyclaceae*_unclassified	-6.67 ± 9.92		-1.43 ± 1.98	
Roseburia	-14.75 ± 37.47	-2.4 ± 3.33	-1.84 ± 1.71	-13 ± 17.73
Ruminobacter	-3.57 ± 5.82	-4.52 ± 0	-1.13 ± 1.3	-4.66 ± 0
*Ruminococcaceae*_unclassified	-9.89 ± 32.99	-0.68 ± 0.83	-0.59 ± 1.1	-1.84 ± 2.31
Ruminococcus	-32.37 ± 71.52	-6.54 ± 9.57	-5.85 ± 6.22	-18.29 ± 37.82
Rummeliibacillus	0.09 ± 0.02	0.09 ± 0	0.35 ± 0.02	0.36 ± 0
Saccharofermentans	-0.06 ± 0.35	-0.41 ± 0	-0.09 ± 0.92	-0.31 ± 0
Scardovia		0.09 ± 0.05		0.31 ± 0.07
Schwartzia	-1.21 ± 1.18	-0.06 ± 0.13	-0.5 ± 0.56	-0.16 ± 0.29
Selenomonas	-11.48 ± 26.18	-0.34 ± 0.54	-0.93 ± 0.7	-0.93 ± 1.14
Sharpea	-0.3 ± 0.4	-0.01 ± 0.2	0.11 ± 0.28	0.13 ± 0.29
Snodgrassella	-8.61 ± 19.36	-0.68 ± 1.09	-1.01 ± 1.66	-3.63 ± 5.82
*Sphaerobacteraceae*_unclassified		0.05 ± 0		0.27 ± 0
Sphingobacterium	-0.62 ± 0		-0.13 ± 0	
Sphingobium	0.05 ± 0.09	0.02 ± 0.01	0.25 ± 0.04	0.2 ± 0.09
Sphingomonas	0.11 ± 0.07		0.28 ± 0.01	
*Spirochaetaceae*_unclassified	-0.02 ± 0.18	0.1 ± 0	0.06 ± 0.62	0.54 ± 0
Spirosoma		0.05 ± 0		0.27 ± 0
Sporanaerobacter	-0.12 ± 0.47	0.09 ± 0.01	0.2 ± 0.31	0.34 ± 0.01
SR1_unclassified	-0.34 ± 0	0.1 ± 0	-0.9 ± 0	0.54 ± 0
Staphylococcus		-0.07 ± 0.25		-0.13 ± 0.66
Stenotrophomonas	0.1 ± 0.04	0.05 ± 0	0.3 ± 0.05	0.27 ± 0
Streptococcus	-4.66 ± 10.64	-0.15 ± 0.43	-0.17 ± 0.71	-0.13 ± 0.68
Streptomyces		0.06 ± 0		0.36 ± 0
*Subdivision5*_unclassified	0.02 ± 0.21	-0.14 ± 0.29	0.11 ± 0.58	0.01 ± 0.36
Succiniclasticum	-4.49 ± 13	-0.7 ± 1.31	-0.28 ± 0.6	-2 ± 3.32
Succinivibrio	-14 ± 35.28	-2.18 ± 2.44	-1.81 ± 2.02	-3.82 ± 6.63
*Succinivibrionaceae*_unclassified	-0.62 ± 0.73		-0.16 ± 0.39	
Sulfurospirillum	-1.45 ± 0.96	-0.21 ± 0	-0.77 ± 0.53	-2.15 ± 0

*Synergistaceae*_unclassified	-6.37 ± 15.28	-1.14 ± 1.94	-0.83 ± 0.61	-3.42 ± 5.15
Synergistes	-8.77 ± 13.95	-1.55 ± 1.51	-1.52 ± 2.55	-2.81 ± 2.91
Thermoactinomyces	0.08 ± 0.01	0.09 ± 0.05	0.53 ± 0.02	0.3 ± 0.05
*Thermoplasmata*_unclassified	-3.62 ± 11.35	-0.68 ± 1.95	0.01 ± 0.63	-7.16 ± 23.42
Thermus		0.19 ± 0		0.31 ± 0
Tissierella	0.1 ± 0.01	0.09 ± 0.03	0.35 ± 0.02	0.31 ± 0.04
Treponema	-2.86 ± 6.4	-0.72 ± 0.56	-0.29 ± 0.73	-2.52 ± 3.15
Veillonella	-0.16 ± 0.4	0.06 ± 0.06	0.09 ± 0.22	0.19 ± 0.26
*Veillonellaceae*_unclassified	-1.94 ± 2.12	-0.65 ± 1.32	-0.35 ± 0.37	-0.84 ± 1.42
*Verrucomicrobia*_unclassified	-0.19 ± 0		-0.53 ± 0	
Victivallis	-2.22 ± 2.91	0.06 ± 0	-1.13 ± 0.96	0.27 ± 0
Weissella	-2.96 ± 3.96	-0.35 ± 0.73	-0.95 ± 0.56	-0.85 ± 1.59
Xanthobacter	0.09 ± 0.09	-0.01 ± 0	0.29 ± 0.03	0.16 ± 0
*Xanthobacteraceae*_unclassified		0.06 ± 0		0.36 ± 0
*Xanthomonadaceae*_unclassified	-15.22 ± 48.02	-0.19 ± 0.53	-0.29 ± 1.66	-0.4 ± 1.44
Zoogloea	0.05 ± 0		0.27 ± 0	

Table A.9. $rDNA_{influent}$/ $rDNA_{reactor}$ and $rRNA_{influent}$/ $rRNA_{reactor}$ values for different genus or family observed in the bioreactor samples.

Genus or Family	$rDNA_{influent}$/ $rDNA_{reactor}$	$rRNA_{influent}$/ $rRNA_{reactor}$	Genus or Family	$rDNA_{influent}$/ $rDNA_{reactor}$	$rRNA_{influent}$/ $rRNA_{reactor}$
Acetobacter	0.04 ± 0.04	0.08 ± 0.2	*Lactobacillales*_unclassified	1.33 ± 1.88	3.18 ± 1.51
*Acetobacteraceae*_unclassified	0.02 ± 0.02	0.02 ± 0.03	*Lactobacillus*	1.15 ± 1.09	1.01 ± 1.22
*Acidaminococcaceae*_unclassified	0.84 ± 1.72		*Lactococcus*	1.59 ± 1.17	0.81 ± 0.82
Acidaminococcus	0.47 ± 0.61	0.54 ± 0.69	*Leuconostoc*	4.15 ± 6.56	3.43 ± 2.96
Acinetobacter	7.04 ± 4.18	15.35 ± 7.65	*Megasphaera*	1.25 ± 1.65	2.21 ± 2.14
Aeromonas	5.73 ± 5.82		*Methanobrevibacter*	0.06 ± 0.11	0.07 ± 0.2
*Alcaligenaceae*_unclassified	1.12 ± 1.41	1.88 ± 1.89	*Methanomassiliicoccus*	0.63 ± 0.7	0.5 ± 0.32
Alcaligenes	0.23 ± 0.32		*Methanosphaera*	0.41 ± 0.51	1.02 ± 1.61
Allisonella	1.04 ± 1.54	1.39 ± 1.76	*Microbacteriaceae*_unclassified	0.11 ± 0.11	0.14 ± 0.09
*Alphaproteobacteria*_unclassified	15.72 ± 15.72		*Microvirgula*	2.71 ± 3.85	6.62 ± 6.79
Anaerocella	4.79 ± 4.37	192.62 ± 105.44	*Mitsuokella*	2.71 ± 2.71	
Anaerofilum	1.03 ± 1.03		*Mogibacterium*	1.31 ± 2.75	3.66 ± 3.98
*Anaerolineaceae*_unclassified	1.28 ± 1.79	7.25 ± 11.86	*Neisseriaceae*_unclassified	2.06 ± 1.26	
Anaeroplasma	3.63 ± 3.48	0.96 ± 0.92	*Nitrospirillum*	2.45 ± 1.87	9.48 ± 6.07
Anaerovibrio	1.9 ± 1.67	1.3 ± 1.29	*Nocardiopsis*	0.75 ± 1.09	
Arcobacter	14.19 ± 15.04	57.87 ± 37.82	*Oligosphaera*	5.73 ± 5.73	
Asteroleplasma	0.34 ± 0.39		*Olsenella*	0.12 ± 0.11	0.06 ± 0.07
Azoarcus	10.42 ± 4.65		*Oscillibacter*	6.58 ± 6.86	18.22 ± 18.1
Azospira	1.83 ± 1.83		*Pandoraea*	0.63 ± 0.74	
*Bacillales*_unclassified	0.45 ± 0.64	1.2 ± 1.68	*Paraprevotella*	5.18 ± 4.68	45.4 ± 41.31

*Bacteria*_unclassified	0.56 ± 1.84	1.23 ± 1.52
*Bacteroidales*_unclassified	4.14 ± 2.58	4.86 ± 2.72
Bacteroides	3.43 ± 3.09	14.67 ± 8.2
*Bacteroidetes*_unclassified	4.5 ± 5.61	1.86 ± 1.56
Barnesiella	4.03 ± 5.38	
*Betaproteobacteria*_unclassified	1.19 ± 1.35	2.22 ± 2.52
*Bifidobacteriaceae*_unclassified	1.53 ± 1.67	
Bifidobacterium	0.6 ± 0.52	0.48 ± 0.4
Bilophila	1.52 ± 1.01	1.23 ± 1.41
*Brucellaceae*_unclassified	2.73 ± 2.2	
*Burkholderiales*_unclassified	0.41 ± 0.51	0.38 ± 0.27
Butyricicoccus	1.32 ± 0.97	
Butyrivibrio	5.54 ± 7.92	14.1 ± 5.61
Camelimonas	2.42 ± 2.42	
*Candidatus_Endomicrobium*_unclassified	2.84 ± 3.08	
*Candidatus_Saccharibacteria*_unclassified	1.09 ± 1.09	
Cellulosilyticum	20.68 ± 11.19	23.46 ± 18.08
*Chloroflexi*_unclassified	1.54 ± 1.97	
Chryseobacterium	0.45 ± 0.52	
Cloacibacillus	2.16 ± 1.96	6.17 ± 4.78
*Clostridia*_unclassified	0.01 ± 0.02	0.52 ± 0.71
*Clostridiales_Incertae_Sedis_XIII*_unclassified	2.67 ± 3.58	
*Clostridiales*_unclassified	0.15 ± 0.14	0.09 ± 0.07
Clostridium_IV	3.92 ± 3.31	31.73 ± 18.88
Clostridium_sensu_stricto	3.71 ± 5	1.22 ± 0.92
Clostridium_XlVa	6.46 ± 6.31	24.4 ± 10.65
Pectinatus		0.82 ± 1.08
*Planctomycetaceae*_unclassified	0.78 ± 1.76	
Pleomorphomonas		1.36 ± 1.31
*Porphyromonadaceae*_unclassified	4.36 ± 6.87	1.42 ± 1.26
Prevotella	1.73 ± 0.79	4.52 ± 3.2
*Prevotellaceae*_unclassified	3.96 ± 4.62	3.34 ± 4.87
*Proteobacteria*_unclassified	3.21 ± 5.31	2.89 ± 2.76
Proteus	0.93 ± 1.01	2.94 ± 2.09
Pseudobutyrivibrio	123.77 ± 120.6	
Pseudoclavibacter	0.03 ± 0.03	0.02 ± 0.03
*Pseudomonadaceae*_unclassified	2 ± 1.37	1.26 ± 1.21
Pseudomonas	14.04 ± 12.26	15.99 ± 24.19
Pseudoramibacter	0.01 ± 0.01	0.01 ± 0.02
Pseudoscardovia	1.46 ± 1.65	0.51 ± 0.69
Psychrobacter		0.83 ± 0.48
Pyramidobacter	1.69 ± 1.91	5.23 ± 4.98
*Rhizobiaceae*_unclassified	0.58 ± 0.83	1.91 ± 1.83
*Rhodobacteraceae*_unclassified	1.35 ± 1.9	2.01 ± 1.46
Rhodococcus	0.16 ± 0.25	0.58 ± 0.72
*Rhodocyclaceae*_unclassified	3.52 ± 3.4	
Roseburia	7.39 ± 9.96	14.73 ± 17.26
Ruminobacter	3.85 ± 4.67	38.54 ± 34.49
*Ruminococcaceae*_unclassified	2.18 ± 3.41	3.81 ± 6.42
Ruminococcus	6.32 ± 4.74	29.78 ± 26.87
Rummeliibacillus		0.03 ± 0.03
Saccharofermentans	9.39 ± 11.82	4.26 ± 4.1

*Comamonadaceae*_unclassified	0.07 ± 0.11	0.04 ± 0.05
Comamonas	2.26 ± 2.22	20.83 ± 10.96
Coprococcus	0.08 ± 0.08	0.15 ± 0.12
*Coriobacteriaceae*_unclassified	0.91 ± 1.66	0.08 ± 0.12
Corynebacterium	0.39 ± 0.42	0.83 ± 1.06
Desulfovibrio	1.84 ± 2.25	11.2 ± 8.69
Dialister	1.33 ± 3.61	0.62 ± 0.62
Dysgonomonas	1.46 ± 1.19	
Eggerthella	1.21 ± 1.41	0.47 ± 0.56
Elusimicrobium	18.3 ± 26.84	
Empedobacter	2.97 ± 2.82	23.73 ± 15.68
Enhydrobacter	10.64 ± 7.51	1.17 ± 0.56
*Enterobacteriaceae*_unclassified	2.89 ± 3.26	0.05 ± 0.06
Enterococcus	2.8 ± 3.04	1.48 ± 1.9
*Erysipelotrichaceae*_unclassified	0.49 ± 0.94	0.22 ± 0.27
*Eubacteriaceae*_unclassified	3.56 ± 3.55	2.62 ± 3.79
Eubacterium	0.65 ± 0.76	1.07 ± 1.66
*Euryarchaeota*_unclassified		2.47 ± 1.64
Faecalibacterium	0.41 ± 0.77	
*Firmicutes*_unclassified	1.84 ± 3.15	1.2 ± 2.52
*Flavobacteriaceae*_unclassified	0.01 ± 0.02	
*Gammaproteobacteria*_unclassified	5.2 ± 7.76	11.19 ± 22.24
Gordonia	0.86 ± 0.86	
Hathewaya	14.46 ± 18.55	2.23 ± 1.92
Ignatzschineria	3.26 ± 3.26	
Intestinimonas	5.48 ± 5.68	8.65 ± 5.63
Kurthia	68.75 ± 57.73	80.09 ± 58.24
Schwartzia	1.23 ± 0.92	1.36 ± 1.48
Selenomonas	1.66 ± 1.22	3.24 ± 2.39
Sharpea	0.59 ± 0.92	0.3 ± 0.33
Snodgrassella	2.71 ± 2.91	7.07 ± 9.01
Sphingobacterium	5.83 ± 2.76	
Sphingobium	0.12 ± 0.19	0.38 ± 0.22
*Spirochaetaceae*_unclassified	4.68 ± 6.14	26.06 ± 25.04
Sporanaerobacter	0.09 ± 0.15	0.13 ± 0.14
SR1_unclassified	7.92 ± 7.92	3.5 ± 3.36
Staphylococcus		0.44 ± 0.24
Stenotrophomonas	1.19 ± 1.85	
Streptococcus	2.2 ± 2.43	1.32 ± 1.63
Streptomyces		1.79 ± 1.72
*Subdivision5*_unclassified	5.52 ± 7.77	3.34 ± 3.65
Succiniclasticum	0.97 ± 1.18	1.84 ± 1.64
Succinivibrio	3.69 ± 3.75	15.03 ± 22.46
*Succinivibrionaceae*_unclassified	1.31 ± 1.11	
Sulfurospirillum	5.12 ± 3.42	19.27 ± 12.85
*Synergistaceae*_unclassified	2.87 ± 2.76	11.07 ± 11.41
Synergistes	3.09 ± 3.26	6.27 ± 4.42
*Thermoplasmata*_unclassified	0.13 ± 0.14	0.64 ± 0.61
Treponema	2.68 ± 3.81	6.14 ± 6.96
Veillonella	0.75 ± 0.61	0.52 ± 0.52
*Veillonellaceae*_unclassified	1.5 ± 1.1	2.88 ± 4
*Verrucomicrobia*_unclassified	7.36 ± 5.62	
Victivallis	3.23 ± 2.68	1.69 ± 0.8
Weissella	2.08 ± 1.19	0.95 ± 0.76

Lachnospira	7.67 ± 8.94		*Xanthobacter*	0.05 ± 0.06	0.34 ± 0.33
*Lachnospiraceae*_unclassified	0.45 ± 0.5	0.4 ± 0.46	*Xanthomonadaceae*_unclassified	0.29 ± 0.34	0.32 ± 0.17
*Lactobacillaceae*_unclassified	6.69 ± 3.11	2 ± 2.6			

*Values are reported as means with standard deviations of time series data.

A.2 Figures

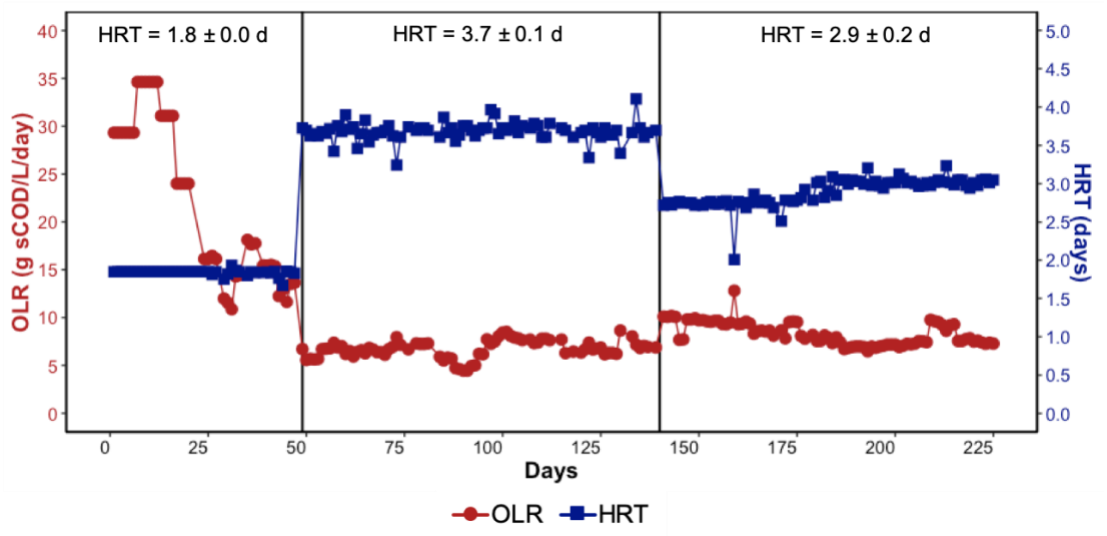

Figure A.1. Hydraulic retention time (HRT) with corresponding organic loading rate (OLR) over time. The vertical lines represent change of HRT on Days 49 and 140. The OLR is a function of soluble chemical oxygen demand (sCOD) of the influent (g sCOD L^{-1}), flow rate of the influent (L d^{-1}), and working volume of the bioreactor (L). MCCAs volumetric production rate was significantly different (p=6.61E-09) between HRTs but there was no particular trend. The longest HRT of 3.7 ± 0.1 days led to lowest average MCCAs volumetric production rate of 3.0 ± 1.1 mmole $L^{-1}d^{-1}$ while the MCCAs production was similar (p=0.48) between HRTs 1.8 ± 0.0 days (4.7 ± 1.5 mmole $L^{-1}d^{-1}$) and 2.9 ± 0.22 days (5.2 ± 1.4 mmole $L^{-1}d^{-1}$).

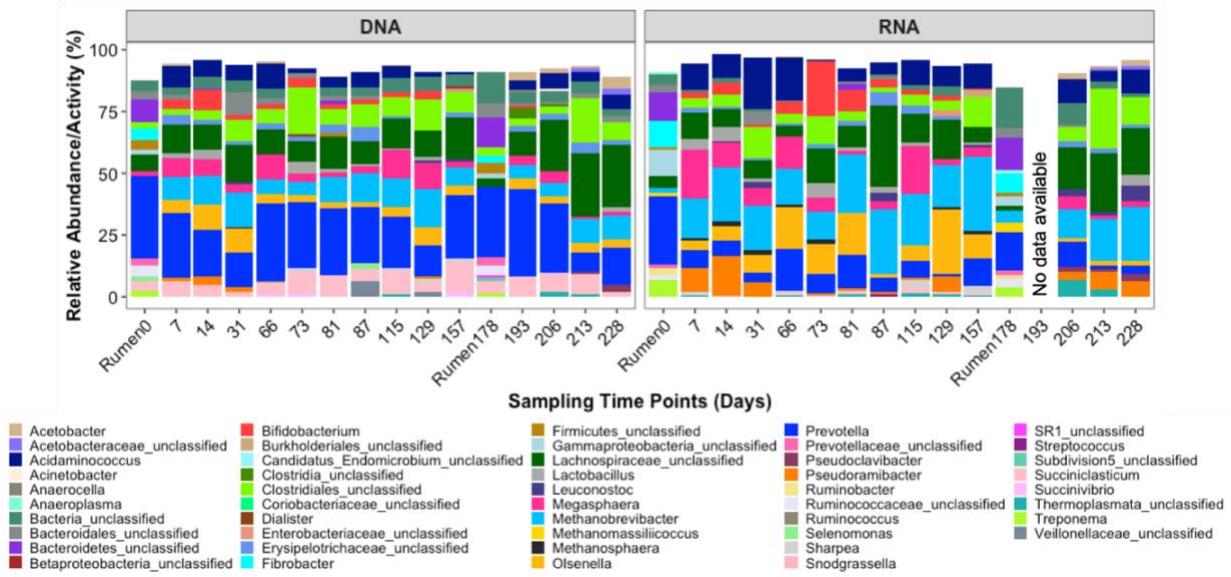

Figure A.2. Relative abundance and activity of 15 most abundant microbial groups classified to the genus or family level in rumen inocula and the bioreactor samples over time. The relative abundance and activity were determined as percentages normalized to the total number of 16S rRNA gene sequences and 16S rRNA sequences, respectively. The top 15 microbial groups represented 87.5-95.8% and 84.5-98.3% of the total relative abundance and relative activity, respectively.

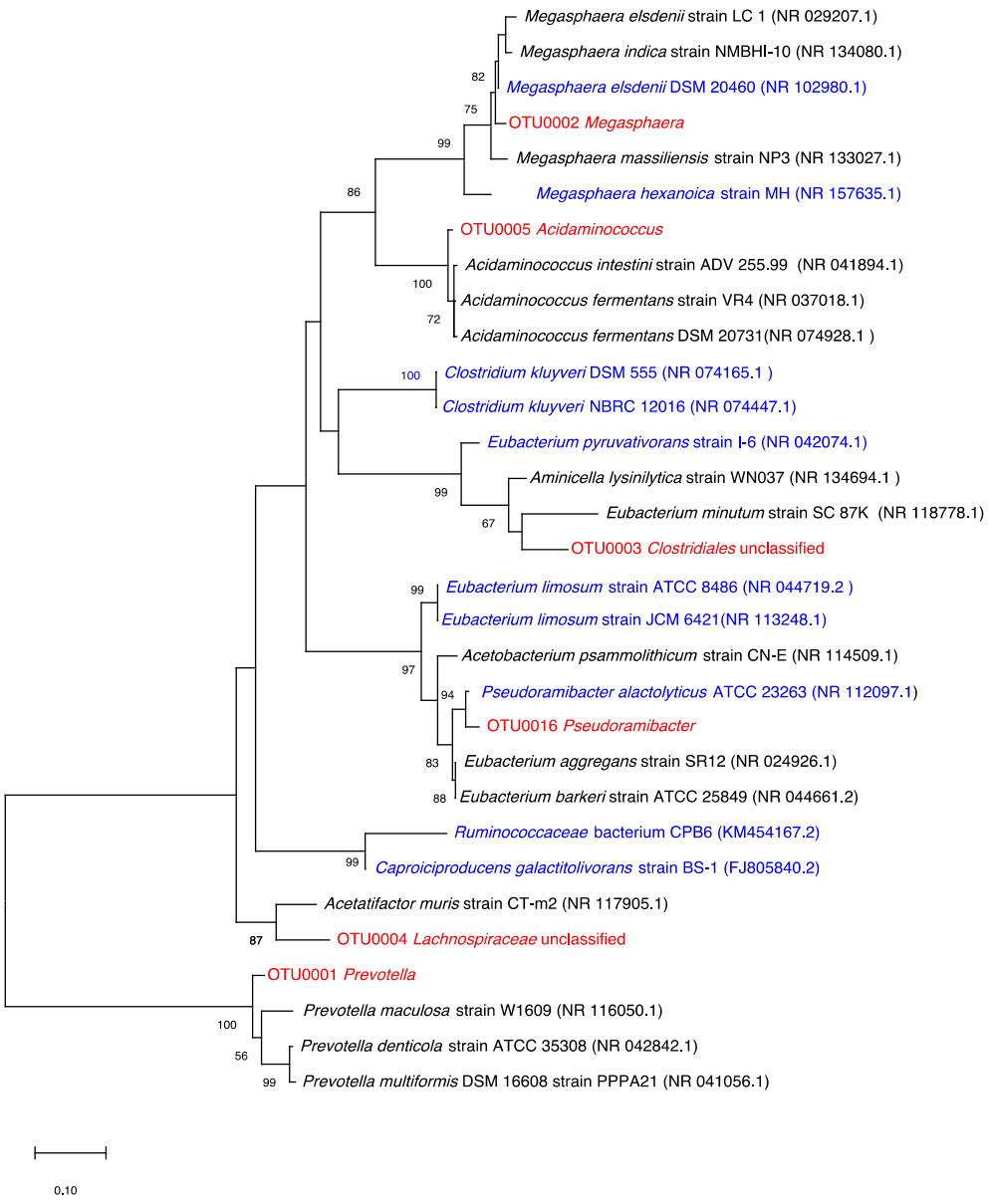

Figure A.3. Phylogenetic tree of 16S rRNA gene sequence of the dominant bacterial OTUs (in red). The GenBank accession numbers are given in parentheses. The reference sequences are shown in black while the known chain elongating microorganisms are shown in blue. The numbers at the nodes of the branch indicate bootstrap values. The scale bar of 0.10 represents 10% substitutions per nucleotide base pair.

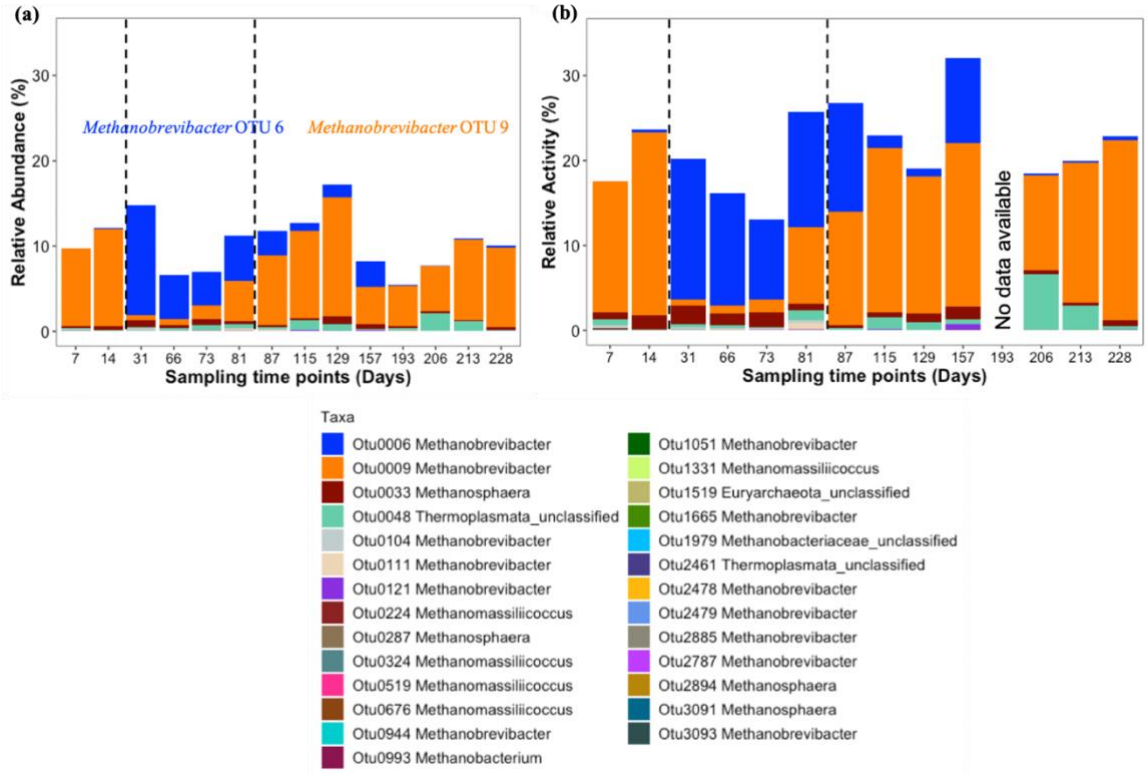

Figure A.4. Relative abundance (a) and relative activity (b) of methanogens on OTUs level in the bioreactor samples over time. The relative abundance and relative activity were determined as percentages normalized to the total number of 16S rRNA gene sequences and 16S rRNA sequences, respectively. The dashed lines represent start and end of wasting bioreactor content on Days 20 and 82, respectively, to decrease solids retention time.

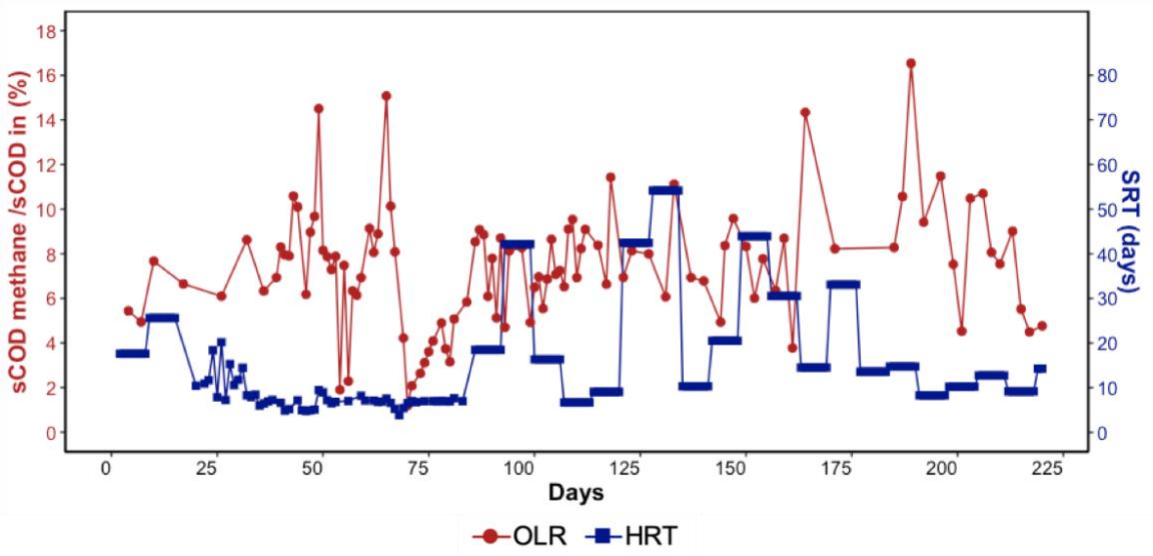

Figure A.5. Percentage of influent soluble chemical oxygen demand (sCOD) used up in methane production and solids retention time (SRT) over time.

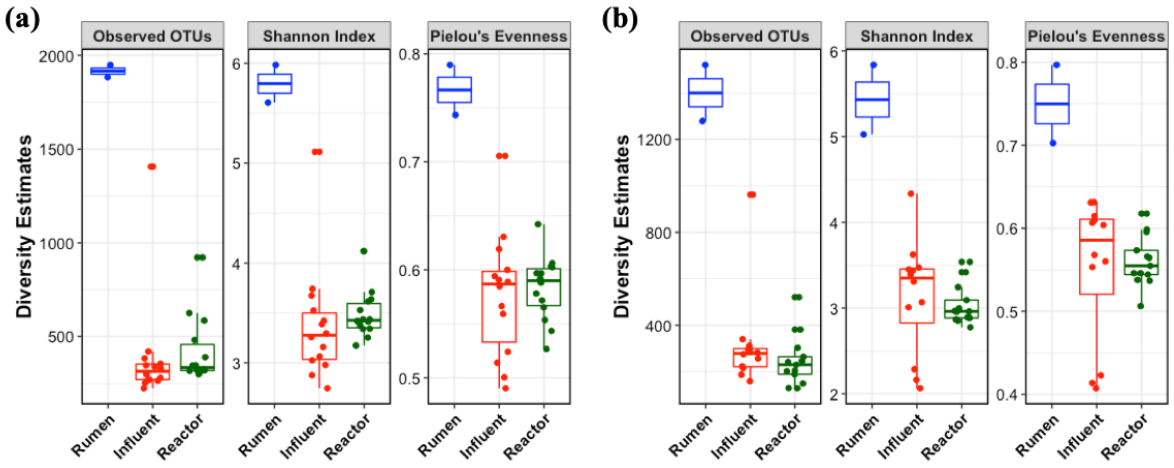

Figure A.6. Alpha diversity indices of the microbial community based on 16S rRNA gene sequencing (a) and 16S rRNA sequencing data (b) between inoculum, influent, and bioreactor samples.

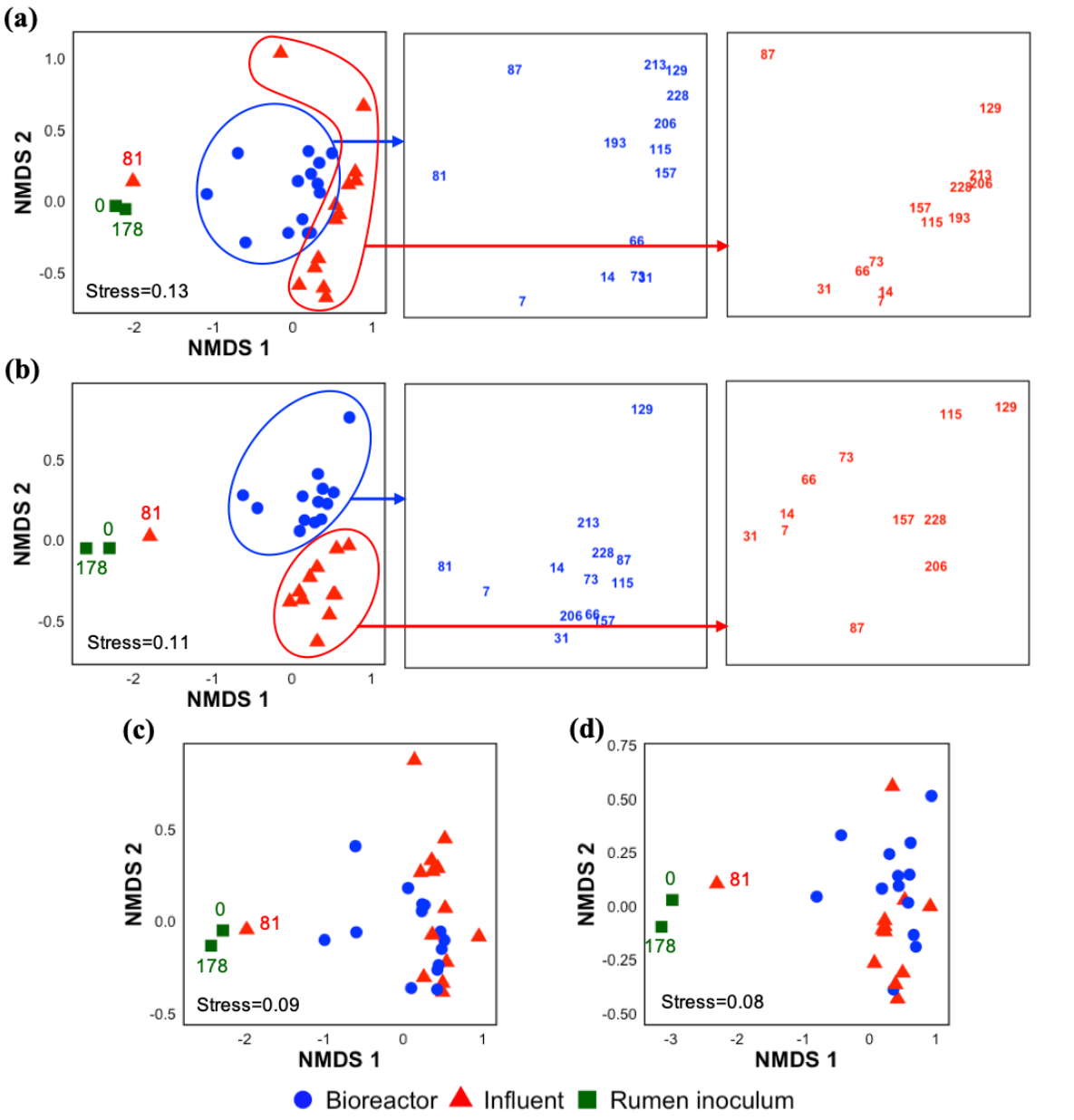

Figure A.7. Non-metric multidimensional scaling (NMDS) ordination plot based on Bray-Curtis dissimilarity index of the bacterial community at OTU level using 16S rRNA gene sequencing (a) and 16S rRNA sequencing data (b) and Jaccard index using 16S rRNA gene sequencing (c) and 16S rRNA sequencing data (d) in the rumen inocula, bioreactor, and influent samples. The numbers correspond to sampling time points.

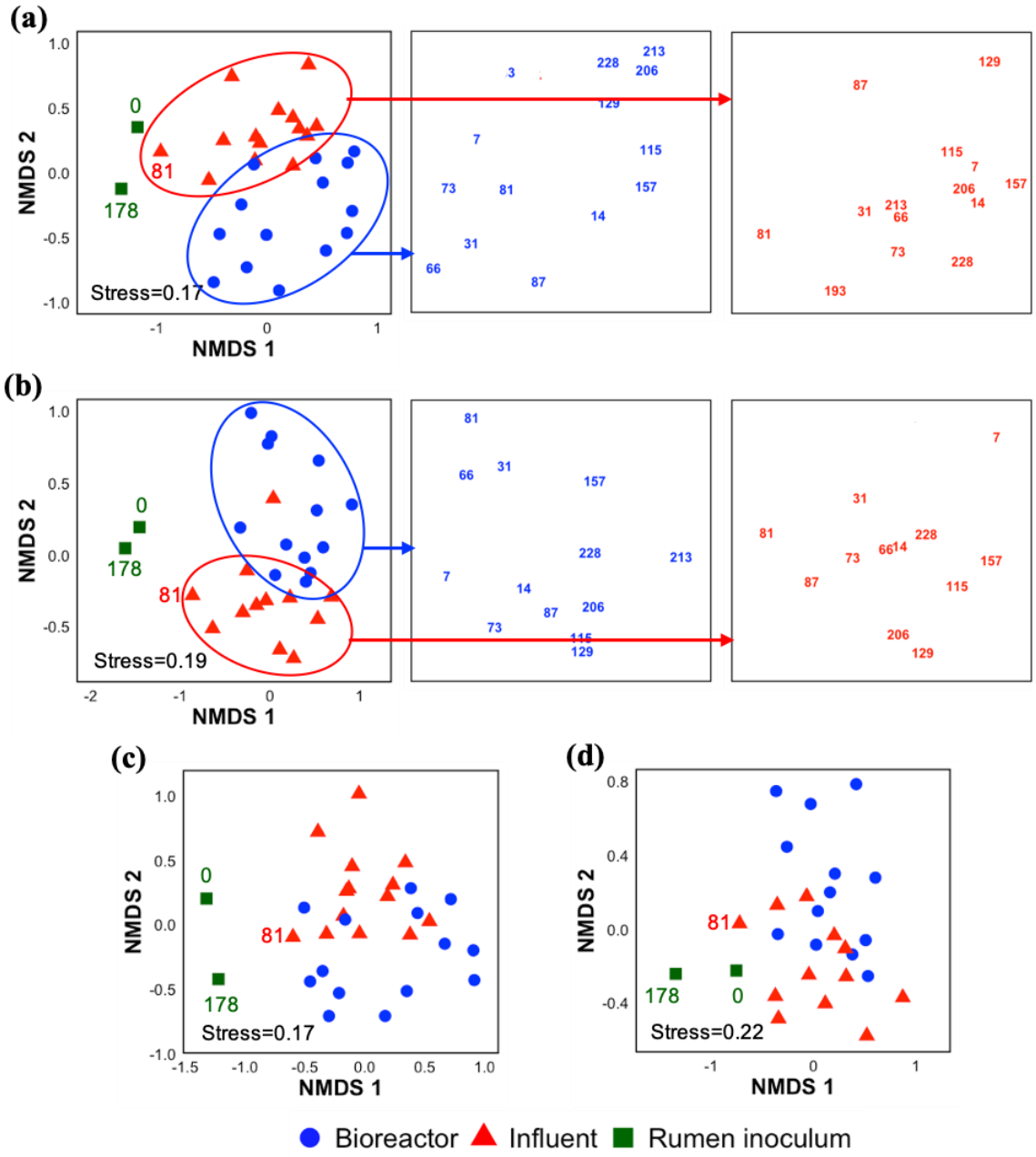

Figure A.8. Non-metric multidimensional scaling (NMDS) ordination plot based on Bray-Curtis dissimilarity index of the archaeal community at OTU level using 16S rRNA gene sequencing (a) and 16S rRNA sequencing data (b) and Jaccard index using 16S rRNA gene sequencing (c) and 16S rRNA sequencing data (d) in the rumen inocula, bioreactor, and influent samples. The numbers correspond to sampling time points.

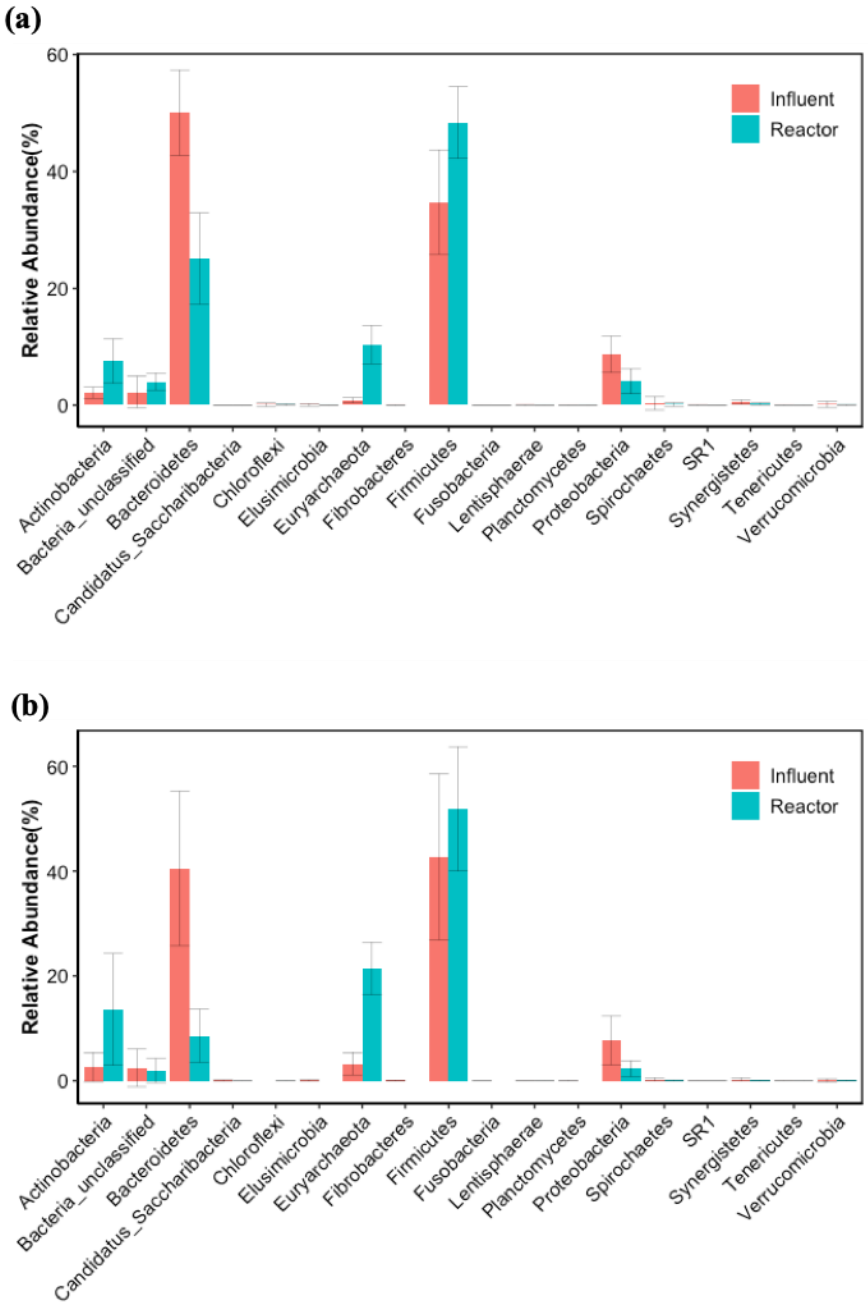

Figure A.9. Comparison of community composition at the phylum level based on 16S rRNA gene sequencing (a) 16S rRNA sequencing (b) between influent and bioreactor samples. The data represent averages and error bars represent the standard deviations of data collected at different sampling time points.

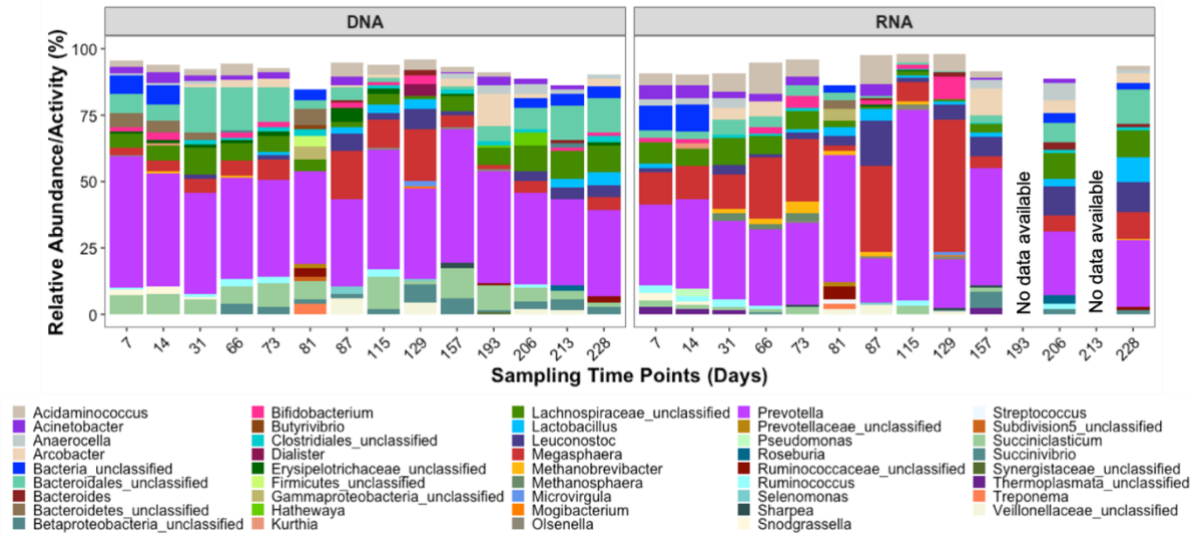

Figure A.10. Relative abundance and activity of 15 most abundant microbial groups classified to the genus or family level in the influent samples over time. The top 15 microbial groups represented 84.5-96.2% and 86.3-98.2% of the total relative abundance and relative activity, respectively.

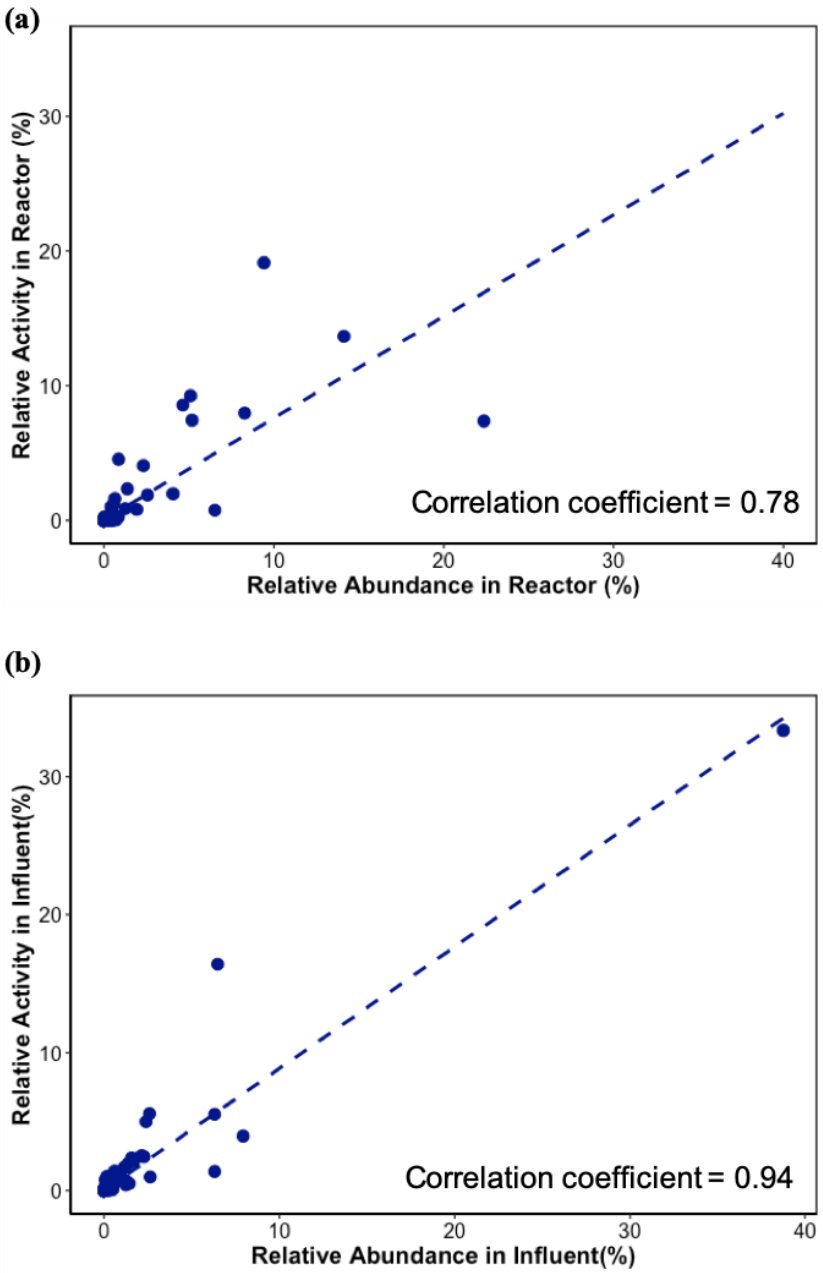

Figure A.11. Correlation of relative abundance and relative activity of microbial groups identified to the genus level observed in the bioreactor (a) and influent (b) samples. The relative abundance and relative activity were determined as percentages normalized to the total number of 16S rRNA gene sequences and 16S rRNA sequences, respectively. The average values of relative abundance and relative activity corresponding to all sampling time points were used.

A.3 References

Mei, R., Narihiro, T., Nobu, M.K., Kuroda, K., Liu, W.T., 2016. Evaluating digestion efficiency in full-scale anaerobic digesters by identifying active microbial populations through the lens of microbial activity. Sci. Rep. 6, 1–10. https://doi.org/10.1038/srep34090

Milo, Ron, Phillips, R., 2015. Cell Biology by the Numbers. Garland Science.

APPENDIX B

Supplementary Information for Chapter 3

Effect of Methanogenic Inhibitor on Competitive Reactions During Ethanol Chain Elongation

B.1 Materials and Methods

B.1.1 Thermodynamic calculations

The change in Gibbs free energy at standard condition (ΔG^o) of temperature 273 K and activities of 1 M and 1 atm (for gaseous substrate) was calculated from the standard Gibbs energies of formation according to equation 1.

$$\Delta G^o\ (kJ) = \sum G_f^o products - \sum G_f^o reactants \quad (1)$$

Where, G_f^o is Gibbs free energy of formation of each reactant and product.

The standard Gibbs free energy values were corrected for temperature using the Gibbs-Helmholz equation. The change in Gibbs free energy at reactor condition ($\Delta G_R'$) for different reactions was calculated according to the Nernst's equations 2 and 3 using the measured concentrations of reactants and products in the reactor. The G_f^o values were taken from Kleerebezem and Loosdrecht (2017) and Thauer et al. (1977)

$$\Delta G_R'(kJ) = \Delta G^o + R \times T \times lnQ \quad (2)$$

$Q = \frac{\{C\}^c\{D\}^d}{\{A\}^a\{B\}^b}$ for the reaction aA+bB=cC+dD (3)

Where, R is the universal gas constant (8.314 $*10^{-3}$ kJ $mole^{-1}$ K^{-1}), T is the temperature of the reactor in K (293+37 K in this study), Q is the reaction quotient related to the activities of products A and B and reactants C and D along with their stoichiometric coefficients.

B.2 Tables

Table B.1 Standard Gibbs free energy (ΔG^o) calculated at standard conditions for competitive reactions for acetate production potentially involved during chain elongation.

Eq.	Reactions	ΔG^o (kJ mole^{-1} reaction)
B1	Ethanol oxidation to acetate (Excessive Ethanol Oxidation, EEO) Ethanol + H_2O = Acetate$^-$ + H^+ + 2 H_2 $C_2H_6O + H_2O \rightarrow C_2H_3O_2^- + H^+ + 2\ H_2$	49.6
B2	Hydrogenotrophic methanogenesis $4\ H_2 + CO_2 \rightarrow CH_4 + 2\ H_2O$	-130.7
B3	Syntrophic ethanol oxidation (EEO and hydrogenotrophic methanogenesis) 2 Ethanol + CO_2 = 2 Acetate$^-$ + CH_4 + 2 H^+ $2\ C_2H_6O + CO_2 \rightarrow 2\ C_2H_3O_2^- + CH_4 + 2\ H^+$	-31.5
B4	Direct EEO by a methanogen 2 Ethanol + CO_2 = 2 Acetate$^-$ + CH_4 + 2 H^+ $2\ C_2H_6O + CO_2 \rightarrow 2\ C_2H_3O_2^- + CH_4 + 2\ H^+$	-31.5
B5	Oxidation of ethanol by acetic bacteria $2\ \text{Ethanol} + 2\ CO_2 = 3\ \text{Acetate}$ $2\ C_2H_6O + 2\ CO_2 \rightarrow 3\ C_2H_4O_2$	44.2
B6	Homoacetogenesis 4 H_2 + 2 CO_2 = Acetate$^-$ + H^+ + 2 H_2O $2\ CO_2 + 4\ H_2 \rightarrow C_2H_3O_2^- + H^+ + 2\ H_2O$	-55.0
B7	Propionate oxidation Propionate + 2 H_2O = Acetate$^-$ + 3 H_2 + CO_2 $C_3H_5O_2^- + 2\ H_2O \rightarrow C_2H_3O_2^- + 3\ H_2 + CO_2$	71.7
B8	Butyrate oxidation Butyrate + 2 H_2O = 2 Acetate$^-$ + 2 H_2 + H^+ $C_4H_7O_2^- + 2\ H_2O \rightarrow 2\ C_2H_3O_2^- + 2\ H_2 + H^+$	88.1

Table B.2. ASVs with significant difference in relative activity due to 2-BES addition as observed with DESEq2 analysis

Bacterial ASVs significantly lower after 2-BES addition				
ASVNumber	log2FoldChange	pvalue	padj	Genus
ASV_173	2.88	5.43E-03	3.06E-02	*Acetobacter*
ASV_221	4.14	4.07E-08	1.60E-06	*Acidaminococcus*
ASV_9	4.08	1.46E-09	8.91E-08	*Acidaminococcus*
ASV_119	3.79	8.03E-05	9.19E-04	*Acidaminococcus*
ASV_143	3.56	1.97E-03	1.41E-02	*Acidaminococcus*
ASV_315	3.53	4.70E-03	2.78E-02	*Acidaminococcus*
ASV_62	5.43	2.19E-04	2.16E-03	*Acinetobacter*
ASV_89	5.01	3.19E-06	5.83E-05	*Acinetobacter*
ASV_190	7.09	1.33E-04	1.43E-03	*Bifidobacterium*
ASV_19	3.96	1.00E-06	2.29E-05	*Bifidobacterium*
ASV_95	2.24	6.15E-05	7.26E-04	*Bulleidia*
ASV_144	4.63	2.97E-03	1.94E-02	*Comamonas*
ASV_262	6.34	2.87E-05	4.21E-04	*Escherichia/Shigella*
ASV_33	2.92	1.19E-05	1.90E-04	*Holdemania*
ASV_103	3.00	5.68E-03	3.12E-02	*Lachnospiraceae*_unclassified
ASV_56	2.36	4.99E-03	2.85E-02	*Lachnospiraceae*_unclassified
ASV_201	7.26	3.47E-05	4.79E-04	*Lactobacillus*
ASV_71	5.31	1.42E-04	1.48E-03	*Lactobacillus*
ASV_18	3.69	1.03E-02	4.55E-02	*Lactobacillus*
ASV_54	4.19	4.76E-09	2.49E-07	*Megasphaera*
ASV_2	2.49	1.48E-03	1.13E-02	*Megasphaera*
ASV_322	2.98	6.13E-03	3.25E-02	*Olsenella*
ASV_217	5.28	7.66E-03	3.74E-02	*Phocaeicola*
ASV_53	7.97	1.49E-06	3.22E-05	*Prevotella*
ASV_7	7.24	1.05E-09	7.68E-08	*Prevotella*
ASV_25	6.39	2.15E-03	1.50E-02	*Prevotella*
ASV_66	6.35	2.32E-03	1.57E-02	*Prevotella*
ASV_160	6.21	8.51E-04	7.42E-03	*Prevotella*
ASV_32	4.85	5.94E-08	1.98E-06	*Prevotella*
ASV_458	4.52	1.03E-02	4.55E-02	*Prevotella*
ASV_35	3.49	4.97E-05	6.27E-04	*Prevotella*
ASV_80	5.81	3.88E-03	2.43E-02	*Prevotellaceae*_unclassified
ASV_229	2.16	1.10E-02	4.78E-02	*Pseudoclavibacter*
ASV_164	4.16	9.62E-03	4.40E-02	*Schwartzia*
ASV_60	4.34	1.44E-05	2.19E-04	*Sharpea*
ASV_135	4.94	1.03E-02	4.55E-02	*Succiniclasticum*
ASV_6	2.54	1.61E-04	1.63E-03	*Succiniclasticum*
ASV_270	4.45	4.12E-03	2.51E-02	*Synergistes*
ASV_171	6.15	2.13E-06	4.34E-05	*Weissella*
Bacterial ASVs significantly higher after 2-BES addition				
ASVNumber	log2FoldChange	pvalue	padj	Genus
ASV_234	-2.68	2.64E-03	1.76E-02	*Acetobacter*
ASV_26	-2.46	5.71E-03	3.12E-02	*Acidaminococcus*

ASV_546	-2.44	6.93E-03	3.51E-02	*Bifidobacterium*
ASV_72	-4.57	2.32E-06	4.47E-05	*Bifidobacterium*
ASV_200	-4.90	8.08E-03	3.85E-02	*Carnobacterium*
ASV_43	-3.35	1.86E-03	1.36E-02	*Clostridiales*_unclassified
ASV_466	-3.88	3.28E-04	3.16E-03	*Clostridium_IV*
ASV_239	-23.40	4.52E-24	8.27E-22	*Clostridium_IV*
ASV_151	-23.01	2.67E-23	3.25E-21	*Clostridium_sensu_stricto*
ASV_188	-2.68	7.04E-03	3.51E-02	*Coprococcus*
ASV_549	-3.07	1.75E-03	1.31E-02	*Coriobacteriaceae*_unclassified
ASV_298	-5.90	3.66E-07	8.93E-06	*Enterococcus*
ASV_444	-3.25	4.24E-03	2.54E-02	*Firmicutes*_unclassified
ASV_154	-1.56	6.40E-03	3.35E-02	*Lachnospiraceae*_unclassified
ASV_146	-1.78	8.20E-03	3.85E-02	*Lachnospiraceae*_unclassified
ASV_122	-2.01	1.04E-03	8.85E-03	*Lachnospiraceae*_unclassified
ASV_78	-2.11	3.91E-03	2.43E-02	*Lachnospiraceae*_unclassified
ASV_370	-3.63	4.26E-05	5.57E-04	*Lachnospiraceae*_unclassified
ASV_352	-4.99	5.92E-03	3.19E-02	*Lachnospiraceae*_unclassified
ASV_40	-2.49	3.40E-03	2.18E-02	*Lactobacillus*
ASV_11	-2.69	6.68E-04	6.11E-03	*Lactobacillus*
ASV_480	-4.08	1.19E-03	9.69E-03	*Lactobacillus*
ASV_305	-4.18	1.49E-03	1.13E-02	*Lactobacillus*
ASV_102	-8.24	2.44E-07	6.38E-06	*Lactobacillus*
ASV_45	-7.73	4.37E-08	1.60E-06	*Lactococcus*
ASV_16	-2.19	8.12E-06	1.41E-04	*Leuconostoc*
ASV_243	-2.67	3.64E-04	3.41E-03	*Leuconostoc*
ASV_536	-2.18	8.13E-03	3.85E-02	*Megasphaera*
ASV_147	-2.28	1.11E-03	9.24E-03	*Megasphaera*
ASV_83	-2.62	1.14E-05	1.90E-04	*Megasphaera*
ASV_264	-3.13	1.07E-04	1.19E-03	*Megasphaera*
ASV_251	-4.05	7.75E-09	3.55E-07	*Megasphaera*
ASV_811	-4.06	8.50E-04	7.42E-03	*Megasphaera*
ASV_187	-6.67	4.46E-10	4.08E-08	*Olsenella*
ASV_85	-5.04	5.69E-05	6.94E-04	*Prevotella*
ASV_17	-4.85	1.22E-03	9.72E-03	*Pseudomonas*
ASV_216	-5.60	4.99E-03	2.85E-02	*Pseudomonas*

B.3 Figures

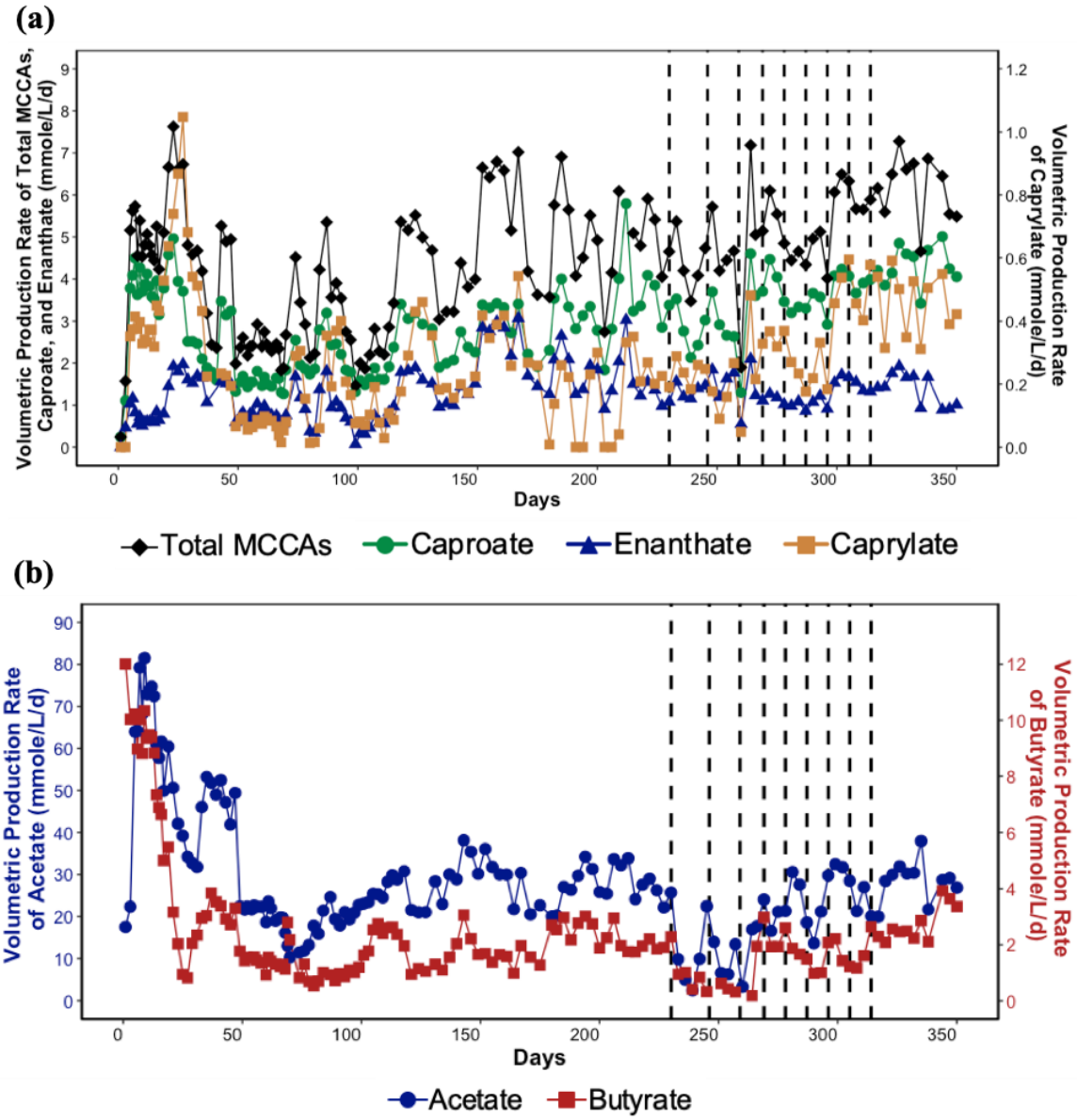

Figure B.1. Volumetric production rate of total MCCAs, caproate, enanthate, and caprylate (a) acetate and butyrate (b) in the reactor over time. The dashed lines represent 2-BES addition. Chapter 2 reports the data in Figure 2.1a until Day 229. These data are repeated here for clarity. The volumetric production rates were determined by subtracting the influent concentration from the corresponding effluent concentration.

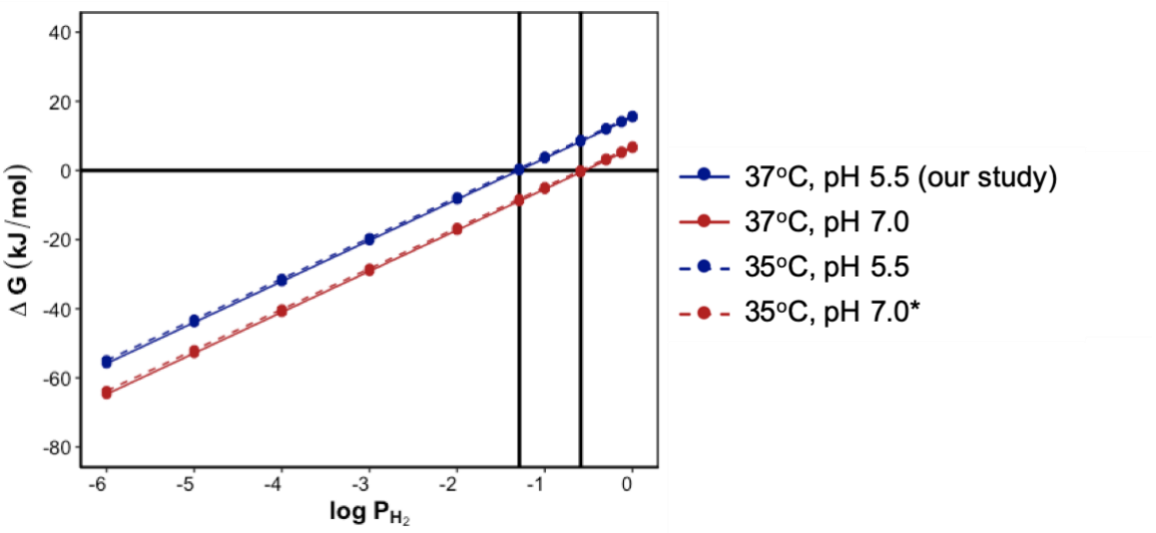

Figure B.2. Gibbs free energy of ethanol oxidation to acetate (EEO) reaction under different pH (H^+ concentration) and temperature conditions assuming 1M of solute (reactant and product) concentration. *conditions used by Grootscholten et al. (2014)

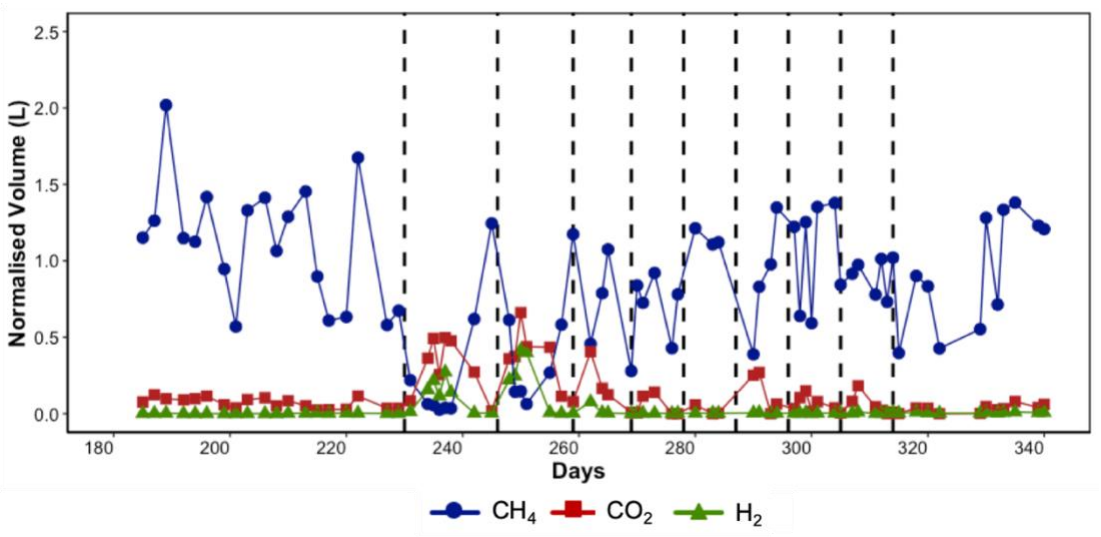

Figure B.3. Daily production of gas showing its composition after 2-BES addition (represented by the dashed lines). Gas volumes were normalized to standard temperature (273K) and pressure (1 atm) condition.

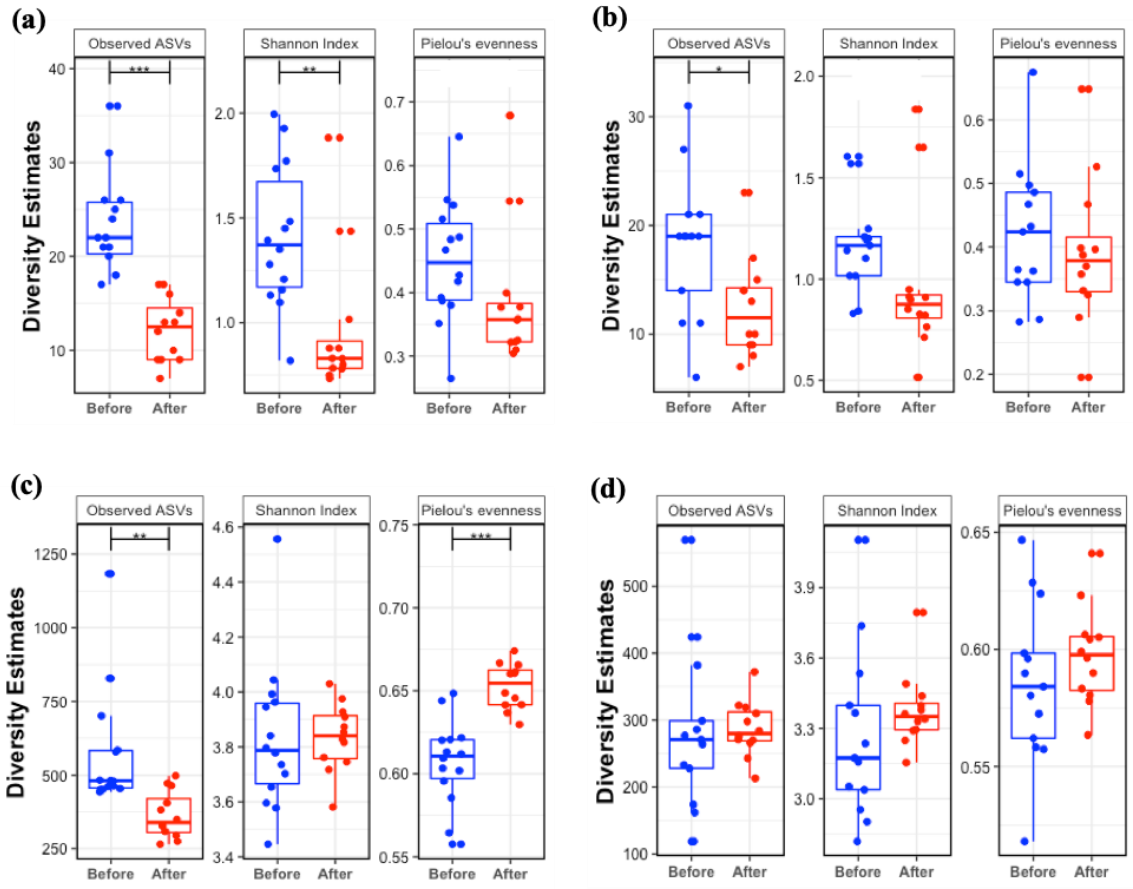

Figure B.4. Alpha diversity indices of the archaeal community based on 16S rRNA gene (a) and 16S rRNA sequencing data (b) and of the bacterial community based on 16S rRNA gene (c) and 16S rRNA sequencing data (d) before (blue) and after (red) the start of 2-BES addition on Day 230. Significant difference is indicated by * (P<0.05), ** (P<0.01), and *** (P<0.001) based on the ANOVA analysis.

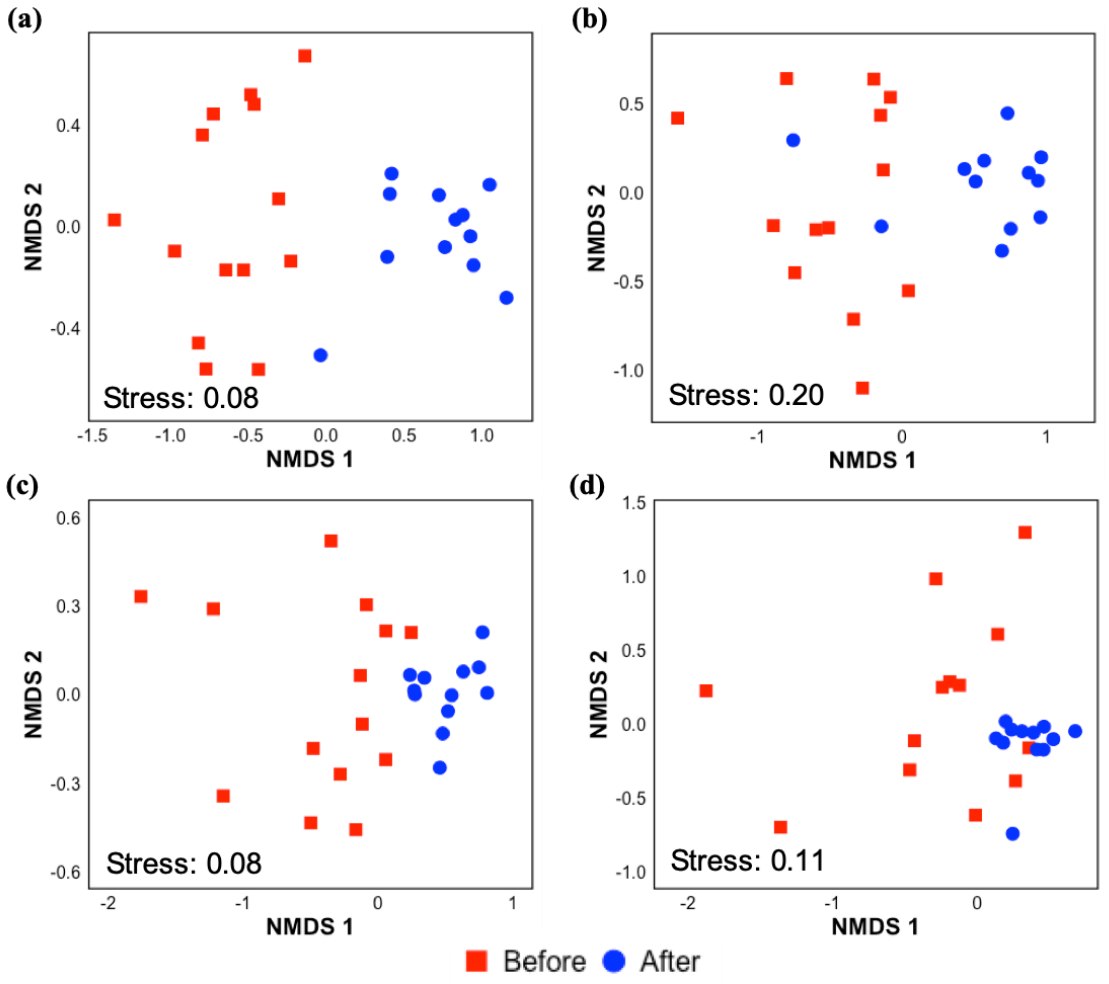

Figure B.5. Non-metric multidimensional scaling (NMDS) ordination plot based on Bray-Curtis dissimilarity index of the archaeal community at ASV level based on 16S rRNA gene (a) and 16S rRNA sequencing data (b) and of the bacterial community at ASV level based on 16S rRNA gene (c) and 16S rRNA sequencing data (d) before and after the start of 2-BES addition on Day 230.

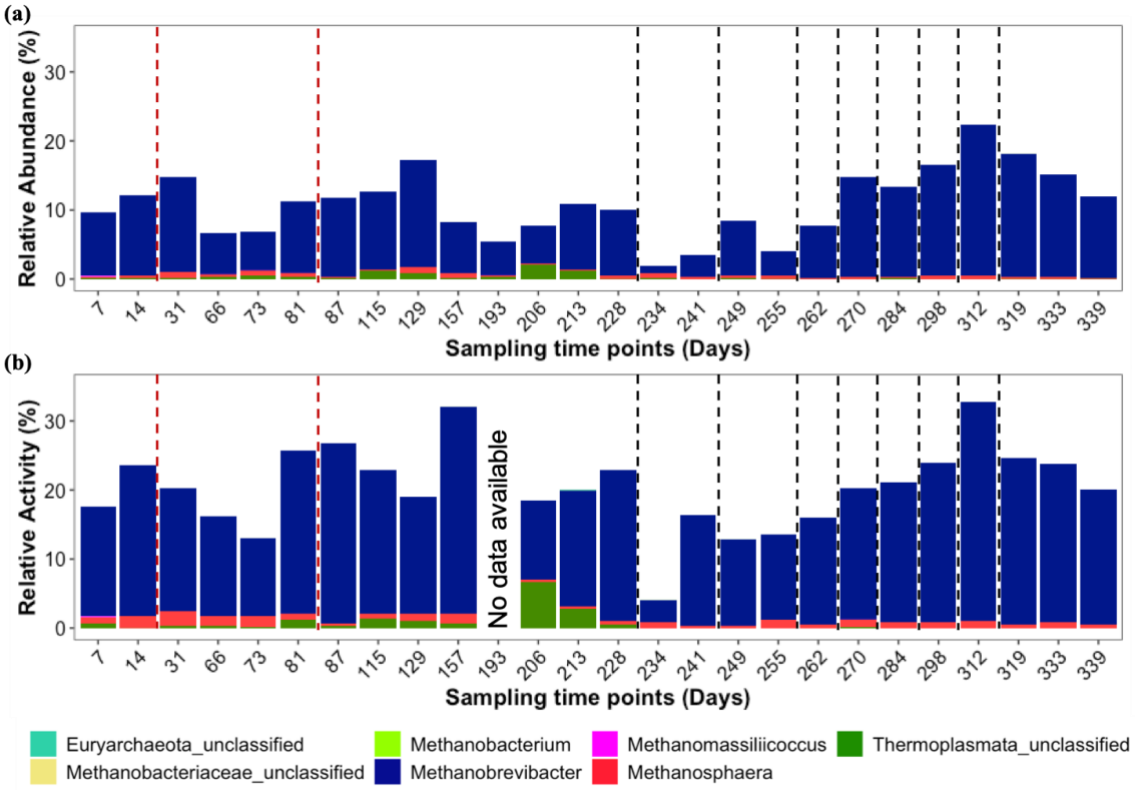

Figure B.6. Relative abundance (a) and activity (b) of methanogens identified to the genus or family level in the reactor samples over time using OTU based clustering approach. The relative abundance and relative activity were determined as percentages normalized to the total number of 16S rRNA gene sequences and 16S rRNA sequences, respectively. The red dashed lines represent start and end of wasting bioreactor content on Days 20 and 82, respectively, for controlling solids retention time and the black dashed lines represent 2-BES additions.

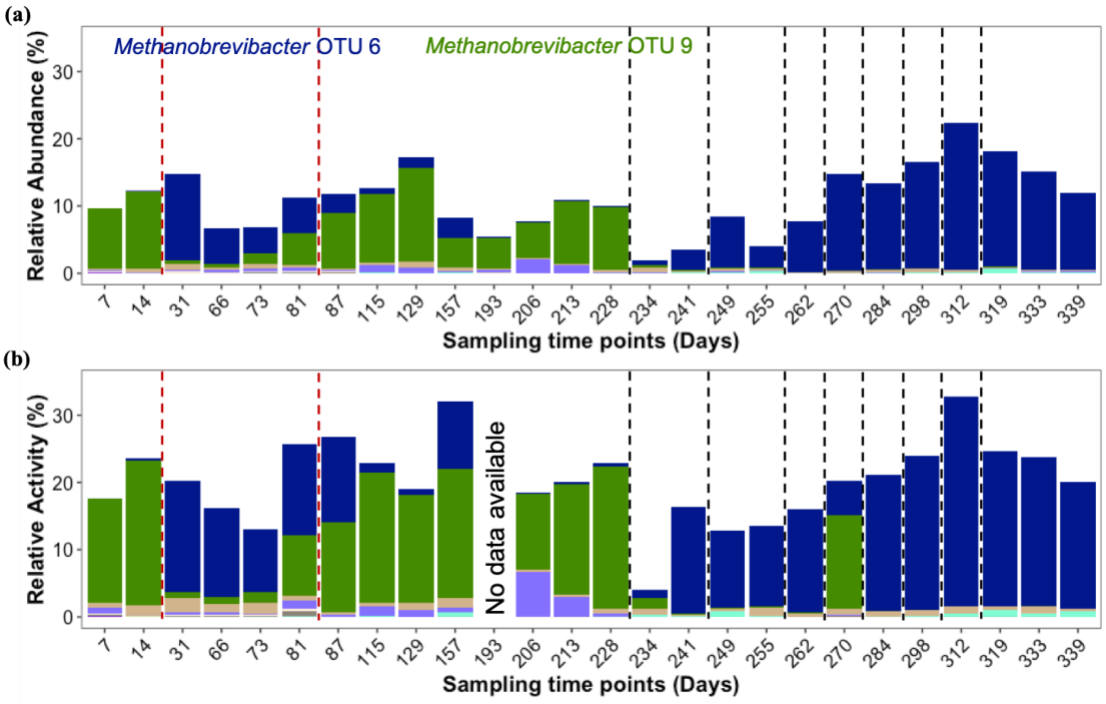

Figure B.7. Relative abundance (a) and activity (b) of methanogens OTUs in the reactor samples over time. The key OTUs discussed in the paper are labeled. The relative abundance and relative activity were determined as percentages normalized to the total number of 16S rRNA gene sequences and 16S rRNA sequences, respectively. The red dashed lines represent start and end of bioreactor content wasting on Days 20 and 82, respectively, for controlling solids retention time and the black dashed lines represent 2-BES additions. Chapter 2 report data until Day 229 in Figure S4.

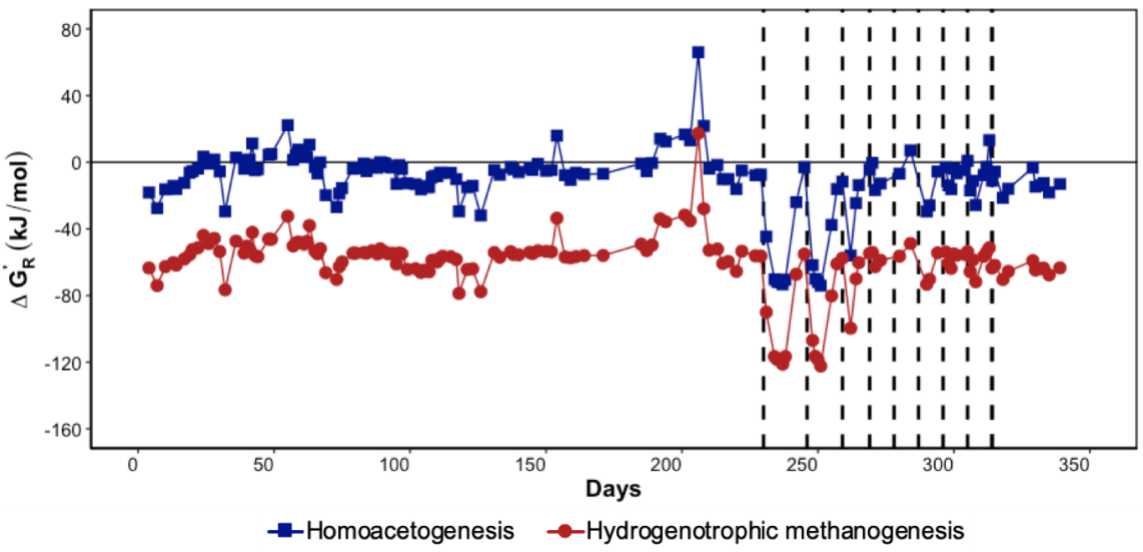

Figure B.8. Gibbs free energy changes for hydrogenotrophic methanogenesis (Table B2, Eq B2) and homoacetogenesis (Table B2, Eq B6) reactions. The calculations were done using concentration of respective reactants and products in the reactor and other reactor conditions (pH 5.5, 37^{o}C). The vertical dashed lines represent 2-BES additions.

B.4 References

Grootscholten, T.I.M., Strik, D.P.B.T.B., Steinbusch, K.J.J., Buisman, C.J.N., Hamelers, H.V.M., 2014. Two-stage medium chain fatty acid (MCFA) production from municipal solid waste and ethanol. Appl. Energy 116, 223–229. https://doi.org/10.1016/j.apenergy.2013.11.061

Kleerebezem, R., Loosdrecht, M.C.M.V.A.N., 2017. A Generalized Method for Thermodynamic State Analysis of Environmental Systems A Generalized Method for Thermodynamic. Crit. Rev. Environ. Sci. Technol. 40, 1–54. https://doi.org/10.1080/10643380802000974

Thauer, R.K., Jungermann, K., Decker, K., Pi, P.P.H.--, 1977. Energy Conservation in Chemotrophic Anaerobic Bacteria. Bacteriol. Rev. 41, 100–180.

APPENDIX C

Supplementary Information for Chapter 4

Impact of Dynamic Membrane Development on Chain Elongation for Medium Chain Carboxylic Acid Production from Organic Waste Streams

C.1 Pertraction system

The pertraction system consisted of two 3M (Charlotte, NC, USA) hollow-fiber, hydrophobic membrane contactors containing forward and backward membranes with a pore size of 0.03 μm and a total membrane surface area of 2.8 m^2. The bioreactor permeate was recirculated through the shell side of the forward membrane contactor at a flow rate of 140 L d^{-1}. A hydrophobic mineral oil solvent with 30 g L^{-1} trioctylphosphine oxide (TOPO), a commonly used extractant for carboxylic acids extraction (Sprakel and Schuur, 2019), was used for preferential extraction of longer chain hydrophobic medium chain carboxylic acids (MCCAs). The oil was recirculated continuously through the lumen of the forward and backward membrane modules at a flow rate of 12 L d^{-1}. An alkaline stripping solution was continuously recycled at 40 L d^{-1} through the shell side of the backward membrane contactor. The alkaline solution was made up of 0.3 M pH 9 buffer solution containing sodium tetraborate and boric acid. The pH of the stripping solution was maintained at pH 9 with automated addition of 1 M NaOH using a valve controlled by a pH controller/transmitter (Jenco ¼ DIN Panel Mount pH/ORP Controller/Transmitter 3676, JJS Technical Services, Schaumburg, IL). A pH gradient between the bioreactor permeate (pH 5.5) and the alkaline stripping solution (pH 9) maintained a concentration gradient of undissociated carboxylic acids creating a driving force for mass transfer of MCCAs across the membranes. In

the forward membrane, MCCAs were extracted into the mineral oil solvent and the undissociated MCCAs recovered in the solvent was transferred across the backward membrane contactor and finally accumulated in the alkaline extraction solution. The shell side of both membranes was maintained at a higher pressure than the lumen side with the help of needle valves to maintain enough transmembrane pressure to prevent oil entrainment into the aqueous solutions.

An intermediate vessel (extraction unit (EU) vessel, Figure C2) was placed between the bioreactor and forward membrane module to enable control of permeate recirculation through the forward membrane at a higher flow rate of 140 L d^{-1} independent of the permeate flow rate from the AnDMBR side. The pH of the permeate in the EU vessel was manually adjusted to 5.5. The EU was integrated with the AnDMBR system on Day 245 but was interrupted on Day270 due to difficulty in controlling constant volume in the EU vessel and was restarted again on Day 314. The EU operation was again stopped on Day 334 due to problems with the meshes. It was restarted on Day 380 with the same set-up except that the reactor permeate was recirculated between the AnDMBR and ultrafiltration unit continuously and a constant volume of permeate left the system (Figure C2).

C.1.1 Trial I

A comparison was done with and without TOPO (extractant) addition in the mineral oil (diluent, organic phase) in Trial I. A synthetic mixture containing ethanol and carboxylic acids including both short chain carboxylic acids (SCCAs, acetate, propionate, butyrate, and valerate at concentrations of 5000, 1000, 1500, and 500 mg L^{-1}, respectively) and MCCAs (caproate, enanthate, and caprylate at concentrations of 2500, 100, and 300 mg L^{-1}, respectively) simulating the bioreactor permeate in concentration and pH (5.5) was used as the feed solution. A conventional liquid-liquid extraction was carried out without membrane contactors where the synthetic feed solution and solvent were mixed and shaken thoroughly to reach equilibrium. Samples were taken every hour for a total of three hours and carboxylic acids concentrations were measured in the aqueous solution and the fraction of extracted acids was calculated. The distribution coefficients for different compounds were calculated as

$$K_{Di} = \frac{C_{i,org}}{C_{i,aq*}} \quad \text{(C1)}$$

Here, $C_{i,org}$ and $C_{i,aq}$ are the equilibrium concentration of component i in the organic phase (solvent) and the aqueous phase, respectively.

Figure C3. shows that the fraction of MCCAs extracted to the organic phase is larger for the trial conducted with mixture of mineral oil and TOPO compared to the one without TOPO. The fraction of caproic acid increased from 73.1% to 96.4% due to the addition of TOPO. However, the difference was small for enanthic and caprylic acids. An extractant like TOPO enhances extraction efficiency because of stronger interaction with MCCAs due to complexation facilitated by stronger Van der Waals force and hydrogen bonding.(Sprakel and Schuur, 2019) The K_{Di} values (Table C.2) for MCCAs are greater than 1 in the organic phase showing that they are preferentially present in the organic phase while SCCAs such as acetic acid and propionic acid prefer the aqueous phase ($K_{Di} < 1$). It is also clear that the distribution coefficients increase when TOPO is added to the organic solvent. Higher distribution coefficients lead to a larger driving force for mass transfer of carboxylic acids from the aqueous to the organic phase and, therefore, improve the extraction. Therefore, it was decided to use a mixture of mineral oil and TOPO for MCCAs extraction.

C.1.2 Trial II

Trial II consisted of two sets of experiments where the first one was conducted using synthetic solution of SCCAs and MCCAs (similar composition as Trial I) and the second one used bioreactor effluent. The objective of Trial II was to examine the extraction efficiency of the LLX unit. The flow rates of aqueous feed solution, organic solvent, and alkaline stripping solution were set at 200 L d^{-1}, 20 L d^{-1} and 40 L d^{-1}, respectively. The experiment was conducted semi-continuously for 78 hours with periodic addition of MCCAs at 48 and 72 hours to mimic MCCAs production in the bioreactor. The concentrations of ethanol, SCCAs, and MCCAs were measured in the aqueous feed and stripping solutions during the experiments.

To determine mass transfer coefficient (k), mass balance was done as shown below:

$$\frac{dM_a}{dt} = V_a \frac{dC_a}{dt} = -kA\Delta C = -kA(C_a - C_a^*) \quad \text{(C2)}$$

The depletion of carboxylic acids (dM_a/dt [g hr^{-1}]) from the aqueous feed solution of volume (V_a [m^3]) is equal to the mass transfer rate, which is proportional to the mass transfer coefficient k [m

hr^{-1}], the membrane surface area A [m^2] and the driving force, i.e., the concentration difference between the aqueous feed concentration C_a [g m^{-3}] and the equilibrium concentration C_a^* [g m^{-3}]. The equilibrium aqueous concentration C_a^* can be written as

$$C_a^* = \frac{C_o}{K_D} \quad \text{(C3)}$$

Here, C_o is the concentration in the organic phase and K_D is the distribution coefficient. Mass balance was done as follows.

$$V_a(C_a^o - C_a) = V_a(C_o - C_o^0) \quad \text{(C4)}$$

with V_o [m^3] the organic phase volume and $C_o^0 = 0$ and C_a^0 the initial concentrations in the organic phase and feed phase, respectively. After rearranging and integrating the equations, the equation for a normalized concentration function C_N was plotted logarithmically. The slope of this curve was equal to $\frac{kA}{V_a}(V+1)$ with V = $\frac{V_a}{V_o K_D}$ and the value of k can be calculated.

$$C_N = \frac{C_a(V+1) - VC_a^o}{C_a^o} = \exp\left(-\frac{kA}{V_a}(V+1)t\right) \quad \text{(C5)}$$

The concentration of SCCAs remained relatively constant in the aqueous feed solution (Figure C.3a) while the MCCAs increased in the stripping solution with time (Figure C.3b) showing the effectiveness of the LLX unit to separate MCCAs from a synthetic mixture of SCCAs and MCCAs. At the end of 78 hours, 52%, 60.9%, and 61.5% of total caproic, enanthic, and caprylic acids were recovered in the stripping solution. The mass transfer coefficients for caproic, enanthic, and caprylic acids were 2.46, 6.62, and 11.90 mm/d, respectively showing that the extraction rate increases with the carbon chain length of the carboxylic acids. The longer the hydrocarbon tail of the carboxylic acids, the higher is its hydrophobicity, which leads to stronger Van der Waals force between the MCCAs and the organic solvent. A similar experiment was conducted with a reactor effluent from another operational chain elongation reactor (Chapter 2) as the feed solution to confirm the effectiveness of LLX unit with real waste stream. 46.92%, 51.43%, and 48.36% of total caproate, enanthate, and caprylate were recovered in the stripping solution at the end of a 30-

hour experiment confirming that the LLX unit could be integrated with a bioreactor system for MCCAs extraction.

C.2 Calculations

The soluble chemical oxygen demand (sCOD) of the influent (mixture of ethanol rich waste beer+SCCAs rich permeate, g sCOD L^{-1}), flow rate of the influent (L d^{-1}), and working volume of the bioreactor (L) were taken into account to calculate organic loading rate (g sCOD L^{-1} d^{-1}). The volumetric production rate (mmole L^{-1} d^{-1}) of MCCAs was determined as the permeate MCCAs concentration (mmole L^{-1}) divided by corresponding HRT (d, working volume (L) divided by permeate flow rate (L d^{-1})). Net permeate MCCAs concentration was used for the volumetric production rate calculation by subtracting the concentration of the respective compound already present in the influent from the gross values. The product yield was calculated by dividing sCOD of MCCAs produced by fermentable influent sCOD (sCOD of MCCAs already present in the influent was subtracted from the measured sCOD in the influent).

The volumetric production rate of MCCAs, r_n (mmole L^{-1} d^{-1}) after integration with the extraction unit (EU) was determined by using mass balance approach given below

$$r_n = \frac{m_{prod\,1,n} + m_{acc\,2,n} + m_{acc\,3,n} + m_{acc\,4,n}}{V_R} \quad \text{(C6)}$$

$$m_{prod\,1,n} = C_{p,n} \times V_{p,n} + C_{ML,n} \times V_{ML,n} - C_{i,n} \times V_{i,n} - C_{EU\,perm,n} \times V_{recirc,n}$$

$$m_{acc\,2,n} = C_{p,n} \times V_{p,n} - C_{EU\,perm,n} \times V_{recirc,n} - C_{EU\,perm,n} \times V_{out,n}$$

$$m_{acc\,3,n} = 0$$

$$m_{acc\,4,n} = \frac{C_{b,n} \times V_{b,n} - C_{b,m} \times V_{b,m}}{n-m}$$

Here,

$m_{prod\,1,n}$ = amount of MCCAs produced by AnDMBR on day n [mmole d^{-1}]

$m_{acc\,2,n}$ = amount of MCCAs accumulated in the EU perm vessel on day n [mmole d^{-1}]

$m_{acc\ 3,n}$ = amount of MCCAs accumulated in the solvent vessel on day n [mmole d^{-1}]

$m_{acc\ 4,n}$ = amount of MCCAs accumulated in the stripping buffer on day n [mmole d^{-1}]

$C_{p,n}$ = amount of MCCAs in AnDMBR permeate on day n [mmole d^{-1}]

$C_{ML,n}$ = amount of MCCAs in influent on day n [mmole d^{-1}]

$C_{i,n}$ = amount of MCCAs in AnDMBR mixed liquor on day n [mmole d^{-1}]

$C_{EU\ perm,n}$ = amount of MCCAs in EU permeate vessel on day n [mmole d^{-1}]

$V_{p,n}$ = volume of permeate leaving the system on day n [L]

$V_{ML,n}$ = volume of mixed liquor wasted on day n [L]

$V_{i,n}$ = volume of influent added to AnDMBR on day n [L]

$V_{recirc,n}$ = volume of permeate recirculated on day n [L]

$V_{out,n}$ = volume of permeate leaving the EU perm vessel on day n [L]

V_R = working volume of AnDMBR [L]

$C_{b,n}$,$C_{b,m}$ = amount of MCCAs in stripping buffer on days n and m [mmole d^{-1}]

$V_{b,n}$,$V_{b,m}$ = volume of stripping buffer solution on days n and m [L]

Extraction efficiency was calculated using equation C7. The amount of MCCAs accumulated in the buffer solution over time with respect to the amount of MCCAs added to the EU perm vessel from the bioreactor was considered for the calculation.

$$\eta_n = \frac{m_{b,n} - m_{b,m}}{\sum_{i=m}^{n-1} m_{perm\ added,i}} \times 100 \qquad \text{(C7)}$$

$$\eta_n = \frac{C_{b,n} \times V_{b,n} - C_{b,m} \times V_{b,m}}{\sum_{i=m}^{n-1} C_{perm,i} \times V_{perm\ added,i}} \times 100$$

Here,

n_n = extraction efficiency on day n [%]

$m_{b,n}$, $m_{b,m}$ = mass of MCCAs extracted in stripping buffer solution on day n and m respectively [mg]

$m_{perm\ added,I}$ = mass of MCCAs added to EU perm vessel [mg]

$C_{b,n}$, $C_{b,m}$ = concentration of MCCAs in the stripping buffer solution on day n and m respectively [mg L^{-1}]

$V_{b,n}$, $V_{b,m}$ = volume of stripping buffer solution on day n and m respectively [L]

$C_{perm,i}$ = concentration of MCCAs in EU perm vessel on day i [mg L^{-1}]

$V_{perm\ added,i}$ = volume of AnMBR permeate added into the EU perm vessel on day i [L]

C.3 Sequencing data processing

The sequences were processed with DADA2 v1.16 (Callahan et al., 2016) in R (version 3.6.1) according to the online pipeline tutorial. The forward and reverse reads were truncated at positions 240 and 200 bp, respectively, based on the read quality profiles and the expected error rate was set to 2. An error model for the data was generated followed by dereplication of the sequences to combine all identical sequences into unique sequences. The core sample inference algorithm was applied to infer true biological sequences with the pool=TRUE option to increase sensitivity to distinguish between sequencing error and real biological variation in the amplicon sequences that may be present at very low read counts across multiple samples thus allowing detection of rare taxa. The paired-end reads were merged and non-target length sequences were removed from the sequence table followed by chimeras removal. Finally, taxonomy was assigned with the naïve Bayesian Classifier method within the DADA2 package using the Ribosomal Database Project (RDP, Version 16).

C.4 Tables

Table C.1. Chemical composition of inoculum and substrate

Parameter	Unit	Rumen Content (Day 0)	Rumen Content (Day 175)	Chain Elongation Inoculum (Day 175)	Waste Beer (Batch 2)	Waste Beer (Batch 3)	Waste Beer (Batch 4)	SCCA rich permeate
TS	$g\ L^{-1}$	23.2 ± 0.1	45.2 ± 0.8	20.2 ± 0.2	30.0 ± 0.2	52.2 ± 0.1	55.1 ± 0.1	N.A.
VS	$g\ L^{-1}$	14.0 ± 0.0	33.8 ± 0.6	12.6 ± 0.3	27.8 ± 0.1	48.6 ± 0.1	52.3 ± 0.2	N.A.
TSS	$g\ L^{-1}$	6.0 ± 0.3	N.A.	11.3 ± 0.5	1.3 ± 0.1	1.7 ± 0.0	1.3 ± 0.0	N.A.
VSS	$g\ L^{-1}$	4.5 ± 0.1	N.A.	9.5 ± 0.1	1.2 ± 0.1	1.6 ± 0.0	1.3 ± 0.0	N.A.
sCOD	$g\ L^{-1}$	15.3 ± 0.1	N.A.	N.A.	130.2 ± 0.1	177.0 ± 0.8	162.1 ± 9.0	N.A.
Ethanol	mM	0.0 ± 0.0	N.A.	17.4 ± 0.2	1024.2 ± 4.6	1147.5 ± 5.9	1128.5 ± 7.0	2.5 ± 3.0
SCCAs	mM	80.5 ± 0.3	N.A.	141.6 ± 0.2	0.0 ± 0.0	0.0 ± 0.0	0.0 ± 0.0	136.3 ± 100.9
MCCAs	mM	0.0 ± 0.0	N.A.	19.8 ± 0.4	0.0 ± 0.0	0.0 ± 0.0	0.0 ± 0.0	4.4 ± 4.9
Lactate	mM	N.A.	N.A.	N.A.	N.A.	N.A.	20.2 ± 0.6	N.A.

Values are reported as means with standard deviations of technical or biological replicates. Permeate values are averaged over 435 days. SCCAs include n-acetate, n-propionate, n- and iso-butyrate, and n- and iso-valerate. MCCAs include n-caproate, n-enanthate, and n-caprylate. Waste Beer Batch 2, 3, and 4 were used from Days 1- 72, Days 73-287, and Days 288-435 respectively. N.A. stands for not available.

Table C.2. Distribution coefficients between aqueous and organic phases for SCCAs and MCCAs with and without TOPO

Compound	Distribution coefficient (K_{Di})	
	without TOPO	with TOPO
Acetic acid	0.02	0.06
Propionic acid	0.04	0.32
Butyric acid	0.18	1.36
Valeric acid	0.64	6.28
Caproic acid	2.71	26.58
Enanthic acid	10.09	44.50
Caprylic acid	25.40	91.12

Table C.3. Biomass sampling points (days of reactor operation) from inoculum, bad beer, influent, reactor, and biofilm samples

Samples	DNA	RNA
	Days	
Rumen inoculum	0, 175	0, 175
Chain elongation biomass	175	175
Influent and Bioreactor	12, 27, 41, 89, 118, 145, 166, 181, 201, 215, 222, 243, 271, 292, 320, 348, 365, 383, 412, 435	12, 27, 41, 89, 118, 145, 166, 181, 201, 215, 222, 243, 271, 320, 365, 383, 412, 435
Biofilm	41, 89, 145, 222, 271, 320, 365, 383, 412, 435	41, 89, 145, 222, 271, 320, 365, 383, 412, 435

C.5 Figures

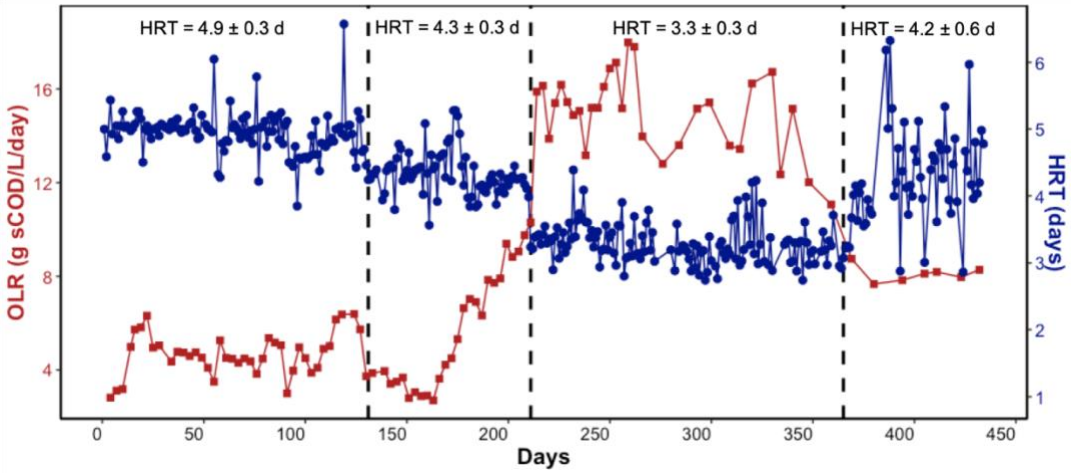

Figure C.1. Hydraulic retention time (HRT) with corresponding organic loading rate (OLR) over time. The vertical dashed lines represent changes in HRT on Days 130, 210, and 364.

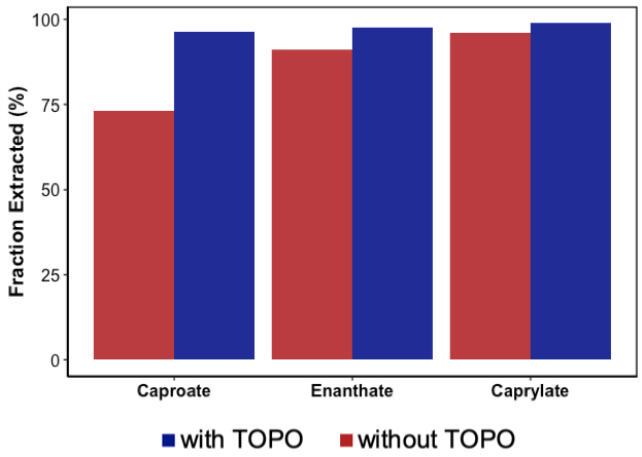

Figure C.2. Comparison of fraction of caproate, enanthate, and caprylate extracted during liquid-liquid extraction to the solvent (organic phase) with and without extractant TOPO.

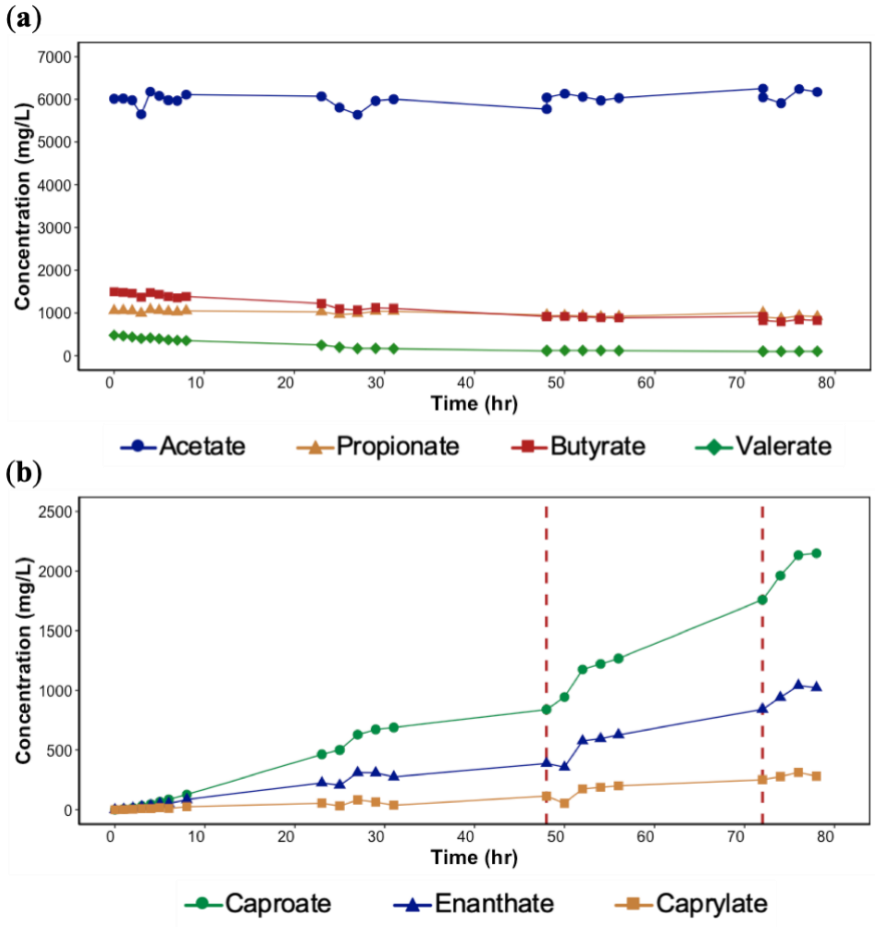

Figure C.3. Concentration profiles of SCCAs (acetate, propionate, butyrate, and valerate) in the aqueous feed solution (a) and MCCAs (caproate, enanthate, and caprylate) in the stripping solution. The vertical red lines represent addition of MCCAs.

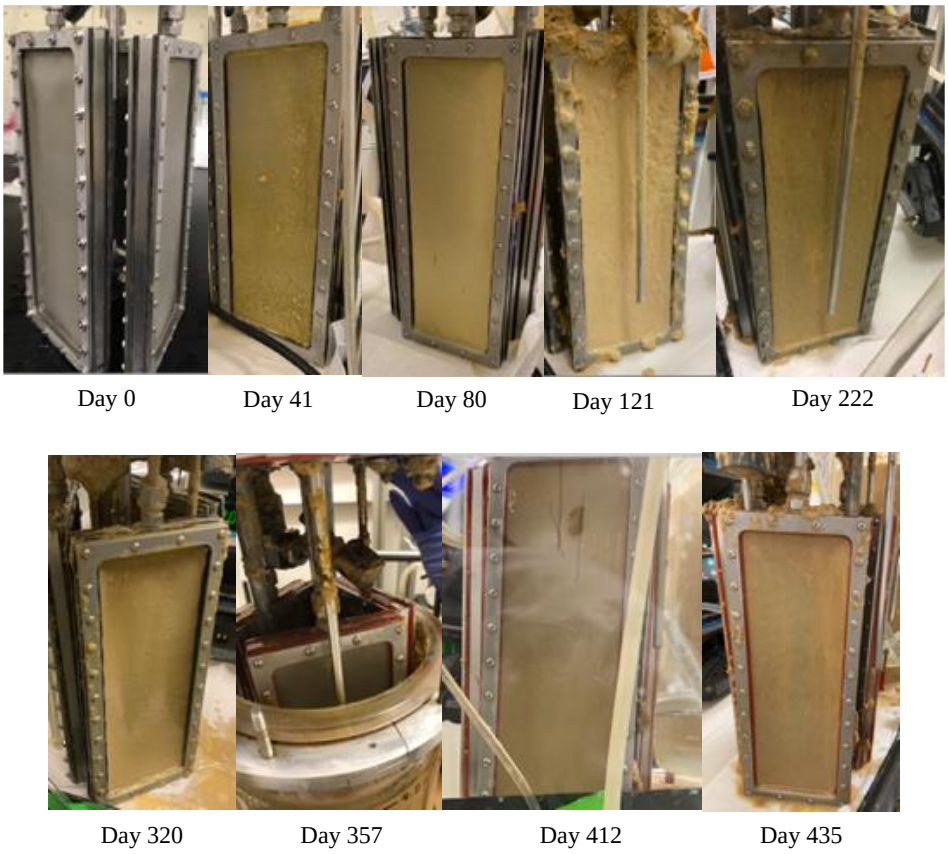

Figure C.4. Dynamic membrane formation over time

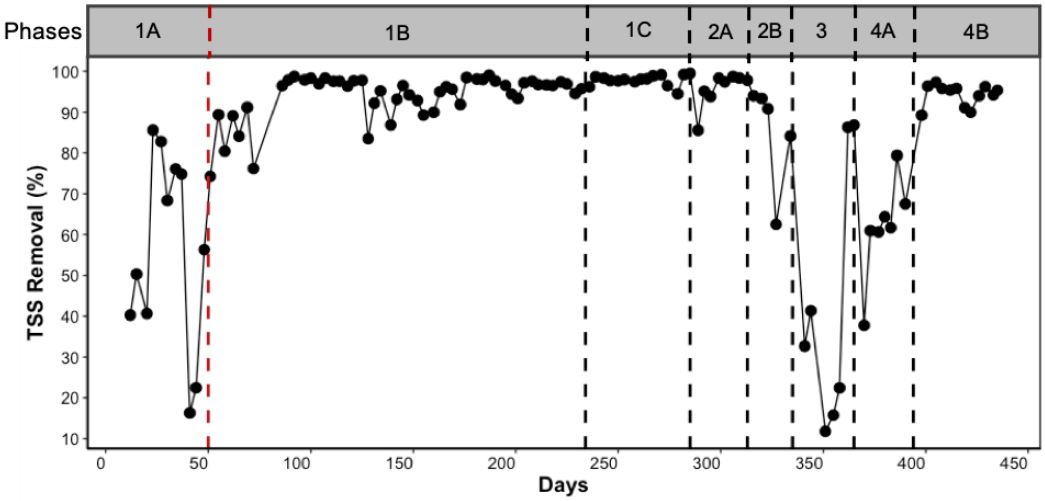

Figure C.5. Total suspended solids (TSS) removal over time. The vertical red dashed line represents a switch to the continuous filtration mode on Day 50 and the vertical black dashed lines represent different experimental phases.

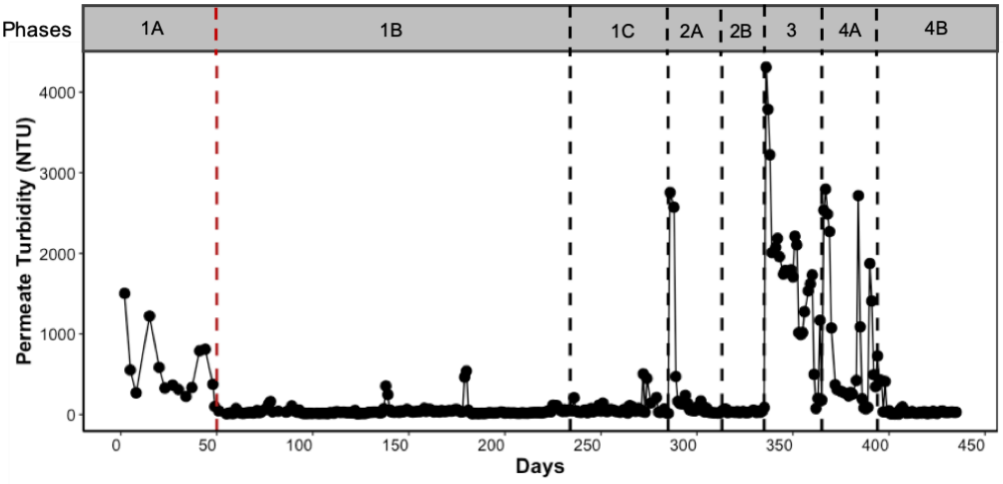

Figure C.6. Turbidity measured in the permeate samples over time. The vertical red dashed line represents a switch to the continuous filtration mode on Day 50 and the vertical black dashed lines represent different experimental phases.

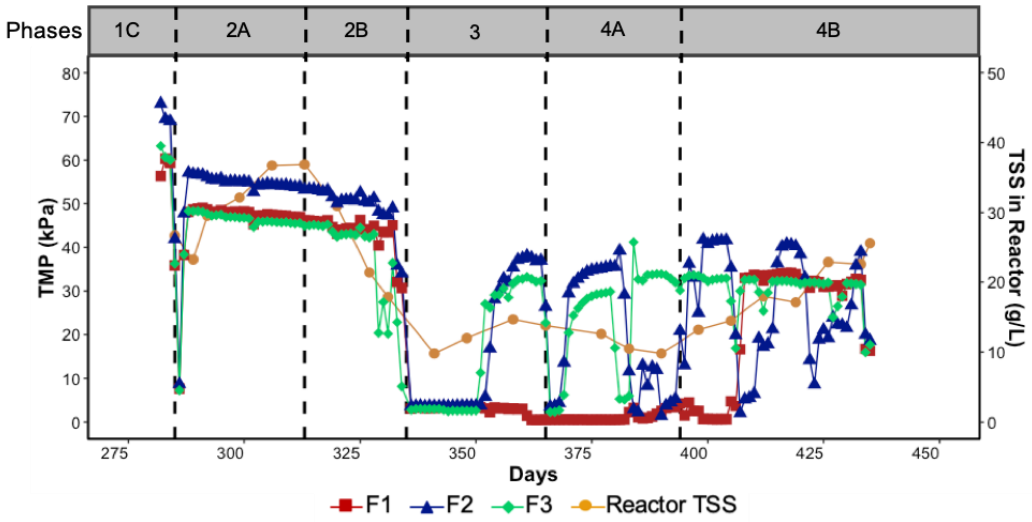

Figure C.7 Transmembrane pressure (TMP) profiles of the three meshes, F1, F2, and F3 over time versus the TSS concentration in the bioreactor. The TMP dropped whenever the meshes were replaced or flushed with water. The vertical dashed lines represent different experimental phases.

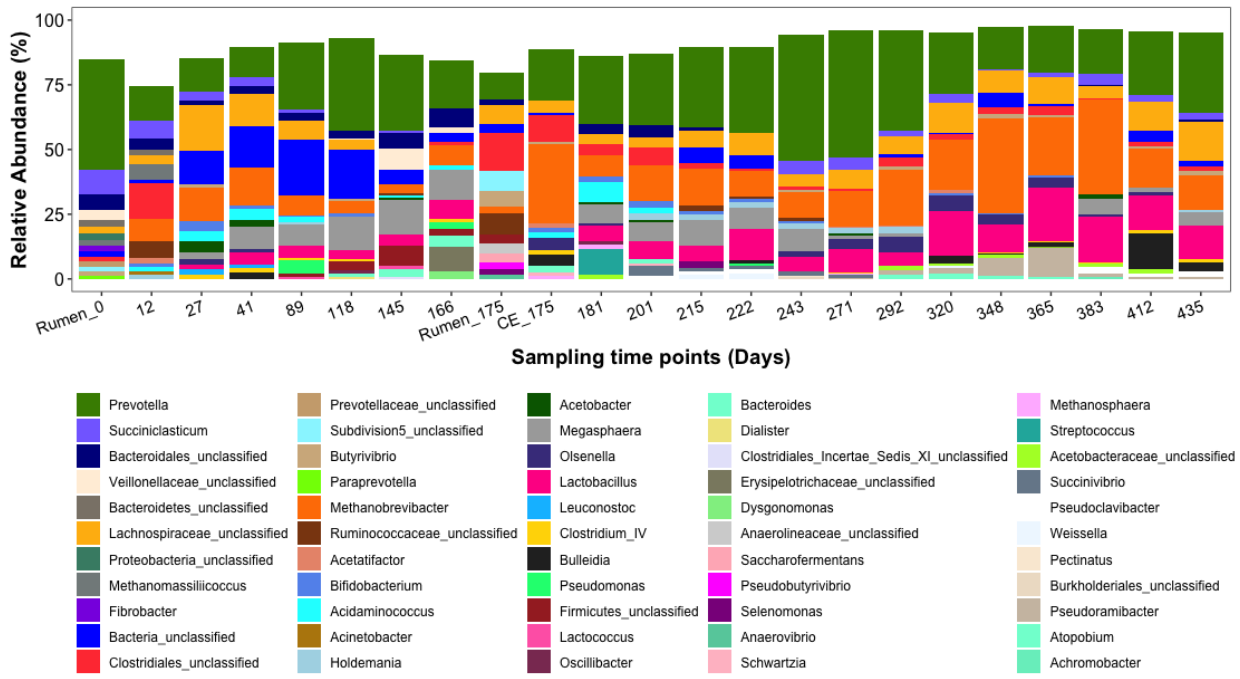

Figure C.8. Relative abundance of 15 most abundant microbial groups identified to the genus or family level in the bioreactor samples over time. The relative abundance was determined as percentages normalized to the total number of 16S rRNA gene sequences. The top 15 microbial groups represent 74.6-97.9% of the total relative abundance.

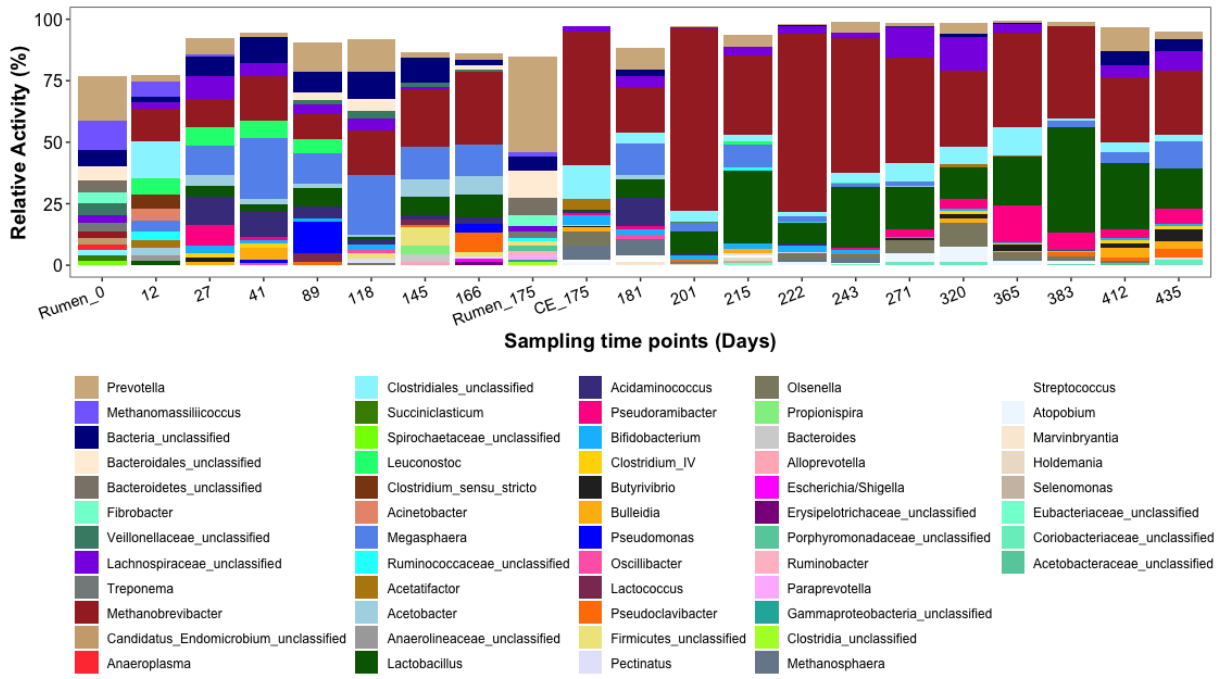

Figure C.9. Relative activity of 15 most abundant microbial groups identified to the genus or family level in the bioreactor samples over time. The relative activity was determined as percentages normalized to the total number of 16S rRNA sequences. The top 15 microbial groups represent 76.7-99.5% of the total relative activity.

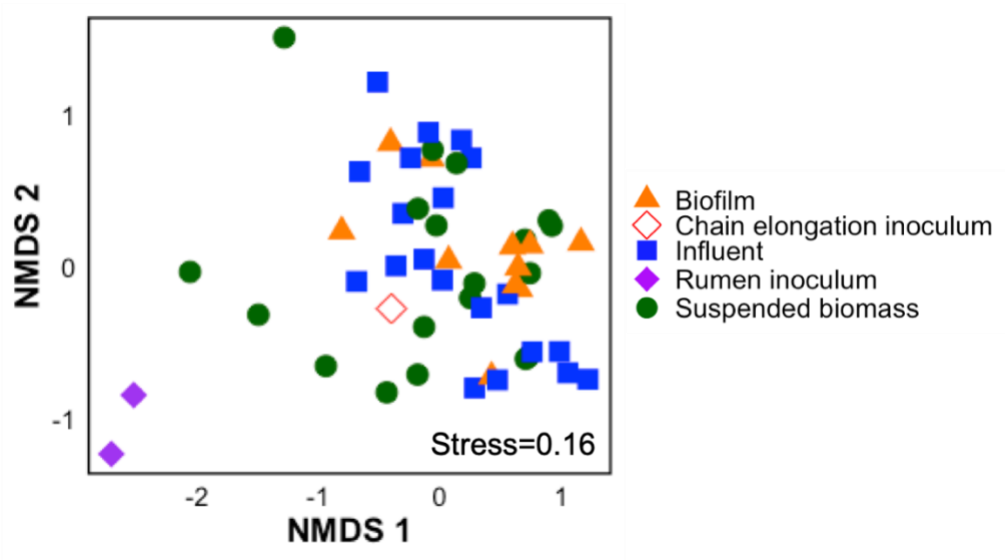

Figure C.10. Non-metric multidimensional scaling (NMDS) ordination analysis at ASV level based on Bray-Curtis dissimilarity index using 16S rRNA gene sequencing data in the rumen inoculum, chain elongation inoculum (CE_175), influent, suspended biomass, and biofilm samples. The numbers correspond to sampling time points.

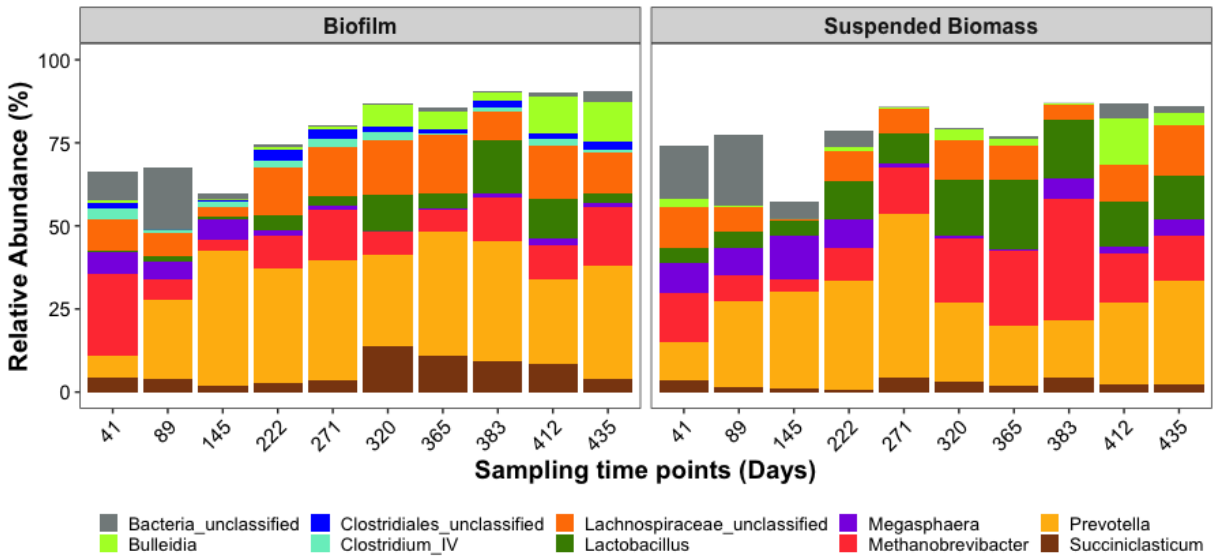

Figure C.11. Relative abundance of the microbial groups present at relative abundance greater than 1% in at least 50% of the samples (n=10 in each group) classified to the genus or family level in the biofilm and suspended biomass samples.

APPENDIX D

Supplementary Information for Chapter 5

Environmental Life Cycle Assessment of Caproic Acid Recovery from Brewery Waste Streams

D.1 Detailed description of the BW-CA system

A two-phase anaerobic digester system was modeled for caproic acid production from brewery waste (BW-CA) based on the two-phase lab-scale anaerobic bioreactor system, acidogenic (Fonoll et al., 2019) and chain elongation (Chapter 4) bioreactors operated at the University of Michigan. The amount of spent grain needed was determined based on the concentration of short chain carboxylic acids (SCCAs) produced during hydrolysis and acidogenesis of spent grain, volume of waste beer generated at the Jolly Pumpkin brewery (a midsize craft brewery in Dexter, MI, USA), and the concentration of ethanol in the waste beer. The chain elongation stoichiometric equations were used to determine the ratio in which ethanol and SCCAs react (Angenent et al., 2016). Jolly Pumpkin brewery generates around 162 L of waste beer per day (personal communication with Doug Knox, sustainability manager of Jolly Pumpkin brewery). The two-phase digester system was scaled up linearly to treat 162 L of waste beer and 37.5 kg of spent grain. The overview of model process parameters including the input and output for the baseline scenario is given in Table D.1. The major unit processes are described below.

Acidogenic digester

Brewery spent grain was used as input for the first phase acidogenic digester to produce SCCAs. The operational parameters and SCCAs concentration and yield (g chemical oxygen demand

$(COD)_{SCCAs}$ per $gCOD_{fed}$) was based on the lab-scale system operated at the University of Michigan and the study conducted by Liang and Wan (2015). The digester was operated at a hydraulic retention time (HRT) of 10 days, temperature 39^{o}C, and pH of 6.3 (adjusted with NaOH dosing). The SCCAs rich permeate was sent to the second phase chain elongation digester for caproic acid production.

Chain elongation digester

The chain elongation digester was fed mixture of SCCAs rich permeate from the acidogenic digester and waste beer. Waste beer contains 4-8% of ethanol depending on the type of the beer. It was assumed that the waste beer contained 6% (60 g L^{-1}) of ethanol. The digester was operated at an HRT of 3 days, temperature 37^{o}C, and pH of 5.5. NaOH supplementation maintained a pH at 5.5 in the digester. Both the acidogenic and chain elongation digester were configured as an anaerobic dynamic membrane bioreactor (AnDMBR) equipped with stainless steel meshes. The meshes served as support structure for the development of the dynamic membrane layer, which was responsible for efficient filtration to produce low solids containing permeate. The biogas produced from both digesters was flared.

Liquid-liquid extraction

The liquid-liquid extraction (LLX) unit consisted of a hollow-fiber, hydrophobic membrane contactor (Liqui-Cel EXF 10X28 Series) from 3M (Charlotte, NC, USA). A hydrophobic mineral oil solvent with 30 g L^{-1} trioctylphosphine oxide (TOPO) was used for the preferential extraction of hydrophobic caproic acid. The life cycle impact data for TOPO was not available in the Ecoinvent database. Hence, emissions for trimethylamine, a closer derivative of tri-octylamine, a commonly used extractant for carboxylic acids(Sprakel and Schuur, 2019), was used instead.

Distillation

Caproic acid extracted into the mineral oil+TOPO solvent was sent to a distillation system to recover caproic acid in high purity (Saboe et al., 2018). The solvent was recycled back to the LLX unit after the first solvent distillation step while caproic acid was recovered in the second distillation column. It was assumed that 95% of the solvent was replenished while the remaining 5% was lost and sent to the municipal wastewater treatment plant.

Wastewater treatment

The wastewater generated from the BW-CA process was discharged directly to a municipal wastewater treatment plant and the emissions during the treatment process were calculated using the Ecoinvent database. Emissions can vary depending on the process undergone, influent characteristics, and the effluent discharge limit, however, this was outside the scope of this paper.

Digestate handling

The digestate disposal was modeled for 55% land application, 25% landfill, and 20% incineration. Centrifuge dewatering was performed to thicken the digestate with the addition of polyacrylamide polymer (5.5 kg per ton of dry solids) (Hospido et al., 2005). The digestate was transported and distributed to a local farm 10 miles away from the brewery for land application. For landfilling and incineration, the digestate was assumed to be transported to a landfill and an incinerator 14 miles and 40 miles away from the brewery, respectively. The transportation distances were based on the closest farm, landfill, and incinerator located from the Jolly Pumpkin Brewery. The proximity of agricultural land, landfill, and incinerator will affect the transportation emission. The ash produced after incineration was disposed to the landfill. For the land application, the digestate was directly applied to the land as Class B biosolids without lime stabilization as it was coming from food grade digesters and the digesters were also operated at mesophilic temperature and long retention time (Pennington, 2018). Fecal coliform in the brewery digestate treated under mesophilic temperature (31-37ºC, similar to this study) has been found to be 25 Most Probable Number (MPN) g^{-1} dry weight digestate, which is below the U.S. EPA limit of 2.0E+06 MPN g^{-1} dry weight for Class B biosolids (Babel and Pecharaply, 2009; U.S EPA, 1994). Heavy metals released from the land application of sewage sludge have been a concern (Hospido et al., 2005); however, the amount of heavy metals in brewery sludge after digestion was found to be comparatively lower (Babel and Pecharaply, 2009), hence impacts due to digestate application related to heavy metals were also not considered in this study. Nutrients in the form of nitrogen and phosphorus present in land-applied digestate were assumed to offset mineral fertilizer use. The nitrogen and phosphorus concentrations in the digested brewery sludge were taken from the literature (Babel and Pecharaply, 2009). It was assumed that 50% of the total N as NH_3-N and 70% of the total P present in the digestate were bioavailable for plant uptake (Lundin et al., 2000).

Diesel consumption during digestate land application was assumed to be 0.73 kg ton^{-1} of digestate (Hospido et al., 2005). Impact data for the use of nitrogen- and phosphorus-based synthetic fertilizer was obtained from the Ecoinvent database.

D.2 Material, chemical, and energy requirement

Chemical consumption

NaOH consumption by both digesters was calculated using lab-based data and corroborated with the theoretical calculation. The Henderson Hasselbalch equation was used to calculate the number of moles of undissociated carboxylic acids produced under the digester pH (6.3 and 5.5) conditions. It was assumed that the same number of moles of NaOH (OH^-) was required to neutralize the acid produced. This calculation did not consider the buffering capacity of the system.

Membrane material and cleaning

The membrane material consumption for the two-phase digesters and LLX unit and water and chemicals required for membrane cleaning were included in the life cycle inventory. The membrane material weight was calculated based on the dimension and density of the membrane components. Stainless steel was used to make LLX membrane housing and the support material for the dynamic membrane formation in the first and second phase digesters. The hollow fiber membrane used in the LLX unit for caproic acid extraction was made up of polypropylene. The membranes were cleaned with NaOH solution once a month following the manufacturer's instructions. A lifetime of 5 years, as suggested by 3M, was used for the hollow fiber membrane. The stainless steel meshes used in the digesters were assumed to be replaced every two and a half years. However, the impact of membrane lifetime must be evaluated carefully and these assumptions should be verified once AnDMBRs are implemented on a full scale.

Energy calculations

Natural gas was combusted in a boiler for steam generation to heat the two-phase digesters and the distillation column. Brewery wastewater has temperature ranging from 25^oC to 42^oC (Chaitanyakumar et al., 2011). A temperature of 25^oC was used for the baseline scenario. Heat requirement was estimated based on the mass of liquid to be heated, specific heat capacity of the

liquid, and temperature of the brewery wastewater (25^{o}C) and the acidogenic and chain elongation digesters. The specific heat capacity of the mixture of acidogenic permeate and waste beer fed into the chain elongation digester was assumed to be similar to water (4.182 KJ kg^{-1} ^{o}C^{-1}). The specific heat capacity of 2.207 KJ kg^{-1} ^{o}C^{-1} was used for the spent grain. The amount of natural gas needed was calculated based on the amount of heat required and the calorific value of natural gas (3.66E-02 MJ L^{-1}). The heat loss from the digesters was not considered. For the distillation column, the energy input of 2.6 MJ kg^{-1} of caproic acid produced was used based on the Saboe et al. (2018) study. The emission due to natural gas extraction and burning was included by deriving the impact data from the Ecoinvent database. Electrical energy requirement for centrifuge dewatering was assumed to be 49.09 kWh ton^{-1} of dry solids (Hospido et al., 2005). Pumping power requirement was calculated using equation 3.2 from Judd (2010). The mechanical mixing energy requirement of 8 kW/1000 m^{3} was used (Grady Jr et al., 2011). Energy input using average mid-west electricity production was used for BW-CA system.

D.3 Caproic acid production from PKO-CA

In the reference system (PKO-CA), caproic acid was recovered from palm kernel oil (PKO), which was extracted from palm kernel, a byproduct produced during crude palm oil (CPO) production. The life cycle inventory (Table D.3) was built from an LCA study conducted by the Malaysian Palm Oil Board (MPOB) (Choo et al., 2011; Muhammad et al., 2010; Subramaniam et al., 2010a, 2010b; Zulkifli et al., 2010). During the life cycle of PKO production, palm oil seedlings were first grown in a nursery to minimize the immature period in the plantation field and to ensure a high early yield (Choo et al., 2011; Muhammad et al., 2010). The 12-15 months old seedlings were then cultivated in the plantations for fresh fruit branches (FFB) production. In the MPOB study, it was assumed that FFB was produced on land previously used for palm oil cultivation without displacing prior crop production to other areas, hence impacts due to land use effect were excluded (Zulkifli et al., 2010). FFB was transported to the palm oil mill for further processing. CPO was obtained from the mesocarp and PKO was obtained from the palm kernel present inside the nut of the FFB (Subramaniam et al., 2010a). Mass-based allocation was used to allocate the impacts of the seedling and plantation stages, as shown in Figure D.1. The palm kernels were transported to kernel crushing plants for PKO production (Subramaniam et al., 2010b). The kernel crushing plant was assumed to be located near the palm oil mill and used electricity generated at the palm oil

mill. PKO contains 0.5 % caproic acid by weight (Anneken et al., 2012). It was assumed that 100% of caproic acid present in the PKO was recovered. The shell after nut cracking and pressed mesocarp fiber left after mechanical pressing of palm fruits were used as boiler fuel to produce steam at the palm oil mill. The steam thus produced was used to run a turbine for electricity generation (Subramaniam et al., 2010a). The electricity generated on-site met almost 89% of the total electricity demands of the PKO-CA system while the remaining electricity was derived from the local grid. Diesel and electricity required for machinery, farm equipment, water consumption, and emissions due to fertilizer and pesticide use were considered during the life cycle impact assessment of PKO-CA system. The sea freight distance was calculated assuming transportation from Kuantan Port, Malaysia to Michigan City Harbor, U.S. Alternately, LCIA data for production of PKO and fatty acid production from vegetable oil was also derived from Ecoinvent database to compare with the results based on the MPOB study. Fatty acid and vegetable oil were used as substitutes for caproic acid and PKO, respectively.

D.4 Sensitivity Analysis

NaOH consumption

Excessive ethanol oxidation to acetate (EEO) leads to high base consumption due to production of acetic acid. A previous study demonstrated that operation at longer HRT can control EEO and decrease NaOH consumption from 0.67 kg NaOH per kg of caproic acid at HRT 1 day to 0.32 kg NaOH per kg of caproic acid at HRT of 4 days (Roghair et al., 2018). Alternate data for NaOH consumption was derived from this study for the sensitivity analysis. Operation at longer retention time increases the footprint of the system; however, this was not considered in the current analysis.

Biogas capture

Biogas was assumed to be combusted on-site in a boiler for heat generation that offsets the use of natural gas to meet the heating demand. The remaining heat was generated by using natural gas. Calorific value of biogas i.e 0.021 MJ L^{-1} was used to calculate the amount of heat generated from the biogas combustion. The CO_2 released from the biogas burning was excluded as biogenic CO_2.

100% land application

In this scenario, all the digestate produced in the BW-CA system was diverted towards land application.

D.5 Tables

Table D.1 Key process parameters for the production of one kg of caproic acid in the BW-CA system

Unit Process	Parameters	Value	Unit
Acidogenic digester	Hydraulic retention time	10	days
	Temperature	39	^{o}C
	pH	6.3	
	Dilution water	2.3	L kg^{-1} spent grain
	NaOH consumed	6.0E-03	g NaOH $gCOD^{-1}_{fed}$
	SCCAs yield*	0.25	$gCOD_{SCCAs}$ $gCOD^{-1}_{fed}$
	Biogas production	1.2E-02	L $gCOD^{-1}_{fed}$
	Digestate produced	0.11	kg digestate kg^{-1} spent grain
	SCCAs rich permeate produced	0.60	kg permeate kg^{-1} spent grain
Chain elongation digester	Hydraulic retention time	3	days
	Temperature	37	^{o}C
	pH	5.5	
	NaOH consumed	0.149	g NaOH $gCOD^{-1}_{fed}$
	Caproic acid yield	0.3	gCOD $gCOD^{-1}_{fed}$
	Biogas production	2.1E-02	L $gCOD^{-1}_{fed}$
	Digestate produced	3.0E-03	kg digestate $gCOD^{-1}_{fed}$
	Permeate produced	8.1E-03	kg permeate $gCOD^{-1}_{fed}$

*SCCAs yield include C2, C3, C4, and C5

Table D.2. Life cycle inventory of BW-CA for one kg of caproic acid for the baseline scenario.

Inputs/Outputs	Unit	Values
Electricity	kWh	0.2
Water	L	3.6E+01
NaOH	kg	1.3
Trioctylphosphine oxide	kg	3.5E-04
White mineral oil	kg	9.8E-03
Natural gas	MJ	9.2
Diesel	MJ	3.1E-03
Stainless steel (membrane)	kg	2.0E-01
Polypropylene (membrane)	kg	1.2E-02
Polyacrylamide	kg	9.6E-04
Digestate	kg	2.8E+01
Wastewater	L	6.0E+01
Transportation	tkm	5.5E-03

Table D.3. Life cycle inventory of PKO-CA for 1 kg of caproic acid. The inventory data was derived from different literature studies*

Inputs/Outputs	Unit	Values
Electricity	kWh	2.5
Water	L	8.0E+02
Diesel	MJ	2.2E+01
Natural gas	MJ	2.6
Transportation	tkm	2.7E+01
Fertilizer	kg	4.5
Pesticide	kg	8.7E-05
Polyethylene	kg	1.1E-03

*(Choo et al., 2011; Muhammad et al., 2010; Subramaniam et al., 2010a, 2010b; Zulkifli et al., 2010)

Table D.4. Life cycle impact data derived from Ecoinvent database for different activities used for BW-CA and PKO-CA systems

Activity	Ecoinvent item	Unit
Electricity for mixing, pumping, dewatering	market for electricity, high voltage, production mix [MRO, US only]	kWh
Water consumption in the acidogenic digester	Water, deionised, from tap water, at user {RoW}| market for | Alloc Def, Results	L
Extraction of natural gas (offset by biogas)	Market for natural gas, high pressure [RoW]	m3
Heat from natural gas (offset by biogas)	Heat production, natural gas, at industrial furnace >100kW [RoW]	MJ
NaOH for pH control in the digesters	Sodium hydroxide to generic market for neutralising agent, [GLO])	kg
Digester Membrane material (mesh)	Market for wire drawing, steel [GLO]	kg
Digester Membrane material (housing)	Market for metal working, average for steel product manufacturing [GLO]	kg
Extraction unit hollow fiber membrane material	Market for polypropylene granulate [GLO]	kg
Wastewater treatment at WWTP	Wastewater, from residence {RoW}| treatment of, capacity 1.1E10l/year | Alloc Def, U	m3
Triethyl amine (TOPO substitute) as extractant	Market for triethyl amine [GLO]	kg
Mineral oil as diluent	Market for WASTE mineral oil [RoW]	kg
Transportation	Transport, freight, light commercial vehicle [RoW]	metric ton km
Polymer for thickening	Market for polyacrylamide [GLO]	kg
Digestate application	Market for diesel, burned in agricultural machinery [GLO]	MJ
N fertilizer offset	Market for nitrogen fertilizer, as N [GLO]	kg
P fertilizer offset	Market for Phosphate fertiliser, as P_2O_5 [GLO])	kg
Landfill disposal	Treatment of Municipal Solid waste, sanitary landfill [RoW]	kg
Incineration	Treatment of digester sludge, municipal incineration [GLO]	kg
PKO-CA		
Electricity requirement	Market for electricity, high voltage [MY]	MJ
K fertilizer application	Market for potassium fertiliser, as K_2O [GLO]	kg
Pesticide application	Market for [thio]carbamate-compound [GLO]	kg
Pesticide application	Market for pyrethroid-compound [GLO]	kg

Pesticide application	Market for organophosphorus-compound, unspecified [GLO]	kg
Pesticide application	Market for pesticide, unspecified [GLO]	kg
	Market for urea, as N [GLO]	kg
Pesticide application	Market for glyphosate [GLO]	kg
Polybags for plantation stage	Market for polyethylene, high density, Granulate [GLO]	kg
Transportation from Malaysia to the U.S.	Marker for transport, freight, sea, transoceanic ship [GLO]	metric ton km
Animal feed offset with spent grain	Market for maize silage [GLO]	kg
	Ethanol production from maize [RoW]	kg
	Market for ethanol, without water, in 99.7% solution state, from ethylene [GLO]	kg
	Ethanol production from grass [RoW]	kg

Table D.5. Alternate scenarios modeled for sensitivity analysis

Parameter	Description	Baseline
Digestate handling	100% land application	55% land application, 25% landfill, and 20% incineration
Source of heating	Biogas combustion for heat generation	Natural gas
Lower NaOH consumption	0.32 kg NaOH per kg of caproic acid	1.32 kg NaOH per kg of caproic acid

Table D.6. Total life cycle impacts calculated per functional unit for PKO-CA system

Unit Process	Global Warming	Acidification	Carcinogenics	Non-Carcinogenics	Respiratory Effects	Eutrophication	Ozone Depletion	Ecotoxicity	Photochemical Oxidation
	kg CO_2-eq	moles of H^+-eq	kg benzene-eq	kg toluene-eq	kg PM2.5-eq	kg N	kg CFC-11-eq	kg 2,4-D eq	kg NO_x-Eq
Electricity	7.3	1.7	7.73E-03	13.59	1.66E-02	7.64E-04	1.89E-07	1.74	1.14E-02
Diesel	4.4	1.8	1.54E-02	33.51	9.66E-03	1.83E-03	4.58E-07	5.26	2.61E-02
Natural gas	2.0E-01	4.6E-02	9.27E-05	5.46E-01	2.18E-04	9.62E-06	1.90E-08	1.13E-02	1.15E-04
Water	1.4	3.8E-01	4.24E-03	7.89	3.61E-03	2.31E-04	3.55E-07	4.62E-01	3.10E-02
Transportation	1.4	5.6E-01	4.3E-03	6.4	2.7E-03	7.2E-04	2.2E-07	3.7E-01	8.7E-03
Fertilizer	48.5	10.5	1.36E-01	3.55E+02	3.38E-02	13.37	2.24E-06	11.91	9.09E-02
Pesticide	6.0E-04	5.2E-04	3.55E-06	9.76E-03	2.78E-06	2.21E-06	1.23E-10	1.80E-03	1.65E-06
Polyvinylchloride	1.9E-03	5.3E-04	1.03E-04	1.14E-01	2.83E-06	2.65E-07	1.62E-11	1.03E-04	3.81E-06
Polyethylene bag	2.2E-03	4.1E-04	2.23E-07	4.55E-03	1.59E-06	2.31E-07	1.61E-11	4.49E-05	4.44E-06
Total	6.3E+01	1.5E+01	1.7E-01	4.2E+02	6.7E-02	1.3E+01	3.5E-06	2.0E+01	1.7E-01

Table D.7. Comparison of total life cycle impacts of BW-CA including various scenarios and PKO-CA

Impact categories	Unit	BW-CA				PKO-CA
		(baseline*)	100% land application	biogas capture, 25ºC	lower NaOH	
Global warming	kg CO_2-eq	4.5	4.4	3.9	3.2	6.3E+01
Acidification	moles of H^+-eq	2.4	2.4	2.3	2.1	1.5E+01
Carcinogenics	kg benzene-eq	1.4E-02	1.4E-02	1.4E-02	9.4E-03	1.7E-01
Non-carcinogenics	kg toluene-eq	1.2E+02	1.2E+02	1.2E+02	1.1E+02	4.2E+02
Respiratory effects	kg PM2.5-eq	8.1E-03	8.2E-03	7.5E-03	4.8E-03	6.7E-02
Eutrophication	kg N	4.1E-03	-2.5E-03	4.1E-03	3.8E-03	1.3E+01
Ozone depletion	kg CFC-11-eq	1.1E-06	1.1E-06	1.1E-06	4.1E-07	3.5E-06
Ecotoxicity	kg 2,4-D eq	8.3	8.3	8.3	7.8	2.0E+01
Photochemical oxidation	kg NO_x-eq	1.4E-02	1.4E-02	1.3E-02	1.1E-02	1.7E-01

D.6 Figures

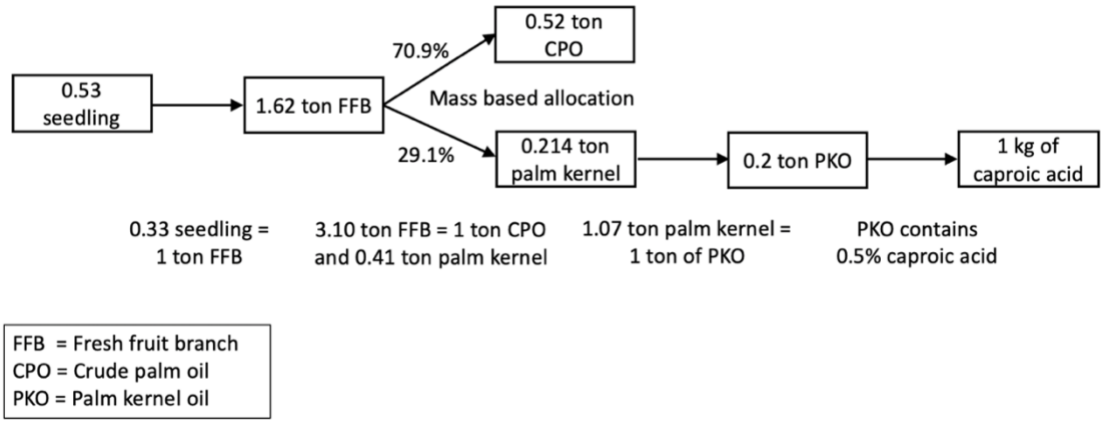

Figure D.1. Processes involved in production of one kg of caproic acid from palm kernel oil shown with mass-based allocation

D.7 References

Angenent, L.T., Richter, H., Buckel, W., Spirito, C.M., Steinbusch, K.J.J., Plugge, C.M., Strik, D.P.B.T.B., Grootscholten, T.I.M., Buisman, C.J.N., Hamelers, H.V.M., 2016. Chain Elongation with Reactor Microbiomes: Open-Culture Biotechnology to Produce Biochemicals. Environ. Sci. Technol. 50, 2796–2810. https://doi.org/10.1021/acs.est.5b04847

Anneken, D.J., Both, S., Christoph, R., Fieg, G., Steinberner, U., Westfechtel, A., 2012. Fatty acids:Ullmann's Encyclopedia of Industrial Chemistry. https://doi.org/10.1002/14356007.a10

Babel, S., Pecharaply, A., 2009. Anaerobic co-digestion of sewage and brewery sludge for biogas production and land application 6, 131–140.

Chaitanyakumar, D., Unnisa, S.A., Rao, B., Kumar, G.V., 2011. Efficiency Assessment of Combined Treatment Technologies : A Case Study of Charminar Brewery Wastewater Treatment Plant 1, 138–145.

Choo, Y.M., Muhamad, H., Hashim, Z., Subramaniam, V., Puah, C.W., Tan, Y., 2011. Determination of GHG contributions by subsystems in the oil palm supply chain using the LCA approach. Int. J. Life Cycle Assess. 16, 669–681. https://doi.org/10.1007/s11367-011-0303-9

Fonoll, X., Meuwissen, T., Aley, L., Shrestha, S., Raskin, L., 2019. The rumen membrane bioreactor: Transforming food waste into volatile fatty acids at the small scale, in: IWA 16th World Congress on Anaerobic Digestion.

Grady Jr, C.L., Daigger, G.T., Love, N.G., Filipe, C.D., 2011. Biological wastewater treatment, CRC press. https://doi.org/10.1017/CBO9781107415324.004

Hospido, A., Moreira, M.T., Martín, M., Rigola, M., Feijoo, G., 2005. Environmental evaluation of different treatment processes for sludge from urban wastewater treatments: Anaerobic digestion versus thermal processes. Int. J. Life Cycle Assess. 10, 336–345. https://doi.org/10.1065/lca2005.05.210

Judd, S., 2010. The MBR Book: principles and applications of membrane bioreactors for water and wastewater treatment. Elsevier. https://doi.org/10.1016/B978-1-85617-481-7.50005-2

Liang, S., Wan, C., 2015. Carboxylic acid production from Brewer's spent grain via mixed culture fermentation. Bioresour. Technol. 182, 179–183. https://doi.org/10.1016/j.biortech.2015.01.082

Lundin, M., Bengtsson, M., Molander, S., 2000. Life cycle assessment of wastewater systems: Influence of system boundaries and scale on calculated environmental loads. Environ. Sci. Technol. 34, 180–186. https://doi.org/10.1021/es990003f

Muhammad, H., Hashim, Z., Subramaniam, V., Tan, Y.A., Wei, P.C., Let, C.C., May, C.Y., 2010. Life cycle assessment of oil palm seedling production (part 1). J. Oil Palm Res. 22, 878–886.

Pennington, M., 2018. Anaerobic digestion facilities processing food waste in the United States in 2015: Survey results. United States Environ. Prot. Agency.

Roghair, M., Liu, Y., Strik, D.P.B.T.B., Weusthuis, R.A., Bruins, M.E., Buisman, and C.J.N., 2018. Development of an Effective Chain Elongation Process From Acidified Food Waste and Ethanol Into n-Caproate. Front. Bioeng. Biotechnol. 6, 1–11. https://doi.org/10.3389/fbioe.2018.00050

Saboe, P.O., Manker, L.P., Michener, W.E., Peterson, D.J., Brandner, D.G., Deutch, S.P., Kumar, M., Cywar, R.M., Beckham, T., Karp, E.M., 2018. In situ recovery of bio-based carboxylic acids. Green Chem. 20, 1791–1804. https://doi.org/10.1039/c7gc03747c

Sheets, J.P., Yang, L., Ge, X., Wang, Z., Li, Y., 2015. Beyond land application : Emerging technologies for the treatment and reuse of anaerobically digested agricultural and food waste. Waste Manag. 44, 94–115. https://doi.org/10.1016/j.wasman.2015.07.037

Sprakel, L.M.J., Schuur, B., 2019. Solvent developments for liquid-liquid extraction of carboxylic acids in perspective. Sep. Purif. Technol. 211, 935–957. https://doi.org/10.1016/j.seppur.2018.10.023

Subramaniam, V., May, C.Y., Muhammad, H., Hashim, Z., Tan, Y.A., Wei, P.C., 2010a. Life cycle assessment of the production of crude palm oil (part 3). J. Oil Palm Res. 22, 895–903.

Subramaniam, V., May, C.Y., Muhammad, H., Hashim, Z., Tan, Y.A., Wei, P.C., 2010b. Life cycle assessment of the production of crude palm kernel oil (part 3a). J. Oil Palm Res. 22, 904–912.

U.S EPA, 1994. A plain English guide to the EPA Part 503 Biosolids Rule.

Zulkifli, H., Halimah, M., Chan, K.W., Choo, Y.M., Mohd Basri, W., 2010. Life cycle assessment for oil palm fresh fruit bunch production from continued land use for oil palm planted on mineral soil (part 2). J. Oil Palm Res. 22, 887–894.